Winter 1-1-2012

The Physiological Effects of Phycobilisome Antenna Modification on the Cyanobacterium Synechocystis sp. PCC 6803

Lawrence Edward Page
Washington University in St. Louis

WASHINGTON UNIVERSITY IN ST. LOUIS

Division of Biology & Biomedical Sciences

Biochemistry

Dissertation Examination Committee:
Himadri Pakrasi, Chair
Tuan-Hua David Ho
Joseph Jez
Tom Smith
Gary Stormo
Yinjie Tang

The Physiological Effects of Phycobilisome Antenna Modification on the Cyanobacterium *Synechocystis* sp. PCC 6803

by

Lawrence Edward Page II

A dissertation presented to the
Graduate School of Arts and Sciences
of Washington University in
partial fulfillment of the
requirements for the degree
of Doctor of Philosophy

December 2012

St. Louis, Missouri

Table of Contents

List of Figures

Chapter 1

Chapter 2

Chapter 3

Chapter 4

Appendix Chapter 1

Appendix Chapter 2

Appendix Chapter 3

Appendix Chapter 4

Appendix Chapter 5

List of Tables

Chapter 2

Chapter 3

Chapter 4

Appendix Chapter 2

Appendix Chapter 3

Appendix Chapter 4

Appendix Chapter 5

Abbreviations

APC	Allophycocyanin
$\alpha^{PC}\beta^{PC}$	The αβ phycobiliprotein dimer that is made up of phycocyanin subunits.
$\alpha^{APC}\beta^{APC}$	The αβ phycobiliprotein dimer that is made up of allophycocyanin subunits.
CHL	Chlorophyll
DCMU	3-(3,4-dichlorophenyl)-1,1-dimethylurea
L_C	Core-Core linker protein
L_{CR}	Core-rod linker protein
L_{CM}	Core-membrane linker protein
L_R	Rod-rod linker protein
λ_{max}	Wavelength of maximum absorption
PB	Phycobilin
PBS	Phycobilisome
PBP	Phycobiliprotein
PC	Phycocyanin
PCB	Phycocyanobilin
PE	Phycoerythrin
PEC	Phycoerythrocyanin
PMB	p-hydroxymecuribenzoate
PSI	Photosystem I
PSII	Photosystem II
SANS	Small Angle Neutron Scattering

Synechocystis 6803	*Synechocystis* sp. PCC 6803
WT	Wild Type

Acknowledgements

First and foremost, I would like to thank my family. The support and encouragement of my loving mother Donna, father Randy, and Sister Lori gave me the strength and resolve to finish this degree program. I would also like to thank my extended family members, who have been extremely supportive, as well. I would especially like to thank my aunt Nancy, aunt Margie, and uncle Chuck, as they have been a source of inspiration for me throughout my life and this graduate program. Last, but definitely not least, I would like to thank the newest member of the Page family, my wife Christine for her help, support, and love. This truly would not have been possible without your constant encouragement.

Next, I would like those who steered me towards a career in science. Three high school teachers were especially important to me in this regard: Donna Malkmus, Darlene Jones, and Joyce Barker. They encouraged me at a young age to pursue my passions, and gave me the courage to do well in school. I would also like to thank my cousin, Keith. I could have put him in the family section, but I felt that he belongs here, as he was undoubtedly the strongest influence in my decision to pursue a Ph.D. I can still remember the Thanksgiving weekend we spent in his lab at Emory genotyping my family for a specific genetic marker. That was my first experience with performing an experiment where the outcome was unknown, and that was enough to get me hooked on scientific research. Next, I would like to thank my professor from my undergraduate lab, Bruce McClure. The experience working on the molecular biology of pollen/pistil interactions was what led to my obsession with photosynthesis, and his instruction has made me a much stronger scientist. In his lab, I was fortunate to be the first mentee of graduate student Chris Lee. He is a scientific inspiration and lifelong friend.

Now, moving on to my graduate education. I met Himadri during my senior year as an undergraduate at the University of Missouri. He gave a presentation on photobiological hydrogen production that was so mind-blowing, I lost sleep for several nights thereafter dreaming of all the possibilities of a hydrogen economy. From then on, I knew I wanted to work on photosynthesis and biological production of molecules that are useful for mankind. I was fortunate to be accepted to the graduate program at Washington University, and even more fortunate still to be allowed to work in his laboratory. I cannot emphasize enough how thankful I am to be counted among the lifelong Pakrasi Lab members.

My thesis also would not have been possible without all of the other Pakrasians. Daily interaction with the lab is what makes coming to work a joy, and in getting to know the lab members so well, it has become difficult to distinguish coworkers from friends. I would like to especially thank my coffee buddies, Jeff Cameron, Bert Berla and Kim Wegener, who provide interesting daily conversations on all sorts of topics (sometimes even science). I would also like to thank Michelle Liberton, who has been absolutely instrumental in teaching me an array of techniques that I use in the lab on a daily basis. I would like to thank all of the rest of the Pakrasi Lab, there is not enough space to name everyone, but rest assured that I am forever grateful for all of the help you have given me along the way.

Finally, I would like to thank my thesis committee. Your guidance and thoughtful questions while developing my thesis have pushed me to become a much better scientist. My committee chair, Tuan-Hua David Ho, asked incredibly insightful questions throughout my time as a graduate student. Bob Blankenship was a wonderful collaborator and mentor who brought a deep knowledge of a wide variety of photosynthetic life forms. Yinjie Tang has been a teacher, mentor, and collaborator, and as an engineer, a committee member who brings a fresh

perspective that draws on his knowledge of a diverse array of microbial metabolisms. Joe Jez has been an insightful committee member, a great source of help in biochemistry, and a key source of guidance between committee meetings. Gary Stormo has drawn on his insight in all things genetic to help me with my understanding of an organism from the basis of their genome sequence. It has truly been an exciting (and sometimes intimidating) experience to get to learn from such great minds during the development of my dissertation.

The following paragraphs acknowledge the specific contributions to individual chapters in this thesis. Ghada Ajlani generously provided the CB, CK, and PAL mutants used throughout the body chapters of the thesis.

Chapter 3 is reproduced in part with permission from Liberton, M., Page, L. E., O'Dell, W. M. B., O'Neill, H., Mamontov, E., Urban, V. S., and Pakrasi, H. B. submitted to the *Journal of Biological Chemistry* in 2012. The first three authors contributed equally to the work. M. Liberton performed the electron microscopy contained therein with the help of Howard Berg at the Donald Danforth Plant Science Center. Liberton, Page, O'Dell, O'Neill, and Urban performed the neutron scattering and data analysis. Mamontov performed the quasi-elastic neutron scattering and data analysis. This work was supported as part of the Photosynthetic Antenna Research Center (PARC), an Energy Frontier Research Center funded by the U.S. Department of Energy, Office of Science, Office of Basic Energy Sciences under Award Number DE-SC 0001035. The Bio-SANS instrument used in these studies is a resource of the Center for Structural Molecular Biology at Oak Ridge National Laboratory that is supported by the U.S. Department of Energy, Office of Science, Office of Biological and Environmental Research Project ERKP291. Bio-SANS is located at the Oak Ridge National Laboratory's High Flux Isotope Reactor and the BaSiS instrument is located at the Spallation Neutron Source. Both

neutron sources are sponsored by the Scientific User Facilities Division, Office of Basic Energy Sciences, U.S. Department of Energy.

Chapter 4 is reproduced in part with permission from Page, L. E., Liberton, M., and Pakrasi, H. B. submitted to the *Journal of Applied and Environmental Microbiology*. The work was performed at Washington University as part of the Photosynthetic Antenna Research Center, an Energy Frontier Research Center funded by the U.S. Department of Energy, Office of Science, Office of Basic Energy Sciences under Award Number DE-SC 0001035.

Appendix 1 was reproduced in part with permission from the American Chemical Society. This was written as a book chapter arising from a conference on carbon capture and sequestration. The authors gratefully acknowledge the support of the Sponsors of GCEP, ExxonMobil, GE, Toyota, and Schlumberger, and of the International Center for Advanced Renewable Energy and Sustainability at Washington University (I-CARES) that made this workshop and report possible. We would also like to thank Gayle Geren, Suzanne Loui, and Marylin Roberts, for ensuring the smooth running of the workshop at Washington University in St. Louis. We also thank staff at GCEP, especially Emilie Hung for her helpful comments on this review, Clare Swan for web support and Girley Tegama for additional administrative support for the workshop. Lastly, we would like to express our sincere gratitude to all the speakers and participants in the workshop for sharing their knowledge and expertise that made the workshop a success and for their valued efforts in helping bring this review together. Distinguished speakers we thank are: Richard Axelbaum, Washington University in St. Louis; Bob Blankenship, Washington University in St. Louis; Yusuf Chisti, Massey University, New Zealand; Maria Ghirardi, National Renewable Energy Laboratory; Ben Hankamer, The University of Queensland, Australia; Marcel Janssen, Wageningen University, Netherlands; Nir

Keren, Hebrew University, Israel; Olaf Kruse, University of Bielefeld Center for Biotechnology, Germany; Pete Lammers, New Mexico State University and Solix Biofuels; Steve Mayfield, The Scripps Research Institute; Ladislav (Lada) Nedbal, Institute of Systems Biology and Ecology, Academy of Sciences for the Czech Republic; Don Ort, University of Illinois, Urbana-Champaign; John Raven, University of Dundee, UK; Adel Sarofim, University of Utah; Richard Sayre, Donald Danforth Plant Science Center; Lou Sherman, Purdue University; Alison Smith, University of Cambridge, UK; and Martin Spalding, Iowa State University.

Appendix 2 was reproduced in part with permission from an article submitted to the *Journal of Biomedicine and Biotechnology* written by X. Feng, L. Page, J. Rubens, L. Chircus, P. Colletti, H. B. Pakrasi, and Y. J. Tang. This study was supported in part by an NSF Career Grant (MCB0954016) to Y. J. Tang and in part by a DOE Bioenergy Research Grant (DEFG0208ER64694) to HBP. The authors are grateful to all of the students (Bing Wu, Arul Varman, Yin Wang, Stephanie Suen, Craig Jacobson, and Wenying Liu) in the 2010 Metabolic Engineering class (ChE596) at Washington University for their useful input during class discussions.

Appendix 3 was reproduced in part with permission from an article submitted to the *Journal of Microbiology* written by X. Feng, A. Bandyopadhyay, B. Berla, L. Page,
B. Wu, H. B. Pakrasi, and Y. J. Tang. This study was supported in part by a U. S. Department of Energy (DOE) bioenergy research grant (DEFG0208ER64694) and in part by a grant from the National Science Foundation (MCB0954016). The authors are also grateful to Jing Jiang, Jeff Cameron and Dr. Jana Stöckel for their kind help with measurements and discussion.

Appendix 4 was reproduced in part with permission from an article submitted to the *Journal of Bacteriology* written by W. M. Sattley, M. T. Madigan, W. D. Swingley, P. C.

Cheung, K. M. Clocksin, A. L. Conrad, L. C. Dejesa, B. M. Honchak, D. O. Jung, L. E. Karbach, A. Kurdoglu, S. Lahiri,1 S. D. Mastrian, L. E. Page, H. L. Taylor, Z. T. Wang, J. Raymond, M. Chen, R. E. Blankenship, and J. W. Touchman. This work was supported by the U.S. National Science Foundation Phototrophic Prokaryotes Sequencing Project (grant 0412824). W.D.S. was funded by a Japanese Society for Promotion of Science Postdoctoral Fellowship for Foreign Researchers (grant P07141). M.C. was funded by Australian Research Council Discovery Project grant DP0665169. Partial support for the participation of P.C.C. and L.E.K. in this research was provided by a grant to Washington University from the Howard Hughes Medical Institute through the Undergraduate Biological Sciences Education Program. D.O.J. was partially supported by National Science Foundation grant MCB0237567. We thank Aaron Collins for helpful discussions and assistance with graphics

Appendix 5 was reproduced in part with permission from an article written in the *Proceedings of the National Academy of the Sciences, U. S. A.* written by W. D. Swingley, M. Chen, P. C. Cheung, A. L. Conrad, L. C. Dejesa, J. Hao, B. M. Honchak, L. E. Karbach, A. Kurdoglu, S. Lahiri, S. D. Mastrian, H. Miyashita, L. Page, P. Ramakrishna, S. Satoh, W. M. Sattley, Y. Shimada, H. L. Taylor, T. Tomo, T. Tsuchiya, Z. T. Wang, J. Raymond, M. Mimuro, R. E. Blankenship, and J. W. Touchman. The authors thank Paul Stothard for assistance with the generation of the circular genome and plasmid maps, Brendon Hill at 454 Life Sciences for coordination of 454 sequencing, and Jonathan Eisen for helpful discussions. This work was supported by the U.S. National Science Foundation Phototrophic Prokaryotes Sequencing Project Grant 0412824 and by a Grant-in-Aid for Creative Scientific Research (no. 17GS0314) from the Japanese Society for Promotion of Science. W.D.S. is funded by the Japanese Society for Promotion of Science Postdoctoral Fellowship for Foreign Researchers (no. P07141). M.C. is

funded by an Australian Research Council Discovery Project (DP0665169). Partial support for the participation of P.C.C. and L.E.K. in this research was provided by a grant to Washington University from the Howard Hughes Medical Institute through the Undergraduate Biological Sciences Education Program.

My specific contributions to each chapter follow here. I wrote and conducted all experiments contained in chapters 1, 2, 4 and 5. For chapter 3, I was part of a research team (including M. Liberton, W. M. B. O' Dell, H. O'Neill, and V. Urban) that conducted the small angle neutron scattering experiments. I was also responsible for approximately half of the data analysis carried to convert the data to publication ready form. I assisted in the writing and editing of the submitted manuscript, and helped to prepare the figures. For appendix 1, I part of a three person team (with J. Milne and J. Cameron) that prepared the manuscript, and as such, was responsible for one third of the writing. For appendix 2, I was responsible for generating Figure 3 and assisting with writing and editing of the manuscript. For appendix 3, I was responsible for conducting the photosynthetic measurements used to generate Figure 3, and assisting in preparation and editing of the manuscript. For appendices 4 and 5, I was part of a large interdisciplinary team that manually annotated the genomes. I also edited the manuscripts during their preparation.

My dissertation is

dedicated to my family:

Christine, Donna, Lori

and Randy

List of Publications

Feng, X., Bandyopadhyay, A., Berla, B., **Page, L**., Wu, B., Pakrasi, H. B. and Tang, Y. J. 2010. Mixotrophic and photoheterotrophic metabolism in *Cyanothece* sp. ATCC 51142 under continuous light. *Microbiology*. 156:2566-2574.

Feng, X. **Page, L.,** Rubens, J., Chircus, L., Colletti, P., Pakrasi, H.B., and Tang, Y.J. 2010. Bridging the Gap between Fluxomics and Industrial Biotechnology. *Journal of Biomedicine and Biotechnology.* 2010: ID 460717.

Lee, C.B. **Page, L.E**., McClure, B.A., and T.P. Holtsford. 2008. Post-pollination hybridization barriers in *Nicotiana* Section *Alatae. Sexual Plant Reproduction.* 21:183-191.

Liberton, M., **Page, L. E.**, O'Dell, W. M. B., O'Neill, H., Mamontov, E., Urban, V. S., and Pakrasi, H. B. 2012. Organization and Flexibility of Cyanobacterial Thylakoid Membranes Examined by Neutron Scattering. *Journal of Biological Chemistry*. Accepted.

Page, L. E., Liberton, M., Sato, H. and Pakrasi, H. B. 2010. Phycobilisome Antenna Deletion in a Cyanobacterium Does Not Improve Photosynthetic Energy Conversion Efficiency or Productivity in a Bench-Scale Photobioreactor System. (*In*) Kuang, T., Lu, C., and Zhang, L (*Eds*.) Photosynthesis research for Food, Fuel, and Future: Proceedings of the 15th International Conference on Photosynthesis, Beijing.

Page, L. E., Liberton, M., and Pakrasi, H. B. 2012. Phycobilisome antenna truncation reduces photoautotrophic productivity in *Synechocystis* sp PCC 6803, a cyanobacterium. *Applied and Environmental Microbiology.* 78, 17:6349.

Sattley, W. M., Madigan, M., Swingley, W. D., Cheung, P. C., Clocksin, K., Conrad, A. L., Dejesa, L., Honchak, B. M., Jung, D., Karbach, L. E., Kurdoglu, A., Lahiri, S., Mastrian, S. D., **Page, L**., Taylor, H. L., Wang, Z. T., Raymond, J., Chen, M., Blankenship, R., and Touchman, J. 2008. The genome of *Heliobacterium modesticaldum*, a phototrophic representative of the Firmicutes containing the simplest photosynthetic apparatus. *Journal of Bacteriology*. 190, 13:4687–4696.

Swingley, W. D., Chen, M., Cheung, P. C., Conrad, A. L., Dejesa, L. C., Hao, J., Honchak, B. M., Karbach, L. E., Kurdoglu, A., Lahiri, S., Mastrian, S. D., Miyashita, H., **Page, L**., Ramakrishna, P., Satoh, S., Sattley, W. M., Shimada, Y., Taylor, H. L., Tomo, T., Tsuchiya, T., Wang, Z. T., Raymond, J., Mimuro, M., Blankenship, R. E., and Touchman, J. 2007. Niche adaptation and genome expansion in the chlorophyll d-producing cyanobacterium *Acaryochloris marina*. *Proceedings of the National Academy of Sciences, USA*. 105, 6:2005-2010**.**

You, L., **Page, L**., Feng, X., Berla, B., Pakrasi, H. B., and Tang, Y. J. 2012. Metabolic pathway confirmation and discovery through 13C-labeling of proteinogenic amino acids. *Journal of Visualized Experiments.* E3583.

Abstract of the Dissertation

Phycobilisomes are the large, membrane extrinsic light harvesting antenna of cyanobacteria. They function to absorb light energy and deliver it efficiently to the photosystems, thereby increasing photosynthetic light absorption. Wild type phycobilisomes in the model organism *Synechocystis* sp. PCC 6803 (*Synechocystis* 6803) consist of a tricylindrical core from which six rods radiate. The colored phycobiliproteins are held together by colorless linker polypeptides.

Several phycobilisome truncation mutants have been generated in *Synechocystis* 6803. The first, CB, has truncated phycobilisome rods; the second, CK, has only the phycobilisome core; and the third, PAL, has no phycobilisomes at all. Together, these mutants construct a series of increasingly truncated phycobilisomes which are useful for studying the physiology of antenna truncation in cyanobacteria.

In this dissertation, the physiological effects of antenna truncation are examined from three perspectives. First, the effect of partial and complete phycobilisome removal on the expression and activity of photosystem II is examined using a variety of assays that center around fluorescence and oxygen evolution. Second, the overall effects of antenna truncation on thylakoid membrane spacing and structure is explored using electron microscopy and small angle neutron scattering. Finally, the effects of antenna truncation on culture-wide biomass productivity are examined in a variety of setting, including a bench-scale photobioreactor. Together, these studies represent a comprehensive examination of the physiological effects of antenna truncation on *Synechocystis* 6803.

Chapter 1

Introduction to Photosynthetic Light Harvesting Antenna Complexes and the Cyanobacterial Phycobilisome

Introduction

The role of cyanobacteria in the evolution of life on earth

There are five distinct phyla of bacteria capable of performing photosynthesis, the process of capturing light energy, storing it, and using it to drive cellular processes (Balows *et al.,* 1992; Blankenship, 2002; Madigan *et al.,* 1997). Four of these are anoxygenic, and thus do not evolve oxygen as a byproduct (Blankenship *et al*., 1995). The fifth phylum, cyanobacteria, makes up the oldest oxygen-evolving organisms. Cyanobacteria are truly ancient: the fossil record indicates they are roughly 3.5 billion years old (Schopf, 1993). They have also played a very significant role in the evolution of life on earth. They are the original terraformers, responsible for fundamentally altering the composition of the earth's atmosphere by generating the oxygen that is present today. This oxygen had profound effects on the evolution of life, as it paved the way for aerobic metabolisms and precipitated iron from the world's oceans.

Early endosymbiosis of a unicellular cyanobacterium is the source of the eukaryotic chloroplast (Mereschowsky, 1905; Martin, W. and Kowallik, 1999). Thus, cyanobacteria are the ancestral origin of the photosynthesis occurring in all eukaryotic organisms, from unicellular green algae to vascular plants. With very few exceptions, it can be said that all life on earth directly or indirectly depends on oxygenic photosynthesis for its survival, through production of oxygen and conversion of carbon dioxide into sugars.

Synechocystis *sp. PCC 6803 as a model organism for the study of photosynthesis*

Because of their remarkable history and their ancestral role in the evolution of "modern" oxygenic photosynthesis, cyanobacteria are critical for basic photosynthetic research.

Synechocystis sp. PCC 6803 (*Synechocystis* 6803) is one of the most important model cyanobacteria. One of the most important driving forces for its adoption as a model organism was the discovery that it is naturally competent for the uptake and incorporation of exogenous DNA into its genome (Grigorieva and Shestakov, 1982; Williams, 1988). Genetic engineering technology based on the transformability of this organism facilitated its wide use for the elucidation of gene function. It was also the first photosynthetic organism to have its genome fully sequenced, which is very important for the understanding of the organism's overall metabolism (Kaneko *et al.,* 1996; Kaneko and Tabata, 1997). *Synechocystis* 6803 is readily cultured in a variety of settings, including on solid media and liquid culture, providing ready access to genetically-stable cellular material (Allen, 1968). It has a short generation time (6-24 hours), allowing for the harvesting of large numbers of cells in a relatively short period of time. It can also be grown photoautotrophically, photomixotrophically, or heterotrophically, the latter allowing for creation of photosynthetic knockout mutants (Rippka, 1979).

Oxygenic photosynthesis

The cellular location of photosynthesis in *Synechocystis* 6803 and all other photosynthetic organisms is the thylakoid membrane, a specialized lipid bilayer. There, four major intrinsic protein complexes and several soluble energy-carrying intermediates work in concert to harvest light energy and convert it into stable chemicals used for cell growth. Two of the major intrinsic protein complexes, Photosystem I and Photosystem II, are capable of absorbing light, which is the main catalyst driving photoautotrophic growth.

The simplest conceptual view of photosynthesis is as a linear electron transport chain (Figure 1), though *in vivo*, the four major protein complexes are not present in equimolar ratios.

Oxygenic photosynthesis begins when light energy reaches the Photosystem II enzyme, creating a charge separation that is used to split water. The resulting excited electrons are then transferred to the second complex, cytochrome b_6f, via plastoquinone carriers. Cytrochrome b_6f translocates protons into the thylakoid lumen and simultaneously transfers electrons from plastoquinone to plastocyanin. The third complex, Photosystem I, then accepts the electrons from plastocyanin, and with the help of additional light energy, reduces ferredoxin. This ferredoxin is converted into the important cellular energy carrier NADPH. The luminal protons generated in this process build up a gradient that the final major protein complex, ATP synthase, uses to turn ADP into ATP. ATP and NADPH are used as the driving force for cellular growth in a wide variety of downstream processes.

Light harvesting antenna complexes

As mentioned above, only two enzymes in the photosynthetic electron transport chain, PSI and PSII, are capable of absorbing light. In all known chlorophyll-based photosynthetic organisms, pigment-protein antenna complexes exist that aid in the light absorption process (Green and Parson, 2002). The primary function of light harvesting antenna complexes is to greatly increase the efficiency of photosynthesis by absorbing additional light and transferring the energy to reaction centers. This is necessary in photosynthetic organisms because, in most situations, light energy is a relatively dilute energy source compared to the size of a single chlorophyll molecule. Even at full sunlight, only ten photons per second on average would strike a given chlorophyll molecule (Blankenship, 2002). The photosystems can catalyze orders of magnitude more reactions per second, so without the presence of antenna complexes, a great deal of catalytic capacity would be wasted.

It is important to note that antenna systems do not perform photochemistry themselves. Rather, they collect light via excited electronic states, and through a series pigment-pigment transfers, efficiently deliver this energy to the reactions centers where catalysis occurs. For efficient energy transfer to occur, these pigments must be arranged in highly organized conformations. As a result, in almost all cases (the chlorosome being the only known counterexample), the pigments are bound to proteins that coordinate the arrangement of the pigments in the complex (Blankenship, 2002, Frigaard *et al.* 2001).

The resulting antenna structures are highly ordered, and arranged so that the pigments within are very densely packed in conformations that optimize energy transfer. Energy transfer within antenna systems is not totally random, however, as in addition to trapping light energy, antenna systems have evolved to funnel the trapped energy towards the reaction centers. Energetic funneling is accomplished generally by locating the pigments that absorb higher energy, lower wavelength light towards the periphery of the antenna complex, while lower energy, high wavelength absorption pigments are located progressively closer to the reaction centers. As a result, antenna complexes can not only trap light energy efficiently, but also deliver that energy to the reaction centers with minimal loss.

Though all antenna systems show functional conservation, their wide structural variation indicates that they are likely an example of convergent evolution. Thus, antenna complexes are advantageous to photosynthetic organisms competing for light energy in the wild. It is also likely that they are multiple answers to the same basic problem: how to most efficiently collect light of varying quality (wavelength) and quantity (intensity) (Sidler, 1994).

The phycobilisome of cyanobacteria

Some of the most well-studied antenna complexes are the phycobilisomes (PBSs) of cyanobacteria. The most common PBSs are hemi-discoidal pigment-protein complexes that sit on the cytoplasmic face of the thylakoid membrane. PBSs absorb in the spectral gap of the chlorophyll (CHL) in the photosystems (500-660 nm), allowing cyanobacteria to absorb light in the entire visible spectrum (Adir, 2005; Ajlani, 1995). In addition, PBSs deliver absorbed light with an energy transfer efficiency of >90%, primarily to PSII (Glazer, 1989; Grabowski and Gantt, 1978; MacColl, 1998; Searle *et al.,* 1978). The PBS can functionally link more than 600 energy absorbing pigments to a single PSII dimer (Glazer, 1989). There is also evidence for PBS energy transfer to PSI, both *in vitro* and *in vivo*, but whether this is a specific interaction or a transient phenomenon is still unclear (Aspinwall *et al.,* 2004; Kirilovsky and Ohad 1986; Rakhimberdieva *et al.,* 2001).

PBS structural analysis began after their initial description and subsequent biochemical isolation (Gantt and Conti, 1965; Gantt and Conti 1966; Gantt and Conti 1969; Gantt and Lipschultz, 1972; Gray and Gantt, 1975). In PBSs, there are two main classes of protein: the phycobiliproteins (PBPs) that coordinate the pigments and make up about 85% of the mass of a PBS, and the linker proteins that are colorless and make up about 15% of the mass of a PBS (Tandeau de Marsac and Cohen-Bazire, 1977). The pigments, known as phycobilins (PBs), are covalently bound to the PBPs through cystein residues, and are open chain linear tetrapyrroles whose biosynthetic precursors are biliverdins (Beale, 1994).

In all PBSs, there are two main substructures: the core and the rods. The core sits closest to the membrane surface and interacts directly with the photosystems. The rods radiate out from

the core, and do not interact with the membrane directly. Several linker proteins hold the PBS together: the rod-rod linker (L_R) connects PC rod hexamers together, the core-rod linker (L_{CR}) connects the PC rod hexamers to the APC hexamer core, the core-core (L_C) linker connects the APC hexamers to each other, and the core-membrane linker (L_{CM}) connects the PBS core to PSII and (possibly PSI) on the thylakoid membrane.

There are two fundamental PBPs, α and β, that make up the most basic building block of the PBS, and are present in 1:1 stoichiometry (Sidler, 1994) (Figure 2). The α and β subunits differ in molecular mass and the number of PBs they coordinate. These two subunits form a heterodimer (αβ) that forms a toroidal 3-part aggregate $(\alpha\beta)_3$. There is a different PBPαβ for each type of pigment comprising a complete phycobilisome. The naming convention is to use the superscript abbreviation for the PBP that comprises a given subunit. For example, $\alpha^{PC}\beta^{PC}$ designate the αβ dimer of PC.

The number of PBP types found in a PBS varies by cyanobacterial strain. Each PBP is differentiated by the wavelength of maximum absorption (λ_{max}). The PBS core is made up primarily of ($\alpha^{APC}\beta^{APC}$) trimers, with λ_{max}=652 nm. In the rods, there are up to three different PBPs, depending on the cyanobacterium. Located closest to the core is an ($\alpha^{PC}\beta^{PC}$) hexamer, λ_{max}=620 nm, which is found in all PBS rods. Further from the core, phycoerythrin (PE), λ_{max}=560 nm or phycoerythrocyanin (PEC), λ_{max}=575 nm are sometimes found. Typically, $\alpha^{PE}\beta^{PE}$ and $\alpha^{PEC}\beta^{PEC}$ are found in the rods of cyanobacterial strains that undergo chromatic adaptation, and neither PE or PEC are found in *Synechocystis* 6803 (Ajlani *et al.,* 1995; Bryant, 1982). Importantly, the arrangement of the PBPs in PBSs are from the shortest wavelengths at the rod ends to the longest wavelengths at the PBS core, which allows for efficient energy funneling, as mentioned above.

Phycobilisome structure in Synechocystis *6803*

In seeking to define the PBS structure in a transformation-competent cyanobacterium, a random mutagenesis screen in *Synechocystis* 6803 for mutants with altered pigments and PBS content was conducted using the chemical p-hydroxymercuribenzoate (PMB) (Elmorjani *et al.,* 1986). PMB was used because it is effective in enriching for a population of mutants defective in their photosynthetic capacity (Astier *et al.,* 1984). The 1986 study by Elmorjani was very important for understanding *Synechocystis* 6803 PBSs for three main reasons. First, it led to the successful isolation of two PC-less mutants, PMB10 and PMB11, which could be used to purify pure PBS cores. Second, these mutants led to the identification of the linker polypeptides by location within the PBS and by molecular weight. Finally, it allowed for the determination of the basic PBS structure of *Synechocystis* 6803: a three-cylinder core (of four $(\alpha^{APC}\beta^{APC})_3$ each) from which six rods (of three $(\alpha^{PC}\beta^{PC})_6$ each) radiate.

Building on this knowledge, several partial and complete PBS mutants were generated using targeted mutagenesis. Starting with the PMB11 mutant, a PBS-deficient mutant was generated by knockout of *apcE* (encoding L_{CM}) and *apcAB* (encoding $\alpha^{APC}\beta^{APC}$) (Ajlani and Vernotte, 1998; Capuano, *et al.,* 1991; Capuano *et al.,* 1993). Therefore, PAL is a PBP-less mutant with intact photosystems (Ajlani and Vernotte, 1998). Upon characterization, Ajlani and Vernotte found that PAL grew much more slowly than the WT strain and had an increased PSII:PSI ratio.

In addition to a complete PBS knockout mutant, two intermediate antenna mutants have also been generated by targeted mutagenesis. The first, CB was generated by knockout of *cpcC1* and *cpcC2* (which encode the proximal and distal L_R proteins). Because

both of the genes encoding the L_R proteins were knocked out, the CB mutant can construct a complete PBS core, but can only coordinate one PC hexamer per rod, held to the core by the still-present L_{CR} (Ughy and Ajlani, 2004). The CB mutant and several others from the same study were primarily used to show that transcriptional regulation of the L_R genes is what adjusts the rod length, and thus the light harvesting capacity of the PBS.

The second partial antenna knockout, CK, was generated by knockout of *cpcA* and *cpcB* (which encode the $\alpha^{PC}\beta^{PC}$ subunits), as well as *cpcC1* and *cpcC2*. As a result, CK has no PBS rods but retains the intact PBS core (Thomas *et al.,* 2006). CK has been used to determine the site of Ferredoxin:NADP oxidoreductase binding, the role of the PBS in state transitions, and the structural organization of PBSs via single particle analysis (Arteni *et al.,* 2009, Stadnichuk *et al.,* 2009, and Thomas *et al.,* 2006).

Together, wild type (WT), PMB10, PMB11, CB, CK, and PAL have been used in a series of studies that were crucial for the elucidation of PBS structure in *Synechocystis* 6803. Additionally, WT, CB, CK, and PAL represent a series of antenna mutants with increasingly truncated PBSs (Figure 2). These three mutants have proven to be extremely valuable for testing another hypothesis, as well: whether PBS antenna truncation can be used to increase photoautotrophic productivity.

Antenna mutants and photoautotrophic productivity

The antenna that evolved in photosynthetic organisms is relatively large, and efficient at harvesting light at low intensities. In a photosynthetic microbe's native habitat, this provides a competitive advantage even if the harvested light is not used for photochemistry. This is because harvesting any available light prevents a nearby

competing photosynthetic organism from using that light for its own photochemistry (Ort *et al.,* 2011). Therefore, a strain with a large antenna system that is efficient at harvesting light would be expected to evolve as the optimal antenna setup. This has been shown to be the case in many strains of photosynthetic microbe, from eukaryotic green algae to cyanobacteria. Most photoautotrophic microbes possess antenna that saturate at one quarter of the intensity of full sunlight (Melis 2009).

In biotechnological settings, where the goal is to maximize culture-wide productivity, these large antenna pose a potential problem. An antenna that saturates at one quarter of full sunlight intensity means that the excess light must be dissipated by nonphotochemical means. This is wasteful in microbial monoculture for two reasons: first, the organisms at the surface of incident light are quickly light saturated, and must dissipate the excess without performing photochemistry. Second, in dense cultures, organisms at the surface of the incident light shade the organisms below. Therefore, it is possible that optimization of light harvesting antenna size may maximize areal monoculture productivity.

In green algae, decreasing antenna size has been shown *in silico* and *in situ* to increase photosynthetic production efficiency. Modeling efforts on the *tla1* strain of *Chlamydomonas reinhardtii* indicate an increase in light-driven hydrogen production over the wild-type strain by as much as 300% is possible (Melis, 2009). A different *Chlamydomonas reinhardtii* mutant, the antenna mutant *stm6Glc4T7* was found to be similarly more efficient at light harvesting, and productivity increases in terms of hydrogen production and biomass accumulation were observed, though increases were not compared to the WT strain directly (Beckmann *et al*., 2009). In terms of pure

photoautotrophic biomass productivity, partial antenna reduction by RNA interference was determined to be optimal (Perrine *et al.,* 2012).

These productivity advantages are significant, and may drastically reduce the market price of commodities produced from green algal biomass. Importantly, this effect has only been demonstrated in eukaryotic green algae. There, the light harvesting complex II (LHCII) antenna is a membrane intrinsic protein complex composed pigmented primarily by chlorophyll (Melis, 1996). The physiological effects and changes in photoautotrophic productivity of light harvesting antenna truncation mutants have yet to be explored in cyanobacteria.

This Work

In this study, an analysis of the physiological effects of antenna modification on cyanobacterial physiology at the photosystem level (Chapter 2), membrane level (Chapter 3), and whole-culture level (Chapter 4) are presented. The model organism *Synechocystis* 6803 was used because of the detailed phycobilisome structural information that exists. In all three cases, WT and the previously-generated CB, CK, and PAL are tested to determine whether a partial (CB and CK) or complete (PAL) antenna truncation mutant may provide an advantage over WT.

In Chapter 2, a detailed analysis is presented of changes to the antenna mutants at the photosystem level. First, western blots are used to examine PSI and PSII titers. Then, the physiological effects of the observed changes in photosystem titer are examined, including an examination of light saturated PSII-mediated oxygen evolution in whole cells, flash-induced PSII turnover on a Joliot-type electrode, and flash-induced changes in fluorescence. Together, these data show that PSII is increasingly upregulated and impared in S-state turnover as a result of

increasingly truncated antenna. This is likely a physiological adaptation to the decreased absorption and delivery of excited states to the PSII reaction center.

Chapter 3 addresses the changes that occur with antenna truncation at the thylakoid membrane level. Electron microscopy was used to examine changes in thylakoid membrane curvature and spacing in fixed cells. These images provided the basis for assignment of peak distances correlating to membrane spacing *in vivo* using Small Angle Neutron Scattering (SANS). Due to the non-invasive nature of SANS, it was possible to measure dynamic changes in membrane spacing. Time-resolved membrane rearrangement due to exposure to light and dark was examined, as was the effect of the PSII inhibitor 3-(3,4-dichlorophenyl)-1,1-dimethylurea (DCMU) on membrane rearrangement. This study demonstrates the important structural role that phycobilisomes play in setting proper thylakoid membrane curvature and spacing.

In chapter 4, the effects of antenna truncation on whole-culture growth rates and biomass productivity are presented. This study represents a direct test of whether antenna truncation in cyanobacteria is an effective technique for boosting photoautotrophic productivity. The antenna mutants are presented in a variety of settings, from shake flasks in an ambient air environment and low light to an optimized bench-scale photobioreactor at high light and elevated carbon dioxide. In all cases, the detrimental physiological changes discussed above lead to a decrease in photoautotrophic productivity in the antenna mutants.

Taken together, the body chapters of this thesis represent a comprehensive story of the myriad of changes that occur when PBS antenna systems are truncated or removed. The physiological effects of PBS antenna truncation and removal are significant, and cause global changes in PSII expression and thylakoid membrane organization that are too detrimental to

boost photoautotrophic productivity.

References

Adir, N. (2005) Elucidation of the molecular structures of components of the phycobilisome: reconstructing a giant. *Photosynth. Res.* 85: 15-32

Ajlani, G. and Vernotte, C. (1998) Construction and characterization of a phycobiliprotein-less mutant of *Synechocystis* sp. PCC 6803. *Plant Mol. Biol.* 37:577-580

Ajlani, G., Vernotte, C., Di Magno, L., and Haselkorn, R. (1995) Phycobilisome core mutants of *Synechocystis* PCC 6803. *Biochim. Biophys. Acta.* 1231: 189-196

Allen, M. M. (1968) Simple conditions for the growth of unicellular blue-green algae on plates. *J. Phycol*. 4:1– 4

Arteni, A. A., Ajlani, G., and Boekema, E. J. (2009) Structural organization of the phycobilisomes from *Synechocystis* sp. Strain PCC6803 and their interaction with the membrane. *Biochim. Biophys. Acta.* 1787:272-279

Aspinwall, C. L., Sarcina, M. and Mullineaux, C. W. (2004) Phycobilisome mobility in the cyanobacterium *Synechococcus* sp. PCC7942 is influenced by the trimerisation of Photosystem I. *Photosynth. Res*. 79: 179–187

Astier, C., Elmorjani, K., Meyer, I., Joset, F., and Herdman, M. (1984) Photosynthetic mutants of the cyanobacteria *Synechocystis* sp. strain PCC 6714 and PCC 6803: sodium p-hydroxymercuri-benzoate as selective agent. *J. Bact.* 158:659-664

Balows, A., Trüper, H. G., Dworkin, M., Harder, W., and Schliefer, K.-H. (eds.) (1992) *The Prokaryotes*. Spriner-Verlag, Berlin

Beale, S. I. (1994) Biosynthesis of Cyanobacterial Tetrapyrrole Pigments Hemes, Chlorophylls, and Phycobilins. p 519-558. *In* Bryant, D. A. (ed), The molecular biology of cyanobacteria. Kluwer Academic Publishers, Dordrecht, The Netherlands

Beckmann, J., F. Lehr, G. Finazzi, B. Hankamer, C. Posten, L. Wobbe, O. Kruse. (2009) Improvement of light to biomass conversion by deregulation of light harvesting protein translation in *Chlamydomonas Reinhardtii*. *J. Biotechnol.* 14: 70-77

Bernát, G., Waschewski, N., and Rögner, M. (2009) Towards efficient hydrogen production: the impact of antenna size and external factors on electron transport dynamics in *Synechocystis* PCC 6803. *Photosynth. Res.* 99:205-216

Blankenship, R. E., Madigan, M. T., and Bauer, C. E. (eds) (1995) *Anoxygenic Photosynthetic Bacteria*. Kluwer Academic Press, Dordrecht

Blankenship, R. E. (2002) *Molecular Mechanisms of Photosynthesis*. Blackwell Science, Oxford, UK.

Bryant, D. A. (1982) Phycoerythrocyanin and phycoerythrin: properties and occurrence in Cyanobacteria. *J. Gen. Microbiol.* 128: 835-844

Capuano, V., Braux, A.-S., Tandeau de Marsac, N., and Houmard, J. (1991) The "Anchor Polypeptide" of Cyanobacterial Phycobilisomes. Molecular characterization of the *Synechococcus* sp. PCC 6301 apce gene. *J. Biol. Chem.* 266, 11:7239-47

Capuano, V., J-C. Thomas, N. Tandeau de Marsac, N., and Houmard, J. (1993) An *in vivo* approach to define the role of the LCM , the key polypeptide of cyanobacterial phycobilisome. *J. Biol. Chem*. 268: 8277–8283

Elmorjani, K., Thomas, J.-C., and Sebban, P. (1986) Phycobilisomes of wild-type and pigment mutants of the cyanobacterium *Synechocystis* sp. PCC 6803. *Arch. Microbiol.* 146: 186-191

Frigaard, N.-U., Vassilieva, E. V., Li, H., Milks, K.J., Zhao, J. and Bryant, D.A. (2001) The remarkable chlorosome. In: PS2001 Proceedings of the 12th International Congress on Photosynthesis, Vol. S1. CSIRO Publishing, Melbourne, Brisbane, Australia

Gantt, E., and Conti, S. F. (1965) The ultrastructure of *Porphyridium cruentum. J. Cell Biol.* 26: 365-81

Gantt, E. and Conti, S. F. (1966) Granules associated with the chloroplast lamellae of *Porphyridium cruentum. J. Cell Biol.* 29: 423-434.

Gantt, E. and Conti, S. F. (1969) Ultrastructure of blue-green algae. *J. Bacteriol.* 97: 1486-1493.

Gantt, E. and Lipschultz, C. A. (1972) Phycobilisomes of *porphyridium cruentum*; isolation. *J. Cell Biol.* 54: 313-324

Glazer, A. N. (1989) Light Guides. Directional energy transfer in a photosynthetic antenna. *J. Biol. Chem.* 264: 1-4

Grabowski, J. and Gantt, E. (1978) Excitation energy migration in phycobilisomes: comparison of experimental results and theoretical predictions. *Photochem. Photobio1*. 28: 47-54

Gray, B. H. and Gantt, E. (1975) Spectral properties of phycobilisomes and phycobiliproteins from the blue-green alga *Nostoc* sp. *Photochem. Photobiol.* 21: 121-128

Green, B. R. and Parson, W. W. (2003) (Eds) *Light-Harvesting Antennas in Photosynthesis.* Kluwer Academic Press, Dordrecht, The Netherlands

Grigorieva, G., and Shestakov, S. (1982) Transformation in the cyanobacterium *Synechocystis* sp. PCC 6803. *FEMS Microbiol. Lett*. 13(4): 367–370

Kaneko, T., and Tabata, S. (1997) Complete Genome Structure of the Unicellular Cyanobacterium *Synechocystis* sp. PCC 6803. *Plant Cell Physiol.* 38, 11: 1171-1176

Kaneko, T., Sato, S., Kotani, H., Tanaka, A., Asamizu, E., Nakamura, Y., Miyajima, N., Hirosawa, M., Sugiura, M., Sasamoto, S., Kimura, T., Hosouchi, T., Matsuno, A., Muraki, A., Nakazaki, N., Naruo, K., Okumura, S., Shimpo, S., Takeuchi, C., Wada, T., Watanabe, A., Yamada, M., Yasuda, M., and Tabata, S. (1996) Sequence Analysis of the Genome of the Unicellular Cyanobacterium *Synechocystis* sp. Strain PCC 6803. II. Sequence Determination of the Entire Genome and Assignment of Potential Protein-coding Regions. *DNA Res.* 3: 109-136

Kirilovsky, D. and Ohad, I. (1986) Functional assembly *in vitro* of phycobilisomes with isolated Photosystem II particles of eukaryotic chloroplasts. *J. Biol. Chem.* 261: 12317–12323

MacColl, R. (1998) Cyanobacterial phycobilisomes. *J. Struct. Biol*. 124: 311–34

Madigan, M. Martinko, J. M., and Parker, J. (1997) *Brock Biology of Microorganisms*. Prentice-Hall, Upper Saddle River, NJ

Martin, W. and Kowallik, K. V. (1999) Annotated English translation of Mereschkowsky's 1905 paper 'Über Natur und Ursprung der Chromatophoren im Pflanzenreiche.' *Eur. J. Phycol.* 34:287-295

Melis, A. (1996) Excitation energy transfer: functional and dynamic aspects of *Lhc (cab)* proteins. In: Ort, D., and Yokum, C [eds]. Oxygenic Photosynthesis: the light reactions. Kluwer, Dordrecht, pp 523-538.

Melis, A. (2009) Solar energy conversion efficiencies in photosynthesis: Minimizing the chlorophyll antennae to maximize efficiency. *Plant Science*. 177:272-280

Mereschkowsky, C. (1905) Über Natur und Ursprung der Chromatophoren im Pflanzenreiche. *Biol. Centralbl.* 25:593-604

Ort, D., Zhu, X., and Melis, A. (2011) Optimizing Antenna Size to Maximize Photosynthetic Efficiency. *Plant Physiol.* 155:79-85

Perrine, Z., Negi, S., and Sayre, R. T. (2012) Optimization of photosynthetic light energy utilization by microalgae. *Algal Res.* 1, 2: 134-142

Rakhimberdieva, M. G., Boichenko, V. A., Karapetyan, N. V. and Stadnichuk, I. N. (2001) Interaction of phycobilisomes with Photosystem II dimers and photosystem I monomers and trimers in the cyanobacterium *Spirulina platensis*. *Biochemistry* 40: 15780–15788

Rippka, R., Deruelles, J., Waterbury, J. B., Herdman, M., Stanier, R. Y. (1979) Generic assignments, strain histories and properties of pure cultures of cyanobacteria. *J. Gen. Microbiol.* 111:1- 61

Schopf, J. W. (1993) Microfossils of the early archean apex chert – new evidence of the antiquity of life. *Science.* 260: 640–646

Searle, G. F. W., Barber, J., Porter, G., and Tredwell, C. J. (1978) Picosecond time-resolved energy transfer in *Porphyridium cruentum.* II. In the isolated light harvesting complex (phycobilisomes). *Biochim. Biophys. Acta.* 501: 246-256

Sidler W.A., (1994) Phycobilisome and phycobiliprotein structures, p 139 –216. *In* Bryant, D. A. (ed), The molecular biology of cyanobacteria. Kluwer Academic Publishers, Dordrecht, The Netherlands

Stadnichuk, I. N., Lukashev, E. P., and Elanskaya, I. V. (2009) Fluorescence changes accompanying short-term light adaptations in photosystem I and photosystem II of the cyanobacterium *Synechocystis* sp. PCC 6803 and phycobiliprotein-impaired mutants: State 1/State 2 transitions and carotenoid-induced quenching of phycobilisomes. *Photosynth. Res*. 99: 227-241

Tandeau de Marsac N. and Cohen-Bazire, G. (1977) Molecular composition of cyanobacterial phycobilisomes. *Proc. Natl. Acad. Sci.* 74:1635-1639

Thomas, J. C., B. Ughy, B. Lagoutte, and G. Ajlani. (2006) A second isoform of the ferredoxin:NADP oxidoreductase generated by an in-frame initiation of translation. *PNAS*. 103, 48:18368-18373

Ughy B., and Ajlani, G. (2004) Phycobilisome rod mutants in *Synechocystis* sp. PCC 6803. *Microbiol.* 150:4147-4156

Williams, J. G. K. (1988) Construction of specific mutations in photosystem II photosynthetic reaction center by genetic engineering method in *Synechocystis* 6803. *Methods Enzymol.* 167: 766–778

Figure 1. The photosynthetic electron transport chain. The four major protein complexes participating in oxygenic photosynthesis are shown in solid grey. Thick arrows indicate electron movement and thin arrows indicate proton movement. Photosystem II, PSII; cytochrome *b6f*, CYT; photosystem I, PSI; ATP Synthase, ATP Syn; plastocyanin, P; Ferredoxin, FD; ferredoxin-$NADP^+$ reductase, FNR

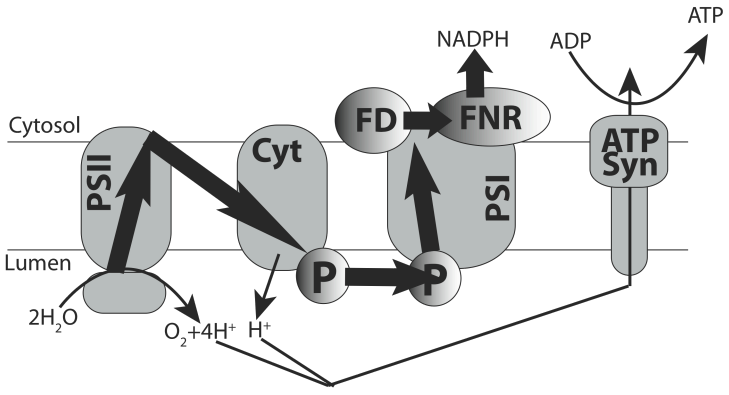
ATP
NADPH
ADP
FD
FNR
Cytosol
Cyt
PSII
PSI
ATP
Syn
Lumen
P
P
2H2O
O2+4H+
H+

Figure 2. Basic building blocks of a phycobilisome. Top row: the building of a single PBS rod from the basic α^{pc} and β^{pc} PBPs to a complete rod. Middle row: the building of the PBS core from the basic α^{apc} and β^{apc} PBPs up to a complete tri-cylindrical core. Bottom row: the PBS mutations in the strains used in this thesis.

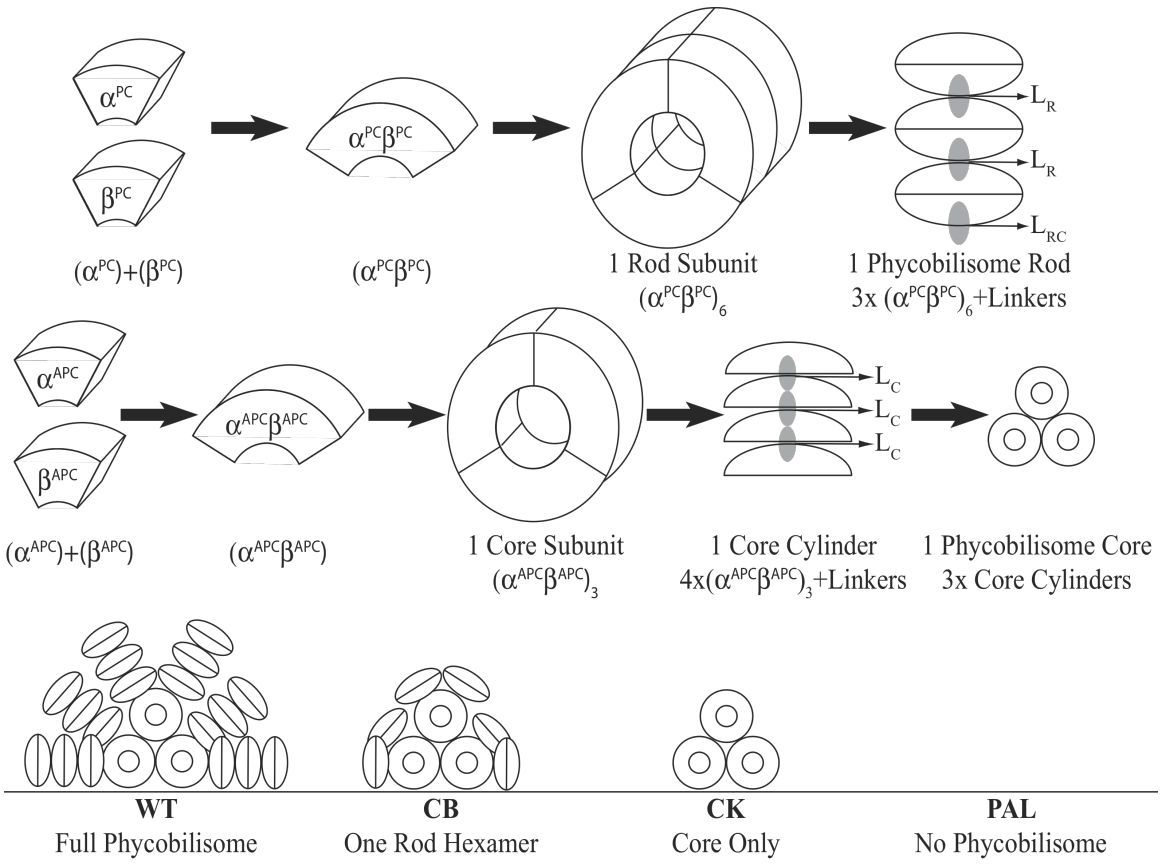
α^{PC}
β^{PC}
$(\alpha^{PC})+(\beta^{PC})$
$\alpha^{PC}\beta^{PC}$
$(\alpha^{PC}\beta^{PC})$
1 Rod Subunit
$(\alpha^{PC}\beta^{PC})_6$
L_R
L_R
L_{RC}
1 Phycobilisome Rod
3x $(\alpha^{PC}\beta^{PC})_6$+Linkers
α^{APC}
β^{APC}
$(\alpha^{APC})+(\beta^{APC})$
$\alpha^{APC}\beta^{APC}$
$(\alpha^{APC}\beta^{APC})$
1 Core Subunit
$(\alpha^{APC}\beta^{APC})_3$
L_C
L_C
L_C
1 Core Cylinder
4x$(\alpha^{APC}\beta^{APC})_3$+Linkers
1 Phycobilisome Core
3x Core Cylinders
WT
Full Phycobilisome
CB
One Rod Hexamer
CK
Core Only
PAL
No Phycobilisome

Chapter 2

Physiological consequences of phycobilisome antenna truncation on expression and function of Photosystem II

Introduction

Cyanobacteria are among the most ancient organisms capable of oxygenic photosynthesis, a process that is driven by two enzymes that are capable of harvesting light to power photochemistry: photosystem I (PSI) and photosystem II (PSII). A large pigment protein complex known as the phycobilisome (PBS) associates with the cyanobacterial thylakoid membrane and greatly increases the absorption and transfer of light energy towards the photosystems (Glazer, 1989). A set of antenna reduction mutants have been generated in the model cyanobacterium *Synechocystis* sp. PCC 6803 (*Synechocystis* 6803) by taking advantage of the fully sequenced genome (Kaneko *et al.,* 1996; Kaneko and Tabata, 1997) and genetic engineering capabilities (Grigorieva and Shestakov, 1982; Williams, 1988) available in this organism. Partial and total PBS reduction mutants harbor a set of mutations that effectively reduce the pigment and protein content by disrupting the structural genes necessary to build a complete WT PBS.

In *Synechocystis* 6803, the PBS is a hemi-discoidal complex made up of a three-cylinder core from which six rods radiate (Elmorjani *et al.,* 1986). The most basic building block of a PBS is a phycobiliprotein (PBP) heterodimer with α and β subunits that coordinate chromophores called phycobilins. Two different PBPs assemble into a toroidal trimer $(\alpha\beta)_3$ in the core cylinders or hexamer $(\alpha\beta)_6$ in the rod cylinders. The core and rod cylinders are held together by colorless linker polypeptides filling the central cavity that are arranged to optimize directional energy transfer towards the thylakoid membrane (Glazer, 1989). The PBS core is composed of three cylinders of 4 trimeric allophycocyanin (APC) disks each, while the six rod cylinders are composed of four hexameric phycocyanin (PC) disks each (Elmorjani *et al.,* 1986).

The genes *cpcC1* and *cpcC2* encode two linker polypeptides that connect the two outer rod hexamers to the rest of the PBS (Ughy and Ajlani, 2004). Therefore, the CB mutant, which is Δ*cpcC1*, Δ*cpcC2,* has only one PC hexamer per rod. The remaining rod hexamer can still be coordinated to the PBS core because the core-rod linker is still present. A complete PBS rod knockout, CK, has also been generated (Thomas *et al.,* 2006). Like CB, CK is also Δ*cpcC1*, Δ*cpcC2,* and it is Δ*cpcA*, Δ*cpcB* as well. The genes *cpcA* and *cpcB* encode the PC PBPs that form the basic structural units of the PBS rod.

A random mutagenesis screen using the chemical p-hydroxymercuribenzoate (PMB), effective at enriching for pigment mutants (Astier *et al.,* 1984), was successful in isolating the PC deficient mutants PMB10 and PMB11 (Elmorjani *et al.,* 1986). The PMB11 background was then used to generate PAL, a Δ*apcE*, Δ*apcAB* mutant (Ajlani and Vernotte, 1998). The *apcE* gene encodes the core-membrane linker (Capuano, *et al.,* 1991; Capuano *et al.,* 1993), and *apcAB* encodes the rod PBPs. As a result, PAL is devoid of PBSs, but retains intact photosystems.

In *Synechocystis* 6803, reduction of the PBS has been found to decrease photoautotrophic productivity in monoculture in a variety of settings (Page *et al.,* 2012). In this paper, we have used the same series of antenna truncation mutants, CB, CK, and PAL, to examine the effects of antenna truncation on PSII function. First, the ratio of PSI to PSII was determined using western blots and low temperature spectroscopy. Then, a Clark-type electrode was used to examine the amount of functional PSII in each strain by determination of steady-state oxygen evolution rates. Then, a flash train was used in conjunction with oxygen evolution and fluorimetry to examine changes in S-state turnover in the antenna mutants. Together, these results indicate that the antenna mutants express increasing levels of functional PSII to compensate for the loss of the

PBS. The increased PSII titer leads to progressively higher oxygen evolution rates, but these mutants also demonstrate difficulty in S-state turnover. Overall, the detrimental physiological changes that occur in light harvesting and delivery to PSII are likely enough to cause the previously observed reduction in photoautotrophic productivity.

Materials and Methods

Strains and Growth Conditions

Stock cyanobacterial strains were maintained on solid BG11 plates (Allen, 1968) with antibiotic selection (CB and CK, 10 μg/ml kanamycin; PAL, 10 μg/ml chloroamphenicol and spectinomycin) at 30^{O}C under constant 30 μmol photons m^{-2} s^{-1} white fluorescent light. Liquid cultures were started from plates in 250 ml Erlenmeyer flasks containing 100 ml BG11 and grown at 30 ºC in 30 μmol photons m^{-2} s^{-1} light on an orbital shaker at 150 rpm with appropriate antibiotics. For use in measurements, strains were sub-cultured at ten percent by volume into fresh 250 ml Erlenmeyer flasks in the same growth conditions, and antibiotics were omitted. The cultures were harvested by centrifugation at 8,250 x g on day 3-5 and normalized to equal chlorophyll (Chl) concentrations. For normalization, Chl concentration was determined by extracting cells in methanol and measuring absorbance at 652 and 665 nm in an Olis DW 2000 spectrophotometer (SLM-Aminco, Urbana, Illinois) (Porra *et al.,* 1989).

Western Blots

Total membranes were prepared as in Norling *et al.,* 1998. Proteins from whole membrane preparations were loaded at 5 μg Chl and separated by molecular weight by SDS-PAGE as described previously (Laemmli, 1970**)** using a resolving gel with 16% acrylamide and 6 M urea. After transfer to 0.22 μm nitrocellulose, CP43 and PsaA/B were detected by using specific antiserum against each protein, and both were reacted with goat-antirabbit horseradish peroxidase conjugated antiserum (Pierce Biotech, Rockford, IL) developed in West Pico (Pierce Biotech, Rockford, IL) for 5 min. Blots were visualized in a Fujifilm LAS-1000plus imager (Fujifilm, Stamford, CT) for 1 to 5 min.

Oxygen Saturation Curves

Photosystem II-mediated oxygen evolution was measured in whole cells on a Clark-Type oxygen electrode (Mannan and Pakrasi, 1993). Briefly, cells were normalized to 5 μg/ml and incubated at 30 ºC and 30 μmol photons m^{-2} s^{-1} light in a water bath. For measurement, 0.5 mM 2.6-di-chloro-p-benzoquinone (Eastman Kodak Co., Rochester, New York) and 1 mM K_3FeCN_6 (Sigma Aldrich, St. Louis, MO) were added to samples, and they were exposed to the measurement light intensity using neutral density filters. Oxygen evolution rate at a given light intensity was measured in triplicate. Curves for calculation of K_m and V_{max} were fitted using Kaleidagraph (Synergy Software, Reading, PA).

Low Temperature Fluorescence

Fluorescence emission spectra were taken at 77K on a Fluoromax-2 fluorometer (Jobin Yvon, Cedex, France). Excitation at 435 nm was used to excite Chl, while excitation at 600 nm was used to excite phycobilisomes (Kashino *et al.,* 2002). Fluorescence emission spectra excited at 435 nm were normalized by $(F-F_{640})/(F_{720}-F_{640})$. Fluorescence emission spectra excited at 600 nm were normalized by F/F_{640}.

Flash-Induced Oxygen Evolution

Oxygen evolution was measured as described previously (Bricker *et al.,* 2001). Cells were normalized to 40 μg CHL per ml. They were then spun at RCF=16,000 x g for 5 min, and applied to the bare platinum electrode (Artisan Scientific Co., Urbana, IL) as a paste. Cells were dark-adapted for two minutes before electrode polarization at 0.65V for ten seconds. A series of

flashes were supplied by an integrated, computer-controlled Xenon flash lamp (20 μs width at ½ height). Twenty flashes were applied at 200 millisecond intervals.

The collected data were processed by distilling out maximum peaks using in-house Oxygen Revolution software. Peak data was fitted to a four-step homogenous model for Mn cluster S-state cycling (Meunier, 1993). Calculations were carried out using MathCad software (MathSoft Engineering and Education, Inc., Cambridge, MA).

Flash-Induced Fluorescence

S-state fluorescence was measured at room temperature using the FL200 dual-modulated kinetic fluorometer (Photon Systems Instruments, Brno, Czech Republic) with FluorWin software (version 3.6.3.3) (Nedbal *et al.,* 1999). Chl concentration was adjusted to 10 μg/ml, and cells were dark-adapted for three minutes before measurement. Spectra were normalized by division to the minimum fluorescence value at each time interval (to correct for baseline drift), and offset on the Y-axis for clarity. Three technical replicates were performed, and one representative trace is shown.

Results

Estimation of Active PSII Expression

Western blots with antibodies to CP43 and PsaA/B were used as indicators for PSII and PSI, respectively (Figure 1). When loaded at equal Chl concentrations, PSII titers in the PBS antenna mutants gradually increased as PBSs are truncated, while the amount of PSI centers generally decreased as antenna are truncated. PSII-mediated oxygen evolution indicates that the active PSII reaction center titer is increasing in the mutants (rather than the PSI titer decreasing), as the antenna mutants evolve progressively more oxygen per Chl at saturation. When fitted to Michaelis-Menten kinetics, V_{max} was found to increase as antenna are truncated.

Low Temperature Fluorescence

When CHL is excited at 435 nm, and traces are normalized to PSI emission (at 720 nm), fluorescence emission spectra again showed evidence of an increase in the PSII:PSI ratio (Figure 2A). The PSII peaks at 685 and 695 nm gradually increase over WT in CB and CK. In PAL, they are significantly higher than any of the other mutants. This same trend has been observed in WT, CK, and PAL before using this method (Stadnichuk *et al.,* 2009).

By exciting PBSs at 600 nm, energy transfer to the photosystems can be tracked (Figure 2B). There, phenotypic differences in the PBSs become apparent, as there is a smaller PC emission signal at 645 nm in CB, and none in CK and PAL. The APC peak at 660 nm is present in WT, CB, and CK, but missing in PAL. Changes in the protein environment around PSII are evident in the two PSII peaks (685 nm and 695 nm). In WT and CB, for instance, the 695 nm peak is higher than at 685 nm. In CK, however, the 685 peak is higher, and in PAL, the two

peaks are approximately equal. These results can be interpreted to mean that proximal PBS rod plays a role in energy transfer to PSII, which will be discussed below.

Determination of S-state turnover

In 1969, Joliot and coworkers measured the oxygen evolution of dark-adapted green algae and isolated spinach chloroplasts under a series of short saturating flashes and discovered that photosynthetic organisms evolve oxygen in a four-step cycle (Joliot, *et al.,* 1969). This led to the proposal of a linear four-step model of charge cooperation that has become the most widely accepted model of S-state advance in the field (Kok *et al.,* 1970). Subsequently, the occurrence of damping in the four-step oscillating system was attributed to double hits and misses, both of which serve to get some PSII reaction centers out of sync with the overall population by one step (Forbush *et al.,* 1971). Backwards transitions were added to this model, improving the accuracy of the model in relation to experimental data (Packham *et al.,* 1988), and the eigenvalue method for calculating the contribution of each of these variables to the damping rates was published (Meunier, 1993).

In this study, series of flash trains were used to evaluate the ability of the antenna truncation mutants to undergo S-state transitions and evolve oxygen. All four strains show the ability to evolve oxygen on the third and fourth flash (Figure 4). The antenna mutants also evolve more oxygen on average than WT, when data is not normalized to average oxygen evolution (data not shown). The damping rate is significantly increased in the antenna mutants, however. CB and CK are significantly more damped than WT, but still show cyclic oxygen evolution out to the twentieth flash. In PAL, damping is extreme, being so severe as to flatten oxygen evolution to the average by the eighth flash.

In fitting the data, the antenna mutants show similar calculated S-state distributions to WT (Table 1). The probability of a single hit occurring decreases as antenna size decreases, with minor differences between WT and CB (4.4%) and CK and PAL (1.3%). A significant (12.3%) jump occurs between CB and CK. Concurrently, misses increase as antenna size decreases, with a similarly large jump seen between CB and CK (10.1%). Therefore, again, WT and CB group together, as do CK and PAL.

Flash fluorescence is another method of observing changes in S-state turnover (Nedbal, *et al.,* 1999). Here again, WT and CB group together, while CK and PAL show a more dramatic phenotype. WT and CB show little difficulty in charge delivery to downstream acceptors, as the valleys between flashes are mostly smooth. In CK and PAL, however, there are sharp disturbances in the return to the base level fluorescence.

Discussion

Western blots (Figure 1), PSII-mediated oxygen evolution (Figure 2), low temperature fluorescence (Figure 3A), and average oxygen evolution rates on the flash electrode (data not shown) all demonstrate the physiological response to decreasing PBS antenna size is to increase PSII expression. PSII-mediated oxygen evolution in Figure 2 shows evidence that the additional PSIIs expressed are active, as the mutants evolve progressively more oxygen at saturation. The increase in PSII expression is expected, as it has been previously reported using a variety of other methods (Ajlani and Vernotte, 1998; Collins *et al.,* 2012; Stadnichuk *et al.,* 2009). The likely explanation is that the PBS primarily delivers excitation energy to PSII (Sidler, 1994).

The reason behind the need to upregulate PSII becomes clear when looking at the flash-induced oxygen and fluorescence data (Figure 4 and Figure 5). During flash-induced oxygen evolution, an increase in damping occurs from the onset of antenna truncation, where CB and CK show a much higher rate of damping than WT. PAL is affected even more significantly, as it only completes two full turnovers of the S-state clock before the oxygen evolution signal is completely damped out (WT completes 5 when the measurement stops). Curve fitting to this data shows that the reason behind this increase in damping is a concurrent decrease in single hits, primarily at the expense of misses (Table 1). When decreasing antenna size, an increase in misses is to be expected, as pigment number per antenna also decreases.

There is an important correlation between the miss rates in the flash-induced oxygen evolution (Table 1) and in the PSII-mediated oxygen evolution (Figure 2). In Figure 2 at the highest light intensity: 8,250 μmol photons*m^{-2}*sec^{-1}, it appears that CK and PAL express very similar amounts of PSII. Likewise, WT and CB group closer to each other than CK and PAL. In Table 1, the single hit rates are similar in this regard, with WT and CB forming a group and CK

and PAL forming a group. The reason for this is presumably the drastic increase in misses that occur between CB and CK.

The fact that CB shows minor deviation from WT, while there is a significant jump between CB and CK in most data, indicates there is a significant change that occurs with the complete removal of PC rods. Flash-induced fluorescence traces (Figure 5) show one phenotypic change. CK and PAL have very inconsistent "valleys" during the dark periods, whereas in WT and CB, the signal mostly decays smoothly.

There are several possible explanations for this significant change between CB and CK. PBSs have been proposed to play a significant role in thylakoid membrane spacing and structure (Olive, *et al.,* 1997). Electron micrographs of WT and the three antenna mutants show a distinct change in thylakoid membrane curvature in CK and PAL that is not seen in WT and CB (Liberton *et al.,* 2012). Another possibility for the distinct change in the transition from CB to CK is that *Synechocystis* 6803 has physiological mechanisms to compensate for removal of some, but not all of its PC. In conditions where nitrogen is limiting, the PBSs are degraded in an organized manner, and the nitrogen in their PBPs is recycled for essential cellular processes (Elmorjani *et al.,* 1987; Yamanaka and Glazer, 1980). The PC to APC ratio decreases from 2.7 at the onset of nutrient limitation to 1.3 after 34 hours, while levels of APC remain relatively constant during this time (Richaud *et al.,* 2001). The final possibility for this significant change between the CB and CK mutants has to do with downstream processes. There is preexisting evidence for this, as well. The proximal rod hexamer has been found to prevent proteolysis in the Ferredoxin-NADP(+) Reductase complex in cyanobacteria (Thomas *et al.,*2006). Therefore, removal of the proximal rod hexamer, but not the two distal rods, would be expected to have a large effect on substrate channeling and the natural physiology of the organism.

The removal of the proximal rod hexamer in the transition from CB to CK has major physiological consequences for *Synechocystis* 6803. The difficulties in S-state turnover increase (Figure 3), the chances of single hits occurring in PSII decrease (Table 1), and the ability to transfer absorbed energy to downstream processes decreases (Figure 5). All of these changes result in a drastic increase in the amount of PSII expressed in CK and PAL, which represents a significant metabolic burden on these cells. Therefore, removal of the proximal PC hexamer causes a drastic physiological change for *Synechocystis* 6803. However, the differences between WT and CB, in this study and others, is much less detrimental to the light harvesting capabilities of the organism (Liberton *et al.,* 2012; Page, *et al.,* 2012). If PBS truncation for improved photoautotrophic productivity is to be pursued, the CB mutant would likely be the best starting point, though further mutation is necessary to re-balance photoautotrophic growth with the decreased antenna size.

References

Ajlani, G. and Vernotte, C. (1998) Construction and characterization of a phycobiliprotein-less mutant of *Synechocystis* sp. PCC 6803. *Plant Mol. Biol.* 37:577-580

Allen, M. M. (1968) Simple conditions for the growth of unicellular blue-green algae on plates. *J. Phycol.* 4:1-4

Astier, C., Elmorjani, K., Meyer, I., Joset, F., and Herdman, M. (1984) Photosynthetic mutants of the cyanobacteria *Synechocystis* sp. strain PCC 6714 and PCC 6803: sodium p-hydroxymercuri-benzoate as selective agent. *J. Bact.* 158:659-664

Bricker, T. M., Lowrance, J., Sutton, H. M., and Frankel, L. K. (2001) Alterations of the oxygen-evolving apparatus in a (448)Arg → (448)S mutant in the CP47 protein of Photosystem II under normal and low chloride conditions. *Biochemistry*. 40: 11483-11489

Capuano, V., Braux, A.-S., Tandeau de Marsac, N., and Houmard, J. (1991) The "Anchor Polypeptide" of Cyanobacterial Phycobilisomes. Molecular characterization of the *Synechococcus* sp. PCC 6301 apce gene. *J. Biol. Chem.* 266, 11:7239-47.

Capuano, V., J-C. Thomas, N. Tandeau de Marsac, N., and Houmard, J. (1993) An *in vivo* approach to define the role of the LCM , the key polypeptide of cyanobacterial phycobilisome. *J. Biol. Chem*. 268: 8277–8283

Collins, A. M., Liberton, M., Jones, H. D. T., Garcia, O. F., Pakrasi, H. B., and Timlin, J. A. (2012) Photosynthetic Pigment Localization and Thylakoid Membrane Morphology Are Altered in *Synechocystis* 6803 Phycobilisome Mutants. *Plant Phys*. 158, 4: 1600-1609

Elmorjani, J. and Herdman, M. (1987) Metaboic control of phycocyanin degradation in the cyanobacterium *Synechocystis* PCC 6803: a glucose effect. *J. Gen. Microbiol.* 133:1685-1694

Elmorjani, K., Thomas, J.-C., and Sebban, P. (1986) Phycobilisomes of wild-type and pigment mutants of the cyanobacterium *Synechocystis* sp. PCC 6803. *Arch. Microbiol.* 146: 186-191

Forbush, B., Kok, B., and McGloin, M. P. (1971) Cooperarion of charges in photosynthetic O2 Evolution-II. Damping of flash yield. *Photochem. Photobiol.* 14: 307-321

Glazer, A. N. (1989) Light Guides. Directional energy transfer in a photosynthetic antenna. *J. Biol. Chem.* 264: 1-4

Grigorieva, G., and Shestakov, S. (1982) Transformation in the cyanobacterium *Synechocystis* sp. PCC 6803. *FEMS Microbiol. Lett*. 13,4: 367–370

Joliot, P., Barbieri, G, and Chabaud, R. (1969) Un noveau modèle des centres photochemiques du système II. *Photochem. Photobiol.* 10:309-329

Kaneko, T., and Tabata, S. (1997) Complete Genome Structure of the Unicellular Cyanobacterium *Synechocystis* sp. PCC 6803. *Plant Cell Physiol.* 38,11: 1171-1176

Kaneko, T., Sato, S., Kotani, H., Tanaka, A., Asamizu, E., Nakamura, Y., Miyajima, N., Hirosawa, M., Sugiura, M., Sasamoto, S., Kimura, T., Hosouchi, T., Matsuno, A., Muraki, A., Nakazaki, N., Naruo, K., Okumura, S., Shimpo, S., Takeuchi, C., Wada, T., Watanabe, A., Yamada, M., Yasuda, M., and Tabata, S. (1996) Sequence Analysis of the Genome of the Unicellular Cyanobacterium *Synechocystis* sp. Strain PCC 6803. II. Sequence Determination of the Entire Genome and Assignment of Potential Protein-coding Regions. *DNA Res.* 3: 109-136

Kashino Y., Lauber, W. M., Carroll, J. A., Wang, Q., Whitmarsh, J., Satoh, K., and Pakrasi, H. B. (2002) Proteomic analysis of a highly active photosystem II preparation from the cyanobacterium *Synechocystis* sp. PCC 6803 reveals the presence of novel polypeptides. Biochemistry 41: 8004-8012

Kok, B., Forbush, B., and McGloin, M. (1970) Cooperation of charges in photosynthetic O2 evolution I. A linear four step mechanism. *Photochem. Photobiol.* 11:457-475

Laemmli, U. K. (1970) Cleavage of Structural Proteins during the Assembly of the Head of Bacteriophage T4. *Nature*. 227, 680–685

Liberton, M., Page, L. E., O'Dell, W. M. B., O'Neill, H., Mamontov, E., Urban, V. S., and Pakrasi, H. B. (2012) Organization and Flexibility of Cyanobacterial Thylakoid Membranes Examined by Neutron Scattering. *J. Biol. Chem.* Submitted

Mannan, R. M., and Pakrasi, H. B. (1993) Dark Heterotrophic Growth Conditions Result in an Increase in the Content of Photosystem II Units in the Filamentous Cyanobacterium *Anabaena variabilis* ATCC 29413. *Plant Physiol*. 103: 971–977

Meunier, P. (1993) Oxygen evolution by Photosystem II: the contribution of backward transitions to the anomalous behavior of double-hits revealed by a new analysis method. *Photosyn. Res.* 36: 111-118

Nedbal, L. Trtilek, M., and Kaftan, D. (1999) Flash fluorescence induction: a novel method to study regulation of Photosystem II. *J. Photochem. Photobiol. B: Biol.* 48:154-157

Norling, B., Zak, E., Andersson, B., and Pakrasi, H. B. (1998) 2-D isolation of pure plasma and thylakoid membranes from the cyanobacterium *Synechocystis* sp. PCC 6803. *FEBS Letters*. 436:189-192

Olive, J., Ajlani, G., Astier, C., Recouvreur, M., and Vernotte, C. (1997) Ultrastructure and light adaptation of phycobilisome mutants of *Synechocystis* sp. PCC 6803. *Biochim. et.*

Biophys. Acta. 1319: 275-282

Packham, N. K., Hodges, M., Etienne, A. L., and Briantais, J. M. (1988) Changes in the flash-induced oxygen yield pattern by thylakoid membrane phosphorylation. *Photosynth. Res.* 15: 221-232

Page, L. E., Liberton, M., and Pakrasi, H. B. (2012) Reduction of Photoautotrophic Productivity in the Cyanobacterium *Synechocystis* sp. Strain PCC 6803 by Phycobilisome Antenna Truncation. *Appl. and Env. Microbiol.* 78, 17: 6349-6351

Porra, R. J., Thompson, W.A., and Kriedemann, P.E. (1989) Determination of accurate extinction coefficients and simulatneous equations for assaying chlorophylls a and b extracted with four different solvents: verification of the concentration of chlorophyll standards by atomic absorption spectroscopy. *Biochim. Biophys. Acta.* 975: 384–339

Richaud, C., Zabulon, G., Joder, A., and Thomas, J.-C. (2001) Nitrogen or Sulfur Starvation Differentially Affects Phycobilisome Degradation and Expression of the *nblA* Gene in *Synechocystis* Strain PCC 6803. *J. Bact.* 183, 10: 2989-2994.

Sidler W.A., (1994) Phycobilisome and phycobiliprotein structures, p 139 –216. *In* Bryant, D. A. (ed), The molecular biology of cyanobacteria. Kluwer Academic Publishers, Dordrecht, The Netherlands

Stadnichuk, I. N., Lukashev, E. G., and Elanskaya, I. V. (2009) Fluorescence changes accompanying short-term light adaptations in photosystem I and photosystem II of the cyanobacterium *Synechocystis* sp. PCC 6803 and phycobiliprotein-impaired mutants: State 1/State2 transitions and carotenoid-induced quenching of phycobilisomes. *Photosynth. Res.* 99:227-241

Thomas, J. C., B. Ughy, B. Lagoutte, and G. Ajlani. (2006) A second isoform of the ferredoxin:NADP oxidoreductase generated by an in-frame initiation of translation. *PNAS*. 103, 48:18368-18373

Ughy B., and Ajlani, G. (2004) Phycobilisome rod mutants in *Synechocystis* sp. PCC 6803. *Microbiol.* 150:4147-4156

Williams, J. G. K. (1988) Construction of specific mutations in photosystem II photosynthetic reaction center by genetic engineering method in *Synechocystis* 6803. *Methods Enzymol.* 167: 766–778

Yamanaka, G. and Glazer, A. N. (1980) Dynamic aspects of phycobilisome structure. *Arch. Microbiol.* 124, 39-74

	WT	CB	CK	PAL
Km	762±103	1151±128	843±151	1175±217
Vmax	587±23	720±26	913±49	1011±62
S0	34.9±1.6	33.7±1.4	36.3±3.1	31.7±0.7
S1	42.5±1.5	39.1±1.3	40.5±3.1	49.3±0.7
S2	12.8±1.3	14.6±1.0	10.7±2.0	11.6±0.4
S3	9.8±1.1	12.6±0.8	12.4±1.3	7.4±0.3
Misses	10.6	14.3	24.4	24.9
Single Hits	86.7	82.3	70.0	68.7
Double Hits	4.9	-0.9	3.0	2.6
Deactivation	-1.5	3.8	3.2	3.7

Table 1. Changes in photosynthetic performance of antenna mutants.

Kaleidagraph was used to determine K_m and V_{max} of data from Figure 2. S-state distribution was calculated from a homogenous four-step mechanism for Mn cluster cycling from Figure 4 (See Materials and Methods)(Meunier, 1993).

Figure 1. Western blots of photosystem proteins. Immunoblot detection of the Photosystem I proteins PsaA/B and Photosystem II protein CP43 were used to quantify Photosystem amounts. Lanes were loaded at 5 μg Chl. Hairlines are the lines of best fit calculated in Kaleidagraph and used to calculate K_m and V_{max}.

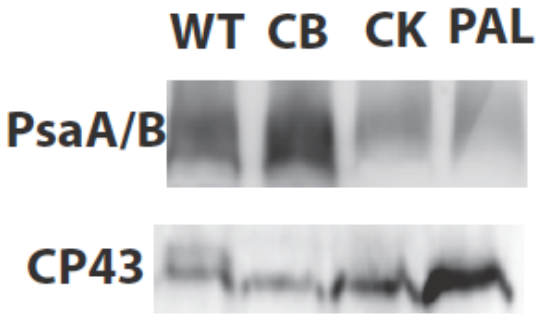
WT CB CK PAL
PsaA/B
CP43

Figure 2. Photosystem II-mediated oxygen evolution. Light saturation curves measured on a Clark-type oxygen electrode in the presence of KFeCN and DCBQ. Error bars represent one standard deviation of three technical replicates.

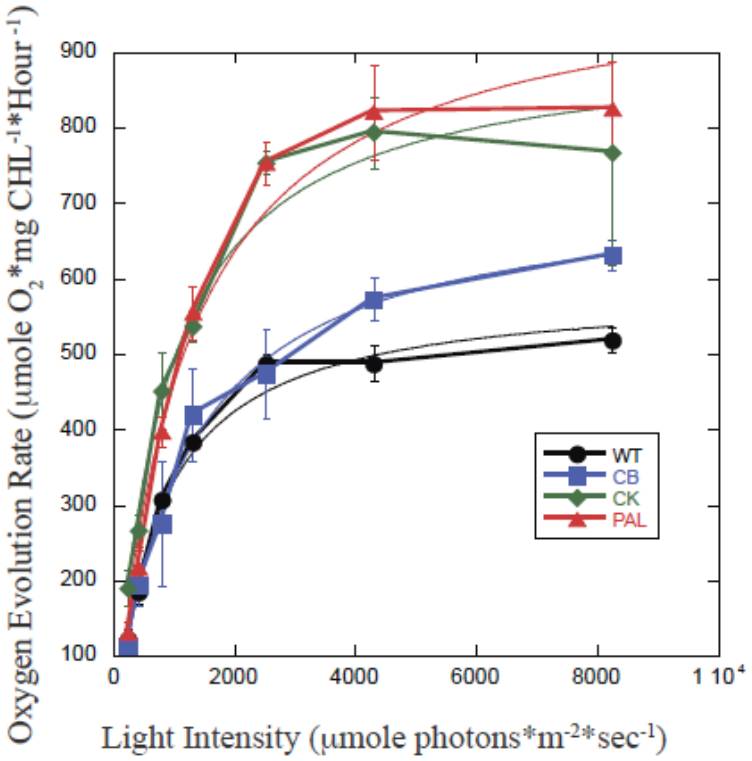
Oxygen Evolution Rate (μmole O2*mg CHL-1*Hour-1)
900
800
700
600
500
400
300
200
100
0
2000
4000
6000
8000
1 10^4
Light Intensity (μmole photons*m-2*sec-1)
WT
CB
CK
PAL

Figure 3. Low Temperature Fluorescence Emission Spectra. Fluorescence emission spectra at 77K were recorded with 435 nm (A) and 600 nm (B) excitation. Samples were loaded at equal 5 μg/ml Chl concentration (Porra *et al.,* 1989). Spectra excited at 435 nm were normalized to $(F-F_{640})/(F_{720}-F_{640})$, and spectra excited at 600 nm were normalized by F/F_{640}.

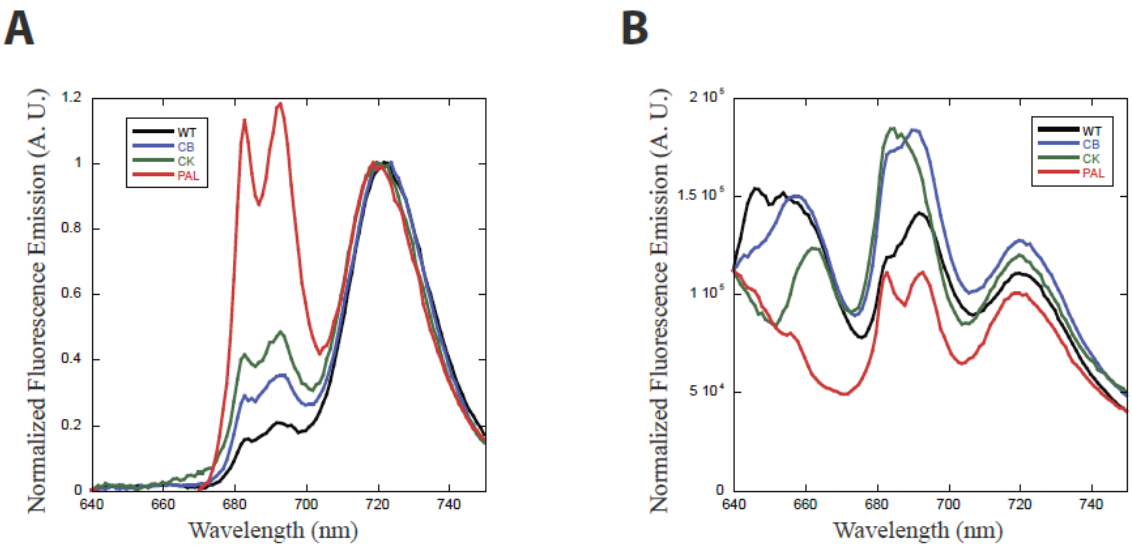
A
B
Normalized Fluorescence Emission (A. U.)
Wavelength (nm)
WT
CB
CK
PAL
0
0.2
0.4
0.6
0.8
1
1.2
640
660
680
700
720
740
5 10⁴
1 10⁵
1.5 10⁵
2 10⁵

Figure 4. Flash-Induced Oxygen Evolution. Flash-induced oxygen evolution was measured on a bare platinum electrode polarized at 650 mV. Samples were applied as a paste in concentrations of 40 μg Chl/ml. Each trace is an average of three technical replicates normalized to the average oxygen evolution rate of the entire trace.

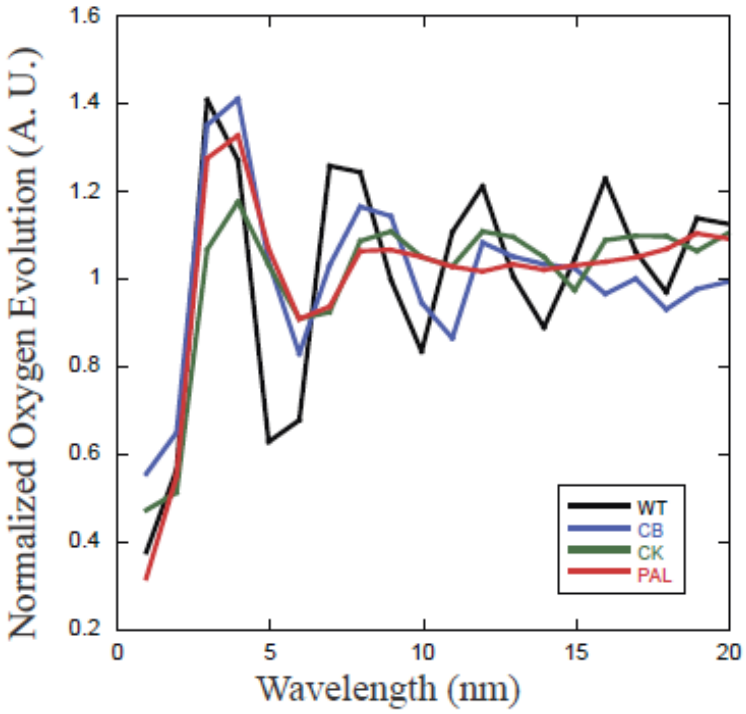
Normalized Oxygen Evolution (A. U.)
Wavelength (nm)
1.6
1.4
1.2
1
0.8
0.6
0.4
0.2
0
5
10
15
20
WT
CB
CK
PAL

Figure 5. Flash-Induced Fluorescence. Flash-induced Chl fluorescence was measured at room temperature on an FL-200 Dual-Modulated Kinetic Fluorometer as in Nedbal *et al.,* 1999. Spectra were normalized by division to the minimum fluorescence value at each time interval (to correct for baseline drift), and offset on the Y-axis for clarity. Three technical replicates were performed, and one representative trace is shown. Samples were loaded on an equal (10 μg/ml) Chl basis.

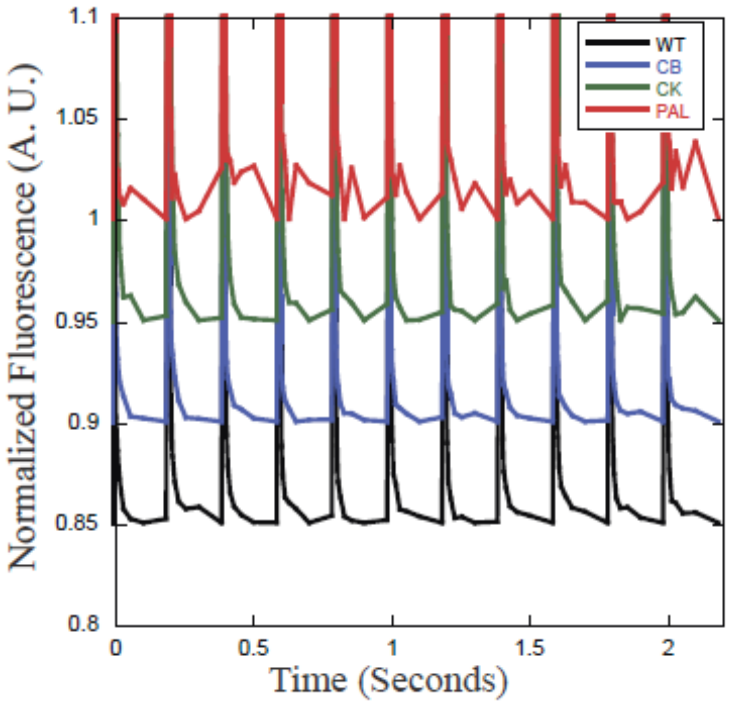
WT
CB
CK
PAL
Normalized Fluorescence (A. U.)
1.1
1.05
1
0.95
0.9
0.85
0.8
0
0.5
1
1.5
2
Time (Seconds)

Chapter 3

Organization and Flexibility of Cyanobacterial Thylakoid Membranes Examined by Neutron Scattering

Introduction

In photosynthetic organisms like plants, algae, and cyanobacteria, the light reactions occur in the highly specialized thylakoid membranes that house the components of the photosynthetic electron transfer chain. While plant thylakoids are arranged in stacked grana and unstacked stroma membranes, and algal thylakoids can be appressed or separated depending on the strain (Larkum *et al.,* 2003), cyanobacterial thylakoids typically do not stack or appress and are more uniformly sheet-like (Liberton *et al.,* 2008). Cyanobacterial strains display differences in intracellular organization, in particular having various arrangements of the thylakoid membranes within the cell interior (Liberton *et al.,* 2008). The organization of the thylakoid membrane system in cyanobacterial cells has been explored by different techniques, including recent work using electron tomography to show the three-dimensional arrangement of the membrane system (Liberton *et al.,* 2010; Nevo *et al.,* 2009*).* While these studies have begun to show the complexity and spatial detail of these membrane systems, such work provides static views of what are undoubtedly dynamic structures. To date there is little information exploring the rearrangements of the thylakoid membrane system in response to environmental stimuli such as light or temperature in live cyanobacterial cells. In order to thoroughly understand the form and function of cyanobacterial thylakoid membranes, studies are needed that incorporate high resolution measurements of membrane structure with information of how the organization of these membranes change in response to environmental inputs.

Probing the structural responses of the thylakoid membrane systems of photosynthetic organisms to light is of particular interest. In *Synechocystis* 6803, growth in low light (0.5 μmol photons $m^{-2}s^{-1}$) with glucose as a carbon source resulted in inflated thylakoid lumens measuring up to 300 nm (van de Meene *et al.,* 2012). Kirchhoff and colleagues used cryoelectron

microscopy to examine vitreous sections and found that the grana lumen in *Arabidopsis thaliana* expands in the light, thereby increasing the lumenal volume and presumably facilitating protein diffusion (Kirchhoff *et al.,* 2011). Earlier studies of the thylakoid membranes in the marine algae *Ulva* and *Porphyra* demonstrated a reproducible and reversible light-induced flattening of the thylakoid lumenal space as measured by electron microscopy of chemically fixed samples and micro-densitometry (Murakami and Packer, 1970). Recently, Nagy and coworkers used small-angle neutron scattering (SANS) to examine the *Synechocystis* 6803 PAL mutant and found a light-induced increase in repeat distances that they attributed to periodic spacing between adjacent thylakoid membrane pairs (Nagy *et al.,* 2011). These data demonstrate the need for additional studies to understand the effect of light on the organization of thylakoids in detail, and to clarify whether illumination results in expansion or contraction of the membrane system.

Obtaining structural information from photosynthetic organisms under changing conditions requires non-destructive techniques capable of probing the membrane systems of live cells. Studies using light microscopy approaches such as fluorescence recovery after photobleaching (FRAP) and hyperspectral confocal fluorescence microscopy (HCFM) have led to intriguing findings regarding the mobility of photosynthetic components and the organization of photosynthetic pigments within cyanobacterial cells (Mullineaux, 1999; Collins *et al.,* 2012). SANS can also be used to characterize periodically organized biological membrane systems on smaller length scales by observing diffraction from regularly spaced structural features separated by ~1-200 nm (Sadler and Worchester, 1982). Both the accessible length scales and the ability to examine individual components of biological systems using contrast matching has led to the

application of SANS in studies of cyanobacteria, eukaryotic algae, plant thylakoids (Nagy *et al.,* 2011; Nagy *et al.,* 2012) and mammalian mitochondria (Murugova *et al.,* 2011).

In order to examine thylakoid membrane organization in cyanobacterial cells under different conditions, we used a correlative approach incorporating both transmission electron microscopy and SANS. These techniques both provide complementary data at the length scales relevant to the study of biological structures, including membranes. We compared the thylakoid membrane organization in wild type *Synechocystis* 6803 cells to that of mutants in which the phycobilisomes have been truncated by varying degrees. These mutants are CB (containing one phycocyanin hexamer per rod), CK (lacking phycocyanin rods but still possessing the allophycocyanin core), and PAL (lacking functionally assembled phycobilisomes) (Ajlani and Vernotte, 1998; Ughy and Ajlani, 2004; Arteni *et al.,* 2009). Our results showed that the distances between thylakoid membrane layers is correlated with the size of the phycobilisome light harvesting antenna complexes and that these distances change reversibly and rapidly upon illumination, with strain-specific differences. Furthermore, our data indicated that the photosynthetic membranes in *Synechocystis* 6803 have a structural plasticity that is tied to the function of the photosynthetic electron transfer chain.

Materials and Methods

Electron microscopy

Cells were prepared for electron microscopy as previously described in (Liberton *et al.,* 2010). Cultures of WT, CB, CK, and PAL cells were grown for 5 days in liquid BG11 (Allen, 1968) with appropriate antibiotics, harvested by centrifugation, resuspended in a small volume, and loaded into planchettes for high pressure freezing (Bal-Tec). Thin sections (~80 nm) were cut from resin-embedded material and imaged using a LEO 912AB electron microscope equipped with a ProScan digital camera. Measurements were taken using Soft Imaging Systems' iTEM software and are given as the results of 20-30 measurements per cell type.

Small angle neutron scattering

SANS measurements were performed using the Bio-SANS instrument (Lynn *et al.,* 2006) at the High Flux Isotope Reactor, Oak Ridge National Laboratory. Cyanobacterial suspensions were in BG11 media prepared with H_2O (H-media), D_2O (D-media), or a mixture of the two. Cells grown in standard H-BG11 were harvested by centrifugation, washed twice in 10 ml of fresh media (with D_2O depending on the experiment), resuspended in 5 ml of media, and equilibrated overnight at 30˚C under ~25 μmol photons $m^{-2}s^{-1}$ white fluorescent light with 150 rpm shaking. All cultures were then adjusted to the same optical density (measured at λ = 730 nm). SANS measurements were carried out in 1 mm path cylindrical cells at 30ºC. The sample enclosure was equipped with a lighting apparatus that illuminated each sample position with ~ 20 ⌈mol photons $m^{-2}s^{-1}$ cool white LED light. A dark enclosure was also installed to allow for dark adaptation of individual samples. Three different configurations of the Bio-SANS instrument

were employed to collect data over the scattering vector range of $0.003 < q < 0.7$ Å^{-1} with sample-to-detector distances of 1.1, 6.8 and 15.3 m and a neutron wavelength of 6 ± 0.15 Å.

Data analysis

SANS data were analyzed using routines implemented in IGORPro software (Wavemetrics). The scattering intensity curves, *I(q)*, were obtained by azimuthally averaging the processed two-dimensional detector images which were normalized to incident-beam monitor counts and corrected for detector dark current, pixel sensitivity and solid angle geometry. Scattering from the quartz cell and appropriate media was subtracted with a volume fraction of 0.95 used to scale the intensity of the buffer scattering before subtraction. The resulting intensity profiles are presented in absolute scattering cross sections per unit volume and per solid angle. Individual diffraction peak q positions were determined by fitting each scattering profile with a variable number of pseudo-Voigt curves and a single underlying power-law function with exponent ≈ 2.5. Diffraction peak positions were equated to corresponding repeat distances through the relation $q = 2\pi / d$ where q is the peak center in reciprocal space (Å^{-1}) and d is the repeat distance (Å).

Quasi-elastic neutron scattering

QENS experiments were performed on the backscattering spectrometer (BASIS) at the Spallation Neutron Source, Oak Ridge National Laboratory (Mamontov and Herwig, 2011). The samples were prepared as described above and placed in rectangular aluminum cells with colorless sapphire windows to allow for illumination with white light (~280 ⌈mol photons m^{-2}s^{-1}). The raw data were converted from time-of-flight to energy transfer at selected q values using standard BASIS data reduction software, and data analysis was performed using the DAVE

software package (Azuah *et al.,* 2009). Data fitting was carried out using the jump diffusion model, $G(q) = \hbar Dq2 / (1 + Dq2\tau)$, where $\hbar$ is the reduced Planck's constant, D is the translational diffusion coefficient, and τ is the residence time between diffusion jumps.

Results

We have used transmission electron microscopy (TEM) to examine the thylakoid membrane systems in *Synechocystis* 6803 wild type (WT) and the phycobilisome mutant strains CB, CK, and PAL (Collins *et al.,* 2012). Thin section electron micrographs of high pressure frozen cells showed that the distances between thylakoid membranes were greatest in WT cells with intact phycobilisomes and smallest in the PAL mutant in which phycobilisomes were absent (Figure 1). In all strains, we measured the thickness of the membrane pairs that enclose the lumenal space and form a single thylakoid, and the interthylakoidal distances between the membrane pairs. The thickness of the thylakoid membrane pair was consistently ~150 Å in all strains, but the distances between membrane pairs varied considerably. We report the distance between membrane pairs in two ways: as the membrane-to-membrane boundary distance across the width of the interthylakoidal space, and as the center-to-center repeat distance between the thylakoid layers. The membrane-to-membrane distance is relevant for discussing the space available to the phycobilisome antenna in the cytoplasmic region, while the center-to-center repeat distance is the measurable quantity directly obtained in SANS.

Wild type cells (Fig. 1A) showed the characteristic intracellular arrangement of *Synechocystis* 6803: layers of ~3-6 concentric membrane pairs generally conforming to the curvature of the cell envelope, with a central cytoplasmic region largely devoid of thylakoid membranes, but in which other cellular components were found. We measured the interthylakoidal distances between membrane pairs as averaging 400 ± 80 Å in WT cells, consistent with reported measurements of 300-500 Å (Olive *et al.,* 1997; van de Meene *et al.,* 2006). The center-to-center thylakoid membrane distance was 550 Å for WT cells (Fig. 1B and Table 1). In terms of overall cell morphology and thylakoid membrane organization, the CB

strain (which contains only one phycocyanin hexamer per rod) appears very similar compared to WT (Fig. 1C). Measurements of interthylakoidal distances averaged 330 ± 60 Å, and center-to-center membrane distance was 480 Å for CB (Fig. 1D and Table 1). In the CK strain, which possesses only the APC core, distances between thylakoid membrane layers averaged 320 ± 20 Å (Fig. 1E), with center-to-center distances of 470 Å (Fig. 1F and Table 1). In the PAL mutant (Fig. 1G), thylakoid membranes consistently formed straight bands with little curvature (Collins *et al.,* 2012). The interthylakoidal distances in PAL averaged 190 ± 30 Å, with center-to-center membrane distances of 340 Å (Fig. 1H and Table 1).

Periodic cellular structures were indicated in the SANS profiles obtained from samples suspended in 100% D-media by the appearance of diffraction peaks above power-law and incoherent scattering backgrounds as shown for WT in Fig. 2A. A series of samples equilibrated in 0%, 20%, 40%, 60%, 80%, and 100% D-media were measured to determine the scattering contrast match points(s) of the diffracting structures and to identify their general molecular composition (*viz.,* protein, lipid, *etc.*). Fig. 2B shows that the contrast for the structure diffracting at the lowest-*q* was "matched" (i.e., disappeared) at ~17% D-media, a value known to correspond to lipid structures. The scattering profile of WT in 20% D-media (Fig. 2A) demonstrated that all diffraction peaks were largely matched at this media scattering length density (SLD) and pointed to the ordered thylakoid membranes observed by TEM as the source of all of the diffraction measured from these samples.

The small-angle scattering observed for all strains equilibrated in 100% D-media and incubated in light is shown in Fig. 3A. The scattering profiles from all strains showed significant differences in the observed diffraction at the lowest *q* (Peak 1). Based on the length scale of both this periodicity and the periodic thylakoid arrangements from TEM, we attributed this diffraction

feature to the thylakoid membrane center-to-center period (Table 1). The systematic shortening of this period with antenna truncation can be seen in the shift to higher *q* values for this feature. Including the thylakoid repeat features, up to five distinct peaks, depending upon the strain, could be observed with small strain-to-strain variations in both the *q* positions and relative intensities (Table 1). A putative assignment of all the diffraction features observed from the WT sample is presented in the following discussion.

To determine whether changes to the SANS profiles would occur if cells were incubated in the dark, cells were dark adapted for 1 hour, and data were collected in an identical manner as for cells in the light. SANS data from cells in the dark showed changes in the *q* positions and relative intensities, but the overall pattern of the profiles remained fairly consistent for each strain (Fig. 3B). All strains have a first peak at 0.010 $Å^{-1}$ to 0.017 $Å^{-1}$ and a third peak centered at ~0.042 $Å^{-1}$. However, Peaks 2, 4, and 5 are only present in a subset of the strains (Table 1). Peak 2 is clearly observed in WT in the dark at approximately 0.022 $Å^{-1}$. In the light this peak is strongly reduced but still discernible as a shoulder (Fig. 3A), and the curve shape suggests yet another peak at ~0.016 $Å^{-1}$ in WT in light. Peak 2 is weakly present in CB but not in the other mutant strains. There is a fourth peak in all strains except WT in dark from 0.045-0.071 $Å^{-1}$. A fifth peak is present in WT and CK (Table 1).

The trend in changes between light and dark was not consistent among the strains (Table 1). The values that corresponded to the largest scale (Peak 1, Table 1) showed a small dark-induced expansion in the CB mutant, but CK and PAL showed a contraction in this distance in the dark with changes of 37.4 Å for CK and 25.8 Å for PAL. No change in position of Peak 1 was discernible for WT, but its intensity was clearly reduced in response to illumination. Peaks 3, 4, and 5, observed at larger *q,* which corresponds to smaller distances, mostly showed

expansion in light. This effect was clearest for Peak 3 with ~8% expansion in the wild type and 4% to 5% expansion in the mutants. All four strains showed a reduction in scattering intensity for the peaks at smaller $q < 0.025$ Å^{-1} (distances > 250 Å) when exposed to light. In contrast, scattering intensity for the higher q peaks clearly increased for WT. Similarly, in all 3 mutants the intensity of Peak 4 at $q \sim 0.045$ Å^{-1} increased when cells were exposed to light.

Time-series measurements were made to characterize the timescale of the transition between the dark- and light-adapted states. Samples of WT, CK and PAL strains were adapted to darkness for one hour before a series of five-minute measurements during illumination began. SANS from the WT strain (Fig. 4A) showed that the dark-to-light changes occurred rapidly, with the majority happening within the first ten minutes of illumination. In contrast, however, structural changes in the PAL mutant only began to appear after 30 minutes of illumination (Fig. 4B), with change occurring up to 2 hours. Reversed light-to-dark time-series measurements were conducted for the CK strain. The dark adapted structures were largely recovered within 20 minutes (Figs. 4C-D).

To determine if these changes depended upon functional photosynthetic electron transport, we incubated dark-adapted cells with 3-(3,4-dichlorophenyl)-1,1-dimethyl urea (DCMU), an inhibitor of electron transport from photosystem II. DCMU treatment did not perturb the dark-adapted structure. However, the SANS measured from these samples after 30 minutes of illumination (Fig. 5) showed little change from the corresponding dark state and demonstrated the dependence of the light-induced changes on an intact electron transport chain.

It was of interest to investigate if the light-induced structural rearrangements observed by SANS that are attributed to a swelling of the thylakoid lumen resulted in changes in the intracellular dynamics of the cyanobacteria. Quasi-elastic neutron scattering is ideally suited to

investigate dynamics on a pico- to nanosecond time frame. Measurements on the SNS backscattering spectrometer, BASIS, were carried out in order to assess the effect of light on the microscopic dynamics of the cyanobacteria and its intracellular water. Both the faster water dynamics and the slower cellular dynamics could be measured simultaneously due to the combination of a high energy resolution and a wide dynamic range of the BASIS. It was possible to analyze the translational dynamics of the intracellular water up to $q = 0.7$ Å^{-1} and the internal dynamic motions of cellular components up to $q = 0.9$ Å^{-1}. Fig. 6 shows the q-dependence of the quasielastic signal broadening (half-width at half-maximum) for WT *Synechocystis* 6803 cells measured with and without light. Data for *Escherichia coli* are presented for comparison. The broader q-dependent component originates from the intracellular water, whereas the narrower q-independent component originates from the cellular components of the bacteria. Unlike the measured dynamics of water, which is clearly translational, the internal dynamics of the bacteria is of localized character resulting in q-independent broadening of the scattering signal. The q-dependence of the water data shown in Fig. 6 was fitted with the jump diffusion model described above. The results of the fitting are shown in Table 2. Within the accuracy of the experiment, the fit values obtained are essentially the same for cells in the light- and dark-adapted states and also similar to the translational diffusion coefficient bulk water (29.8×10^{-10} m^2 s^{-1}) (Mille, 1973). Thus, the space accessible to the intracellular water in cyanobacteria is not sufficiently restricted to affect its translational dynamics, despite the profound structural changes in the membranes observed in the SANS experiment. Similarly, the measured internal dynamics of the cyanobacteria are not affected by light either; the relaxation times calculated from the q-independent broadening component as $\tau = \hbar / \Gamma(q)$ are $(157 \pm 21)\times10^{-12}$ s and $(153 \pm 21)\times10^{-12}$ s with and without light, respectively. In the case of *E. coli*, the diffusion coefficient of water was

similar to the values obtained with the cyanobacteria (Table 2) but the dynamics cellular components exhibited a significantly slower relaxation time, $(175 \pm 15)\times10^{-12}$ s, as is evident in Fig. 6. This possibly reflects the notable differences in the cellular architectures of the two bacterial species.

Discussion

Cyanobacteria such as *Synechocystis* 6803 have a highly organized thylakoid membrane architecture, and it has been proposed that rearrangements in the membrane system, and the spacing between membrane layers, play a role in the cellular regulation of photosynthesis (Collins *et al.,* 2012). Ideally, investigation of membrane architecture in cyanobacteria requires real-time *in situ* studies that can follow the time course of reorganization in response to external stimuli such as light or other environmental conditions. However, techniques that combine the required spatial resolution with the capability to resolve changes over time are rare. TEM is the method of choice for determining cell physiology at the nano- to meso-scale and has been used extensively to determine thylakoid architecture (Nevo, *et al.,* 2009); however, it can rely heavily on fixation of the specimen and does not provide a dynamic picture. Solution scattering techniques, on the other hand, can in principle provide this missing link to the understanding of photosynthesis, but have hardly been used in this field of research until recently (Tang, 2012).

The length scales of interest in this context range from the thickness of individual lipid bilayers to the spacing between thylakoid membrane layers (a few nanometers to just under 100 nanometers), which is covered by small-angle scattering (SAS) techniques using x-rays (SAXS) or neutrons (SANS). However, well-defined peaks are not commonly observed in the small-angle range of scattering data obtained from complex biological systems. In order to observe diffraction-like peaks in biological SAS, well-defined discrete repeat distances must be present in the system, and there must be good contrast between the scattering length densities of the ordered cellular component and the surrounding medium. Both of these prerequisites are fulfilled in cyanobacteria that are equilibrated in D_2O media: the membrane system has been shown to exhibit well defined spacings, and the D_2O-rich cytoplasm and lumen have strong

contrast relative to hydrogen-rich lipid membranes. For a system that is as complex as entire cells, however, the convoluted scattering contributions from a mixture of structural features generally pose great challenges to the interpretation of SAS data. Fortunately, this situation can be greatly improved for SANS by contrast enhancement through selective replacement of hydrogen atoms with its heavier isotope deuterium (^{2}H or D). In cyanobacterial cells, well-organized arrangements of phycobilisomes have been reported (Olive *et al.,* 1997) and a number of other structural features could in principle produce peaks. By using contrast variation, we were able to conclude that the observed peaks are indeed due to membrane repeat distances (Figure 2). Recent work by Nagy et al. has successfully applied SANS to photosynthetic systems (Nagy, *et al.,* 2011; Nagy *et al.,* 2012). Their pioneering study, however, has left many open questions. In the current study, we have developed a more comprehensive picture through correlation of SANS data with TEM images of the same cyanobacterial strains, observation and interpretation of additional diffraction peaks, and application of scattering contrast variation.

SANS data from the four cyanobacterial strains investigated at both light and dark conditions show qualitative agreement (Fig. 3). All profiles can be described by sets of correlation peaks above a power-law baseline (exponent ~ -2.5). The largest repeat distance observed in our studies was found in WT cells at 627 Å (Peak 1). This peak has been predicted previously (Nagy *et al.,* 2011), but this is the first time that it was observed experimentally. The repeat distance agrees well with the expected sum of ~150 Å for thylakoid membrane thickness and an interthylakoidal spacing of ~450 Å (Olive *et al.,* 1997) or 300-500 Å (van de Meene, *et al.,* 2006) as has been reported from TEM data, as well as our own measured interthylakoidal distance of ~400 Å (Fig, 1). The differences seen here among the TEM data are likely due to the

inherent biological variability of the membrane spacing when measured within individual cells, and sample preparation and variations in growth conditions may also contribute.

Studies have shown that modulation of phycobilisome antenna size results in changes to the interthylakoidal distances (Olive *et al.,* 1997). The largest SANS repeat distance (position of Peak 1) systematically decreases with successive reduction of the light harvesting antenna in the order WT, CB, CK, PAL, giving further strong evidence that the size of the phycobilisome is closely related to membrane spacing as reported previously (Collins *et al.,* 2012; Olive *et al.,* 1997). In particular, removal of the phycocyanin rods in CK leads to a reduction of SANS-derived membrane spacing by 170 Å (in light) or 207 Å (in the dark), and the latter number agrees perfectly with the result reported for the phycocyanin-less strain PMB11 by Olive *et al* (Olive *et al.,* 1997). In the mutant strain PΔE, which lacks assembled phycobilisomes, a small interthylakoidal distance of 40 Å was measured (Olive *et al.,* 1997; van de Meene *et al.,* 2006). However, our TEM data did not show as severe a decrease in the interthylakoidal distance in the PAL mutant that lacks phycobilisomes, where the interthylakoidal distances averaged 190 Å. The origin of the differences found in the interthylakoidal distances measured by TEM between these two strains lacking phycobilisomes, PAL and PΔE, is unknown, but may be due in part to fixation methods (high pressure freezing versus chemical fixation). It is interesting that our SANS data showed a repeat distance of 383 Å (light) or 357 Å (dark) for the PAL strain (Peak 1), and this value is similar to our center-to-center membrane distance from PAL TEM images (340 Å) (Table 1).

For a system with appressed membranes, a repeat distance of about 190 Å would be expected, based on the thickness of a thylakoid pair (~150 Å) and an interthylakoidal distance of ~40 Å, as seen in the PΔE strain and as has been measured for appressed thylakoids in other

systems (Larkum *et al.,* 2003). This value was observed by Nagy *et al* (Nagy *et al.,* 2011) and also shows in our SANS data for the PAL mutant as Peak 3. However, a value very close to this is also present in WT, CB, and CK, and this repeat distance varies relatively little among the different strains. These data suggest that all the strains may contain some regions of nearly appressed thylakoids with interthylakoidal distances of 20 Å to 40 Å. We did not see evidence for this in our TEM data; however, SANS gives data averaged over a large population. Moreover, if such appressed membranes form extended stacks, then the diffraction signal would be strongly amplified and even a small concentration of such regions could be visible in the diffraction pattern. In all strains this repeat distance increases in response to illumination. This may be interpreted as an increase in interthylakoidal spacing from 20 to 30 Å in the dark to 30 to 40 Å in the light. However, an alternative interpretation can be given in that the thickness of the lumen also increases in response to light.

SANS data from WT in the dark exhibited a repeat distance of 300 Å (Peak 2 at 0.022 $Å^{-1}$). This corresponds to an interthylakoidal spacing too narrow to accommodate phycobilisomes. In light this peak is attenuated and accompanied by an additional repeat distance of 393 Å (at ~0.016 $Å^{-1}$). The latter value suggests that such thylakoids are separated by a single layer of phycobilisomes. This peak is also weakly present in the CB mutant.

The repeat distances obtained from Peaks 4 and 5 are too small to encompass the width of a thylakoid membrane plus interthylakoidal spacing. Instead, these peaks correspond to distances that are similar to the width of a single thylakoid membrane. Indeed, the repeat distance of the pair of lipid bilayers that enclose the width of the lumen is expected to be approximately 100 to 110 Å, and Peak 5 matches this distance. However, the reason for the absence of Peak 5 in CB and PAL is unknown at this time. Peak 4, with values slightly larger

than Peak 5, might suggest a swollen thylakoid membrane in which the lumen width is increased by approximately 30 Å. Peak 4 is absent in WT in the dark but rises in response to light. Thus, SANS data suggest a swelling of the lumen in response to light exposure in WT. It is at present unknown what the significance of lumen swelling in response to light is, but this is consistent with the findings of Kirchhoff *et al* (Kirchhoff *et al.,* 2011).

In summary, SANS data of WT and mutant *Synechocystis* 6803 cells revealed at least five distinct peaks that could be correlated with TEM images of these same strains. These findings are summarized in Fig. 7, which shows a schematic drawing of our interpretation of these data: Peak 1 is the center-to-center thylakoid membrane repeat distance that may accommodate phycobilisomes, while Peak 2 is a center-to-center repeat distance that is too small for phycobilisomes. Peak 3 originates from a population of appressed membranes in all strains, and Peaks 4 and 5 originate from single thylakoid membrane layers with variable lumenal widths. While raising further questions, these descriptions are the most comprehensive analysis of SANS/TEM data sets to date and may serve as a basis for future such work in other photosynthetic membrane systems.

Our findings show that cyanobacterial cells undergo reversible structural changes in response to light, and that these changes are significantly different among the phycobilisome antenna mutants. These intracellular rearrangements within the thylakoid system were reproducible between biological and technical replicates in *Synechocystis* cells in both the wild type and mutant strains, suggesting that these responses are robust. Future measurements under different light qualities and intensities will probe these intracellular reorganizations further. The ability to directly observe membrane rearrangement in response to light exposure and its dependence on antenna mutations points towards a rich arsenal of interdependent membrane

regulation processes that allow cyanobacteria a rapid and efficient adaptation to changes in light intensity.

References

Ajlani, G., and Vernotte, C. (1998) Construction and characterization of a phycobiliprotein-less mutant of *Synechocystis* sp. PCC 6803. *Plant Molecular Biology* 37, 577-580

Allen, M. M. (1968) Simple conditions for growth of unicellular blue-green algae on plates. *J. Phycol*. 4, 1-4

Arteni, A. A., Ajlani, G., and Boekema, E. J. (2009) Structural organisation of phycobilisomes from *Synechocystis* sp. strain PCC6803 and their interaction with the membrane. *BBA - Bioenergetics* 1787, 272-279

Azuah, R. T. Keller, L. R.; Qiu, Y. M.; Tregenna-Piggott, P. L. W.; Brown, C. M.; Copley, J. R. D.; Dimeo, R. M. . (2009) DAVE: A comprehensive software suite for the reduction, visualization, and analysis of low energy neutron spectroscopic data. *Journal of Research of the National Institute of Standards and Technology* 114, 341-358

Collins, A. M., Liberton, M., Jones, H. D., Garcia, O. F., Pakrasi, H. B., and Timlin, J. A. (2012) Photosynthetic pigment localization and thylakoid membrane morphology are altered in *Synechocystis* 6803 phycobilisome mutants. *Plant Physiol* 158, 1600-1609

Kirchhoff, H., Hall, C., Wood, M., Herbstova, M., Tsabari, O., Nevo, R., Charuvi, D., Shimoni, E., and Reich, Z. (2011) Dynamic control of protein diffusion within the granal thylakoid lumen. *Proceedings of the National Academy of Sciences of the United States of America* 108, 20248-20253

Larkum, A. W. D., and Vesk, M. (2003) Algal plastids: their fine structure and properties. In A.W. Larkum, S.E. Douglas, J.A. Raven, eds, *Photosynthesis in Algae*, Kluwer Academic Publishers, The Netherlands, pp 11-28

Liberton, M., and Pakrasi, H. B. (2008) Membrane Systems in Cyanobacteria. In A. Herrero, E. Flores, eds, *The Cyanobacteria: Molecular Biology, Genomics, and Evolution*. Horizon Scientific Press, Norwich, UK, pp 217-287

Liberton, M., Austin, J. R., Berg, R. H., and Pakrasi, H. B. (2010) Unique thylakoid membrane architecture of a unicellular N_2-fixing cyanobacterium revealed by electron tomography. *Plant Physiol* 155, 1656-66

Lynn, G. W., Heller, W., Urban, V., Wignall, G. D., Weiss, K., and Myles, D. A. A. (2006) Bio-SANS--A dedicated facility for neutron structural biology at Oak Ridge National Laboratory. *Physica B: Condensed Matter* 385-386, 880-882

Mamontov, E., and Herwig, K. W. (2011) A time-of-flight backscattering spectrometer at the Spallation Neutron Source, BASIS. *The Review of scientific instruments* 82, 085109

Mills, R. (1973) Self-diffusion in normal and heavy water in the range 1-45 deg. *J Phys Chem* 77, 685-688

Mullineaux, C. W. (1999) The thylakoid membranes of cyanobacteria: structure, dynamics and function. *Aust. J. Plant Physiol*. 26, 671-677

Murakami, S., and Packer, L. (1970) Light-induced changes in conformation and configuration of thylakoid membrane of *Ulva* and *Porphyra* chloroplasts *in-vivo*. *Plant Physiology* 45, 289-299

Murugova, T. N., Solodovnikova, I. M., Yurkov, V. I., Gordeliy, V. I., Kuklin, A. I., Ivankov, O. I., Kovalev, Y. S., Popov, V. I., Teplova, V. V., and Yaguzhinsky, L. S. (2011) Potentials of small-angle neutron scattering for studies of the structure of "live" mitochondria. *Neutron News* 22, 11-14

Nevo, R., Chuartzman, S. G., Tsabari, O., Reich, Z., Charuvi, D., and Shimoni, E. (2009) Architecture of Thylakoid Membrane Networks. In H. Wada, N. Murata, eds, *Lipids in Photosynthesis: Essential and Regulatory Functions*, Springer Science and Business Media, pp 295–328

Nagy, G., Posselt, D., Kovacs, L., Holm, J. K., Szabo, M., Ughy, B., Rosta, L., Peters, J., Timmins, P., and Garab, G. (2011) Reversible membrane reorganizations during photosynthesis in vivo: revealed by small-angle neutron scattering. *Biochemical Journal* 436, 225-230

Nagy, G., Szabo, M., Unnep, R., Kali, G., Miloslavina, Y., Lambrev, P. H., Zsiros, O., Porcar, L., Timmins, P., Rosta, L., and Garab, G. (2012) Modulation of the multilamellar membrane organization and of the chiral macrodomains in the diatom *Phaeodactylum tricornutum* revealed by small-angle neutron scattering and circular dichroism spectroscopy. *Photosynth Res* 111, 71-79

Olive, J., Ajlani, G., Astier, C., Recouvreur, M., and Vernotte, C. 1997. Ultrastructure and light adaptation of phycobilisome mutants of *Synechocystis* sp. PCC 6803. *Biochim. et. Biophys. Acta.* 1319: 275-282.

Sadler, D. M., and Worcester, D. L. (1982) Neutron diffraction studies of oriented photosynthetic membranes. *J Mol Biol* 159, 467-484

Tang, K. H., and Blankenship, R. E. (2012) Neutron and light scattering studies of light-harvesting photosynthetic antenna complexes. *Photosynth Res* 111, 205-217

Ughy, B., and Ajlani, G. (2004) Phycobilisome rod mutants in *Synechocystis* sp. strain PCC6803. *Microbiology* 150, 4147

van de Meene, A. M., Hohmann-Marriott, M. F., Vermaas, W. F., and Roberson, R. W. (2006) The three-dimensional structure of the cyanobacterium *Synechocystis* sp. PCC 6803. *Arch Microbiol* 184, 259-270

van de Meene, A. M. T., Sharp, W. P., McDaniel, J. H., Friedrich, H., Vermaas, W. F. J., and Roberson, R. W. (2012) Gross morphological changes in thylakoid membrane structure are associated with photosystem I deletion in *Synechocystis* sp PCC 6803. *Biochimica Et Biophysica Acta-Biomembranes* 1818, 1427-1434

Table 1. Distances and peak positions in WT, CB, CK, and PAL cells under light (L) and dark (D) conditions. All measurements are in Å.

	TEM[a]	SANS				
		Peak 1	Peak 2	Peak 3	Peak 4	Peak 5
6803 L	550	627.3	295.7	181.1	138.9	113.7
6803 D		627.1	299.5	167.8	-	114.0
CB L	480	524.1	311.2	181.7	130.3	-
CB D		529.7	308.7	175.0	128.5	-
CK L	470	457.3	-	197.8	144.1	112.1
CK D		419.9	-	188.4	142.9	106.0
PAL L	340	382.7	-	192.4	129.0	-
PAL D		356.9	-	184.8	122.6	-

[a]TEM data report the center-to-center thylakoid membrane distances.

Table 2. Translational diffusion coefficients (D) and mean residence times (τ) obtained from the jump diffusion model of the QENS data. Error is reported as standard deviation.

Organism	D (10^{-10} m^2/s)	τ (10^{-12} s)
Synechocystis 6803 (dark)	28.8 ± 9.7	4.7 ± 3.3
Synechocystis 6803 (light)	27.7 ± 9.7	5.2 ± 3.5
Escherichia coli (dark)	32.1 ± 6.8	6.7 ± 1.8

Figure 1. Transmission electron micrographs of WT and phycobilisome antenna mutants. Whole cell images and enlargements showing thylakoid membrane spacing are shown for WT (A-B), CB (C-D), CK (E-F), and PAL (G-H). White bars depict the center-to-center thylakoid membrane spacing. Labeled are T, thylakoid membranes; P, polyphosphate bodies. Bar = 500 nm in (A), (C), (E), (G) and 50 nm in (B), (D), (F), (H).

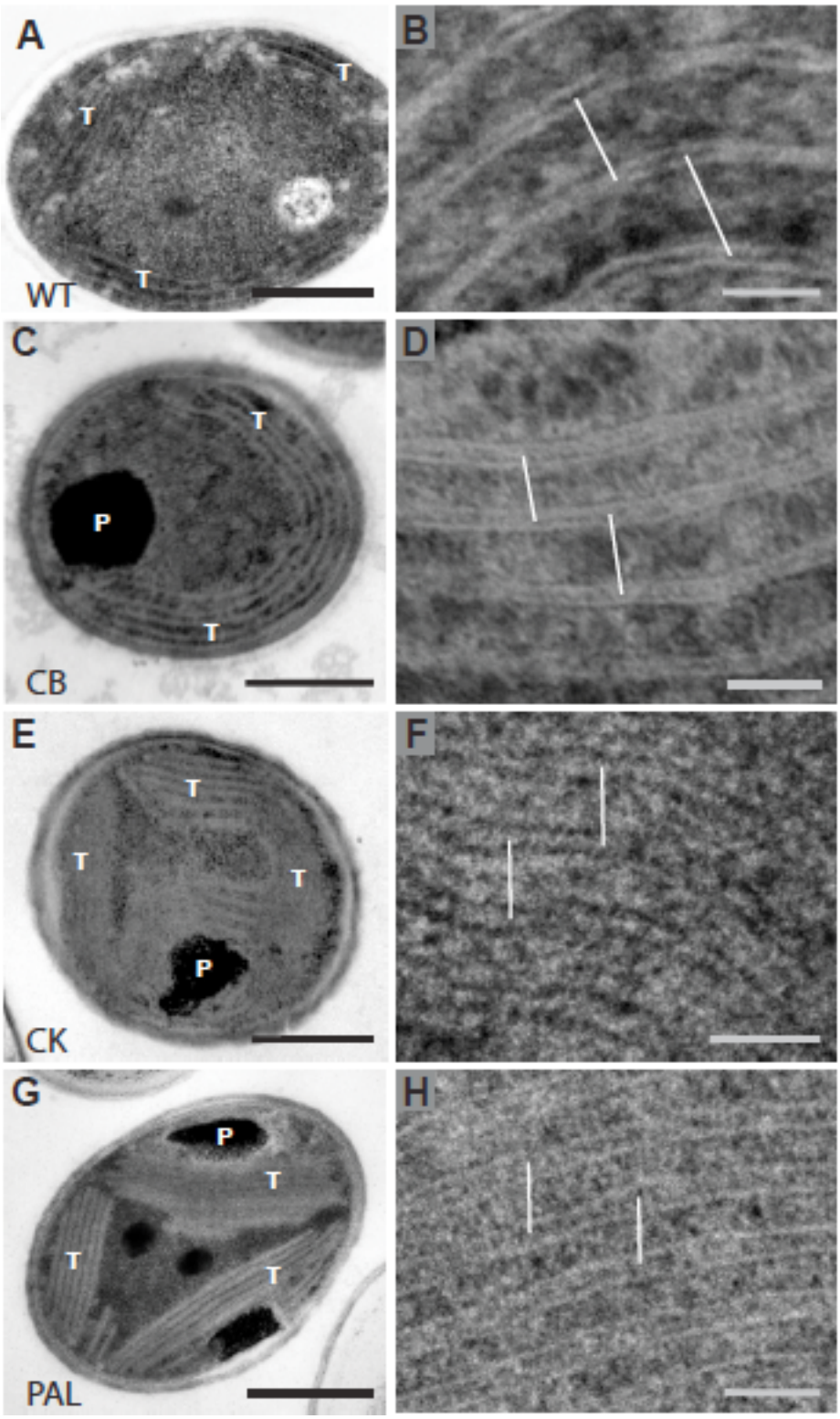
A
T
T
T
WT
B
C
T
P
T
CB
D
E
T
T
T
P
CK
F
G
P
T
T
T
PAL
H

Figure 2. Contrast variation for WT in light and dark. SANS intensity was measured for samples in both light and dark conditions for a range of ratios of D_2O to H_2O. (A) Scattering profiles for samples in dark and equilibrated in 100% D_2O (solid) and 20% D_2O (open). In (B), the square root of scattering intensity for the diffraction peak at lowest q is plotted as a function of D_2O concentration for samples in light (open) and dark (solid). The intensities from samples in 20% D_2O were excluded from the linear regression fits (solid lines). The contrast match point for the major peak is 17.9% in the light and 16.5% in the dark, within the range of a peak that is primarily composed of lipids.

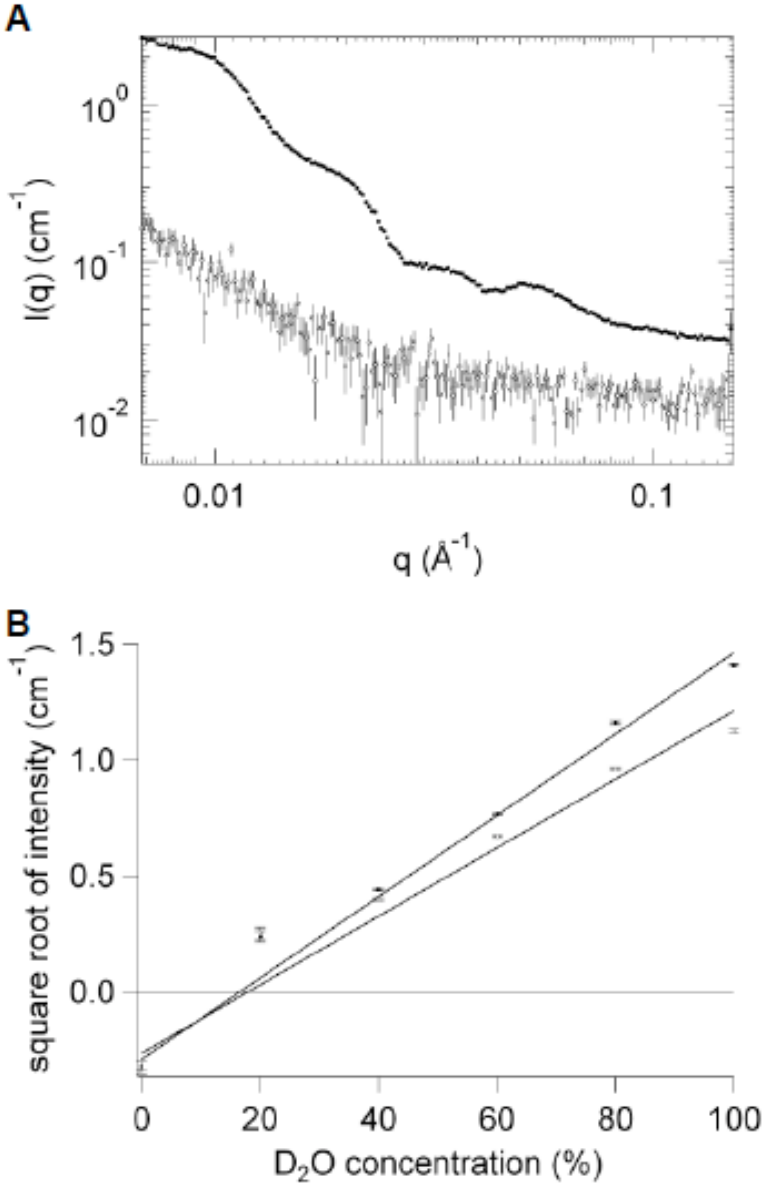
A
10^0
10^{-1}
10^{-2}
I(q) (cm^{-1})
0.01
0.1
q ($Å^{-1}$)
B
square root of intensity (cm^{-1})
1.5
1.0
0.5
0.0
0
20
40
60
80
100
D_2O concentration (%)

Figure 3. SANS data from cyanobacterial cells under light and dark conditions. Scattering intensities from WT (red), CB (blue), CK (green), and PAL (gold) in light (A) and dark (B) over the entire experiment q range are shown. Peaks are labeled 1-5. In (A) intensities for WT and PAL are vertically offset by -12 cm^{-1} and 6 cm^{-1}, respectively. In (B) intensities for WT, CB and PAL are vertically offset by -12 cm^{-1}, -3 cm^{-1} and 6 cm^{-1}, respectively.

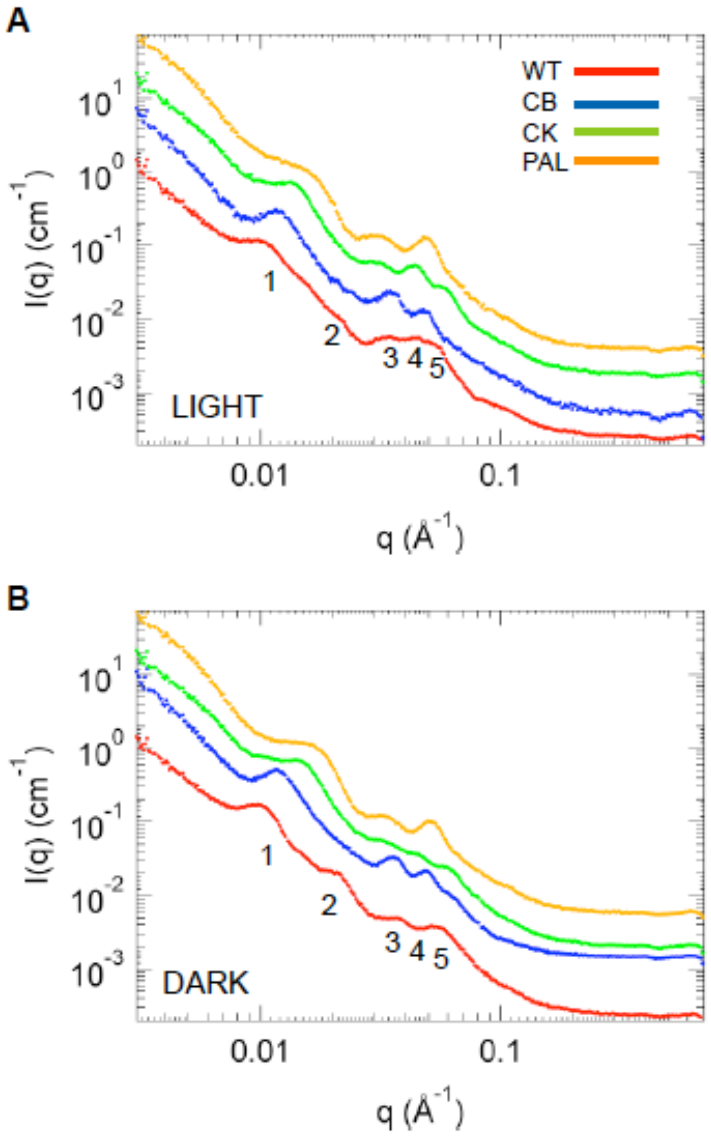
A
WT
CB
CK
PAL
I(q) (cm^{-1})
10^{1}
10^{0}
10^{-1}
10^{-2}
10^{-3}
1
2
3 4 5
LIGHT
0.01
0.1
q (Å^{-1})
B
I(q) (cm^{-1})
1
2
3 4 5
DARK
0.01
0.1
q (Å^{-1})

Figure 4. Time course of dynamic changes in cyanobacterial strains during dark–light transition. (A) WT during the transition from dark to light. (B) PAL during the transition from dark to light, showing that peaks shift slightly in the Q range but do not appear or disappear. (C) CK during light to dark and (D) dark to light transition.

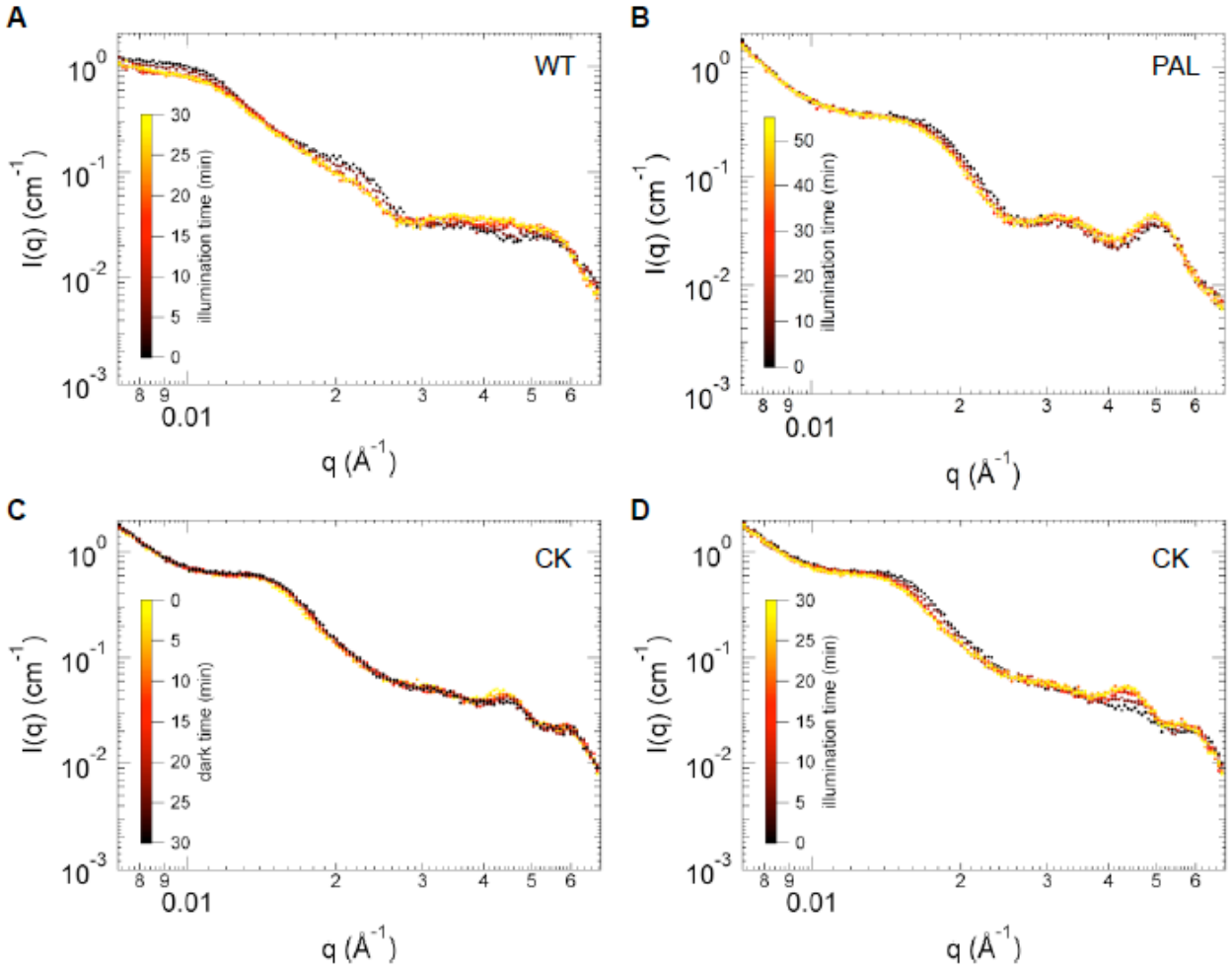
A
WT
B
PAL
C
CK
D
CK
I(q) (cm^{-1})
q (Å^{-1})
illumination time (min)
dark time (min)
0.01

Figure 5. Inhibition of electron transport prevents light/dark induced changes. Strains were pre-incubated in the dark in the presence of DCMU and data were collected in the dark and upon exposure to light for (A) WT, (B) CB, (C) CK and (D) PAL strains. Untreated light (solid red) and dark (solid black) scattering profiles are reproduced from Figure 2 for comparison with the DCMU treated light (open red) and DCMU treated dark (open black) profiles. In (A) intensities were vertically offset by 0.4 cm^{-1} for treated and untreated samples exposed to light. In (B) intensities were vertically offset by 0.7 cm^{-1} for the untreated and by 0.3 cm^{-1} for the treated samples exposed to light. In (C-D) intensities for treated and untreated samples exposed to light were vertically offset by 0.3 cm^{-1}.

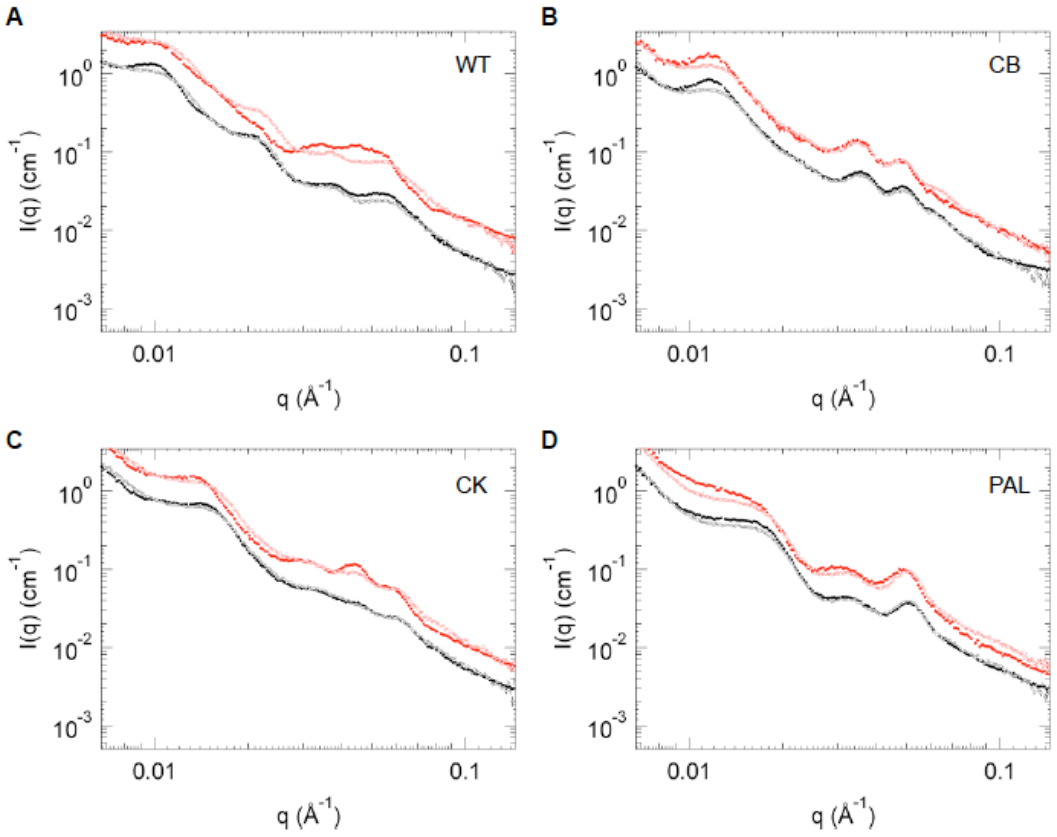
A
WT
B
CB
C
CK
D
PAL
I(q) (cm^{-1})
10^{0}
10^{-1}
10^{-2}
10^{-3}
0.01
0.1
q (Å^{-1})

Figure 6. Quasi-elastic linewidths and fits to jump-diffusion model used to determine average water diffusion coefficients. The half-width at half-maximum values of the *q*-dependent and *q*-independent Lorentzian components of the quasi-elastic energy spectra are shown for WT *Synechocystis* in dark (solid circles), WT *Synechocystis* illuminated with white light (open circles) and BL-21 *E. coli* (solid squares), respectively. Fits of the WT dark, WT illuminated, and *E. coli* dark *q*-dependent linewidths to the jump-diffusion model are shown as solid, dashed, and dotted lines, respectively.

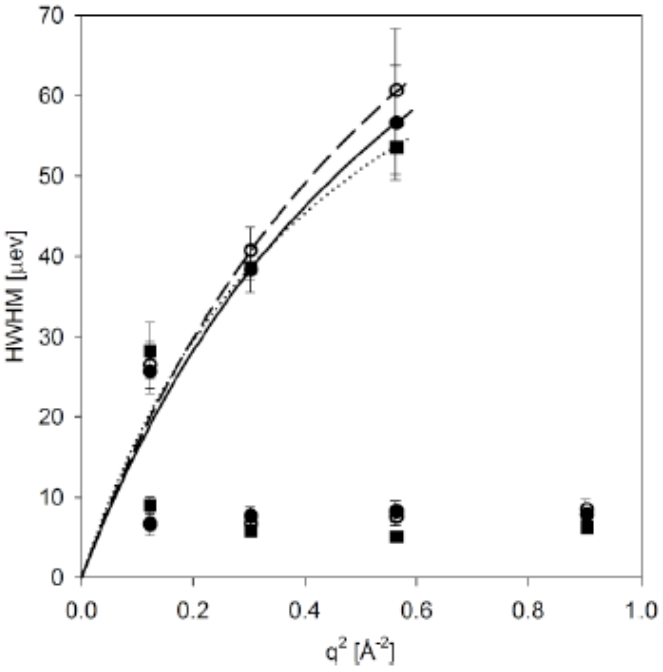
70
60
50
40
30
20
10
0
HWHM [μev]
0.0
0.2
0.4
0.6
0.8
1.0
q² [Å⁻²]

Figure 7. Schematic drawing of thylakoid membrane organization in cyanobacterial cells from SANS data and TEM analysis. Different membrane and phycobilisome arrangements are numbered 1-5 to correlate with SANS peaks: 1, center-to-center repeat distance between thylakoid membrane pairs, shown with WT phycobilisomes; 2, repeat distance between thylakoid membrane pairs insufficient for phycobilisomes; 3, repeat distance originating from closely appressed thylakoid membrane pairs; 4 and 5, repeat distance originating from a single thylakoid membrane layer with lumen of varying size.

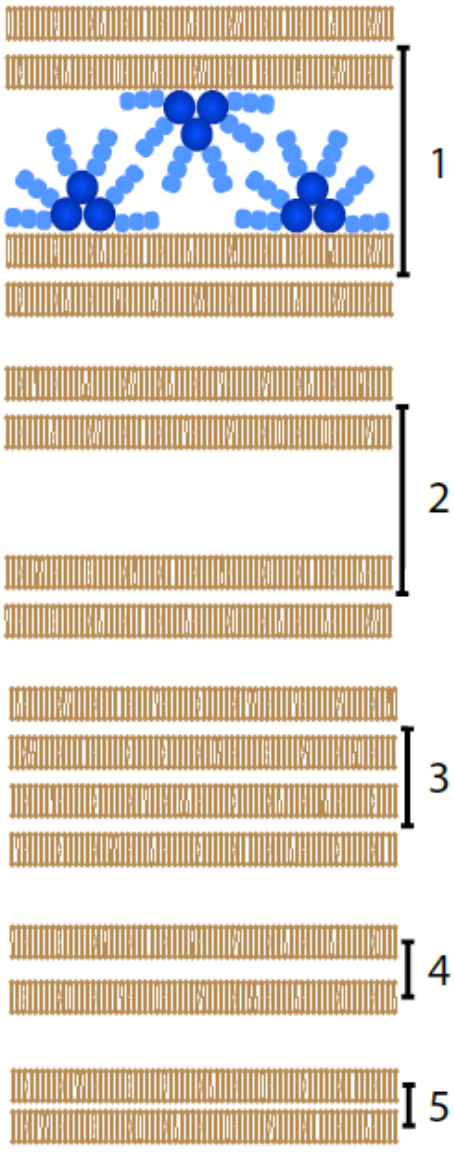
1
2
3
4
5

Chapter 4

Reduction of Photoautotrophic Productivity in the Cyanobacterium *Synechocystis* sp. Strain PCC 6803 by Phycobilisome Antenna Reduction

Introduction

In oxygenic photosynthesis, two enzymes, photosystem I (PSI) and photosystem II (PSII), are capable of harvesting light and using it to drive photochemistry. In all known oxygenic photosynthetic organisms, there exist antenna complexes that harvest light and transfer the energy to the photosystems (Green and Parsons, 2002). These antenna complexes provide a competitive advantage to wild-type (WT) organisms competing for light energy (Melis, 2009). In biotechnological applications, however, photosynthetic organisms are grown in dense monoculture, where antenna complexes are thought to cause inefficient use of available light energy. This is because the organisms at the surface of incident light are quickly saturated and must dissipate excess energy by wasteful non-photochemical processes, and organisms at the surface of the incident light shade those below (Ort *et al.,* 2011).

In the green alga *Chlamydomonas reinhardtii*, the partial reduction of antenna complex pigment content has been shown to improve biomass and hydrogen production. Partial chlorophyll reduction mutants CR-118 and CR-133 grow more quickly and accumulate more biomass than WT (Perrine *et al.,* 2012). The *stm6Glc4T7* mutant, with a 15% reduction in the light harvesting antenna system, was found to be more efficient at converting light to biomass than the *stm6Glc4* parent strain (Beckmann *et al.,* 2009). The *tla1* mutant showed chlorophyll content reduction of 50% in PSI and 65% in PSII (Polle *et al.,* 2003) and increased hydrogen production over the parent strain CC-425 (Kosourov, *et al.,* 2011). Antenna truncation has yet to be explored for biomass production in cyanobacteria.

In the model cyanobacterium *Synechocystis* sp. PCC 6803 (*Synechocystis* 6803), the light harvesting antenna complex is the phycobilisome (PBS), a large membrane-extrinsic hemidiscoidal pigment protein complex (Gantt and Conti, 1966). The PBS is made of a

horizontally-oriented stacked cylindrical core complex from which six rods radiate (Elmorjani *et al.,* 1986). The allophycocyanin (APC) core is made of trimeric α and β $(\alpha^{APC}\beta^{APC})_3$ heterodimers, and the phycocyanin (PC) rods are composed of hexameric $(\alpha^{PC}\beta^{PC})_6$ heterodimers. Several colorless linker proteins connect the rods to the core and the core to the cytoplasmic side of the thylakoid membrane (Capuano *et al.,* 1991; Capuano *et al.,* 1993; Sidler, 1994).

In this work, WT *Synechocystis* 6803 and three previously described mutants(CB, CK, and PAL) that express a series of increasingly truncated phycobilisomes were examined for changes in photoautotrophic productivity. The CB mutant was generated by disruption of the *cpcC1* and *cpcC2* genes (which encode the phycobilisome rod linkers), and as a result the phycobilisomes in this mutant strain contain only one phycocyanin hexamer per rod, instead of three (Ughy and Ajlani, 2004). Another mutant, CK, was generated by disruption of the *cpcA* and *cpcB* genes (which encode the phycocyanin α and β subunits), as well as *cpcC1* and *cpcC2*. CK has no phycocyanin rods but retains the allophycocyanin core (Thomas *et al.,* 2006). The PAL mutant was generated by inactivation of *apcE* gene, encoding the core-membrane linker (Capuano *et al.,* 1991; Capuano *et al.,* 1993), and *apcAB* genes, which encodes α^{APC} and β^{APC} subunits, in a PMB11 mutant background, which lacks phycocyanin (Elmorjani *et al.,* 1986). As a result, PAL lacks phycobilisomes entirely (Ajlani and Vernotte, 1998). Together with the wild type (WT) strain, these strains represent a series of partial and complete antenna truncation mutants in *Synechocystis* 6803.

Here we report the effect of antenna mitigation on biomass productivity, photosynthetic efficiency, and growth rate in *Synechocystis* 6803 WT and the above three phycobilisome antenna mutants in a range of illumination conditions and carbon dioxide concentrations.

Contrary to the findings in algal strains with modified chlorophyll light harvesting antenna, our results show that phycobilisome mitigation in cyanobacteria does not provide an advantage in terms of growth rate or biomass accumulation.

Materials and Methods

Growth and Maintenance of Bacterial Strains. *Synechocystis* 6803 WT and the antenna mutants CB, CK, and PAL were maintained on solid BG11 plates (Allen, 1968) with antibiotic selection (CB and CK, 10 μg/ml kanamycin; PAL, 10 μg/ml chloroamphenicol and spectinomycin) at 30^{O}C under constant 30 μmol photons m^{-2} s^{-1} white fluorescent light. Liquid cultures were inoculated from plates and grown in 250 ml Erlenmeyer flasks containing 100 ml BG11 at 30 ^{O}C in 50 μmol photons m^{-2} s^{-1} light on an orbital shaker maintained at 150 rpm.

Absorption Spectra. Whole cell absorption spectra from cultures growing in photobioreactors were measured using an OLIS DW 2000 spectrophotometer and normalized to the absorbance at 730 nm.

Growth Curves. Liquid cultures in 100 ml BG11 were grown photoautotrophically in 250 ml Erlenmeyer flasks on an orbital shaker at 150 rpm and 30 ^{O}C under white overhead fluorescent lights at 50 μmol photons m^{-2} s^{-1}, with CO_2 provided from ambient air. Growth was determined by daily sampling and measurement of OD_{730} on a BioTek μQuant plate reader. Doubling time was calculated between 0 and 72 hours, when cultures were growing exponentially.

Photobioreactor Specifications. Growth measurements were also carried out in a FMT 150 photobioreactor manufactured by Photon Systems, Inc (Nedbal, *et al.,* 2008). The FMT 150 has an operational volume of 350 ml, and uses blue (455 nm) and red (627 nm) light emitting diodes (LEDs) as the light source. Light delivery has been optimized so that the path length of this flat panel system is a uniform 2 cm. Growth was measured by the integrated densitometer, which

measures changes in optical density at 735 nm (Nedbal *et al.,* 2008). A Mettler-Toledo Clark-type oxygen electrode, integrated into the photobioreactor, was calibrated to measure dissolved oxygen concentrations at the micromolar level and allowed for precise determination of maximum photosynthetic capacity, and respiration on a daily basis (Červený *et al.,* 2009). A custom CO_2 mixing system from Qubit Systems Inc. precisely controlled the CO_2 input rate and concentration.

Growth in Photobioreactors. Prior to photobioreactor inoculation, *Synechocystis* 6803 WT, CB, CK, and PAL cultures were started from plates into 100 ml liquid BG11 media in 250 ml Erlenmeyer flasks with appropriate antibiotics. Upon reaching mid-log phase, cultures were pelleted and resuspended in 5 ml of fresh BG11 and transferred to the photobioreactors. Cultures were then adapted to illumination and CO_2 conditions in continuous turbidostat mode at OD_{735}=0.3 for 3 days. Day 0 samples of batch mode experiments were taken at the end of the continuous mode growth period, and marked the transition to batch-mode growth. During the growth measurements, manual biomass samples were taken daily.

Culture samples and oxygen evolution data were collected daily during the growth curve in Figure 4. An integrated Mettler-Toledo Clark-type oxygen electrode was used to determine respiration (R), photosynthetic oxygen evolution (P), and saturated photosynthetic capacity (Psat) for the entire culture (Červený *et al.,* 2009). Briefly, R is determined by measuring the rate of oxygen consumption in the dark. P is determined by measuring the rate of oxygen evolution with lights set at experimental level and adding R. Psat is determined by using strong actinic light (700 μmol photons m^{-2} s^{-1} red and 600 μmol photons m^{-2} s^{-1} blue) to drive oxygen

evolution, and adding R. These values reflect productivity parameters for the entire culture *in situ*.

Sample Measurements. Biomass accumulation in the photobioreactors was measured by weight before and after oven drying 5 ml samples of liquid culture in aluminum dishes for 24 hours at 105 ^{O}C. Cell count was determined on a Nexcelom Auto M10 cell counter. Chlorophyll and phycobilin concentration was determined spectroscopically (Lichtenthaler, 1987, Porra *et al.,* 1989).

Results

Synechocystis *sp. PCC 6803 phycobilisome antenna mutants.* Whole-cell absorption spectra of the three mutant strains compared to WT is shown in Figure 1, and agrees with previous findings (Collins *et al.,* 2012). The mutant strains show decreasing absorption in the principal phycobilisome peak at ~625 nm. In the CK mutant, which is devoid of phycocyanin, the allophycocyanin shoulders at 590 and 660 become visible (Stadnichuk *et al.,* 2009). In the PAL mutant, the dip at 650 nm indicates a lack of allophycocyanin, which makes up the phycobilisome core, as has been previously reported (Bernát *et al.,* 2009). Additionally, decreasing antenna size correlates to an increase in carotenoid absorption, seen in the shoulder at 490 nm (Bernát, *et al.,* 2009).

Growth comparison of WT and antenna mutants. In order to compare the productivity of WT and the antenna mutants under conditions of intermediate light and extended path length, we grew cells in 250 ml Erlenmeyer flasks and measured OD_{730} at 72-hour intervals. We hypothesized that the antenna mutants might show an initial growth penalty, but might reach a higher stationary phase cell density. Thus growth measurements were extended out to 16 days. The growth profiles under these conditions are shown in Figure 2. The calculated doubling times during the exponential phase of growth (0-72 hours) under these conditions were found to be 25.2±0.5 hours (WT), 22.8±1.1 hours (CB), 29.0±0.5 hours (CK), and 44.9±0.5 hours (PAL). The slower growth for the antenna mutants that we observed is consistent with previous studies on these strains (Bernát *et al.,* 2009). Importantly, in addition to slower growth rates, the antenna mutants also achieved lower culture densities compared to WT from exponential into stationary phase, never exceeding the cell density of WT (Figure 2). This means that under these

illumination conditions, WT excels at photoautotrophic light utilization compared to the antenna mutants.

Growth in bench-scale photobioreactors. To test the effect of antenna mitigation on biomass productivity under optimized conditions, batch-mode growth curves were performed in 350 ml bench-scale photobioreactors. In the photobioreactors, the optical path length is 2 cm, considerably less than in flasks. The photobioreactors were intentionally designed for this path length, as light penetration drops significantly past this point due to scattering, especially for red wavelengths (Ort *et al.,* 2011), according to the Beer-Lambert Law. Additionally, the photobioreactors were designed to precisely control and monitor environmental conditions, enabling a wide range of lighting and CO_2 conditions to be tested to achieve repeatable, consistent batch-mode growth rates.

Initial growth curves were designed to determine conditions under which both WT and the most severe phycobilisome mutant, PAL, could consistently grow and reach stationary phase. Ambient air was bubbled at 350 ml/min and growth was measured by the change in OD_{735} using the integrated densitometer in the photobioreactor. However, all initial experiments were unsuccessful in achieving stationary phase growth using the PAL mutant because the pH increase that accompanies cell growth in batch-mode cyanobacterial cultures (de Vrind-de Jong and de Vrind, 1997; Lucas, 1983) was found to be toxic to the PAL culture (Figure 3). The pH at which growth ceased was consistently ~10.3. This pH is significant in cyanobacterial cultures, because it is the level at which the predominant carbon species in the medium becomes carbonate. To correct pH toxicity, 5% CO_2 was bubbled at a rate of 350 ml/min.

Light intensities of 100 μmol photons m^{-2} s^{-1} blue and 50 μmol photons m^{-2} s^{-1} red together were determined to be optimal because the cultures showed a significantly higher doubling time over that in Erlenmeyer flasks. In addition, less red light was supplied (which prevents heavy bias towards WT growth, as phycobilin absorption is primarily in the red wavelengths), and no special treatment of the cells was necessary to achieve repeatable growth curves. Higher light intensities were tested, but both WT and mutant cultures grew sporadically or photobleached before the start of the experiment (during the 3 day adaptation period of continuous-mode growth at OD_{735}=0.3). Therefore, a 5% CO_2 bubbling rate of 350 ml/min and light intensity of 100 μmol photons m^{-2} s^{-1} blue and 50 μmol photons m^{-2} s^{-1} red were used to generate the data in Figure 3 and Table 1.

Discussion

In *Synechocystis* 6803, a number of mutants with modified phycobilisome antenna have been generated, but not comprehensively studied and compared in terms of productivity. In the present work, we have analyzed the antenna mutants CB, CK, and PAL under different light conditions and CO_2 concentrations, and compared them directly to WT. Contrary to the results obtained in green algae, it appears phycobilisome antenna truncation provides a clear productivity advantage to the cyanobacterial monocultures.

In typical laboratory conditions (Figure 2) of 50 μmol photons*m^{-2}*sec^{-1} cool white fluorescent light, 30^{O}C, in a 250 ml erlenmeyer flask, the path length of the light is longer than in the optimized photobioreactors. There, the reduction in self-shading and surface saturation would be expected to result in a higher stationary phase OD730 in the antenna mutants. This was not the case, however, as the antenna mutants grew progressively more slowly and reached a lower stationary phase than WT. Calculated doubling times were 25.2±0.5 hours (WT), 22.8±1.1 hours (CB), 29.0±0.5 hours (CK), and 44.9±0.5 hours (PAL). The fact that CB grew slightly faster than WT during exponential phase shows that there may be a minor growth advantage conferred at low cell densities, but this effect does not manifest in a higher stationary phase.

The fact that the PAL mutant photobleached (Figure 3) in high light when air was the carbon source, while WT consistently reached stationary phase, suggests that there are other consequences to phycobilisome modification in *Synechocystis* 6803. Additional evidence for this already exists, as hyperspectral confocal fluorescence microscopy has been used to demonstrate changes in photosynthetic pigment localization in these mutants and transmission

electron micrographs have revealed changes to the overall thylakoid membrane architecture (Collins *et al.,* 2012, Liberton *et al.,* 2012).

The other two mutant strains, CB and CK, could grow repeatably in the optimized photobioreactor in 5% CO_2. There, however, growth rate and achieved stationary phase was correlated to the severity of antenna truncation. Calculated doubling times were 13.76±0.48 hours (WT), 19.79±0.33 hours (CB), and 28.14±1.53 hours (CK). In addition to slower growth, in all parameters tested (Table 1) there is a penalty, rather than an advantage, to PBS antenna truncation in these mutants.

To our knowledge, this study is the first to systematically examine the productivity of cyanobacterial phycobilisome antenna mutants, with the goal of determining whether antenna mitigation confers an advantage to these organisms, and to compare these findings to those from algal systems. These data from cyanobacteria can then be used as a baseline to which subsequent analyses can be compared, as pigment concentration, biomass accumulation, and changes in optical density are all reported. Even the least severe of the antenna mutants does not show significant improvements in growth as determined by optical density, and therefore, antenna truncation does not provide a productivity advantage in any of the conditions tested.

References

Ajlani, G. and C. Vernotte. 1998. Construction and characterization of a phycobiliprotein-less mutant of *Synechocystis* sp. PCC 6803. *Plant Mol. Biol*. 37:577-580.

Allen, M. M. 1968. Simple conditions for the growth of unicellular blue-green algae on plates. *J. Phycol.* 4:1-4.

Beckmann, J., F. Lehr, G. Finazzi, B. Hankamer, C. Posten, L. Wobbe, O. Kruse. 2009. Improvement of light to biomass conversion by deregulation of light harvesting protein translation in *Chlamydomonas Reinhardtii*. *J. Biotechnol*. 14: 70-77.

Bernát, G., N. Waschewski, and M. Rögner. 2009. Towards efficient hydrogen production: the impact of antenna size and external factors on electron transport dynamics in *Synechocystis* PCC 6803. *Photosynth. Res.* 99:205-216.

Capuano, V., A. Braux , N. Tandeau de Marsac , and J Houmard. 1991. The 'anchor polypeptide' of cyanobacterial phycobilisomes. Molecular characterization of the *Synechococcus* sp. PCC 6301 *apcE* gene. *J. Biol. Chem*. 266: 7239–7247.

Capuano, V., J-C. Thomas, N. Tandeau de Marsac , and J. Houmard. 1993. An *in vivo* approach to define the role of the LCM , the key polypeptide of cyanobacterial phycobilisome. *J. Biol. Chem*. 268: 8277–8283.

Červený, J., I. Šetlík, M. Trtílek, and L. Nedbal. 2009. Photobioreactor for cultivation and real-time, in-situ measurement of O_2 and CO_2 exchange rates, growth dynamics, and of chlorophyll fluorescence emission of photoautotrophic microorganisms. *Eng. Life. Sci*. 9,3: 247-253.

Collins, A. M., Liberton, M., Garcia, O. F., Jones, H. D. T., Pakrasi, H. B., and Timlin, J A. 2012. Photosynthetic pigment localization and thylakoid membrane morphology are altered in *Synechocystis* 6803 phycobilisome mutants. *Plant Physiol.* 158, 4:1600-1609.

de Vrind-de Jong, E., and J. de Vrind. 1997. Algal Deposition of Carbonates and Silicates, p 267-307. *In* J. Banfield and K. Nealson (ed.), Geomicrobiology: Interactions Between Microbes and Minerals. Mineralogical Society of America, Washington, D. C.

Gantt, E., and S. F. Conti. 1966. Phycobiliprotein localization in algae. *Brookhaven Symp. Biol.* 19: 393-405.

Green, B. R. and W. W. Parson (ed). 2003. Light-Harvesting Antennas. Kluwer Academic Press, Dordrecht, The Netherlands.

Hai, T., H. Ahlers, V. Gorenflo, and A. Steinbuchel. 2000. Axenic cultivation of anoxygenic phototrophic bacteria, cyanobacteria, and microalgae in a new closed tubular glass photobioreactor. *Appl. Microbiol. and Biotechnol*. 53:383-389.

Kosourov, S. N., M. L. Ghirardi, and M. Seibert. 2011. A truncated antenna mutant of *Chlamydomonas reinhardtii* can produce more hydrogen than the parent strain. *Int. J. Hyd. Energy*. 36: 2044-2048.

Liberton, M., Page, L. E., O'Dell, W. M. B., O'Neill, H., Mamontov, E., Urban, V. S., and Pakrasi, H. B. (2012) Organization and Flexibility of Cyanobacterial Thylakoid Membranes Examined by Neutron Scattering. *J. Biol. Chem.* Submitted.

Lichtenthaler, H. 1987. Chlorophylls and Carotenoids: Pigments of Photosynthetic Biomembranes. *Methods in Enzymol.* 148:350-382.

Lucas, W. J. 1983. Photosynthetic assimilation of exogenous HCO3- by aquatic plants. *Ann. Rev. Plant. Physiol*. 33:71-104.

Melis, A. 2009. Solar energy conversion efficiencies in photosynthesis: Minimizing the chlorophyll antennae to maximize efficiency. *Plant Science.* 177:272-280.

Nedbal, L., M. Trtílek, J. Červený, O. Komárek, and H. B. Pakrasi. 2008. A precision photobioreactor system for precise cultivation of photoautotrophic microorganisms and for high content analysis of suspension dynamics. *Biotechnol. and Bioeng*. 100, 5:902-910.

Ort, D., X. Zhu, and A. Melis. 2011. Optimizing Antenna Size to Maximize Photosynthetic Efficiency. *Plant Physiol*. 155:79-85.

Perrine, Z., Negi, S., and Sayre, R. T. 2012. Optimization of Photosynthetic Light Utilization by Microalgae. *Algal Res.* 1, 2: 134-142.

Polle, J. E. W., S-D. Kanakagiri, and A. Melis. 2003. *tla1,* a DNA insertional transformant of the green alga *Chlamydomonas reinhardtii* with a truncated light-harvesting chlorophyll antenna size. *Planta*. 217: 49-59.

Porra, R. J., Thompson, W.A., and Kriedemann, P.E. 1989. Determination of accurate extinction coefficients and simulatneous equations for assaying chlorophylls a and b extracted with four different solvents: verification of the concentration of chlorophyll standards by atomic absorption spectroscopy. *Biochim. Biophys. Acta.* 975: 384–339.

Sidler, W. A. 1994. Phycobilisome and Phycobiliprotein Structures, p. 139-216. *In* D. A. Bryant (Ed.), The Molecular Biology of Cyanobacteria. Kluwer Academic Publishers, Dordrecht, The Netherlands.

Stadnichuk, I. N., E. P. Lukashev, and I. V. Elanskaya. 2009. Fluorescence changes accompanying short-term light adaptations in photosystem I and photosystem II of the cyanobacterium *Synechocystis* sp. PCC 6803 and phycobiliprotein-impaired mutants:

State 1/State 2 transitions and carotenoid-induced quenching of phycobilisomes. *Photosynth. Res*. 99: 227-241.

Thomas, J. C., B. Ughy, B. Lagoutte, and G. Ajlani. 2006. A second isoform of the ferredoxin:NADP oxidoreductase generated by an in-frame initiation of translation. *PNAS* 103, 48:18368-18373.

Ughy B., and G. Ajlani. 2004. Phycobilisome rod mutants in *Synechocystis* sp. PCC 6803. *Microbiol*. 150:4147-4156.

Table 1: Productivity parameters for cells at exponential (24 hours) and stationary (192 hours) phases of growth.

	Result at time point for strain					
	24 h			120 h		
Parameter	WT	CB	CK	WT	CB	CK
Respiration (R; μmol O_2/ml/h)	0.087 ± 0.006	0.075 ± 0.005	0.088 ± 0.007	0.158 ± 0.004	0.155 ± 0.002	0.142 ± 0.007
Photosynthetic O_2 evolution (P; μmol O_2/ml/h)	0.808 ± 0.210	0.562 ± 0.117	0.448 ± 0.054	0.699 ± 0.101	0.588 ± 0.092	0.633 ± 0.156
Saturated photosynthetic O_2 evolution (P_{sat}; μmol O_2/ml/h)	2.284 ± 0.198	1.155 ± 0.194	1.497 ± 0.143	2.436 ± 0.110	1.782 ± 0.252	1.570 ± 0.242
Cell concn (10^{-8} cells/ml)	3.62 ± 0.589	3.37 ± 0.185	1.82 ± 0.21	12.90 ± 1.52	13.03 ± 2.64	9.85 ± 1.18
Biomass concn (mg/ml)	4.70 ± 0.092	4.63 ± 0.069	4.63 ± 0.09	5.80 ± 0.10	5.52 ± 0.09	5.36 ± 0.03
Chlorophyll concn (μg/ml)	7.60 ± 0.918	4.97 ± 0.687	4.37 ± 1.04	32.06 ± 5.79	22.32 ± 1.71	16.42 ± 1.32
Phycobilin concn (μg/ml)	59.43 ± 7.72	19.92 ± 3.37	5.84 ± 1.65	210.91 ± 37.50	92.98 ± 11.92	18.98 ± 3.13

Figure 1. Whole-cell absorption spectra of WT, CB, CK, and PAL strains are represented as black, blue, green, and red traces, respectively. Spectra were corrected with BG11 only baseline and cultures were normalized to the same A_{730}.

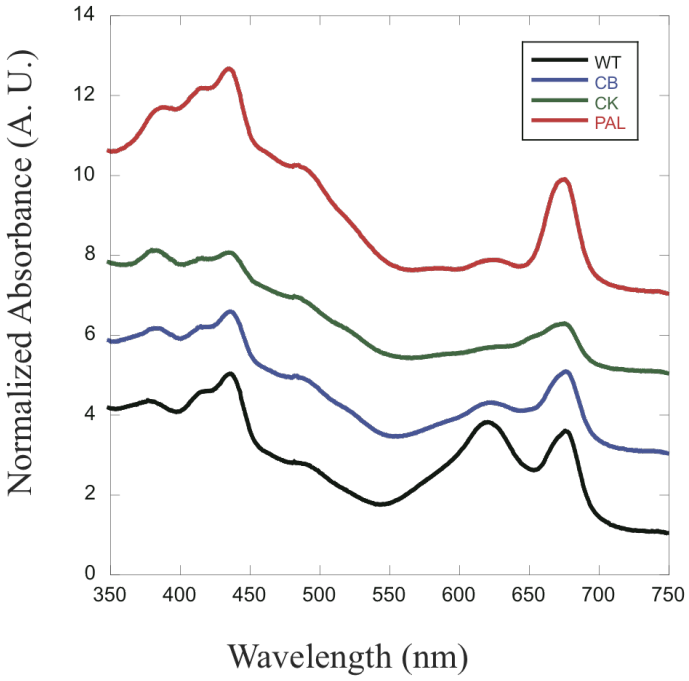
Normalized Absorbance (A. U.)
Wavelength (nm)
WT
CB
CK
PAL
0
2
4
6
8
10
12
14
350
400
450
500
550
600
650
700
750

Figure 2. Growth of WT, CB, CK, and PAL in Erlenmeyer flasks at 30°C in ambient air and 50 μmol photons*m^{-2}*s^{-1} from cool white fluorescent lights. Error bars indicate the standard errors of three biological replicates. When error bars cannot be seen, the error was smaller than the size of the symbol.

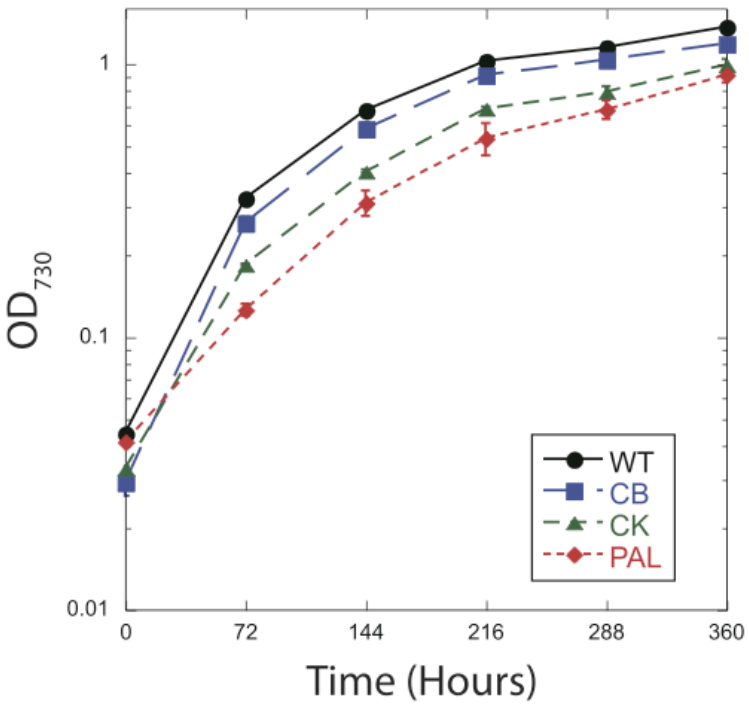
1
0.1
0.01
OD730
0
72
144
216
288
360
Time (Hours)
WT
CB
CK
PAL

Figure 3. Representative growth curves of WT and PAL cultures grown in the FMT-150 photobioreactor with air bubbling at 350 ml per minute, 100 μmol photons*m^{-2}*s^{-1} blue light and 50 μmol photons*m^{-2}*s^{-1} red light, and 30°C.

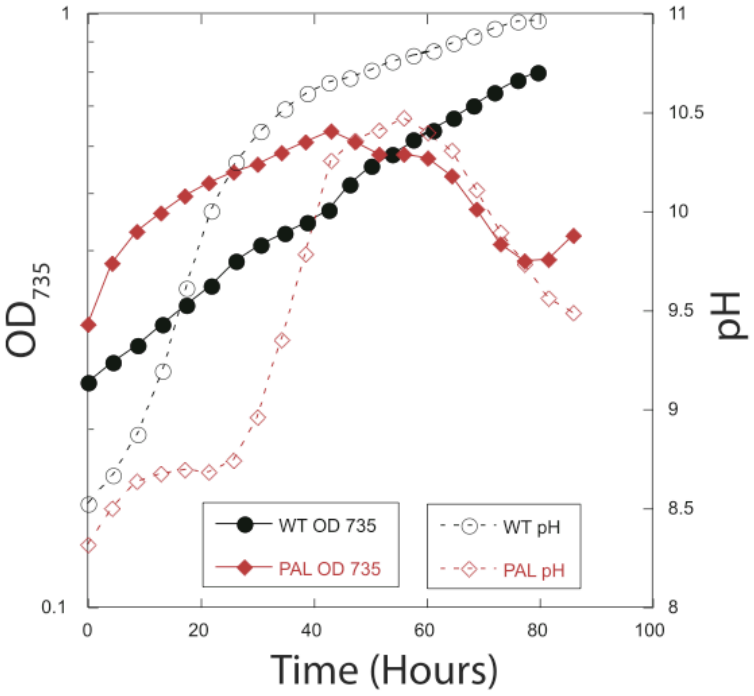
1
0.1
OD735
11
10.5
10
9.5
9
8.5
8
pH
0
20
40
60
80
100
Time (Hours)
WT OD 735
PAL OD 735
WT pH
PAL pH

Figure 4. Cultures grown in the FMT-150 photobioreactor with 5% CO_2 bubbling at 350 ml per minute, 100 μmol photons*m^{-2}*s^{-1} blue light and 50 μmol photons*m^{-2}*s^{-1} red light, and 30°C. Doubling times were calculated from the OD735 during the exponential growth phase. Error bars indicate standard errors for three biological replicates. When error bars cannot be seen, the error was smaller than the size of the symbol.

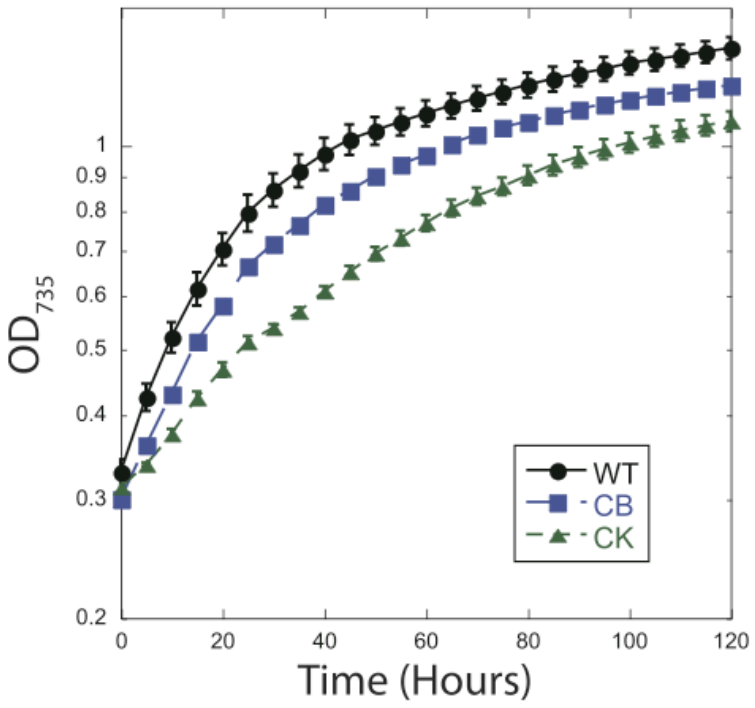
OD735
1
0.9
0.8
0.7
0.6
0.5
0.4
0.3
0.2
0
20
40
60
80
100
120
Time (Hours)
WT
CB
CK

Chapter 5

Conclusion and Future Directions

Introduction

Photosynthetic microbes survive, as do all organisms, by out-competing others for scarce resources found in their native environment. For autotrophs, light is the most important of resources, and as a result, any innovations that provide a competitive advantage in harvesting light should be pervasive. This is true of the light harvesting antenna complex, as there has been wide structural variation found in photosynthetic microbes, all of which contain a variation on a complex that performs the same basic function: improving the efficiency of light energy delivery to the photosystems (Green and Parson, 2003).

The antenna complexes found in the wild have evolved to be very efficient, even at low light intensities. Efficient antenna are advantageous for a variety of reasons, the most important of which is that in many settings, light is a relatively dilute nutrient (Blankenship, 2002). Efficient antenna complexes allow for photosynthesis earlier in the morning and later at night, and in aquatic organisms located below the water's surface. These large, efficient antenna complexes also shade a competitor situated below from light, which provides another competitive advantage (Ort *et al.,* 2011). The downside to antenna setups like this is that they lead to light saturation when intensities are high, such as during the middle of the day and at the surface of incident light. Despite the saturation issues, efficient antenna complexes still provide clear advantage to an individual photosynthetic organism.

In a monoculture setting, however, the goal is to maximize the amount of light utilized by the entire culture, not just the individual organism. In this scenario, shading and light saturation both represent a waste of light energy, and thus should be minimized. One way of doing this is to optimize the light harvesting antenna complexes so as to decrease the amount of light absorbed by an individual organism while increasing the light absorbed by the culture as a

whole. This is precisely the strategy pursued successfully in green algae. There, partial reduction in pigment content of the individual organism's light harvesting antenna has been shown to effectively increase light harvesting by the whole culture. This effect is manifested as an increased biomass and hydrogen productivity over wild-type (WT) organisms at high light intensity (Beckmann, *et al.,* 2009; Kosourov *et al.,* 2011; Melis, 2009; Perrine *et al.,* 2012, Polle *et al.,* 2003).

Antenna reduction in *Synechocystis* sp. PCC 6803

One outstanding question remaining from the studies carried out in green algae is whether antenna reduction can be applied to photosynthetic organisms in general, or whether observed productivity increases are due to aspects that are unique to green algal light harvesting antenna complexes. In this thesis, the model cyanobacterium *Synechocystis* sp. PCC 6803 (*Synechocystis* 6803) has been used to test whether an existing set of partial and complete antenna mitigation mutants improve biomass productivity over WT.

In shake flasks (Chapter 3), where the path length is long enough for self shading to be prevalent, only the partial antenna mutant CB, which expresses phycobilisome rods of only one hexamer instead of the natural three, is there any hint of an improvement (Chapter 3, Figure 2). There, CB grows with a ~10% increase in doubling time over WT. None of the antenna mutants, however, can reach a higher stationary phase than WT, indicating that despite a decrease in culture-wide shading, the antenna mutants do not use light more effectively than WT at high cell density.

Perhaps more importantly, the mutants show more severe growth difficulty in an optimized bench-scale photobioreactor. There, the path length is 2 cm, and the light source is

red and blue LED's optimized for delivery of photosynthetically active radiation. In this setting, the PAL mutant, with complete PBS antenna removal, cannot grow repeatably in either air (Chapter 3, Figure 3) or high CO_2 (not shown). The intermediate antenna mutants can survive in high light and CO_2 (Chapter 3, Figure 4), but grow more slowly than WT, and again, cannot achieve the same stationary phase. Therefore, partial and complete PBS antenna reduction reduced photoautotrophic productivity in a variety of conditions.

Why there is a decrease in productivity in these antenna mutants becomes apparent when taking a deeper look at the physiological consequences of antenna modification on photosystm II (PSII) (Chapter 2) and the thylakoid membranes (Chapter 3). In the antenna mutants, there is a gradual increase in active PSII expression (Chapter 2, Figure 1, 2, and 3) as antenna size decreases. This is presumably how the organisms compensate for the decrease in delivery of light energy to PSII. Accompanying this decrease in light delivery is difficulty in S-state turnover (Chapter 2, Figure 4) and delivery of absorbed charge (Chapter 2, Figure 5). Accompanying these protein level changes in PSII expression and function is the decrease in membrane curvature (Chapter 3, Figure 1) and spacing (Chapter 3, Figure 1 and 3), as seen by both eletron microscopy and small angle neutron scattering. Overall, therefore, the antenna mutants show increasingly detrimental physiological changes that accompany PBS truncation and removal.

One important observation that arises when considering all of the data as a whole is the fact that CB, the least severe antenna mutant, does show a slight increase in growth rate in erlenmeyer flasks (Chapter 4, Figure 2), and a nearly WT behavior in a lot of the physiological parameters measured. This includes similar S-state turnover abilities, in terms both of oxygen evolution and fluorescence, and nearly WT membrane curvature. The possible reason partial

removal of only the PBS rods is not as physiologically challenging to *Synechocystis* 6803 is that in nitrogen deprivation, an orderly degradation of the rods, resulting in a similar situation to the CB mutant, occurs to provide the nitrogen necessary for survival. Therefore, there may already be mechanisms in place for *Synechocystis* 6803 to compensate for partial rod truncation.

Future directions

Synthetic biology is rapidly causing a paradigm shift in the way organisms are optimized for use in biotechnology, as the ability to edit large portions of an organisms genome allows researchers to make changes that are only limited by their own imagination. For the optimization of photosynthetic organisms specifically, this will usher in a new era of genetically-modified microbes that harvest a larger portion of the visible spectrum and divert more of that energy towards production of the desired product. To accomplish this will require modification of both the native metabolism and the light harvesting systems of the wild-type organism.

As discussed above, the partial truncation of PBS rods in the CB mutant does not cause the pervasive difficulties seen in CK and PAL. Therefore, if antenna truncation is to be pursued further in cyanobacteria, using CB as a starting point could provide productivity increases over WT if additional mutations are added. However, due to the physiological changes observed in all of the antenna mutants, it may make more sense to go the opposite direction in cyanobacteria. For example, one could generate strains that harvest as much light as possible by inserting genes for another light harvesting antenna, or modify the phycobilisome to be even more efficient, and then make mutations in the photosystems that allow for the utilization of this absorbed energy. Synthetic biology will allow for even more imaginative mutations to be tested. For example, the

addition of entirely new photosystems, synthetically designed photoenzymes, or a novel form of photosynthesis are all possibilities in the future.

References

Beckmann, J., F. Lehr, G. Finazzi, B. Hankamer, C. Posten, L. Wobbe, O. Kruse. (2009) Improvement of light to biomass conversion by deregulation of light harvesting protein translation in *Chlamydomonas Reinhardtii*. *J. Biotechnol.* 14: 70-77

Blankenship, R. E. (2002) *Molecular Mechanisms of Photosynthesis*. Blackwell Science, Oxford, UK.

Green, B. R. and Parson, W. W. (2003) (Eds) *Light-Harvesting Antennas in Photosynthesis.* Kluwer Academic Press, Dordrecht, The Netherlands

Kosourov, S. N., M. L. Ghirardi, and M. Seibert. (2011) A truncated antenna mutant of *Chlamydomonas reinhardtii* can produce more hydrogen than the parent strain. *Int. J. Hyd. Energy*. 36: 2044-2048

Melis, A. (2009) Solar energy conversion efficiencies in photosynthesis: Minimizing the chlorophyll antennae to maximize efficiency. *Plant Science*. 177:272-280

Ort, D., Zhu, X., and Melis, A. (2011) Optimizing Antenna Size to Maximize Photosynthetic Efficiency. *Plant Physiol.* 155:79-85

Perrine, Z., Negi, S., and Sayre, R. T. (2012) Optimization of photosynthetic light energy utilization by microalgae. *Algal Res.* 1, 2: 134-142

Polle, J. E. W., S-D. Kanakagiri, and A. Melis. (2003) *tla1,* a DNA insertional transformant of the green alga *Chlamydomonas reinhardtii* with a truncated light-harvesting chlorophyll antenna size. *Planta*. 217: 49-59

Appendix Chapter 1

Algal Technologies for Biological Capture and Utilization of CO_2 Require Breakthroughs in Basic Research

Summary

To fully offset the carbon emitted from anthropogenic sources, taking into account the 55% that are captured by enhanced biological and physical processes in the global carbon cycle, an additional 4 Gigatons (Gt) of carbon must be captured per year, and that number is likely to increase. Options for technology that can capture such an immense amount of carbon in the near term are limited. There are real opportunities for achieving significant reductions in CO_2 emissions in the algal field but the current state of research is still very much in the realm of basic science and much needs to be done before we can think about it in technological terms. Biological capture by photosynthetic microbes is an attractive technology because it is renewable, scalable, and may be used to produce fuels and chemicals cheaply. Identification of novel, robust strains, and breakthroughs in bioreactor design and harvesting/extraction technology, are necessary to realize this goal. This chapter, and the workshop from which it is derived assesses the productivity and carbon capture capacity of photosynthetic microbes and outlines the areas in which there are opportunities to achieve significant reductions in CO_2 emissions.

Introduction

The estimated anthropogenic contribution to the carbon cycle in the form of CO_2 released into the atmosphere is approximately 9 Gigatons (Gt) per year. Approximately 7.6 Gt of this is from fossil fuels and 1.4 Gt from land-use change. While as much as 55% of this carbon is absorbed by natural processes, up to 4 Gt are deposited in the atmosphere every year (Lal, 2008).

As much as 65% of this anthropogenic contribution to atmospheric carbon comes from large stationary sources globally, many of these being coal fired-power plants that provide the base-load of electricity demand. In the U.S., these sources supply 60% of electricity and this demand is expected to grow over the next 20 years. If coal is to remain the primary resource for electricity generation in the U.S., carbon emissions are also set to grow.

By the year 2025, 100 GW of new coal-fired steam electricity is expected to be online in the U.S. alone. New plants are expected to be more efficient, making use of integrated gasification combined cycle (IGCC) technology, however the U.S. will still likely rely on the existing fleet of pulverized coal fired power plants as well. These currently supply the base-load electricity, 320 GW capacity and 1,900 billion Kilo-watt hours per year, which is difficult at this time to replace completely by renewable resources.

Carbon capture and storage (CCS) technologies can be used to mitigate these carbon emissions that would otherwise be released to the atmosphere. CO_2 generated in concentrated streams by the combustion of fossil fuels, as in the flue gas from power plants and exhaust gas from cement and steel manufacturing processes, can be captured and sequestered. Additionally, some CCS technologies can capture and sequester atmospheric CO_2. The prevalent use of coal combustion for electricity generation is driving much of the demand for CCS technologies, however some estimates predict the costs of CCS technology to be economically attractive only

after the year 2030, making implementation at a large scale unlikely in the near term (Herzog, 2009).

Photosynthetic biological systems have the potential to make a significant impact in the carbon capture area. In particular, photosynthetic microbes are an attractive option for biological CCS because they have the ability to capture CO_2 , and use the energy in sunlight to store this carbon in forms useful to humans such as fuels, food additives, and medicines. The fact that many algae can have a doubling time of as little as 4 hours makes accumulation of biomass and production of useful molecules realistic on an industrial scale.

To use algae as a carbon capture technology however, a number of important limitations need to be overcome.

Current designs for amine scrubbing for removal of CO_2 from flue stream of coal-fired power plants assume that 90% of the CO_2 is removed (Rochelle, 2009). Algae would need to have the ability to capture as much CO_2 as current CCS technologies are projected to, at similar costs. If less CO_2 is captured by algal technology than by current CCS tecnologies the costs must be significantly lower. The production of biofuels and high value bioproducts would offset the costs of implementing biological organisms as a carbon capture technology as it would in the case of other CCS technologies when fuels are synthesized from the captured CO_2.

Much basic research has been carried out on algae as a production system for fossil fuel alternatives including diesel-like polymers, methane and hydrogen. The U.S. government funded 25 years of research under the Aquatic Species Program (ASP) at the National Renewable Energy Laboratories (NREL), a program that was wound down in 1996, due to lowered price of oil. This research effort led to the isolation of roughly 3000 species of algae that might be useful in this regard (Sheehan *et al*., 1998). Most of these have been lost over the

years due to the absence of culturing necessary to propagate these species. Approximately 300 of these strains have survived and NREL is revisiting the project. Additionally, recent financial investments from the private sector into research towards deployment of algae as a fuel production system indicate that this technology is near the point of profitability. The success stories so far have come mostly from companies producing both fuels and high value products.

As yet, we do not have the means to displace liquid transportation fuels, at scale, with a renewable and sustainable resource. Neither can we capture all of the carbon emitted from stationary fossil fuel sources, by current carbon capture and sequestration methods. The use of algae cultured in non-oceanic environments to capture emissions directly from fossil fuel sources could be a technology that aids in the inexpensive reduction of CO_2 emissions from the energy sector over the coming decades. The ultimate carbon emissions associated with deployment of such a technology would depend on the capacity and efficiency of the algae to capture the carbon and on the use of the stored carbon after capture. When the algae or derived oil is combusted, this stored carbon is again released to the atmosphere. The associated emissions, however, would be offset in part by the algae growth that led to their production, potentially leading to an overall decrease in the amount of anthropogenic carbon released relative to using a fossil source.

Algae produced in this way could be valuable in providing a source for energy dense liquid fuel production not matched currently by other means. The oils derived from algae can be used to produce energy dense fuels such as those used in aviation. Already examples exist where biofuel from algae has been used to power a passenger jet. To meet this demand with another fuel type would be difficult due to the need for a fuel with equivalent energy density to the fossil fuel fuel used currently.

This review discusses the material presented at a workshop held on September 2009 at Washington University in St. Louis. The workshop brought together experts in photosynthesis, bioenergy, microalgae, coal and carbon sequestration to discuss opportunities and challenges in biological CO_2 capture and utilization. The following sections present and discuss these findings and highlight nine game-changing improvements that could enable algae as a carbon capture technology. References to outside and existing literature are made where appropriate to support and help further explain some of the findings.

Game-changing technological improvements

Improvements in delivery, capture, and the metabolic transformation of carbon dioxide into industrially relevant molecules are necessary before algae can be used on a globally significant scale. We feel that the ten topics below are where the largest gains can be made in the near future towards technologies that biologically capture greenhouse gases from fossil fuel sources and contribute to the global energy system.

- Carbon Dioxide Uptake and Utilization
- Light Harvesting Efficiency
- Maximize Biomass Production
- Biofuel/Bioproduct Production
- Bioprospecting and Development of Robust Strains
- Bioreactor Design
- Harvesting and Extraction
- Water Use Efficiency

- Integrated Power Plant Design
- System Analysis

The key limiting factors that can be targeted within each of the above topics are discussed in the following sections.

Overview of photosynthesis, carbon capture and fixation

Algae capture CO_2 and fix it into carbon molecules using photosynthetic processes similar to land plants. The amount of solar energy reaching the earth far exceeds current human energy demand. Photosynthetic organisms have the capacity to harvest a portion of this energy and store it in the form of reduced carbon that can be utilized for both energy and be converted into useful products (Figure 1). There are, however, significant thermodynamic limits imposed on the photosynthetic conversion of sunlight to reduced carbon. The numerous reactions needed to facilitate this process inevitably lead to losses in efficiency.

Photosynthesis begins with absorption of particular wavelengths of light by specialized pigment-protein complexes native to the organism (Figure 2). This absorbed light energy is quickly converted into chemical energy carriers such as NADH and ATP, which fuel subsequent steps in biological carbon capture and fixation. Photosynthetic efficiency is the fraction of total solar radiation that is converted into chemical energy during photosynthesis (Equation 1).

$$2H_2O + CO_2 + \text{energy} \rightarrow CH_2O + H_2O + O_2 \qquad (1)$$

Photosynthetic efficiency is affected by several physical parameters: light intensity, partial pressure of oxygen and CO_2 , temperature, pH and nutrients. However, the degree to which each of these parameters affects a system varies and in some cases will be different between aquatic and terrestrial species.

When all of the losses are summed, the maximal theoretical limit for photosynthetic efficiency at this stage for plants is between 4.6% and 6% for C_3 and C_4 plants, respectively, and 8% for microalgae (Figure 3). C_3 and C_4 plants are distinguished based on metabolism of CO_2. In C_3 plants CO_2 is fixed directly into the three-carbon intermediate 3-phosphoglycerate, whereas in C_4 plants CO_2 is fixed into a four carbon organic acid that is concentrated in specialized carbon fixing tissues. The highest reported efficiencies for C_3 and C_4 plants is about 40% and 60% of the maximum, however, average crop yields fall far below this number (Zhu *et al.,* 2008; Zhu *et al.,* 2010). Assuming a C_3-like metabolism for photosynthetic microbes and minimization of photorespiration by enriching the atmosphere with CO_2 from flue gas, the theoretical efficiency of photosynthesis is 10.6% (from Marcel Janssen, unpublished). In the short term, increasing maximum efficiency may be difficult. During the workshop several interesting ways to increase the maximum efficiencies were discussed and some of these are described under "Light Harvesting Efficiency".

Many factors influence the rate of photosynthesis including light intensity, CO_2 concentration, mass transfer of CO_2 into liquid, temperature, and availability of nutrients. Additionally, the amount of ribulose 1, 5-bisphosphate carboxylase oxygenase (RuBisCO) present in a cell represents an intrinsic limit in the rate of carbon fixation. Other less energy intensive carbon fixation pathways exist in biological organisms and possibly can be used to make the process more efficient. The following sections discuss these factors in more detail.

Carbon Dioxide Uptake and Utilization

As oxygenic photosynthetic organisms, algae are well adapted to capturing ambient CO_2. Growing algae to capture ambient CO_2 will remove carbon dioxide and store it in the form of biomass. Depending on the use of the accumulated biomass, products derived from this process are at best carbon-neutral. Some studies suggest that a 1MW plant facility producing 8323 metric tons of CO_2, or 2269 metric tons C would require a 16 hectare algal bioreactor facility algal facility yielding 80 g dry weight m-2 day-1 or a 64 hectare algal facility yielding 20 g dry weight m-2 day-1 (Ben Hankamer, unpublished).

Bringing a concentrated source of CO_2 , such as the flue gas from a power plant, into contact with algae to increase capture efficiency and productivity has its challenges. Efficiently capturing carbon dioxide from an elevated CO_2 source depends on many factors, but one of the most limiting at present is the ability of the algae to capture and fix carbon at a sufficient rate to avoid acidification of the medium (and thus crash of the culture). Due to this, research is under way to isolate and engineer strains that are tolerant to high CO_2 levels, and are effective at removing large quantities of CO_2 in one pass.

Historically, establishing the limits of carbon uptake and fixation in microalgae represented a major challenge. Green algae can grow at CO_2 concentrations ranging from <=0.01% to > 0.5%. Recent findings in Chlamydomonas indicate that there are typically three tiers of CO_2 concentrations within this range that have distinct carbon concentrating mechanisms (CCMs): very low (< = 0.01%), low (0.03 – 0.4%), and high (> or = 0.5%), (Martin Spalding, unpublished). Ambient CO_2 is at 0.038%. Understanding the differences in CCM that allow strains to flourish at these three levels is needed in order to improve CO_2 fixation.

In addition to the efficiency losses due to carbon delivery to the cell, another well-documented efficiency loss occurs at the cellular site of carbon fixation: RuBisCO. This is due to the fact that there is a secondary oxygenase activity in RuBisCO, which represents a major waste of cellular resources. Ongoing efforts to improve algal carbon uptake efficiency at various CO_2 concentrations are discussed.

Ambient CO_2 concentrations

At ambient CO_2 concentrations (385 ppm), microalgae growing in full sunlight can become carbon-limited. In this scenario the rate of carbon uptake and utilization in the culture exceeds the mass transfer of CO_2 from gas into the media. Significant cellular energy in microalgae is devoted to concentrating and importing CO_2 . In addition, many enzymatic steps are needed to complete the Calvin Cycle leading to reduced carbon building blocks utilized by downstream processes. In order to improve algal CO_2 absorption, ongoing research seeks to grow microalgae with modified carbon concentrating mechanisms and alternative CO_2 utilization pathways.

Elevated CO_2 Concentrations

From a technological point of view it is possible for microalgae to capture carbon from the flue gas emitted from stationary fossil fuel powered sources. Some of the limiting factors identified by various studies are the relatively large land area required, the ability to capture only 25 to 30% of CO_2 in one pass from a flue stream, the cost of pumping the flue gas, and the undeveloped state of this technology (Benemann, 1993).

There are many fundamental questions that still need to be answered regarding microalgal growth at elevated CO_2 concentrations. The most critical determination is the maximum amount of CO_2 sequestered from a given concentration of input gas. There is debate as to the actual amount of CO_2 that can be removed from the input stream. Data presented by Martin Spalding suggested that less than 5% of the CO_2 can be removed from a stream containing >1% CO_2 if the cells are only at a modest density (Figure 4). However, work of others suggests that as much as 70% uptake from a 2% CO_2 stream could be achieved in the blue-green algae, cyanobacteria, which are the largest group of oxygenic photosynthetic prokaryotes. Further results indicate that the maximum amount of CO_2 sequestered from a given concentration of input gas could be 100%. The determination of this limit depends on many factors including the design of the photobioreactor, bubble diameter, bubble lifetime, and culture density (Lada Nedbal, unpublished). Other important factors contributing to the uptake include the pH of the media and the tolerance of the organism to high CO_2. The wide range of values necessitates further research into this key component of carbon capture.

At both ambient and elevated CO_2 concentrations there are important issues to consider when growing algae for the purpose of CO_2 capture and high productivity. The following sections discuss some of these aspects and avenues for potential research opportunities that may lead to increased efficiencies of CO_2 uptake.

Mass Transfer

The mass transfer of carbon dioxide from air into the media can be growth-limiting in dense algal cultures. As discussed above, the transfer of CO_2 from a gas to a liquid depends on

many parameters. The gas flow rate, CO_2 partial pressure and bubble diameter and lifetime in particular can have large influences on the rate of transfer.

Water chemistry also influences the solubility of CO_2 and therefore, to a small extent, the transfer capacity. CO_2 can be dissolved in water according to Henry's law and, to a small extent, reacts with water to form carbonic acid (H_2CO_3). The equilibrium shifts towards HCO_3- (bicarbonate) as the pH increases to a neutral range. HCO_3- is actively transported into microalgae while CO_2 enters the cell by passive diffusion (Figures 5 and 6). The pH of the media plays a major role in mass transfer and can drastically alter growth dynamics of the organism. Controlling pH by the addition of buffering agents can therefore affect mass transfer of CO_2 and carbon uptake by the algae.

Carbon Concentrating Mechanisms

Genetic modification of CCMs may improve the energetic efficiency and rate of carbon uptake in oxygenic photosynthetic organisms. Green algae and cyanobacteria have evolved mechanisms to uptake and concentrate inorganic carbon from the environment (Figures 5 and 6). The strategy utilized depends on the form of carbon encountered. Conversion of CO_2 to HCO_3- in an aqueous environment is pH dependent, with basic environments promoting formation of HCO_3-. Within the cell, enzymatic interconversion takes place in order to transport and concentrate CO_2 at the place of carbon fixation in the chloroplast pyrenoid in green algae or carboxysome in cyanobacteria. Elucidation of the components of both prokaryotic and eukaryotic carbon concentrating systems is underway (Lou Sherman, personal communication). This will allow for the generation and isolation of mutants with enhanced uptake capacity. There

is, however, an energetic cost to operate CCMs. This can be circumvented by growing the algae at high CO_2 concentrations, where a CCM is likely unnecessary.

Increasing Efficiency of the Calvin Cycle

In oxygenic photosynthetic organisms, CO_2 is fixed in the Calvin Cycle by RuBisCO. Substantial losses to photosynthetic efficiency lie between initial charge transfer reactions of photosynthesis and downstream carbohydrate biosynthesis. Depending on the mechanism utilized to fix carbon and the amount of ATP and NADPH utilized, and assuming total incident radiation including infra-red, the maximal theoretical efficiency at this stage (including light capture and energy transduction) is between 8 and 13% before losses due to photorespiration and respiration (Zhu *et al*., 2008).

Photorespiration and Modification of RuBisCO

CO_2 and O_2 are both substrates of RuBisCO. Fixation of CO_2 results in 2 molecules of 3-phosphoglycerate (3-PGA), while fixation of O_2 results in the production of 3-PGA and 2-phosphoglycolate (2-PG), (Buchanan *et al*., 2000). 3-PGA is an intermediate in the reductive C_3 cycle for production of intermediates in biosynthesis and energy production and also for regeneration of Calvin Cycle intermediates. The byproduct of O_2 fixation, 2-PG cannot be utilized by the reductive C_3 pathway and therefore must be recycled to recover the carbon through the photorespiratory C_2 cycle (Buchanan *et al*., 2000). Photorespiratory metabolism inherently decreases carbon fixation efficiency, and estimates are that at current atmospheric CO_2 concentrations, for every three carbons fixed, one oxygen molecule is fixed. To minimize photorespiration, plants have evolved mechanisms to increase CO_2 concentrations by spatially

separating primary CO_2 fixation and RuBisCO activity (C4 plants) or by temporally separating photosynthesis and carbon fixation (CAM plants). Metabolism of CO_2 in C_4 and CAM plants is similar, but in contrast to C_4 plants, CAM plants use CO_2 that is collected at night and stored as malic acid, allowing stomata to remain closed during the day to conserve water.

Algae and cyanobacteria have evolved efficient carbon concentrating mechanisms in order to reduce the oxygenation reaction (Figures 5 and 6). By actively transporting carbon to the site of carbon fixation, photorespiration is reduced due to the increased ratio of carbon to oxygen. Several C_2 pathways to efficiently recycle 2-PG and recover CO_2 have evolved in algae and cyanobacteria (Figure 7).

Because the oxygenase activity of RuBisCO leads to decreased productivity, there has been interest in modifying the enzyme's catalytic properties. Simultaneous enhancement of RuBisCO specificity and catalytic rate has been a scientific goal for a long period of time because of implications for yield in crop-producing plants. However, active site modification of the RuBisCO enzyme has led to the discovery that catalytic rate and specificity are inversely related (Figure 8). RuBisCO may already be optimized and further modifications may not improve function (Tcherkez *et al*., 2006). While increasing enzymatic catalysis may be difficult, there has been interest in modifying Calvin cycle protein levels to increase recycling of intermediates and CO_2 incorporation. This is an active area of investigation.

Secondary Pathways

Diverse carbon capturing pathways have evolved to sustain biomass production in a variety of environments. Several of the limits to carbon fixation using the Calvin cycle native to microalgae have been discussed. In addition to the Calvin cycle, four additional CO_2 fixation

routes have been identified (Figure 9). While several of these pathways require anoxic conditions due to the O_2 sensitivity of some of the enzymes, others can occur during aerobic metabolism. Of particular interest, the 3-hydroxypropionate pathway utilizes the enzymes acetyl-CoA carboxylase and propionyl-CoA carboxylase to fix CO_2 into glyoxylate, an intermediate in carbon metabolism. Genetically engineering alternative CO_2 fixation strategies might be advantageous because they may avoid the regulatory constraints and substrate limitations of native pathways.

A detailed understanding of the diverse mechanisms and pathways for carbon fixation will facilitate an integrated approach for maximal biological carbon uptake. It may be possible to incorporate multiple distinct pathways into a single organism to enhance carbon sequestration. Furthermore, these studies may lead to the development of novel pathways for carbon fixation that do not exist in nature.

Light Harvesting Efficiency

As discussed previously, photosynthetic efficiency is the fraction of total solar radiation that is converted into chemical energy during photosynthesis (Equation 1), and the highest reported values are about 40% and 60% of the maximum for C_3 and C_4 plants, respectively (Zhu *et al.,* 2008, Zhu *et al.,* 2010). Components of this include the biochemical pathways that involve carbon uptake, fixation and metabolism, and potential ways to improve these were dicussed in the previous sections.

$2H_2O + CO_2 + \text{energy} \rightarrow CH_2O + H_2O + O_2$ (1)

Another component that determines overall photosynthetic efficiency is the light harvesting ability of the algae. In the short term, increasing the maximum efficiency of this may be difficult but during the workshop several interesting ways were identified and are discussed in the following sections.

Modification of Antenna Complexes

One major limitation to photosynthesis in full sunlight is that photosynthetic reaction centers quickly become saturated (Figure 10). At low light intensities, in the morning and evening, and in shaded environments, photosynthetic activity increases linearly with light intensities. However in the middle of a sunny day, photosynthetic organs or organisms exposed to full sunlight become saturated and must dissipate this excess energy by non-photochemical means.

In aquatic photosynthetic organisms, light saturation in full sunlight is enhanced by the large antennae complexes that are used to harvest light at low intensity that occurs during self-shading in high density cultures. At high light intensity, light harvesting ability exceeds photosynthetic electron transport capacity. Instead of direct transfer to reaction centers, excess energy is dissipated in the form of heat. These mechanisms have evolved to reduce the formation of reactive oxygen species generated as a byproduct of photosynthesis. Research suggests that in dense cultures of aquatic photosynthetic organisms, fine-tuning the antenna size can increase overall biomass yield, which will facilitate carbon capture (Figure 10 and 11).

Increasing Photosynthetically Active Radiation (PAR)

Another major loss in efficiency is due to the amount of the solar radiation that can be absorbed by photosynthetic pigments. Over half of the solar radiation impacting the earth is outside the range of photosynthetically active radiation (PAR) (400-740 nm). There are additional losses within this spectrum due to reflectance and transmittance of green light. Furthermore, losses due to photochemical inefficiency in the form of heat also represent a substantial fraction. Therefore, even before carbon fixation takes place, approximately 60% of the energy available in total solar radiation is not harvested (Zhu *et al.,* 2008; Zhu *et al.,* 2010).

Increasing the spectrum of solar radiation captured by photosynthesis increases the potential maximal efficiency. Biotechnology and physical science each have promising solutions to this problem. First, it is important to note that the capacity to increase the amount of harvestable sunlight has already evolved in one particular organism, *Acaryochloris marina*. This

organism contains a novel chlorophyll molecule, chl-d, that exhibits a red shifted absorption spectra, extending the photosynthetically active radiation for this organism approximately 40 nm compared to plants, microalgae and related cyanobacteria. Transferring enzymes capable of producing chl-d into other organisms may have the ability to increase the amount of usable wavelengths in the solar spectrum, potentially increasing the maximum efficiency by as much as 5% compared to organisms with only chl-a.

Another way to increase the amount of sunlight that can be utilized is to use materials or chemicals with the ability to shift the wavelength of light from a non-usable wavelength to one that the reaction centers can use. There are many materials capable of shifting light from a short wavelength, high-energy light to a longer wavelength, lower energy light. In fact, this Stokes shift is commonly seen in fluorescent molecules. One target would be to shift green light to red light. This could significantly increase the total amount of photosynthetically active radiation and therefore increase efficiency.

Maximize Biomass Production

Microalgae are attractive for biofuel production because for some species the biomass doubling times are in the range of 4 to 24 hours. Additionally, there are strains that contain up to 80 percent oil by dry weight (Banerjee, *et al.,* 2002; Chisti 2007, Chisti 2008). The accumulation of high biomass over a short time period is desirable and indeed may be essential for making algal culture a viable option for contributing to the energy supply. Currently, ongoing research seeks to confer short doubling times upon strains, and increase yield of high value products from the resulting biomass.

Algae can grow in the presence or absence of light. In the absence of light some algae can grow heterotrophically, using reduced carbon skeletons, such as glucose, as substrate. In this mode of growth, the growth rate is much higher than it can be when algae grow in the presence of light. Under optimal conditions, the maximum photoautotrophic (fueled by sunlight only) growth rate (μ_{max}) is only half that of heterotrophic bacteria because of major differences in the allocation of cellular resources (Raven, 2009).

During photoautotrophic growth, as much as 30% of the total cellular protein is allocated to the processes of photosynthesis and carbon fixation. Typically, RuBisCO accounts for 10% of total protein content of these cells and the apoproteins in the photosynthetic apparatus account for up to 20% (Beardall and Raven, 2010). Additionally, compared to heterotrophs, photoautotrophs have only about half as much of the machinery necessary to make monomers for DNA, RNA, and protein synthesis, and for polymerizing the resulting monomers on an equal cell volume basis. A generalized equation for the specific growth rate of an alga can be expressed in terms of the maximum specific reaction rate R of a catalyst i (e.g. enzyme, transporter, redox agent, pigment-protein complex), and a factor F for the fraction of this reaction rate needed to

account for the observed growth rate, with F varying as a function of environmental factors such as inorganic carbon and light supply. The growth rate hypothesis resulting from this observation is valid for about half of algal species, and says: μ (specific growth rate) is a linear function of rRNA content, with a constant specific reaction rate of rRNA at all rRNA contents (Equation 2).

$$\mu = B_i \bullet C_i \bullet R_i \bullet F_i \quad (2)$$

Where μ = specific growth rate (mol C assimilated • mol C in cell^{-1} • s-^{1}); B_i = mol of catalyst of essential reaction i • mol C in catalyst; C_i = mol C in catalyst • mol C in cell^{-1}; R_i = maximum specific reaction rate of the catalyst of reaction i with the reaction product scaled to units of mol C from mol C of product per mol cell C (mol C transformed • mol catalyst^{-1} • s^{-1}); F_i = fraction of potential R_i in cell needed to account for observed μ.

Algae grown photomixotrophically, where they use not only endogenous but exogenous carbohydrates as an energy source, show a higher μ_{max} than when grown photoautotrophically, but the cost of resulting fuel is increased because of the added cost of reduced carbon sources. Additionally, photomixotrophic growth has many implications for greenhouse gas emissions depending on how the feedstock that provides the reduced carbon was grown, obtained and processed. Growing cultures solely under heterotrophic conditions would also preclude the direct capture of carbon dioxide from fossil fuels sources. Aside from growth on waste carbon sources or in a two-stage production method (See Biofuel/Bioproduct Production), heterotrophic algal growth will likely be prohibitively expensive.

Compared to heterotrophic organisms, photosynthetic organisms require substantially more metal ions for growth due to their important role as redox active cofactors in photosynthetic electron transfer (Shcolnick and Keren, 2006). Among these, iron homeostasis is identified as being critical for optimal growth as it is often a limiting factor under both natural and artificial growth conditions (Nir Keren, personal communication). Additionally, many algae are auxotrophic (requiring a particular nutrient or vitamin for growth) for certain vitamins such as vitamin B_{12}, which they must obtain from the environment. The need to include high value compounds in algal media would increase the cost of production considerably. However, algae can obtain vitamin B_{12} by direct association with bacteria, which obtain fixed carbon from the photosynthetic algae in return (Croft *et al.,* 2005). Mixed cultures such as these might reduce the risk of contamination from other adventitious microorganisms. Maximization of productivity will depend on identification of other factors required for optimal growth.

Biofuel/Bioproduct Production

A large number of products can potentially be made from microalgae ranging from fuels to herbicides, and polymers with desirable biophysical or bioactive properties. The ability to genetically engineer microalgae by the addition of genes encoding enzymes of alternative biosynthetic pathways allows for the production of a wide array of chemicals.

Fuels from Microalgae

A number of fuels can be made by microalgae, including fermentation byproducts, long-chain hydrocarbons, and hydrogen. The specific properties of the molecules being produced will dictate the harvesting strategy to be used (see Harvesting and Extraction) and thus the overall energy balance of the process. Methane, ethane, long chain alcohols, oils, fatty acid esters, and isoprenes can all be made using algae. While chemically diverse, they are biosynthetically derived from acetyl-CoA or related small molecule intermediates, with the exception of methane. The following sections discuss in more detail some of these products and their uses.

Ethanol and Other Fermentative Alcohols

Despite its energy density being less than that of gasoline and most biodiesels, ethanol is an attractive transportation fuel because of its use in the existing fuel infrastructure. Ethanol can be blended into gasoline at various concentrations and used in conventional internal combustion engines, which are reported to perform just as well as those with conventional gasoline. At present however, the production of ethanol and other products of fermentation by algae are currently at yields too low to be economically viable. Ongoing research such as strain

optimization of species that already produce these molecules seeks to increase the yield of fermentative alcohols.

Research also seeks to divert fermentative metabolism from ethanol production into higher-chain alcohols. These alcohols, such as isobutanol, 1-butanol, 2-methyl-1-butanol, 3-methyl-1-butanol and 2-phenylethanol, have more desirable fuel properties such as higher energy content, and hydrophobicities more similiar to gasoline molecules. These can be mixed with other molecules to lead to a fuel with combustion properties similar to current gasoline (Atsumi *et al*., 2008). Simple genetic mechanisms can be used to directly convert ethanol into these other fuels. Though ethanol is a useful biofuel in the near-term, research that moves production to more complex alcohols will undoubtedly prove valuable. Many of these molecules are drop-in or a direct replacement of gasoline and if produced by microalgae, these fuels could in principle be carbon-neutral.

Hydrocarbons and Biodiesel

Another promising route to algal fuel production is the harvest of oils for biodiesel (Chisti, 2007; Chisti 2008). Fatty acids, specifically triacylglycerols (TAGs), can be trans-esterified directly into biodiesel, producing glycerol as the side product. The production of non-polar lipids is in the range of 4-50% of total biomass of various algae strains (Hu *et al*., 2008). Strains that produce remarkably high levels of these oils are now being studied for other desirable characteristics. One example of productivity achieved to date in Fort Collins, Colorado consists of a 6,000 Liter system that can produce 1.5 kg/day dry weight algae biomass with CO_2 enrichment (Pete Lammers, personal communication).

Hydrogen

Hydrogen production from microalgae is achievable now, although at low light-conversion efficiencies and under low irradiation (Ghirardi and Mohanty, 2010) but could reach relatively high efficiency values because the hydrogen production process is independent from the carbon metabolic pathways that account for many of the efficiency losses. The maximum theoretical efficiency is 10-13% (Ghirardi *et al*., 2009). With this in mind, a land area of about 4500 square miles (0.12% of U.S. land area) could effectively supply the transportation fuel demand, with estimated costs as low as $3/kg. The use of hydrogen as a transportation fuel is attractive because it is carbon-free. Its combustion does not produce CO_2 but instead only water.

In green, eukaryotic microalgae, hydrogen production is mediated by the activity of the algal [Fe-Fe] hydrogenase, which catalyzes the reaction in Equation 3:

$$2H^+ + 2e^- \rightarrow H_2 \quad (3)$$

There are some major hurdles to algal hydrogen production, however: the enzymes responsible for hydrogen production are sensitive to oxygen, and are not expressed in its presence; ferredoxin, which supplies electrons to drive hydrogen production, is the major electron donor to other cellular redox processes as well; and if large numbers of electrons are diverted to hydrogen production, the pH gradient across the membrane that is established by electron transport from water is not dissipated through ATP production, thus down-regulating the rates of electron transport through the photosynthetic chain (Lee and Greenabum, 2003). The isolation of natural strain variants that are better adapted at producing hydrogen has given some insights into methods towards alleviating these problems.

If algal hydrogen production is a realistic route to energy generation, there remain major technological limitations to using hydrogen on a global scale. Hydrogen has lower energy density than ethanol. Additionally, use of hydrogen as an energy carrier for transportation will depend a lot on safe storage and distribution technologies, as refueling stations must be constructed and hydrogen fuel cell technology still needs improvements before it is affordable.

Methods to Overcome Losses in Efficiency

To address the problem of oxygen-sensitive hydrogenases, mutants that produce less intracellular oxygen have been generated. Interestingly, these mutants also show accumulation of more oil than wild-type strains (Work *et al*., 2010). Additionally, the oxygen tolerance of hydrogenases varies greatly, according to the amino acid sequence of the enzyme. Biochemical characterization of a variety of algal strains is under way, in order to find hydrogenase homologs that have both high activities and increased oxygen tolerance (Cohen *et al*., 2005). Additionally, a transformation system has been generated that expresses a tagged, active [FeFe] hydrogenase in *E. coli* that allows in vitro characterization of hydrogenase isoforms (King *et al*., 2006). Computational studies of various hydrogenases indicate that two gas diffusion channels allow gas diffusion into the reaction center. Therefore, amino acid substitutions that affect the size of the gas channels are of particular interest. The goal is to create a channel that allows free diffusion of hydrogen, but not oxygen (Cohen *et al*., 2005).

Optimization of Production Parameters

Studies in several labs have identified mutants that produce more hydrogen than wild type strains. Kruse and Hankamer have shown that the *stm6* multi-phenotype mutant of

Chlamydomonas reinhardtii (that cannot transition from linear to cyclic electron transfer) produces H_2 at higher rates and for longer periods of time than its parental strain. Sulfur deprivation, which is known in *Chlamydomonas reinhardtii* to increase hydrogen production, was tested on the *stm6* mutant. Hydrogen production was measured and results indicate the *stm6* strain can produce up to 490% more H_2 over a 300 hour period in sulfur-depleted media when compared to its parental strain, which is not a particularly high H_2-producer.

In an attempt to further boost production, researchers have cloned the HUP1 (hexose uptake protein) hexose symporter from *Chlorella kessleri* into *stm6*, generating the strain known as *Stm6Glc4*. In the presence of 1 mM glucose, H_2 production was seen to increase by 50% compared to the *stm6* strain without the transporter (Figure 12) (Doebbe *et al*., 2007). This essentially created a mixed fermentative/ photosynthetic H_2 production system, and conversion efficiency of glucose to hydrogen was near 100%.

Further strain optimization for enhanced light absorption characteristics has been carried out leading to generation of a truncated antennae mutant optimized for a bioreactor with a depth of 10 cm. With this mutant, in high light (700 μE), cell density reached 0.2g/l biomass in less than 5 days. This equates to a 50% improvement in mid-logarithmic growth rate (Beckmann *et al*., 2009).

Value Added Products

Value added products from algae have the potential to offset running costs when algae are used as a carbon capture technology. However, market prices and demand will determine the value of products from algae, so the ability to produce a wide array of products and to switch among these quickly may be necessary to microalgae, and its products, economically viable.

Advances in genetic engineering and synthetic biology currently underway, will make generation of strains tailored for production of a specific product faster and less expensive.

Current Algae Products

Currently, there are four major profitable products from microalgae: Agar, Alginic acid (used as a stabilizer and emulsifier in shampoos), Carrageenan (extracted from algal cell wall, used as a stabilizer and emulsifier in foods, and toothpastes), and diatomaceous earth. Microalgae are also a source of pigments that have a number of industrial uses. The carotenoids in particular are additives to food as coloring, vitamin supplements, health food products and livestock feed.

Some studies show the worldwide market value of carotenoids is projected to reach over one billion dollars by the end of the decade (Del Campo *et al*., 2007). The market value of one of these pigments, β-carotene, has been projected to reach $253 million by 2009. This pigment is of increasing demand in a variety of market applications including food coloring agent, pro-vitamin A (retinol) in food and feed, as an additive to cosmetics and as a health food product under the antioxidant label. This pigment is conventionally commercially produced from Dunaliella in open ponds (Del Campo *et al*., 2007). The market value for omega-3 fatty acids is presently $1.5 billion dollars, with a majority of this product presently extracted from fish oil. This market is expected to grow to over $10 billion in the next several years and with fish stocks rapidly depleting, production directly from algae may become a significant market.

Therapeutic Proteins

Protein-based therapeutics is one of the fastest-growing sectors of drug development (Manuell *et al*., 2007). Microalgae have the potential to provide high yields of specific classes of recombinant proteins more rapidly and at much lower cost than traditional cell culture (Mayfield *et al*., 2007). For example, algal chloroplasts have proven to be a good system for the production of antibodies (Mayfield *et al.,* 2003; Trans *et al.,* 2009), bioactive mammalian protein, and others of pharmaceutical importance (Manuell *et al.,* 2007; Rasala *et al.,* 2010), and reporter proteins as tools in molecular biology (Mayfield *et al*., 2003). Advantages of microalgae over other expression systems would depend on the actual properties desired in the protein produced. Microalgae have proven successful at producing proteins with disulfide bonds, but that lack glycosylation. The time-scale from initial transformation of gene to production of protein of interest in microalgae is a relatively short two months.

Other Products and Services

Some companies are already producing ingredients for cosmetics from algae growing heterotrophically. This means that the microalgae grow in the dark, with no requirement for a light source, making the growth and production much more efficient than microalgae grown in light. However, a feedstock (glucose, acetate, glycerol etc.,) needs to be supplied to the microalgae, in this case and does not allow/involve the direct capture of CO_2 from a fossil fuel source for algal growth.

Many enzymes are required in the production processes of many industries including food, paper and pulp, cellulosic ethanol, etc. Isolation of these enzymes from naturally occurring sources can be time consuming and costly and sometimes requires expensive purification steps

where losses of enzyme are encountered. Microalgae could be used as a heterologous expression system for the production of many of these enzymes making a contribution to a diverse array of industries.

Bio Prospecting and Development of Robust Strains

As mentioned previously, the DOE ASP identified 3000 strains of algal species that were interesting from a basic research perspective. Recently, there has been a major push towards similar research identifying strains of microalgae that are well suited for use in industrial processes. The isolation of novel strains that are tolerant to unique conditions present in industrial processes is an effective way to bring down up-front costs when designing a process, as a well-suited organism will allow for major input reduction.

Isolating strains with faster growth rates than strains currently available would improve carbon capture and biomass accumulation abilities without the need for genetic modification. Additionally, isolation and study of strains that grow in hypersaline environments may lead to significant water-use savings. Alternatively, considering alternatives to monocultures might mitigate costs required to prevent or deal with contamination. Finally, finding strains that are well suited to an environment with vast and rapid temperature changes may prove useful for minimizing the amount of heating and cooling necessary to keep a culture alive. In all, the opportunity for bio-prospecting right now is immense, and large-scale efforts have a very good chance of finding strains that are naturally suited for bioenergy production.

Bioreactor Design

The physical location in which microalgae are grown has a dramatic effect on the type of system that is the best for productivity. Typically, there are two competing growth systems for microalgal culture: open ponds and enclosed photobioreactors. The strengths and weaknesses of both have been discussed in great detail in recent years (Posten, 2009), and will only briefly be mentioned here.

The major limiting factor to both open pond and enclosed photobioreactor operation is water usage. Typically, sites considered the best for algal production have warm temperatures and high average irradiance throughout the calendar year. In locations with these properties, evaporation from open ponds, and gradual heating of photobioreactors become a problem. The solution to both of these problems is to use more water, either to replace the water lost through evaporation, or to evaporatively cool the photobioreactor. In either situation, total water usage for production processes inflates dramatically, and sometimes reaches the point at which the cost and availability of water renders the process non-viable.

This presents a major opportunity to the scientific community. Major advances in technology for the efficient cultivation of microalgae need to be made before implementation can occur in many regions. Raceway pond design needs to become more resistant to contamination, and resistant to evaporation. Additionally, a low-cost gas delivery technique needs to be designed if algae are to ever capture carbon from power plants. For photobioreactors, major leaps in construction cost and cooling technology must be made before they are price-competitive with ponds.

Harvesting and Extraction

Though algae are very useful for production of high value products through genetic engineering, the harvesting of the desired products can introduce significant costs into the production process. Currently, algae are harvested by centrifugation, which is energetically, very expensive. When producing renewable fuels from algae, up to 50% of the cost comes from harvesting and extraction, and there is a major opportunity for cost savings with innovative harvesting technologies. Improvements in harvesting and extraction technologies will have the biggest effect on renewable fuel prices, as their value per unit volume is relatively low (as compared to other chemicals), and so are profit margins.

Research into harvesting technologies has yielded some interesting insight into the most cost-effective techniques. The biological process of flocculation, in which microalgae clump together and settle out of the media may offer a low-cost method for harvest, as the organisms will self-separate from the media. Flocculation is still poorly understood, however, so current research in that area seeks to understand the molecular factors that trigger flocculation, and identify strains that naturally flocculate.

Another interesting harvesting technique takes advantage of the chemical properties of the chemical being produced. Often, fuel molecules are non-polar, and thus will separate from water on their own. Engineering algae to excrete the molecules or harvesting the molecules while leaving the cell intact would make harvesting trivial, as the molecules will naturally separate from the culture. This process would also make continuous production easier to achieve, as the living cells will continue to produce the desired product instead of being harvested along with the chemical of interest.

The particular harvesting method that will yield the lowest cost will likely be unique to each production process. The fuel produced, algal strain used, and production technique, are the

upstream factors that dictate the cheapest harvesting method. As a result, scientists need to develop an array of low cost, energy-efficient harvesting technologies that can be used in for the wide variety of harvesting conditions that will be present in the future.

Water Use Efficiency

Water requirement for large-scale culture of microalgae has been seen as a major hurdle in achieving sustainable deployment of these organisms for biological CCS. However, the possibility of incorporating microalgal growth and carbon capture with current water systems at coal-fired power plants may make water use less of a concern compared to non-integrated algae growth systems. Used mostly for cooling, freshwater use by power plants is only slightly less than irrigation (the largest use of freshwater), at 132 billion gallons per day in the U.S. (Hutson *et al.,* 2000).

By coupling microalgal growth to existing water-cooling systems or using strains that grow in brackish or wastewater, freshwater requirements for biological capture of CO_2 emissions from that same plant could be low. A typical 500 MW power plant uses 12 million gallons of fresh water per hour, consumes 250,000 gallons per hour, and often sits near a cooling lake (Figure 13). The impacts on water use at power plants due to the deployment of microalgae can and should be done in a fashion that does not increase usage. However, the use of biocide in cooling water for power plants would likely be incompatible with algae production and so this idea may not be practical in systems other than once-through cooling systems.

Integrated power plant design

To capture the carbon given off by coal-fired power plants, existing plants must be retrofitted, and newly designed plants must incorporate carbon capture into the exhaust scrubbing system. The cost of implementing such systems will be the major driving force behind changes, and for algae to be useful, they must be price competitive with non-biological forms of carbon capture (Buhre *et al*., 2005). Furthermore, the type of coal utilized in the plant largely influences the cost of adding biological CCS, as SO_x, NO_x, and heavy metal concentration vary widely in coal deposits (Adel Sarofim, personal communication). The costs associated with CCS will depend on the method of capture and use of advanced separation technologies; whether it is post-combustion or pre-combustion (Rochelle, 2009). Predictions show these costs, in terms of energy penalties, can be approximately 13.5% for separation of CO_2 and another 9% for compression (Herzog, 2009). Storage costs are small in comparison (McCoy and Rubin, 2009). Values in the region of \$52 per tonne/CO_2 for capture and an additional \$10 per tonne CO_2 for transport and storage have been calculated (Hamilton *et al.,* 2009).

Costs of algae production have been calculated to be \$250 per tonne CO_2 in a photobioreactor system (Chisti, 2007) and \$55 per tonne CO_2 in a raceway pond system (Stepan *et al*., 2002). However the energy penalty associated with algae as a CCS technology would likely be zero or negative due to the production of large amounts of biomass that can be used as fuel.

De novo *Design*

Integrating power plant design with algal carbon capture and remediation could be a means of controlling emissions and capturing SO_x, NO_x and heavy metals such as mercury (Hg) and perhaps additional contaminants from the flue stream. Currently, depending on the design of the power plant and emissions control measures that are in place, the energy penalty for controlling these emissions is in the region of 1% for NO_x, 2% for SO_x, and 0.4% for Hg (numbers were calculated from Integrated Environmental Control Software (IECM) assuming a 500-MW power plant burning Appalachian Medium Sulfur coal; SO_x scrubbing consists of a wet flue gas desulfurization unit while NO_x reduction involves a Selective Catalytic Reduction unit), (Wilcox, 2010). However, at present only 30% of all U.S. power plants have NO_x/SO_x scrubbing since the costs of implementing this are less attractive than the actual fines. Regulations for Hg emissions are in place in only 19 states and no other trace metals are regulated or scrubbed (Wilcox, 2010).

The results in Figures 14 and 15 show that microalgae can tolerate SO_2 concentrations up to 400 ppm, and NO concentrations up to 100 ppm (which are levels typically found in flue stream from coal-fired power plants) as long as the acidification of the medium in which the microalgae are growing is prevented (Lee *et al.,* 2002; Matsumoto *et al.,* 1997). While studies that establish the pollutant tolerance limits for algae are important, more research is needed to determine the amounts of contaminant actually removed by the algae. If algae were deployed as a CO_2 capture and storage technology, the ability to sequester pollutants would be an added advantage since an additional technology need not be in place.

Perspective on Feasibility, Sustainability and Impacts

Biofuels produced by microalgae grown on coal-fired power plant flue gases are by definition, not sustainable, since fossil fuels are an unsustainable resource. However, if we consider coal to be a resource available for the next c. 200 years, we can weigh this technology against certain sustainability criteria over this time period. We can also consider this method of carbon capture as a technology that could be applied to coal-fired power plants, natural gas or facilities co-fired with biomass if these were to become adopted at large-scale in the future.

Based on information available from existing technology, land and water are major resources needed to realize carbon capture by algae at power plants (Benemann, 1993). Estimates of land use vary depending on the productivity of algae and whether grown in ponds or photobioreactors. Numbers for water use also vary between these two approaches as pond systems have associated evaporative losses but have the ability to use salt, brackish or wastewater depending on the strain of algae grown. Some working photobioreactors systems employ water reuse/recycling, which helps to lower total water use. Considering the higher reported productivities that can be achieved in photobioreactors compared to those for existing pond systems, there is a trade-off between the capital costs and the apparent benefits and drawbacks of these systems at present.

Siting Issues

The number of suitable sites for deployment of a biological capture technology as described in this review is uncertain as the requirements for land area, type of land, and type and capacity of water resource depend very much on the needs of the algae system employed. Siting

close to the CO_2 source may have its benefits in terms of allowing integrated design and synergy between waste heat and water use of the power plant but the downside is that sufficient land with the desired characteristics may not be available.

Suitable land for raceway pond systems has been suggested to have a slope of no more than 2% for construction costs and water lifting and to have a high clay content to minimize water percolation (Hanova *et al*., 2010). Although the characteristics of surrounding land is important, it need not be restrictive since other options exist such as siting elsewhere with access to a CO_2 pipeline and water source or the use of reactor systems.

Importantly, the effects of land use under any of these scenarios on existing carbon sinks, soil quality and biodiversity must be considered to determine sustainability and impacts on green house gas (GHG) emissions.

Impacts on Local Population

The implementation of algae as a technology to capture and utilize carbon has the potential to have both positive and negative impacts on sites where deployed and on the people living close to those sites.

Benefits for local populations could include improved ground water, lower local emissions of carbon, SO_x, NO_x, and heavy metals such as Hg. A new industry around carbon capture and production of liquid transportation fuels by algae could have the potential to provide local jobs, improve local economy, improve local prosperity, and benefit the social well being of the local population and employees. However, competition with existing local business activities would need to be considered if such a business is to be sustainable and especially if algae were to provide a diversity of high-value products.

Negative impacts on the local population include the risk of contamination of waterways, the possibility of algae blooms and suffocation of other species (plant and animal), and competition for water use.

Research can help to minimize these risks as nutrient dependant strains of algae (where algae cannot grow unless supplied with a particular nutrient/chemical) can be found or engineered (Croft *et al*., 2005). Re-use, treatment, recycling and monitoring of water could minimize total water requirements and the risk of release of contaminants to the surrounding environment. Examples of successful containment due to the growth requirements of algae exist in the San Francisco Bay Area where side-by-side algal salt ponds show no/little apparent cross-contamination between ponds, probably due to differences in their pH and salinity tolerance. The risk of potential negative impacts could be minimized with the right engineering, science and management practices.

Global Impacts

As discussed previously the amount of oil produced by algae varies with strain and growing conditions. Calculations based on reported production from some algae facilities suggests that the contribution from one year's production would meet less than 1/1000th of the current U.S. daily demand of barrels of oil. This highlights the need for game-changing research to improve productivity, but even with these improvements production of oil from algae would make only a small contribution to offset U.S. oil use.

Targeted application of the energy dense fuels from algae, for example for aviation, seems more realistic and practical than attempting to displace liquid fuel use for the whole transportation sector. A major strength of algae, compared to other bioenergy technologies, is its

ability to produce energy dense oils, which can be turned easily into diesel type fuels. This would perhaps be the most appropriate target of an algal oil production system since other non-fossil sources of this fuel are limited. Other oil producing sources, such as oil palm, and bacterial and yeast systems look promising (Peralta-Yahya *et al*., 2011), but scalability and sustainability issues associated with these have yet to be solved. The use of algae compared to these other methods for the production of energy dense liquid fuels should be assessed to determine the most sustainable, efficient and low-cost option.

Systems Analysis

The need for thorough systems analyses on coupling algae growth to CO_2 emissions from power plants to determine the real effects on GHG emissions, and other sustainability criteria is apparent. The amount of fossil fuels that would need to be displaced in addition to the required amount of carbon to be captured by growing the algae to make a substantial reduction in GHG emissions should be determined.

These tasks require developing definitive costs for the various unit processes from producing algal biomass to producing algae oil in the context of land, water needs, and the proximity of a CO_2 source. This would be a complex undertaking, but necessary for assessing the potential of algal technology to contribute to GHG reductions and our energy needs.

Summary and Conclusions

For algae to be deployed as a carbon capture technology and contributor to energy supply the process must be able to compete on a cost basis with other energy related technologies for carbon capture, production of fuels and other services. To be sustainable and deployed on a global scale the amount of water, energy, and land used must also be minimized to help preserve our natural ecosystems and avoid competition over these resources with other uses.

Competing technologies include non-biological carbon capture and storage (CCS) of CO_2 from fossil fuel sources, hydrogen production from fossil fuels and biomass, and production of hydrocarbon fuel molecules by micro-organisms (bacteria or yeast) using sugars derived from biomass feedstocks such as corn, sugarcane and lignocellulosic biomass. Currently, CCS technologies are energy intensive and expensive, often requiring specific operating conditions of temperature, pressure, pH, and concentration in addition to specific citing where the properties of the subsurface allows CO_2 storage. Worldwide there are several carbon storage projects underway (Haszeldine, 2009), but in sum, these projects, including CO_2 injected into oil reserves for enhanced oil recovery, represent only megatons of CO_2 that has been diverted from the atmosphere. It is a seemingly low volume in comparison to the quantities necessary to make a significant impact and indicates the need for additional CCS alternatives.

Algae could be an alternative or additional technology to this if the overall running costs are less and implementation at scale can be achieved. Considerations such as land availability, and water use may limit the potential for the sustainable deployment of algae as a means of capturing carbon from fossil fuel sources globally and these limits need to be assessed by systems analysis. Systems analysis could also help to assess the progress towards minimizing

these needs if some of the key technological advances, as identified by the workshop and discussed in this chapter, are achieved.

Improvements to the rate of carbon capture and fixation by algae can be made by targeting many aspects of algal photosynthesis. Alterations to the light harvesting part of photosynthesis by decreasing light saturation; increasing light capture; and increasing wavelength of light utilized; can all lead to an increase in photosynthetic efficiency. In addition, exploring opportunities in engineering for coupling water use and low-grade heat from power plants to algal growth, complemented with the bio remediation capabilities of algae could further improve sustainability, and lower costs of deployment of algae as a carbon capture technology.

Economics are a key aspect to making algae a viable option for contribution to our energy supply and as a production system for high value products. Technological advances that bring harvesting and extraction costs down, and ultimately finding or engineering organisms that show an order of magnitude increase in efficiency will all impact the extent of deployment of this technology and its successful competition with other carbon capture and liquid fuel production technologies. The production of value added products could potentially offset running costs; however sustaining this with respect to the demands of the market place may be difficult. Having the ability to switch production from one commodity to another on a day to day basis may be important to avoid flooding the markets with a particular product. The goal of achieving carbon capture and production of fuels or high value products at low cost of materials and high efficiency should be the primary goal and the realization of technologies to achieve this should be the focus of fundamental research.

The major findings suggest that focusing research on one area alone will not lead to the necessary improvements but that research focused on a few key aspects of algae biology

provides opportunities for increases in efficiency that together would lead to an order of magnitude improvement in the operating photosynthetic efficiency.

References

Atsumi, S., Hanai, T., and Liao, J. C. (2008) Non-fermentative pathways for synthesis of branched-chain higher alcohols as biofuels. *Nature*. 451:86-89

Badger, M. R. and Spalding, M. H. (2006) CO_2 Acquisition, Concentration and Fixation in Cyanobacteria and Algae. In: Leegood, R., Sharkey, T., von Caemmerer, S. (eds.) *Photosynthesis: Physiology and Metabolism*. 9:369-397. Kluwer Academic Publishers, The Netherlands

Banerjee, A., Sharma, R., Chisti, Y., and Banerjee, U. C. (2002) Botryococcus braunii: A Renewable Source of Hydrocarbons and Other Chemicals. *Crit. Rev. in Biotechnol*. 22: 245–279

Beardall, J., and Raven, J. A. R. (2011) Limits to phototrophic growth in dense culture: CO_2 supply and light. In: Borowitzka, M. (ed), *Algae for Biofuels and Energy, Springer, Germany*. In press

Beckmann, J., Lehr, F., Finazzi, G., Hankamer, B., Posten, C., Wobbe, L., and Kruse, O. J. (2009) Improvement of light to biomass conversion by de-regulation of light-harvesting protein translation in Chlamydomonas reinhardtii. *Biotechnol*. 142:70-77

Benemann, J. R. (1993) CO_2 mitigation with microalgae systems. *Ener. Conv. Mgmt*. 34:999–1004

Buchanan, B. B., Gruissem, W., and Jones, R. L. (eds.) (2000) *Biochemistry and Molecular Biology of Plants*. American Society of Plant Physiology, Rockville, MD

Buhre, B. J. P., Elliott, L. K., Sheng, C. D., Gupta, R. P., and Wall, T. F. (2005) Oxy-fuel combustion technology for coal-fired power generation. *Prog. Ener. Combustn. Sci*. 31:283-307

Chisti, Y. (2007) Biodiesel from Microalgae. *Biotechnol. Adv*. 25:294-306

Chisti, Y. (2008) Biodiesel from Microalgae beats Bioethanol. *Trends in Biotechnol*. 26:126-131

Cohen, J., Kim, K., Posewitz, M., Ghirardi, M.L., Seibert, M., and King, P. (2005) Molecular dynamics and experimental investigation of H_2 and O_2 diffusion in [Fe]-hydrogenase. *Biochem. Soc. Trans.* 33:80-82

Cohen J., Kim, K., King, P.W., Seibert, M., and Schulten, K. (2005) Finding Gas Diffusion Pathways in Proteins: Application to O_2 and H_2 Transport in CpI [FeFe]-Hydrogenase and the Role of Packing Defects. *Structure*. 13:1321-1329

Croft, M.T., Lawrence, A.D., Raux-Deery, E., Warren, M.J., and Smith, A.G. (2005) Algae acquire vitamin B_{12} through a symbiotic relationship with bacteria. *Nature*. 438:90-93

Del Campo, J. A., Garcia-Gonzalez, M., and Guerrero, M. G. (2007) Outdoor cultivation of microalgae for carotenoid production: current state and perspectives. *Appl. Microbiol. Biotechnol*. 74:1163-1174

Doebbe, A., Rupprecht, J., Beckmann, J., Mussgnug, J., Hallmann, A., Hankamer, B., and Kruse, O. (2007) Functional integration of the HUP1 hexose symporter gene into the genome of C. reinhardtii: Impacts on biological H_2 production. *J. Biotechnol*. 131:27-33

Ghirardi, M. L. and Mohanty, P. (2010) Oxygenic hydrogen photoproduction-current status of the technology. *Curr. Sci*. 98:499-507

Ghirardi, M. L., Dubini, A., Yu, J., and Maness, P. C. (2009) Photobiological hydrogen-producting systems. *Chem. Soc. Rev*. 38:52-61

Hagemann, M., Eisenhut, M., Hackenberg, C., and Bauwe, H. (2010) Pathway and Importance of Photorespiratory 2-Phosphoglycolate Metabolism in Cyanobacteria. In: Hallenbeck, P. C. (ed.) *Recent Advances in Phototrophic Prokaryotes, Advances in Experimental Medicine and Biology*. 675, 2:91-108. Springer Science+Business Media, Germany

Hamilton, M. R., Herzog, H. J., and Parsons, J. E. (2009) Cost and U.S. public policy for new coal power plants with carbon capture and sequestration. *Energy Procedia*. 1:4498-4494

Hanova, J., Benemann, J., McMillan, J., and Saddler, J. (2011) Algal Biofuels Status and Prospects. *IEA Bioenergy Annual Report 2010*

Haszeldine, R. S. (2009) Carbon Capture and Storage: How Green Can Black Be? *Science*. 325:1647-1651

Herzog, H. (2009) A research program for promising retrofit technologies. Prepared for the MIT Symposium on Retro-fitting of Coal-Fired Power Plants for CO_2 Emissions Reductions

Hu, Q., Sommerfeld, M., Jarvis, E., Ghirardi, M., Posewitz, M., Seibert, M., and Darzins, A. (2008) Microalgal triacylglycerols as feedstocks for biofuel production: perspectives and advances. *The Plant J.* 54:621-639

Hutson, S. S., Barber, N. L., Kenny, J. F., Linsey, K. S., Lumia, D. S., and Maupin, M. A. (2004) Estimated use of water in the United States in 2000. *Geological Survey Circular 1268*

King P.W., Posewitz, M.C., Ghirardi, M.L., and Seibert, M. (2006) Functional studies of [FeFe] hydrogenase maturation in an Escherichia coli biosynthetic system. *J. Bact*. 188:2163-2172

Lal, R. (2008) Sequestration of atmospheric CO_2 in global carbon pools. *Ener. and Env*. Sci. 1: 86-100

Lee, J. W. and Greenbaum, E. (2003) A new oxygen sensitivity and its potential application in photosynthetic H_2 production. *Appl. Biochem. Biotechnol*. 106, 1-3:303-313

Lee, J. S., Kim, D. K., Lee, J. P., Park, S. C., Koh, J. H., Cho, H. S., and Kim, S. W. (2002) Effects of SO_2 and NO on growth of Chlorella sp. KR-1. *Bioresour. Technol*. 82, 1-4

Manuell, A. L., Beligni, M. V., Elder, J. H., Siefker, D. T., Tran, M., Weber, A., McDonald, T. L., and Mayfield, S. (2007) Robust expression of a bioactive mammalian protein in *Chlamydomonas* chloroplast. *Plant Biotechnol J.* 5:402-412

Matsumoto, H., Sioji, N., Ikuta, Y., and Hamasaki, A. (1997) Influence of CO_2, SO_2 and NO in Flue Gas on Microalgae Productivity. *J. Chem. Eng. Japan*. 82, 1:1-4

Mayfield, S. P., Franklin, S. E., and Lerner, R. A. (2003) Expression and assembly of a fully active antibody in algae. *Proc. Nat. Acad. Sci. USA*. 100:438-42

Mayfield, S. P., Manuell, A. L., Chen, S., Wu, J., Tran, M., Siefker, D., Muto, M., and Marin-Navarro, J. (2007) Chlamydomonas reinhardtii chloroplasts as protein factories. *Curr. Op. in Biotechnol.* 18:126-133

McCoy, S. T., and Rubin, E. S. (2009) Oxy-fuel combustion technology for coal-fired power generation. *Energy Procedia*. 1:4151-4158

Peralta-Yahya, P., Ouellet, M., Chan, R., Mukhopadhyay, A., Keasling, J. D., and Lee, T. S. (2011) Identification and microbial production of a terpene-based advanced biofuel. *Nat. Comm*. 2, 483

Posten, C. (2009) Design principles of photobioreactors for cultivation of microalgae. *Eng. in Life Sci.* 9:165-177

Price, D. R., Badger, M. R., Woodger, F. J., and Long, B. M. (2008) Advances in understanding the cyanobacterial CO_2-concentrating-mechanism (CCM): functional components, Ci transporters, diversity, genetic regulation and prospects for engineering into plants. *J. Exp. Bot.* 59,7: 1441-1461

Rasala, B. A., Muto, M., Lee, P. A., Jager, M., Cardoso, R. M. F., Behnke, C. A., Kirk, P., Hokanson, C. A., Crea, R., Mendez, M., and Mayfield, S. P. (2010) Production of therapeutic proteins in algae, analysis of expression of seven human proteins in the chloroplast of *Chlamydomonas reinhardtii*. Plant. Biotech. J. 8, 6:719-733

Raven, J.A. (2009) Contributions of anoxygenic and oxygenic phototrophy and chemolithotrophy to carbon and oxygen fluxes in aquatic environments. *Aq. Microbial Ecol.* 56:177-192

Rochelle, G.T. (2009) Amine Scrubbing for CO_2 Capture. *Science*. 325:1652-1653

Shcolnick, S. and Keren, N (2006). Metal Homeostasis in Cyanobacteria and Chloroplasts. Balancing Benefits and Risks to the Photosynthetic Apparatus. *Plant Physiol*. 141:805-810

Sheehan, J., Dunahay, T., Benemann, J., and Roessler, P. (1998) A look back at the U. S. Department of Energy's aquatic species program: biodiesel from algae. *U. S. department of Energy Office of Fuels Development: Closeout Report*. National Renewable Energy Laboratory, Golden, CO

Stepan, D. J., Shockey, R. E., Moe, T. A., and Dorn, R. (2002) Carbon dioxide sequestering using microalgal systems. *Final Report prepared for US Department of Energy, Pittsburgh, PA, USA*

Tcherkez, G. G. B., Farquhar, G. D., and Andrews, T. J. (2006) Despite slow catalysis and confused substrate specificity, all ribulose bisphosphate carboxylases may be nearly perfectly optimized. *Proc. Nat. Acad. Sci. USA*. 103:7246-7251

Thauer, R. K. (2007) A Fifth Pathway of Carbon Fixation. *Science*. 318: 1732-1733

Trans, M., Zhou, B., and Mayfield, S. P. (2009) Synthesis and assembly of a full-length human monoclonal antibody in algal chloroplasts. *Biotechnol. and Bioeng*. 104:663-673

Vance, P., and Spalding, M. H. (2005) Growth, photosynthesis, and gene expression in Chlamydomonas over a range of CO_2 concentrations and CO_2/O_2 ratios: CO_2 regulates multiple acclimation states. *Can. J. Bot.* 83:796-809

Wilcox, J. (2010) See http://www.iecm-online.com for further details and current public version of the IECM (2007) software

Work, V. H., Radakovits, R., Jinkerson, R. E., Meuser, J. E., Elliott, L. G., Vinyard, D. J., Laurens, L. M. L., Dismukes, G. C., and Posewitz, M. C. (2010) Increased lipid accumulation in the *Chlamydomonas reinhardtii sta7-10* starchless isoamylase mutant and increased carbohydrate synthesis in complemented strains. *Euk. Cell*. 9:1251-1261

Zhu X. -G., Long, S. P., and Ort, D. R. (2008) What is the maximum efficiency with which photosynthesis can convert solar energy into biomass? *Curr. Opin. Biotechnol*. 19: 153-159

Zhu, X-G., Long, S. P., and Ort, D. R. (2010) Improving Photosynthetic Efficiency for Greater Yield. *Ann. Rev. Plant Biol*. 61: 235-261

Figure 1. Overview of inputs and outputs of photosynthesis in algae. Light, CO_2 and water are utilized by the photosynthetic reactions to produce valuable products such as hydrogen (H_2), oil (including triacylglycerols, TAGS), sugars and starch. H_2 can be utilized as a fuel or light energy carrier in fuel cells. High value products (HVP) can be made to supplement costs and include products such as carotenoids, antibodies or commodities such as organic acids. Legend courtesy of Ben Hankamer, The University of Queensland, Australia.

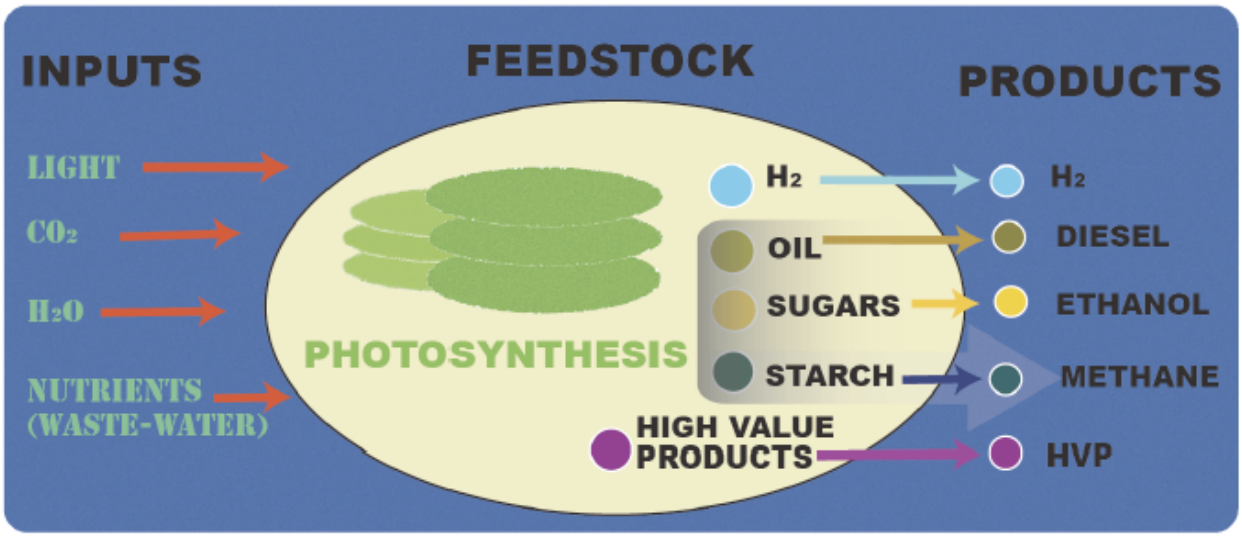
INPUTS
FEEDSTOCK
PRODUCTS
LIGHT
CO2
H2O
NUTRIENTS
(WASTE-WATER)
PHOTOSYNTHESIS
H2
OIL
SUGARS
STARCH
HIGH VALUE
PRODUCTS
H2
DIESEL
ETHANOL
METHANE
HVP

Figure 2. Overview of oxygenic photosynthesis and carbon fixation by the Calvin Cycle. Light driven water oxidation by photosystem II (PSII) releases protons into the lumen and generates O_2, electrons and protons. The protons are utilized by ATP synthase for ATP production. The electrons are shuttled through the electron transfer chain through the light driven protein complex, photosystem I (PSI), to ferredoxin (Fd). Finally, ferredoxin-NADP reductase (FNR) mediates reduction NADP to form NADPH, a soluble reducing equivalent. The Calvin Cycle (C_3 cycle) involves three phases: CO_2 fixation by RuBisCO, followed by reduction using NADPH and ATP and finally regeneration of precursors. Figure courtesy of Don Ort, University of Illinois Urbana-Champaign.

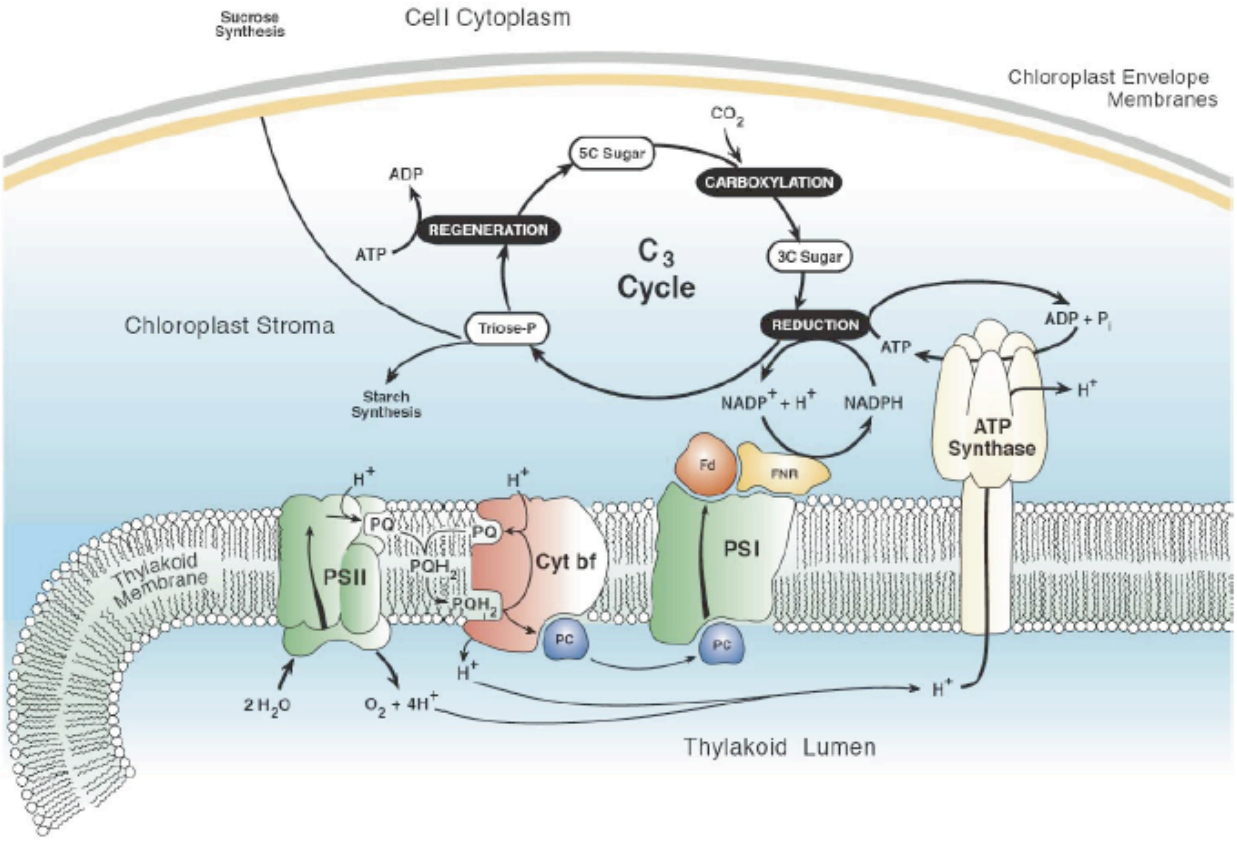
Sucrose Synthesis
Cell Cytoplasm
Chloroplast Envelope Membranes
CO_2
5C Sugar
CARBOXYLATION
ADP
ATP
REGENERATION
C_3 Cycle
3C Sugar
Chloroplast Stroma
Triose-P
REDUCTION
ADP + P_i
ATP
H^+
Starch Synthesis
$NADP^+ + H^+$
NADPH
ATP Synthase
Fd
FNR
PQ
PQH_2
Cyt bf
PSI
PSII
Thylakoid Membrane
PC
$2H_2O$
$O_2 + 4H^+$
Thylakoid Lumen

Figure 3. Maximum Theoretical Photosynthetic Efficiency in Plants and Microalgae. C_3 and C_4 plants have a maximum theoretical yield of 4.6 and 6.0%. Maximum reported yields are 50-60% of theoretical yields, but average yield is 1%. Reproduced with permission from Zhu *et al.,* 2008. Copyright 2008 Elsevier.

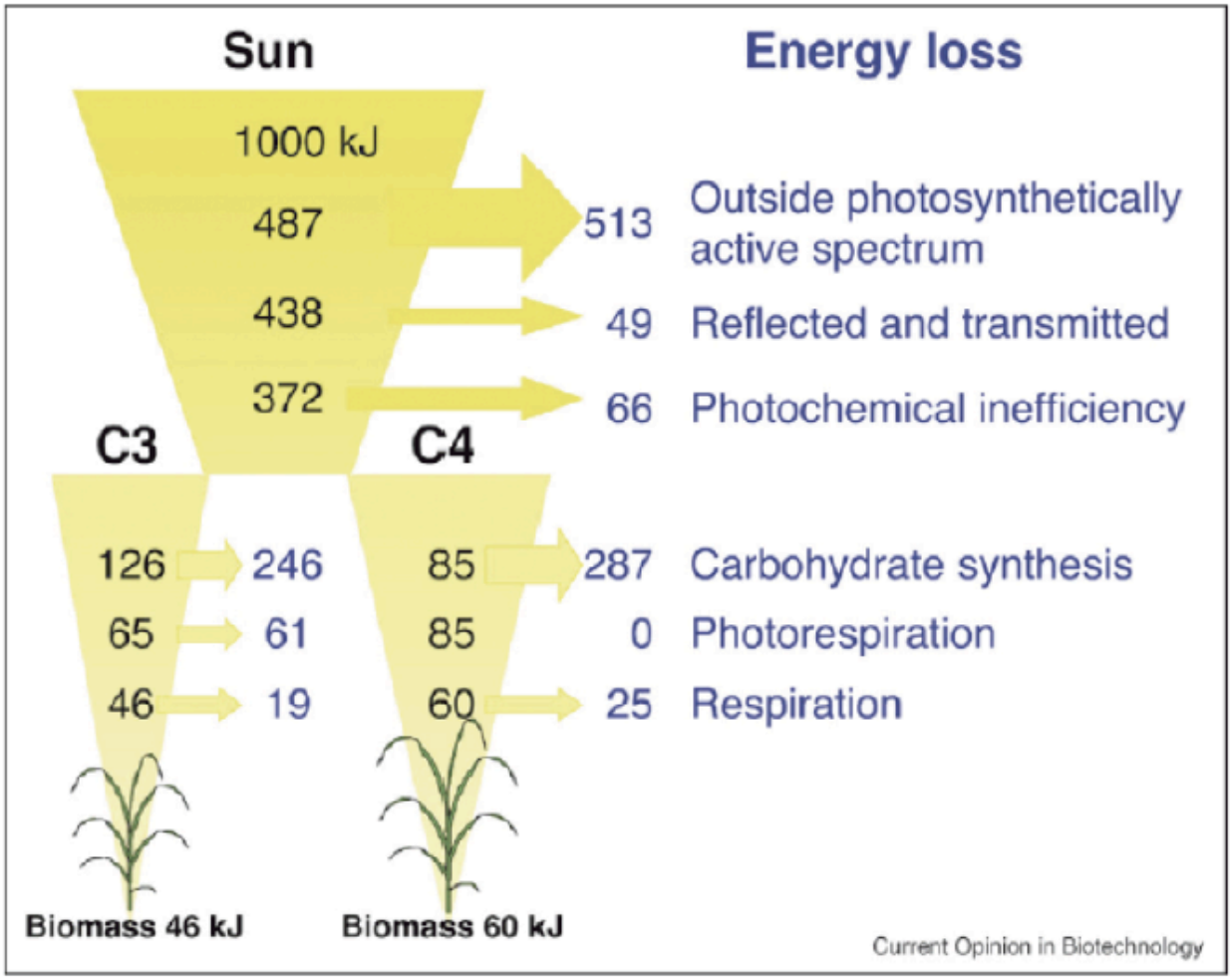
Sun
Energy loss
1000 kJ
487
513
Outside photosynthetically active spectrum
438
49
Reflected and transmitted
372
66
Photochemical inefficiency
C3
C4
126
246
85
287
Carbohydrate synthesis
65
61
85
0
Photorespiration
46
19
60
25
Respiration
Biomass 46 kJ
Biomass 60 kJ
Current Opinion in Biotechnology

Figure 4. The percentage of CO_2 removed from the incoming bioreactor gas stream by a mid-log phase (~1-2x10^6 cells/ml) Chlamydomonas culture over a range of incoming CO_2 concentrations (nominal % CO_2). Each data point represents an independent cell culture. Reproduced with permission from reference (Vance and Spalding, 2005). Copyright 2005 NRC Research Press.

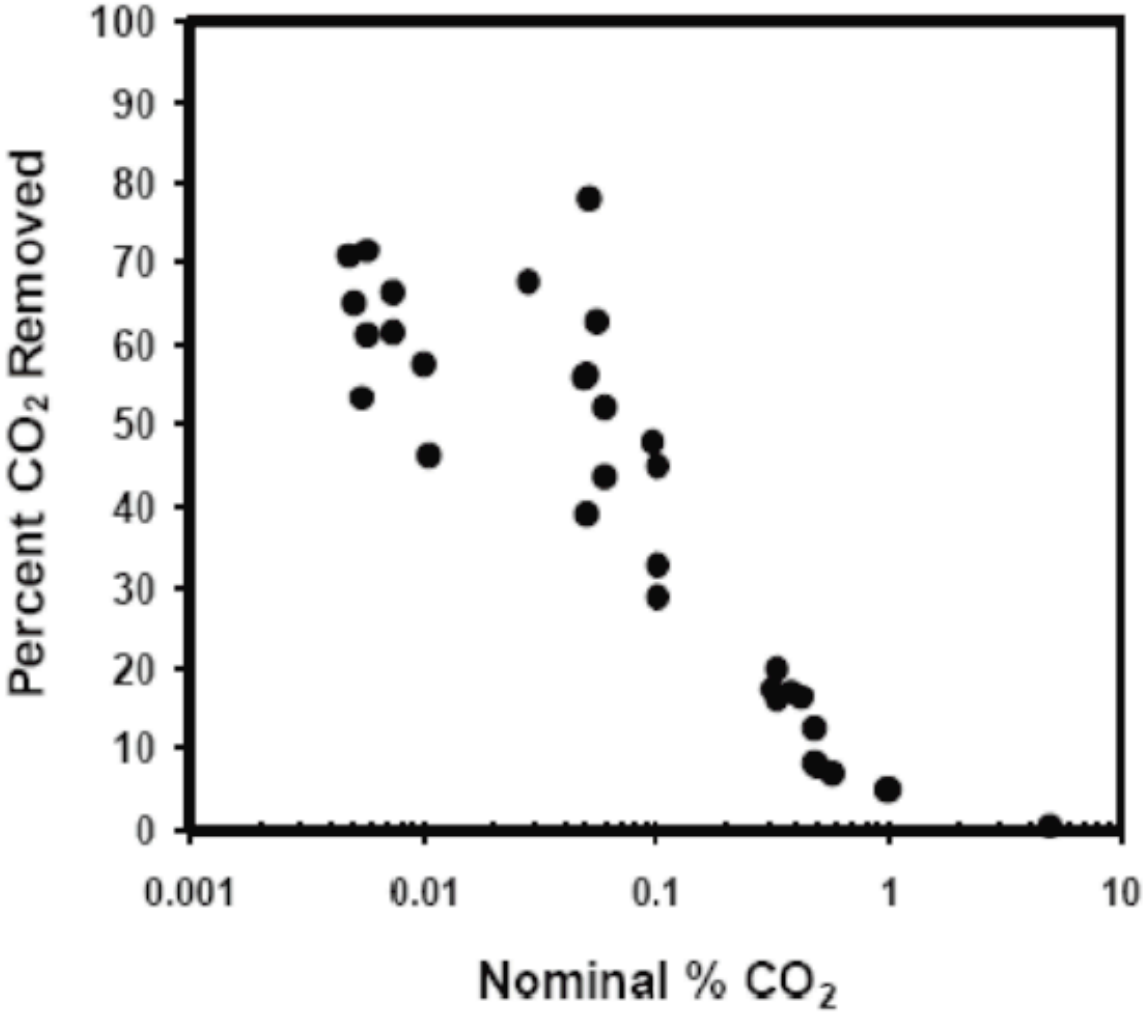

(mid-log phase)

Figure 5. CO_2 concentrating mechanism in a green alga. Bicarbonate (HCO_3-) is transported into the chloroplast and converted into CO_2 by carbonic anhydrase (CA) to provide substrate CO_2 for RuBisCO in the pyrenoid, the site of carbon fixation. Reproduced with permission from Badger *et al.,* 2006. Copyright 2006 Springer.

The CCM in Chlorophyte Algae

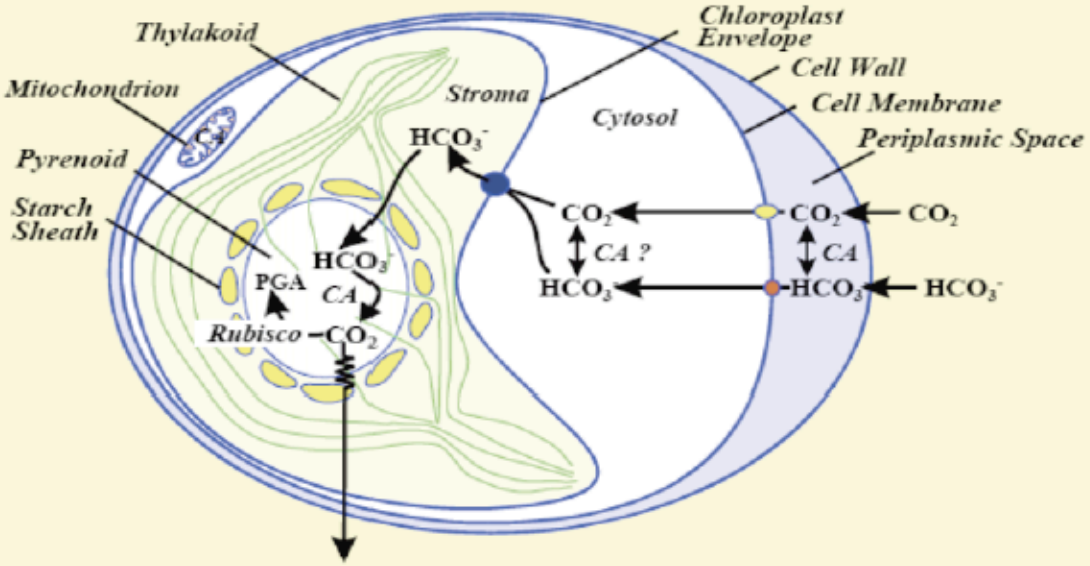

Figure 6. Carbon transport in Cyanobacteria. Bicarbonate (HCO_3-) is actively transported across the membrane using multiple mechanisms tuned to substrate availability. Once internalized, CO_2 is then concentrated in the carboxysome, a bacterial subcompartment housing carbon fixation enzymes. Reproduced with permission from Price *et al.,* 2008.

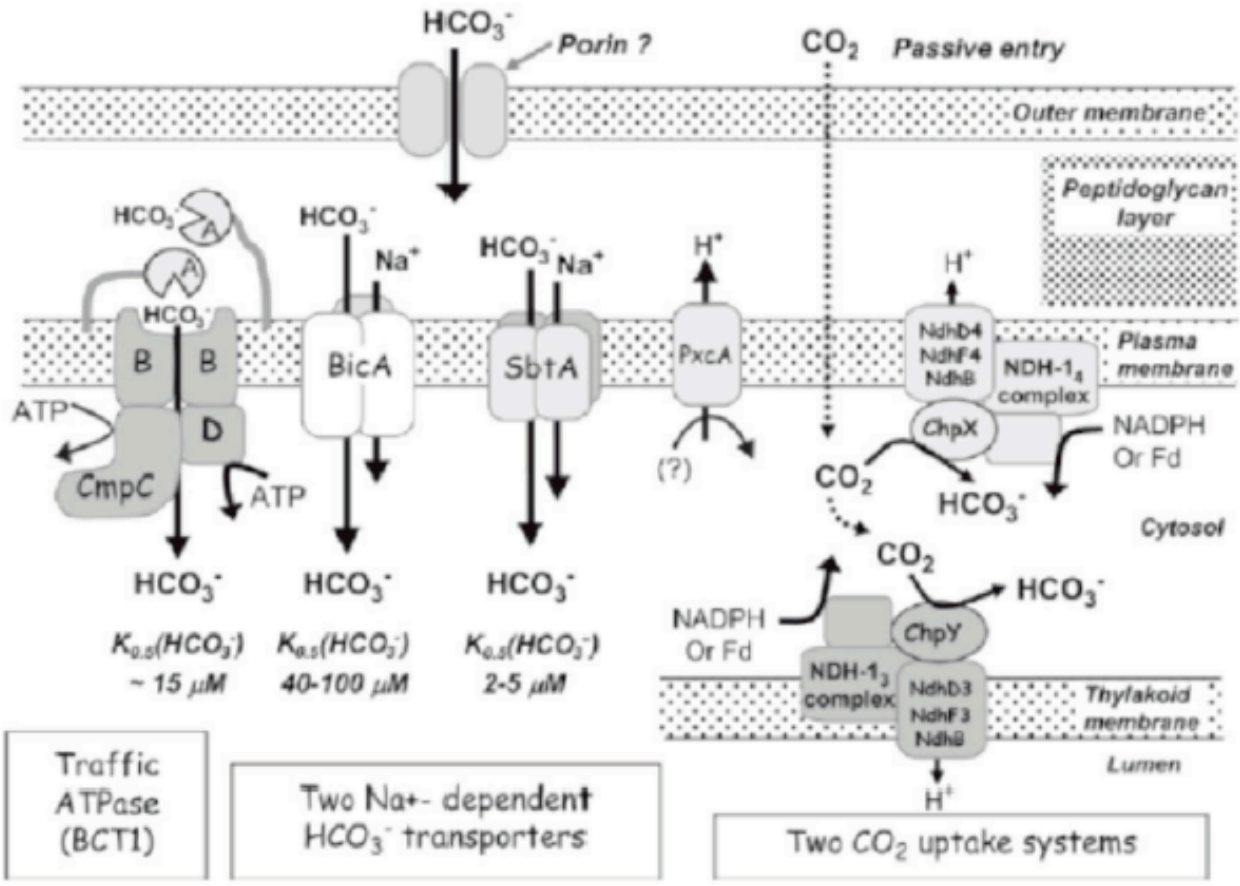
HCO3-
Porin ?
CO2
Passive entry
Outer membrane
Peptidoglycan layer
HCO3-
A
A
HCO3-
B
B
D
ATP
CmpC
ATP
HCO3-
K0.5(HCO3-)
~ 15 µM
HCO3-
Na+
BicA
HCO3-
K0.5(HCO3-)
40-100 µM
HCO3-
Na+
SbtA
HCO3-
K0.5(HCO3-)
2-5 µM
H+
PxcA
(?)
H+
NdhD4
NdhF4
NdhB
NDH-14 complex
Plasma membrane
ChpX
NADPH
Or Fd
CO2
HCO3-
Cytosol
CO2
HCO3-
NADPH
Or Fd
ChpY
NDH-13 complex
NdhD3
NdhF3
NdhB
Thylakoid membrane
Lumen
H+
Traffic ATPase (BCT1)
Two Na+- dependent HCO3- transporters
Two CO2 uptake systems

Figure 7. Cyanobacteria use a plant/bacterial-like photorespiratory pathway. Phosphoglycolate generated as a byproduct of RuBisCO oxygenase activity is metabolized using several pathways. Schematic drawing of the complete photorespiratory 2-PG metabolism in cells of *Synechocystis* sp. strain PCC 6803. 2-PG metabolism is branched into three routes: plant-like glycolate cycle, bacterial-like glycerate pathway, and complete decarboxylation branch (PGP: 2-PG phosphatase, GLD: glycolate dehydrogenase, GGT: glycine/glutamate aminotransferase, GDC: glycine decarboxylase, SHM: serine hydroxymethyltransferase, AGT1: alanine/glyoxylate aminotransferase, HPR1: hydroxypyruvate reductase, GLYK: glycerate kinase, GCL: glyoxylate carboligase, TSR: tartronic semi-aldehyde reductase, GXO: glyoxylate oxidase, ODC: oxalate decarboxylase, FDH: formate dehydrogenase). Reproduced with permission from Hagemann *et al.,* 2010.

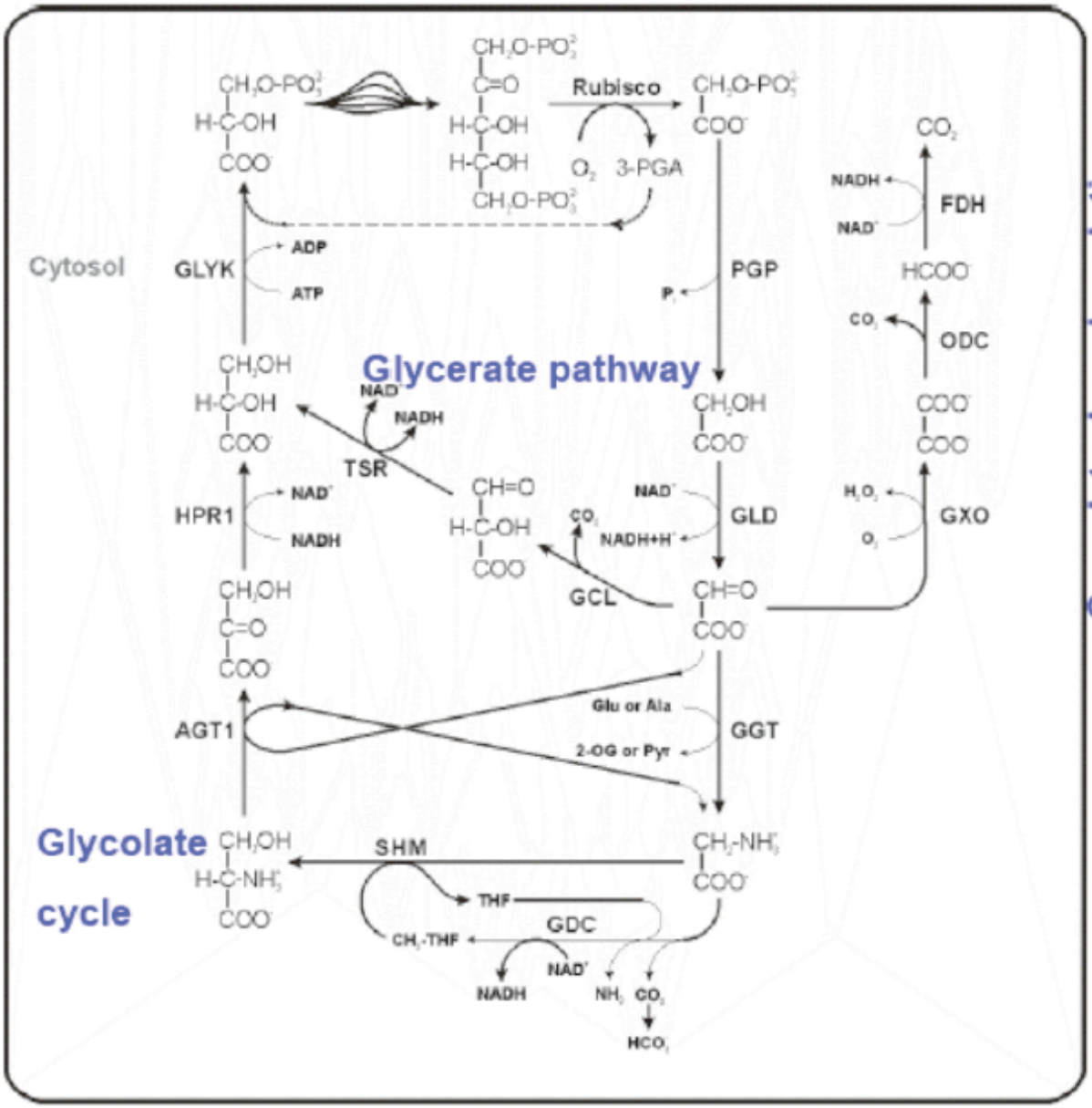
Cytosol
Glycerate pathway
Glycolate cycle
Complete decarboxylation
Rubisco
3-PGA
PGP
GLYK
ADP
ATP
TSR
NAD+
NADH
HPR1
GLD
NADH+H+
GCL
GXO
FDH
ODC
HCOO-
CO2
AGT1
GGT
Glu or Ala
2-OG or Pyr
SHM
THF
CH2-THF
GDC
NH3
HCO3-

Figure 8. Trade-off between RuBisCO specificity and catalytic rate. Carbon fixation competes with photorespiration because CO_2 and O_2 are both substrates for RuBisCO. The oxygenase activity is not desirable as it leads to losses in carbon fixation. Analysis of the natural genetic variation in the kinetic properties of RuBisCO from divergent photosynthetic organisms reveals that forms with higher specificity factors have lower maximum catalytic rates of carboxylation per active site, and vice versa. This inverse relationship implies that higher specificity factors would increase light-limited photosynthesis, while the associated decrease in catalytic rate would lower the light-saturated rate of photosynthesis. The daily integral of CO_2 uptake by a crop canopy is determined by a dynamic combination of light-limited and light-saturated photosynthesis. At current atmospheric CO_2 levels the average specificity factor of current C_3 crops exceeds the level that would be optimal for the present atmospheric [CO_2] of >380 ppm but would be optimal for ~220 ppm, which is close to the average of the last 400,000 years prior to the Industrial Revolution. Canopy simulations reveal that 10% more carbon could be assimilated by C_3 crops if they were operating with a C_4 RuBisCO and this advantage would grow as atmospheric CO_2 levels continue to increase (Zhu *et al.,* 2008; Zhu *et al.,* 2010). Figure courtesy of Don Ort, University of Illinois Urbana-Champaign.

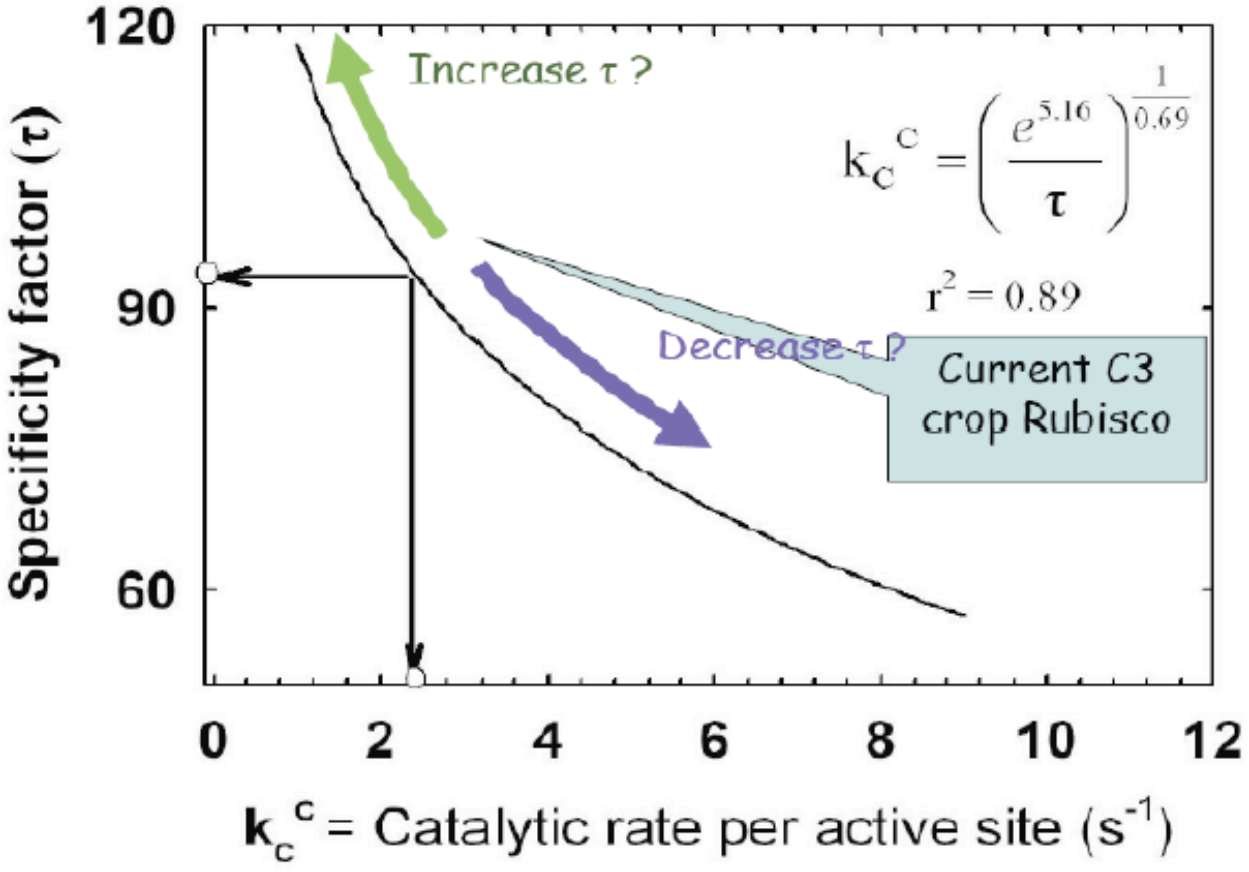
120
90
60
Specificity factor (τ)
Increase τ ?
$k_c^c = \left(\frac{e^{5.16}}{\tau} \right)^{\frac{1}{0.69}}$
$r^2 = 0.89$
Decrease τ ?
Current C3 crop Rubisco
0
2
4
6
8
10
12
k_c^c = Catalytic rate per active site (s^{-1})

Figure 9. Autotrophic Carbon Fixation Pathways. Most photosynthetic organisms can grow autotrophically using only CO_2 as a carbon source. Plants, algae, cyanobacteria and photosynthetic proteobacteria use the Calvin cycle (pathway 1) to fix CO_2 . The green sulfur bacteria use the reductive citric acid cycle (pathway 2), while green nonsulfur bacteria use the 3-hydroxypropionate cycle (pathway 3). The other pathways shown are known only in nonphotosynthetic organisms. Reproduced with permission from Thauer, 2007. Copyright 2007 Science.

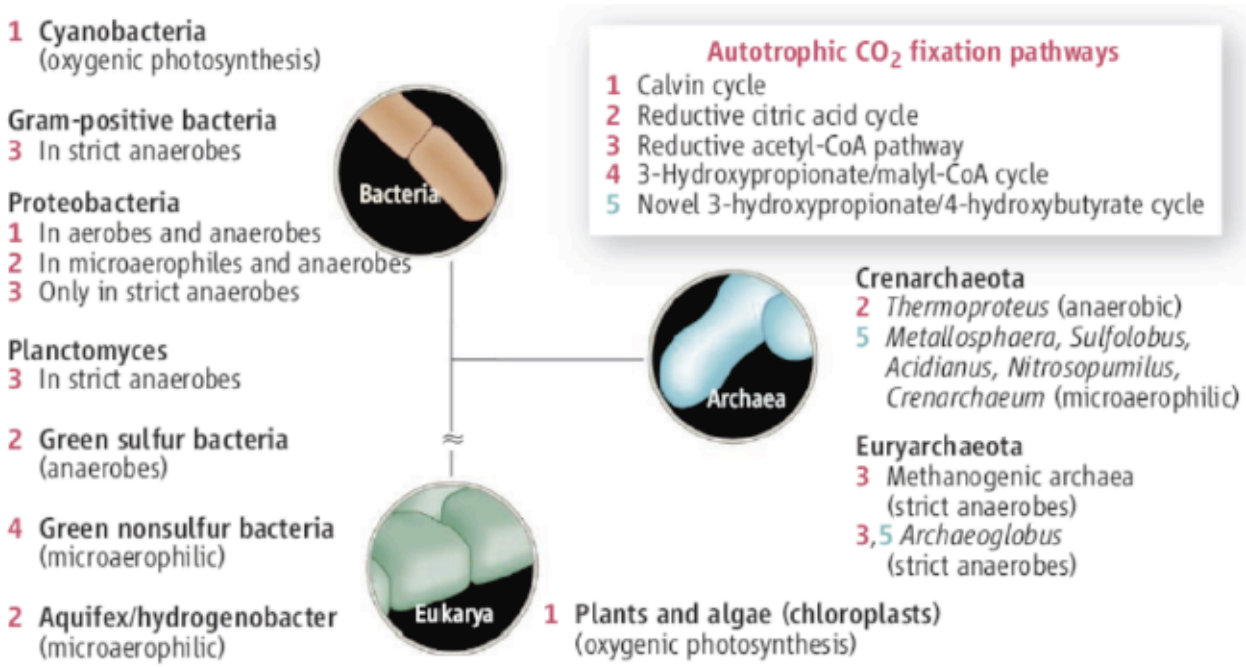
1 Cyanobacteria
(oxygenic photosynthesis)
Gram-positive bacteria
3 In strict anaerobes
Proteobacteria
1 In aerobes and anaerobes
2 In microaerophiles and anaerobes
3 Only in strict anaerobes
Planctomyces
3 In strict anaerobes
2 Green sulfur bacteria
(anaerobes)
4 Green nonsulfur bacteria
(microaerophilic)
2 Aquifex/hydrogenobacter
(microaerophilic)
Bacteria
Archaea
Eukarya
Autotrophic CO_2 fixation pathways
1 Calvin cycle
2 Reductive citric acid cycle
3 Reductive acetyl-CoA pathway
4 3-Hydroxypropionate/malyl-CoA cycle
5 Novel 3-hydroxypropionate/4-hydroxybutyrate cycle
Crenarchaeota
2 Thermoproteus (anaerobic)
5 Metallosphaera, Sulfolobus, Acidianus, Nitrosopumilus, Crenarchaeum (microaerophilic)
Euryarchaeota
3 Methanogenic archaea
(strict anaerobes)
3,5 Archaeoglobus
(strict anaerobes)
1 Plants and algae (chloroplasts)
(oxygenic photosynthesis)

Figure 10. Losses in photosynthesis with increasing light intensity and possible ways to overcome the loss. Qps-eff is photosynthetic efficiency. At high light intensity, photosynthetic antennae complexes dissipate excess energy as heat and fluorescence, leading to less light utilization. To overcome this limitation, one could decrease antennae size, or dilute the light spatially or temporally. Figure courtesy of Ladislav Nedbal, Institute of Systems Biology and Ecology, Academy of Sciences for the Czech Republic.

$Q_{ps\text{-}eff}$ correction for energetic losses to heat, fluorescence (& dynamic effects)

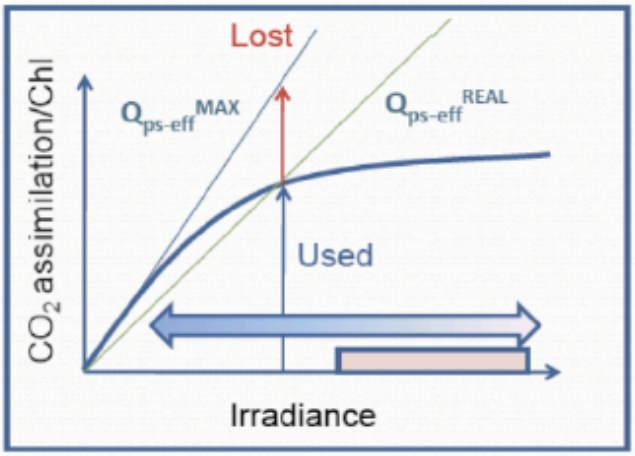

Solution A:
- Decrease the antenna

Solution B:
- Dilute the light technologically in space

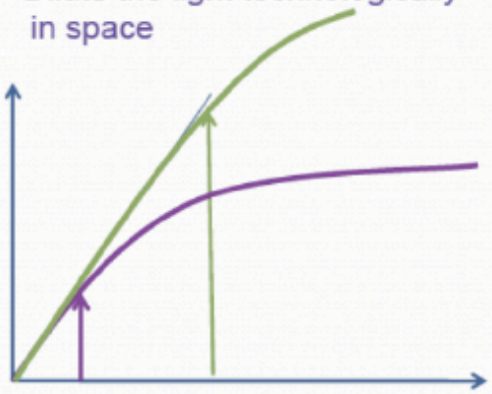

Solution C:
- Dilute the light technologically in time

Figure 11. Photosynthetic rates in algae with varying antennae size. Photosynthetic activity was measured in algae strains with reduced antennae or lacking antennae in air and in high CO_2 at various light intensities. WT, represents wild type, unmodified algae strain; Chl-b deficient is a chlorophyll b deficient algae strain with intermediate light harvesting antennae/complex size (LHC); Chl-b less, represents algae strain with less chlorophyll b than wild type and deficient in LHC. Photosynthetic rates are expressed as the photosynthetic rate in the presence of 10 mM Na bicarbonate minus the photosynthetic rate in air. Figure courtesy of Richard Sayre and Zoee Perrine, Donald Danforth Plant Science Center and Phycal Inc., St. Louis, respectively.

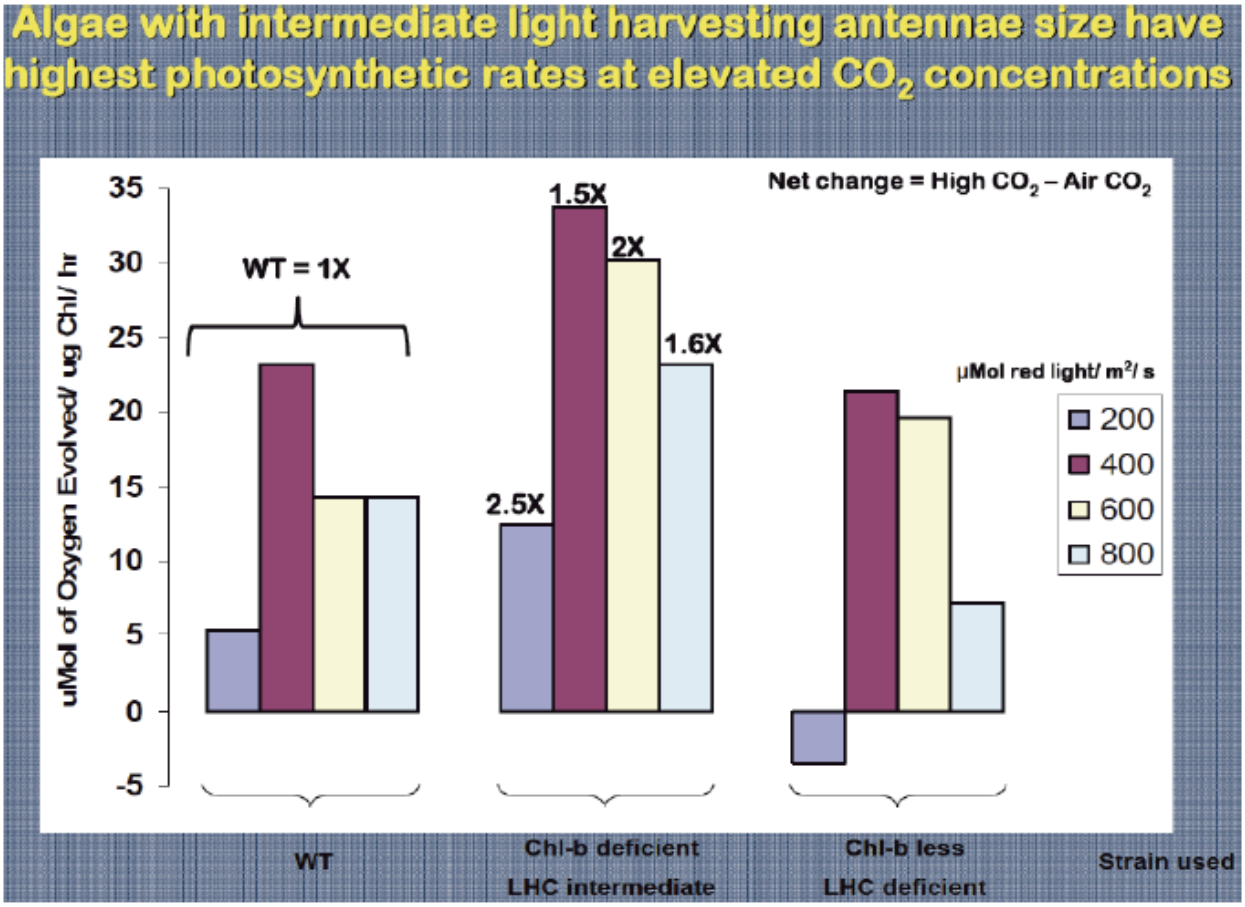
Algae with intermediate light harvesting antennae size have highest photosynthetic rates at elevated CO_2 concentrations
Net change = High CO_2 – Air CO_2
uMol of Oxygen Evolved/ ug Chl/ hr
35
30
25
20
15
10
5
0
-5
WT = 1X
1.5X
2X
1.6X
2.5X
µMol red light/ m^2/ s
200
400
600
800
WT
Chl-b deficient
LHC intermediate
Chl-b less
LHC deficient
Strain used

Figure 12. Influence of glucose on heterotrophic cell cultivation and H_2 production rates in the glucose transporting *Stm6* transformant *Stm6Glc4*. (A) Replication rates of *Stm6* and the transformant *Stm6Glc4* in HSM medium (lacks all carbon sources) supplemented with 100 mM glucose. Each data curve represents an average of at least three measurements. Error bars indicate standard error. (B) Total H_2 production of *Stm6Glc4* as a function of glucose concentration during S-deprivation. Each data curve represents an average of at least three measurements. Error bars indicate standard error. The control measurement (*Stm6Glc4* + 0 mM glucose) was set to 100%. All cell cultures were adjusted to OD750nm = 1.5 (C) Total H_2 production of *Stm6Glc4* compared to *Stm6* in TAP medium containing 1mM glucose during S-deprivation. Each data curve represents an average of three measurements. Error bars indicate standard error. Reproduced with permission from Doebbe *et al.,* 2007.

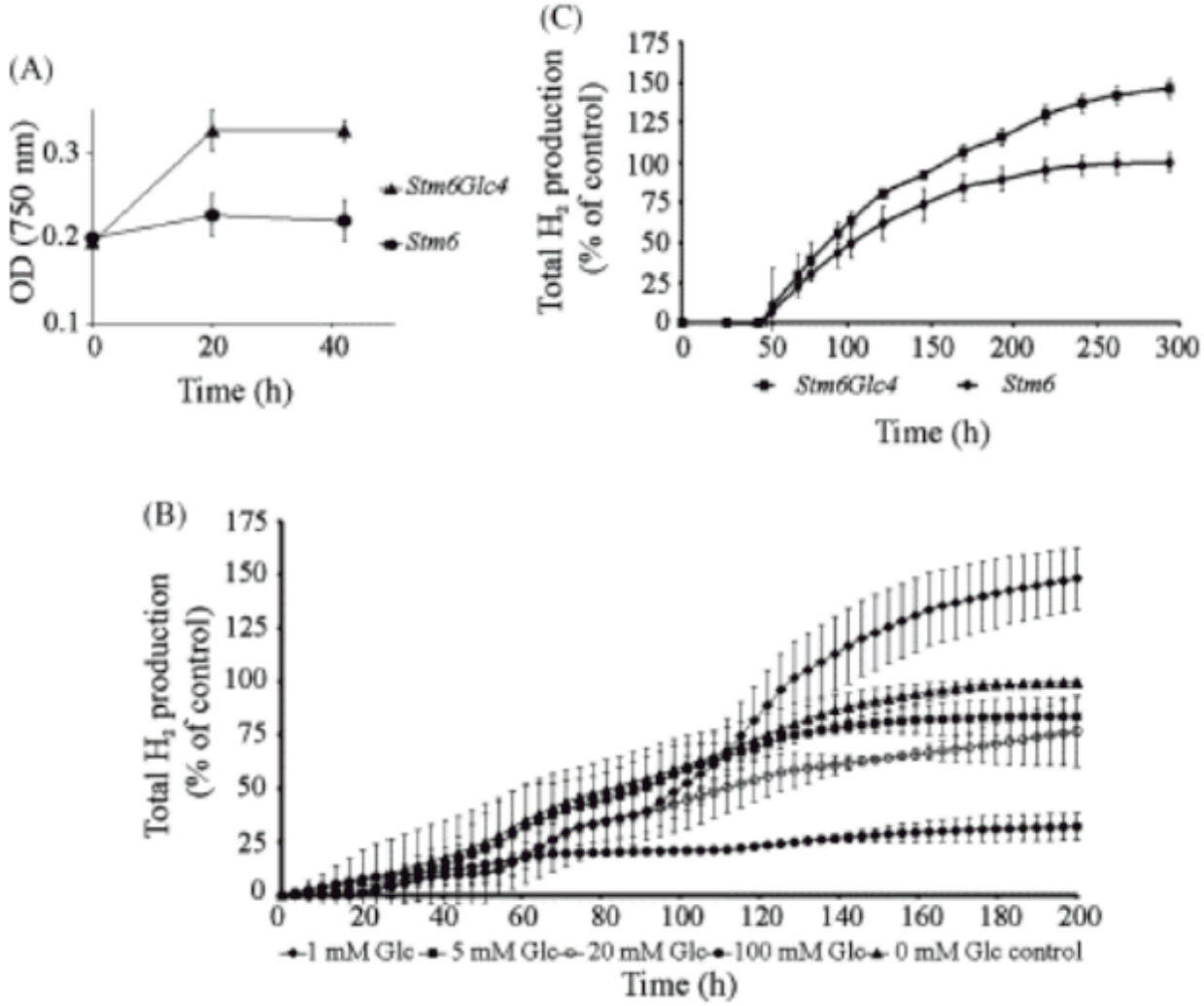
(A)
OD (750 nm)
0.3
0.2
0.1
0
20
40
Time (h)
Stm6Glc4
Stm6
(C)
Total H2 production
(% of control)
175
150
125
100
75
50
25
0
0
50
100
150
200
250
300
Stm6Glc4
Stm6
Time (h)
(B)
Total H2 production
(% of control)
175
150
125
100
75
50
25
0
0
20
40
60
80
100
120
140
160
180
200
1 mM Glc
5 mM Glc
20 mM Glc
100 mM Glc
0 mM Glc control
Time (h)

Figure 13. The Wisconsin Power and Light Columbia Plant uses vast quantities of water per hour, and circulates that water in a large cooling lake located immediately next to the plant. Locations like this may present an opportunity for low cost retrofitting for algal carbon capture (Image from Louis J. Maher Jr., University of Wisconsin).

Figure 14. Summary of studies of microalgae growth in simulated flue gas. Productivity of *Chlorella* sp. KR-1 culture in the presence of NO. Reproduced with permission from Wilcox, 2010. Copyright 2002 Elsevier.

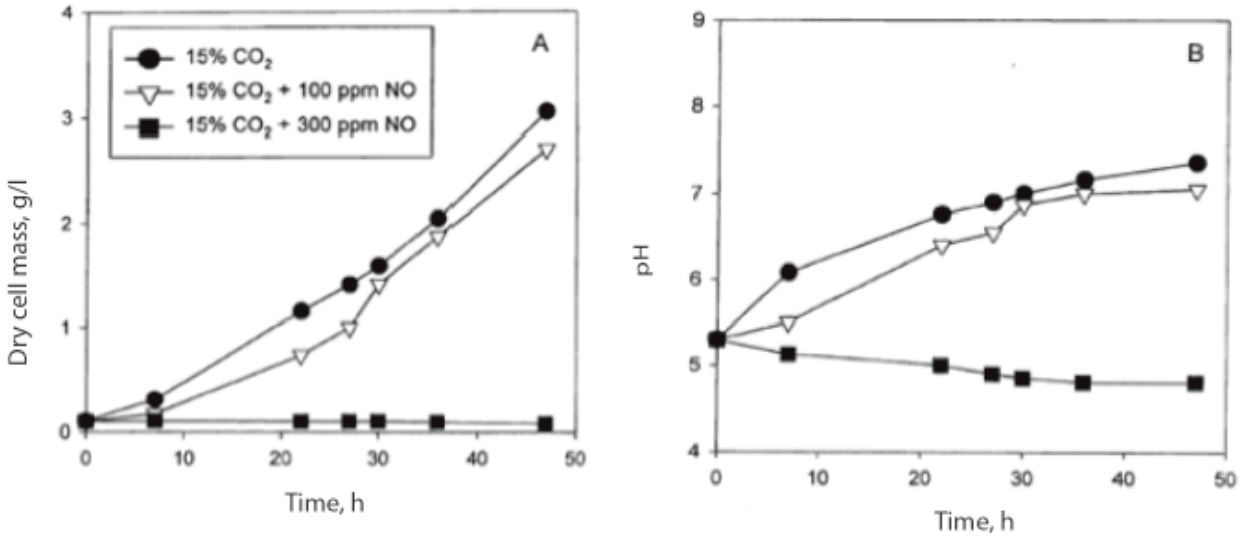
A
15% CO_2
15% CO_2 + 100 ppm NO
15% CO_2 + 300 ppm NO
Dry cell mass, g/l
Time, h
B
pH
Time, h

Figure 15. Productivity of Nannochloropsis salina culture in the presence of SO_2. Results indicate that productivity is not significantly affected by NO and SO_2, at similar concentration levels to that of combustion flue gas, as long as pH is maintained in a favorable range. Redrawn from data from Lee *et al.,* 2002.

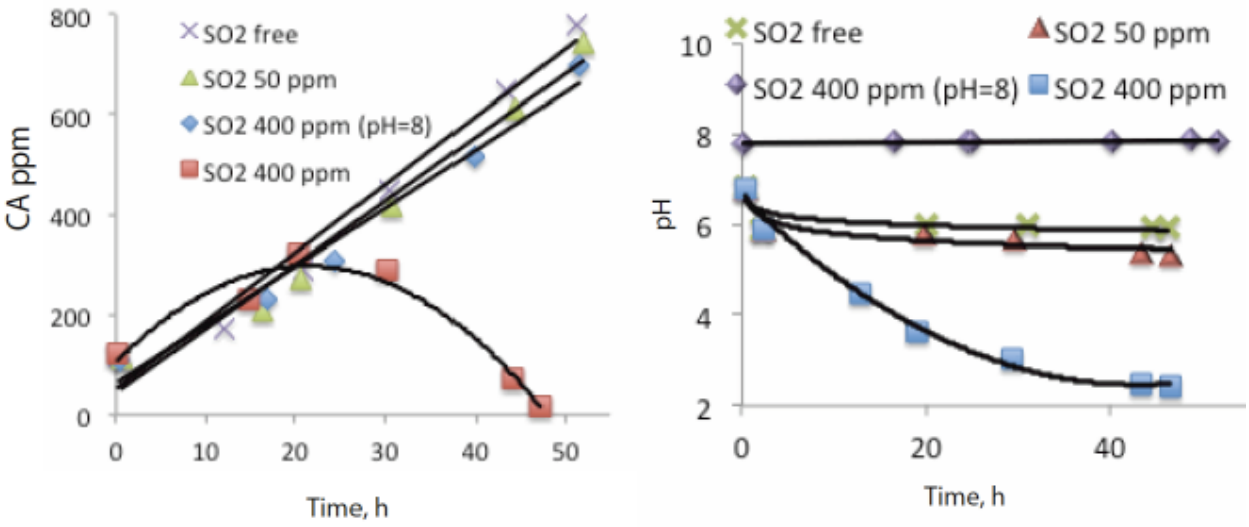
800
600
400
200
0
CA ppm
SO2 free
SO2 50 ppm
SO2 400 ppm (pH=8)
SO2 400 ppm
0
10
20
30
40
50
Time, h
10
8
6
4
2
pH
SO2 free
SO2 50 ppm
SO2 400 ppm (pH=8)
SO2 400 ppm
0
20
40
Time, h

Appendix Chapter 2

Bridging the Gap between Fluxomics and Industrial Biotechnology

Summary

Metabolic flux analysis is a vital tool used to determine the ultimate output of cellular metabolism and thus detect biotechnologically relevant bottlenecks in productivity. ^{13}C-based metabolic flux analysis (^{13}C-MFA) and flux balance analysis (FBA) have many potential applications in biotechnology. However, noteworthy hurdles in fluxomics study are still present. First, several technical difficulties in both ^{13}C-MFA and FBA severely limit the scope of fluxomics findings and the applicability of obtained metabolic information. Second, the complexity of metabolic regulation poses a great challenge for precise prediction and analysis of metabolic networks, as there are gaps between fluxomics results and other omics studies. Third, despite identified metabolic bottlenecks or sources of host stress from product synthesis, it remains difficult to overcome inherent metabolic robustness or to efficiently import and express nonnative pathways. Fourth, product yields often decrease as the number of enzymatic steps increases. Such decrease in yield may not be caused by rate-limiting enzymes, but rather is accumulated through each enzymatic reaction. Fifth, a high-throughput fluxomics tool has not been developed for characterizing nonmodel microorganisms and maximizing their application in industrial biotechnology. Refining fluxomics tools and understanding these obstacles will improve our ability to engineer highly efficient metabolic pathways in microbial hosts.

Introduction

Numerous chemical compounds, ranging from the antimalaria drug artemisinin (Ro, *et al.,* 2006) to the "biofuel" butanol (Atsumi *et al.,* 2008; Atsumi *et al.,* 2009), have been produced with the aid of synthetic biology tools. The ability to efficiently synthesize natural or unnatural products requires a systems-level understanding of metabolism. Functional genomics tools such as genome sequencing, profiling of mRNA transcripts, and proteomics, are widely used to attain a comprehensive knowledge of how metabolic components (genes, proteins and metabolites) are regulated. In contrast to traditional omics tools, flux analysis (measurement of metabolite turnover rates) has become instrumental for physiological prediction and enzymatic rate quantification in metabolic networks (Zamboni and Sauer, 2009). This technology also allows for the identification of metabolic interactions and the knowledge-based design of cellular functions. As such, one can utilize this tool to rationally modify biological hosts and analyze global physiological changes resulting from genetic modifications.

Fluxomics, the cell-wide quantification of intracellular metabolite turnover rates, was first performed via flux balance analysis (FBA). This method uses the stoichiometry of the metabolic reactions in addition to a series of physical, chemical and biological characteristics (thermodynamics, energy balance, gene regulation, etc.) to constrain the feasible fluxes under a given objective function (e.g., maximal biomass production). FBA is an underdetermined model (the number of constraints is smaller than the number of reactions in the metabolic network), which may give unrealistic metabolic readout. In spite of this limitation, FBA provides a useful framework for predicting a wide variety of cellular metabolisms. A complementary approach, ^{13}C-based metabolic flux analysis (^{13}C-MFA) allows for precise determinations of metabolic status under a particular growth condition. The key to ^{13}C-MFA is isotopic labeling, whereby

microbes are cultured using a carbon source with a known distribution of ^{13}C. By tracing the transition path of the labeled atoms between metabolites in the biochemical network, one can quantitatively determine intracellular fluxes.

Flux analysis cannot only provide genetic engineers with strategies for "rationally optimizing" a biological system, but also reveal novel enzymes useful for biotechnology applications (Zamboni and Sauer, 2009). However, flux analysis platforms are still not routinely established in biotechnology companies. This review paper addresses current developments and challenges in the field of fluxomics, which may guide future study to bridge the gap between systems analysis of cellular metabolism and application in biotechnology.

Advances and Limitations in Metabolic Flux Analysis

Steady-State Flux Model

FBA and ^{13}C-MFA concentrate on the stoichiometric (rather than kinetic) properties of metabolic networks. FBA has been widely applied to predict cell growth rate, product yield using different feedstocks, lethality of gene knockouts, and advantageous pathway modifications (Feist *et al.,* 2010). Such a model provides general guidelines for metabolic engineering and thus is a viable first step towards improving biosynthetic yield (Blazeck and ALper, 2010). The hallmark of large scale FBA is the constraint-based reconstruction and analysis toolbox (COBRA) (Becker *et al.,* 2007), which provides a general platform for fluxomics studies.

A number of optimization algorithms and computational strategies for resolving *in silico* and *in vivo* inconsistencies have been proposed to improve the applicability of FBA (Blazeck and Alper, 2010; Kumar and Maranas, 2009). For example, incorporation of thermodynamic principles into FBA can constrain solution space (i.e., energy balance analysis) and obtain both stoichiometrically and thermodynamically feasible fluxes (Boghigian*et al.,* 2010). To describe the "nonoptimal" metabolic behaviors, FBA can use a bilevel optimization approach to estimate the potential trade-off between biomass accumulation and the yield of a desired product (Brugard, *et al.,* 2003). FBA can also relax the objective function for maximization of the biomass and apply a Minimization of Metabolic Adjustment Algorithm to solve fluxes in mutant strains (Boghigian *et al.,* 2010). Such an algorithm calculates fluxes by minimizing the difference between the wild-type flux distributions and the knockout-strain fluxes. Furthermore, FBA can be integrated with metabolic pathway analysis (MPA). MPA is a qualitative technique that examines functional routes existing in a metabolic network without requiring knowledge of reaction rates (Trinh *et al.,* 2009). Combining MPA with FBA can quantitatively trace the

plausible paths for optimal product synthesis, calculate cellular metabolism, and predict phenotypes under genetic manipulations or culture conditions (Schilling *et al.,* 2000). One main advantage of FBA is its capability for genome-scale modeling (including thousands of reactions), which bridge genomic annotation and functional metabolic output. Accordingly, the number of FBA models has increased exponentially since 1999 (Suthers *et al.,* 2009).

^{13}C-MFA aims to rigorously quantify pathway activities in intracellular metabolism by using both the isotopic labeling approach and in silico computation. ^{13}C-MFA is accomplished by feeding microbes a ^{13}C-labeled carbon source, measuring the enrichment pattern of the isotopomer in metabolites (e.g., amino acids), and deciphering the fluxes via computational routines (Zamboni *et al.,* 2009). Since carbon fluxes through a metabolic network generate unique labeling patterns in metabolites, the overall flux distributions can be determined using isotopomer information. Advances in ^{13}C-MFA, including mass spectrometry-based metabolomics and isotopomer modeling approaches (such as novel algorithm using elementary metabolite units), have been discussed in recent papers (Quec *et al.,* 2009; Tang *et al.,* 2009; Zamboni and Sauer, 2009).

Furthermore, open-source software has recently been published that facilitates in silico modelling. For example, WEbcoli is web-based software for flux balance analysis of E.coli (Jung *et al.,* 2009). In addition, OpenFLUX is computationally efficient software for ^{13}C-MFA (Quek *et al.,* 2009), which incorporates the elementary metabolite unit (EMU) framework for calculation of isotopomer balances (Antoniewicz *et al.,* 2007a). User-friendly software such as this allows biologists to perform fluxomics studies with little programming knowledge.

Methodologies for FBA and ^{13}C-MFA share two key characteristics: the use of a metabolic network and the assumption of a steady metabolic state (for internal metabolites).

However, the two techniques have different purposes. FBA profiles the "optimal" metabolism for the desired performance; ^{13}C-MFA measures *in vivo* operation of a metabolic network. The two approaches to flux analysis are complementary when developing a rational metabolic engineering strategy. By comparing existent metabolic fluxes which were empirically determined via 13 C-MFA to the optimal metabolisms predicted by both FBA and other "omics" tools (such as transcription analysis), one can deduce gene targets for solving biotechnologically relevant productivity bottlenecks (Tang *et al.,* 2009). Figure 1 shows that iterative flux analysis and genetic engineering of microbial hosts can remove competitive pathways or toxic byproducts, amplify genes encoding key metabolites, and balance energy metabolism (Blazeck and Halper, 2010).

Metabolic Control and Dynamic Flux Analysis.

FBA and ^{13}C-MFA disregard dynamic intracellular behavior. This avoids the difficulties in developing kinetic models and performing intracellular experimental measurements. However, many biological systems may not maintain a meaningful metabolic (or isotopic) steady state during the fermentation process (Gianchandani *et al,* 2010; Noh *et al.,* 2007; Tang *et al.,* 2007). The description of metabolic perturbation and regulatory mechanisms requires kinetic modeling and control theories. For example, metabolic control analysis (MCA) couples local enzyme kinetics with systematic behavior to predict the control exerted on the targeted pathways by different components (e.g., transcription, enzymes) (Wildermuth, 2000). Although MCA is not a quantitative measurement of flux, MCA can pinpoint bottleneck enzymes (enzymes having the largest effect on the desired flux) in a pathway and allow the analysis of steady-state metabolism in response to changes in the cellular environment (Hoefnagel *et al.,* 2002). In addition to MCA,

the cybernetic approach (a model based on process dynamics and control) has been introduced for study of multienzyme systems and metabolic regulation (Namjoshi *et al.,* 2003). By incorporating both the enzyme kinetics in pathways and the enzyme synthesis kinetics, the cybernetic approach emphasizes microbial process dynamics and control during complicated fermentations (Song *et al.,* 2009).

Both MCA and the cybernetics approach focus on a simplified pathway network. To perform cell-wide quantitative analysis of a dynamic system, it is necessary to integrate the kinetic modeling with FBA and ^{13}C-MFA. Dynamic FBA (dFBA) has been developed to illuminate changing global enzyme activities (Meadows *et al.,* 2010, Gianchandani *et al.,* 2010). To avoid ordinary differential equations and dynamic optimization for describing intracellular metabolism, dFBA can use the Static Optimization Approach (SOA) (Mahadevan *et al.,* 2002) which divides the time-course into numerous small intervals. At each time interval, a steady-state flux is calculated under the assumption of fast intracellular dynamics. By combining stoichiometric FBA for intracellular metabolism with dynamic mass balances on extracellular substrates and products, it is possible to reconstruct dFBA model for genome-scale analysis of microbial metabolisms in industrial fermentations, where product synthesis is often under dynamic control (Hjersted *et al.,* 2007; Oddone *et al.,* 2009).

Recently, ^{13}C-dMFA (dynamic metabolic flux analysis) has been developed for isotopically nonstationary cultures. To profile the flux distributions for fed-batch cultures (slow dynamic metabolism), isotopic pseudosteady state was assumed and two dilution parameters were introduced to account for isotopic transients (Antoniewiecz *et al.,* 2007b). Another approach (Kinetic Flux Profiling) for solving intracellular fluxes is to create a sudden increase of the portion of ^{13}Cin the substrate feed, then measure time-course samples as ^{13}C moves from the

substrate into the metabolites (Yuan *et al.,* 2008). The fluxes can be calculated based on the rates of isotopic enrichment multiplied by the intracellular metabolite concentrations. A similar principle has been proposed for the flux analysis of photoautotrophic microorganisms (Shastri and Morgan 2007) and *E. coli* in an isotopic transient phase (Schaub *et al.,* 2008). If the culture is under both metabolic and isotopic nonstationary state, exploratory and sophisticated ^{13}C-dMFA (dynamic ^{13}C-MFA) models have to be used to calculate both metabolic and isotopic kinetics (Noh *et al.,* 2006; Noh *et al.,* 2007; Wahl *et al.,* 2008). To solve the ^{13}C-dMFA problem efficiently, a set of computational algorithms have been developed for tracing nonstationary isotopomer labeling in response to *in vivo* flux distributions (Noh *et al.,* 2006; Noh *et al.,* 2007; Wahl *et al.,* 2008). The EMU (elementary metabolite unit) framework has also been applied in ^{13}C-dMFA (Antoniewicz, *et al.,* 2007a, Young *et al.,* 2008), because such algorithm can significantly improve computational times for tracing the labeling information (Suthers *et al.,* 2010). To avoid extensive simulation of dynamic isotopomer patterns, the SOA has to be applied by dividing the growth period into small time intervals (30 ~ 60 min), then the "mini" quasi-steady state ^{13}C-MFA can be applied at each time interval based on constraints from simultaneous isotopomer analysis of the fast turnover metabolites (Ruhl *et al.,* 2010). By examining flux profiles over all time intervals, one can resolve the metabolic transients during the entire cultivation period.

Technical Limitations of Fluxomics.

Cell-wide fluxomics tools (i.e., FBA and ^{13}C-MFA) have technical limitations. In genome-scale FBA models, the number of constraints (i.e., the availability of quantitative metabolite data) is much smaller than the number of reactions in the metabolic network. The

calculation of such underdetermined systems depends on objective functions where one assumes that the metabolism optimizes its native "goals" (such as biomass or cofactor production) (Stephanopoulos *et al.,* 1998). This optimization principle has been questioned for several reasons. First, biological systems (e.g., *Bacillus subtilis*) seem to display suboptimal growth performance (Fischer and Sauer, 2005). Second, a previous study examined 11 objective functions in *E. coli* and found no single objective function that can perfectly describe flux states under various growth conditions (Schuetz *et al.,* 2007). For example, unlimited aerobic growth on glucose is best described by a nonlinear maximization of the ATP yield per flux unit, but nutrient-limited continuous cultures favor biomass yield as the objective function. Third, some native cellular processes cannot be simply described by FBA. For example, cyanobacterial species (i.e., *Cyanothece* 51142) maintain their circadian rhythms (e.g., nitrogen fixation and light dependent reaction activities) under nutrient-sufficient and continuous light conditions (Colón-López *et al.,* 1997; Toepel *et al.,* 2008).

The application of ^{13}C-MFA in industrial biotechnology also has several bottlenecks. The most prevalent constriction occurs because current techniques are insufficient for measuring large-scale metabolic networks. Obtaining labeling information of free metabolites rather than amino acids and solving large-scale nonlinear flux models pose two key challenges. As a result, most obtained flux information is limited to central metabolism. To date, only two large-scale ^{13}C-MFA (>300 reactions) have been reported, but many fluxes in their reports cannot be precisely determined due to insufficient constraints (Suthers *et al.,* 2007; Blank *et al.,* 2005). The genome-scale ^{13}C-MFA is still in its infancy and requires further development of the relevant experimental techniques and computational tools (Dauner, 2010). A second issue is that ^{13}C-dMFA is still poorly developed for determining dynamic metabolic behavior. It is difficult for

rapid sampling and precise measurements of metabolites at short time intervals throughout the entire culture period. For example, to measure absolute intracellular metabolite concentrations, one has to grow cell in fully ^{13}C-labeled medium, then the labeled cells are extracted with quenching solvent containing known concentrations of unlabeled internal standards (the concentrations of metabolites are calculated using the isotope ratio-based approach) (Bennett *et al.,* 2008). Such measurement requires extremely high cost of analytical efforts including quick sampling, rapid metabolite extraction, and a high-resolution LC-MS instrument. Furthermore, the time-dependent model includes ordinary differential equations and significantly increases the computational complexity (Noh *et al.,* 2007; Schaub *et al.,* 2008). Third, flux determination assumes that enzymatic reactions are homogenous inside the cell and that there are no transport limitations between metabolite pools. However, eukaryotes have organelles (compartments) that may have diffusion limitations or metabolite channeling (Malaisse *et al.,* 2004; Zamboni *et al.,* 2009). Compartmentalization of amino acid biosynthesis further clouds the obtained amino acid-based labeling information (Blank *et al.,* 2005). Therefore, confident ^{13}C-MFA for eukaryotes not only requires the combination of different analytical tools (GC- MS, LC-MS and NMR) to obtain extensive labeling information (Kleijn *et al.,* 2007), but also adequate sample processing and extraction methods (e.g., separation of compartments by ultracentrifugation). A fourth problem is that some industrial hosts and the great majority of environmental microbes resist cultivation in minimal media, and introducing other nutrient sources often significantly complicates metabolite labeling measurements and flux analyses (Kaeberlein *et al.,* 2002). Finally, a microbial community demonstrates complex metabolic interactions between species. To date, only a few FBA models have been developed for community studies (Stolyar *et al.,* 2007; Taffs *et al.,* 2009). The exchange of metabolites among species is nearly impossible to

unravel by ^{13}C-MFA because complete separation and measurement of metabolites from a single species in a microbial community is impossible (Zamboni and Sauer, 2009). These technical limitations in both FBA and MFA models are responsible for the gap between fluxomics and its applicability in biotechnology.

Integration of Fluxomics with Other "Omics"

It is desirable to integrate the concepts of systems biology (which combines the readouts from transcription as well as protein/metabolite profiling) with fluxomics (Figure 2) (Dauner, 2010). For example, ^{13}C-MFA, enzyme activity assays, and RT- PCR analysis can be used together to study *E. coli* mutants' metabolism (Shimizu, 2004). Additionally, the responses of *E. coli* to genetic modification have been systematically examined by utilizing multiple high-throughput "omics" methods (Ishii *et al.,* 2007). The results illuminate relatively small changes in mRNA and proteins in response to genetic disruptions, which allow the cell to maintain a stable metabolic state under changing growth conditions. A similar approach to the study of *Synechocystis* 6803 has shown that the regulation of some enzymes is sensitive to light conditions (Yang *et al,* 2002). Many other regulatory mechanisms, however, still remain unknown. Furthermore, global regulators in industrial microorganisms have been successfully identified by correlating transcript/transduction levels and metabolic fluxes (Lemuth *et al.,* 2008; Moxley *et al.,* 2009; Nanchen *et al.,* 2008; Tannler *et al.,* 2008). The discovery of functioning regulators provides insight to the entire regulation in metabolic network.

On the other hand, challenges in integrated "omics" studies are also present. The lack of understanding of metabolic regulation at different metabolic levels complicates the rational design of biological systems, which is a major barrier in industrial biotechnology. For example, posttranscriptional regulation poses a significant challenge in integrating fluxomics with other "omics" studies. It is well known that transcript and protein data correlate relatively well for specific pathways, yet this correlation can be poor in cell-wide analyses (Mukhopadhyay *et al.,* 2008). Furthermore, most mRNA expression studies insufficiently predict enzyme activities or flux changes in many *E. coli* pathways (Hua *et al.,* 2007). In studies on the adaptation of *E. coli*

to environmental perturbations, the tricarboxylic acid cycle is found to correlate well with molecular changes at the transcriptional level, but flux alterations in other central metabolic pathways seem to be uncorrelated to changes in the transcriptional network (Fong *et al.,* 2006). Because of the complexity of regulatory mechanisms spanning multiple cellular processes, fluxomics and other "omics" studies may have inconsistent observations which complicate systems-level analyses.

Fluxomics of Microbes for Industrial Biotechnology

FBA allows *in silico* simulations of metabolism in "industrial workhorses," from which desired strains or targeted mutations can be identified. ^{13}C-MFA can assess *in vivo* metabolism of engineered strains under specific growth conditions and validate FBA results. Here, we summarize recent applications of FBA and ^{13}C-MFA for commonly-used industrial chassis (i.e., *E. coli, B. subtilis* and *S. cerevisiae*) and for nonmodel microorganisms (i.e., less-characterized or newly-discovered microorganisms).

Escherichia coli *Model*.

E. coli is the most commonly utilized species in fermentation industry. *E. coli* flux models were reported as early as the 1990s (Varma and Palsson, 1994a; Varma and Palsson, 1994b). For biotechnology applications, the Liao group first applied metabolic pathway analysis (MPA) to guide the genetic manipulation of *E.coli* strains and channel the metabolic fluxes from carbohydrate to the aromatic amino acid pathway (Liao *et al.,* 1996). The Maranas group has integrated cell growth and product synthesis in the OptKnock toolbox (Burgard *et al.,* 2003) and applied it to construct high-performance mutants. The computer-aided designs have shown improved lactic acid, succinate, and 1,3-propanediol production (Fong *et al.,* 2005). FBA can predict lethality in a metabolic network where deletions of more than one nonessential gene mutants may trigger the death of the organism. For example, the Maranas group (Suthers *et al.,* 2009) analyzed the gene/reaction essentiality in a genome-scale model of *E. coli* and systemically identified possible pairs of synthetic lethals: nonessential genes whose simultaneous knockouts would have a potentially lethal effect. Incorporating information about synthetic lethality into the new model will curb the construction of ill-designed biological systems for

biotechnology. Furthermore, FBA can be used to find rate-limiting steps for product synthesis. For example, FBA revealed gene targets, and modification of those genes (i.e., knocking out the genes for pyruvate forming enzymes, overexpression of the glyoxylate shunt and glucose transport system) resulted in more than a ten-fold increase in succinate production (Lee *et al.,* 2002; Lee *et al.,* 2005; Wang *et al.,* 2006). FBA has also been used to improve genetic strategies for the overproduction of secondary metabolites, such as amino acids (Park and Lee, 2008) and lycopene (Alper *et al.,* 2005).

Besides genetic strategies, FBA can provide useful information for the design of optimal fermentation conditions. For example, an FBA model was used to identify nutrient limitations during recombinant interleukin-2 (IL-2) production in *E. coli*. By supplementing specific amino acids, IL- 2 production increased two-fold in fed-batch fermentation (Yegane-Sarkandy *et al.,* 2009). Recently, a reactor-scale dFBA model was developed via a static optimization Approach to analyze *E. coli* metabolism for the production of a biopharmaceutical drug (Meadows *et al.,* 2010). dFBA contains a steady state FBA model embedded within a dynamic kinetic model that describes the time evolution of fermentation process variables (e.g., biomass growth, glucose consumption and products synthesis). Such a model provided guidelines for the optimization of fermentations at the scale of a 1000L process.

The ^{13}C-MFA model was first used to investigate metabolic regulation in *E.coli* under different genetic and environmental conditions (Sauer *et al.,* 1999). ^{13}C-MFA has also been used to examine various biotechnological processes involved in the production of pharmaceuticals, amino acids and polymers. A large scale ^{13}C-MFA with over 300 reactions was successfully developed for amorphadiene (a precursor of the antimalaria drug) producing *E. coli* strains (Suthers *et al.,* 2007). Another study revealed a growth phase-dependent metabolic shift in a

lysine-producing *E. coli* strain (Iwatani *et al.,* 2007). This work was performed in a fed-batch culture with rich medium (containing yeast extract), and metabolic fluxes in both exponential growth and stationary phases were estimated by measuring free metabolites. Metabolic analysis of the stationary phase is important since many products are synthesized during a nongrowth phase. In a third example, ^{13}C-MFA of a 1,3-propanediol producing *E. coli* strain was conducted in fed-batch fermentation (Antoniewicz *et al.,* 2007b). The ^{13}C-MFA results showed a decrease in the split ratio between glycolysis and the pentose- phosphate pathway over the time-course of the culture in response to increasing 1,3-propanediol fluxes.

Bacillus subtilis *Model*.

B. subtilis is the industrial organism of choice for the production of vitamins, antibiotics, enzymes, and nucleosides. The FBA model for *B. subtilis* was constructed based on a combination of genomic, biochemical, and physiological information (Oh *et al.,* 2007). The FBA model was iteratively corrected and improved using information from high-throughput phenotypic screens of mutants, substrate utilization, gene essentiality, and sequence analyses. The *B. subtilis* flux model is mostly studied for riboflavin production, focusing on four aspects: investigating phenotypes of wild type and knock-out strains, assessing production capacity, identifying the impact of different carbon sources on biosynthesis, and characterizing the cellular response to different culture conditions. The Sauer group has extensively investigated riboflavin-producing strains. They first used an FBA model to quantify growth maintenance coefficients, the maximum growth yield, and the specific riboflavin production rate in continuous cultivation (Sauer *et al.,* 1996). Later on, they applied ^{13}C-MFA to the same strain and found that genetic manipulations should target the NADPH balance and riboflavin biosynthetic pathways (Sauer *et*

al., 1997). In other studies on *B. subtilis*, they revealed several guidelines for high-yield riboflavin production (1) they compared the metabolic flux distributions and maintenance energy of eight *Bacillus* strains and discovered that *B. licheniformis* was the most suitable for industrial biotechnology (Tännler *et al.,* 2008), (2) they found that using malate as a substrate resulted in a suppressed respiratory TCA cycle and an enhanced overflow metabolism (Kleijn *et al.,* 2010), and (3) they found the pentose precursors of riboflavin were mainly synthesized via the nonoxidative pentose-phosphate pathway, so any suggested genetic modification should decrease the activity of the oxidative pentose-phosphate pathway (Zamboni*et al.,* 2005). Recently, they developed a ^{13}C-dMFA model for *B. subtilis* to identify the metabolic response of riboflavin overproduction under a glucose-limited fed-batch culture (Rühl *et al.,* 1998). This dynamic flux analysis was obtained by recording changes in labeling patterns of intracellular amino acids under a metabolic pseudosteady state assumption.

Saccharomyces cerevisiae *Model*.

S. cerevisiae is a robust eukaryotic chassis used for the expression of a wide range of products. For example, flux analysis revealed target genes in two native pathways for the overexpression of succinate: the TCA and glyoxylate cycles (Otero *et al.,* 2007). Another study showed the enhancement of sesquiterpene production via *in silico* driven metabolic engineering (Asadollahi *et al.,* 2009). Additionally, flux analysis has been extensively applied for improving ethanol production. First, a number of strategies were developed for the metabolic engineering of redox processes in *S. cerevisiae*, resulting in a decrease in the yield of glycerol by 40% and an increase in ethanol production under both glucose and xylose/glucose growth conditions (Bro *et al.,* 2006). Second, Dikicioglu *et al*. (Dikicioglu *et al.,* 2008) applied a genome-scale FBA model

to analyze respiration-deficient mutants of *S. cerevisiae* for ethanol production. They found that many genetic manipulation strategies (e.g., the overexpression of the glutamate synthase gene) were unnecessary in a respiration-deficient metabolic background. This indicates that the rate limiting steps for ethanol production can change after the initial genetic manipulations of targeted genes. Third, a ^{13}C-MFA model was used to screen ethanol production in 14 hemiascomycetous yeast strains (Blank *et al.,* 2005). This study suggests that *S. cerevisiae* is the ideal ethanol production candidate due to a strong NADPH-driven pentose-phosphate pathway. Other ^{13}C-MFA studies characterized the metabolic shift between oxidative growth and fermentative growth with ethanol production (Frick and Witmann, 2005), investigated alternative carbon substrate (xylose) metabolisms (Grotkjaer, *et al.,* 2005), revealed key factors influencing biomass growth on xylose (Sonderegger *et al.,* 2004), and examined the consumption of ethanol and other storage carbohydrates in a glucose-limited chemostat culture (Van Winden *et al.,* 2005).

Furthermore, a genome-scale FBA indicates an apparent enzyme dispensability, that is, 80% of yeast genes seem to be nonessential for viability under laboratory conditions (Papp *et al.,* 2004). The FBA illustrated the influence of nonessential genes on metabolic robustness and environmental fitness due to genetic buffering through alternative genes, while a ^{13}C-MFA (consisting of over 700 reactions) revealed a similar effect of metabolic network robustness on null mutations (Blank *et al.,* 2005). Understanding the role of these redundant genes is important for a valid and efficient genetic modification.

Nonmodel Microorganisms.

Fluxomics is an important tool for the rigorous study of metabolism in less-characterized microbes that provides novel insights for application of these species to biotechnology. However, fluxomics have not been sufficiently applied to nonmodel microorganisms as compared to model microbial hosts. Table 1 summarizes some milestone papers in fluxomics studies on nonmodel species that are potentially useful for synthetic biology. Compared to the work done in the field of fluxomics for industrial workhorses, far fewer studies have been performed on nonmodel microorganisms. This is due to the complicated growth conditions, poorly-understood metabolic networks, and significant lack of genetic and molecular biology tools. However, nonmodel environmental microorganisms are also important for industrial biotechnology because they often possess native biochemical pathways for chemical synthesis or the ability to utilize cheap substrates (Alper and Stephanopoulos, 2009). Furthermore, flux analysis can be used to discover novel enzymes that can be cloned into industrial microbes to improve their capacity for product synthesis. For example, ^{13}C-MFA revealed a citramalate pathway for isoleucine biosynthesis (independent of the common threonine ammonia-lyase pathway) (Risso *et al.,* 2008; Tang *et al.,* 2007). Citramalate synthase, which has also been detected in some environmental bacteria (Feng *et al.,* 2009; Howell *et al.,* 1999; Wu *et al.,* 2010), can be engineered into *E. coli* for 1-propanol and 1-butanol production. The new pathway bypasses threonine biosynthesis and represents the shortest keto-acid-mediated pathway; as such, it improved biofuel yield 9 to 22-fold (Atsumi and Liao, 2008). Currently, high-throughput genome sequencing methods are mapping genomes in novel microbes at a pace that far exceeds the pace of functional characterization of these species. Therefore, a high throughput ^{13}C-MFA technique is required for screening nonmodel

microorganisms for new enzymes and maximizing their application in industrial biotechnology (Zamboni and Sauer, 2009).

Finding Bottlenecks for Industrial Biotechnology

One of the main goals of fluxomics is to indentify bottlenecks for industrial biotechnology and thereby assist in the creation of rational engineering strategies. Simple measurements of metabolism, however, are not enough to overcome unpredictable challenges in industrial biotechnology. Metabolic regulation is very complex, and systems biology tools are incapable of revealing a general strategy for synthetic biology (Kwok, 2010).

Bottlenecks in industrial biotechnology can be explained from the view of fluxomics. First, metabolic robustness (the ability to maintain metabolic performance under genetic or environmental perturbations) is a long-recognized key property of microbial systems (Stelling *et al.,* 2004). This basic mechanism is often responsible for the gap between computationally aided design and final experimental outcomes. For example, a ^{13}C-MFA study indicates that *E. coli* shows remarkable robustness in the central carbon metabolism in the presence of genetic variation, and is even more flexible in response to altered environmental conditions (e.g., different nutrients or oxygen levels) (Sauer *et al.,* 1999). Analyses of *E. coli* components at multiple "omics" levels also reveal unexpectedly small changes in messenger RNA, proteins and metabolite levels for most genetic disruptions. This is because *E. coli* actively regulates enzyme levels to maintain a stable metabolic state in the presence of perturbations (Fong *et al.,* 2006; Ishii *et al.,* 2007). Similarly, *B. subtilis* shows rigidity and suboptimal performance for its flux regulation in over 137 genetic backgrounds (Fischer and Sauer, 2005). Furthermore, gene essentiality and pairwise genetic interactions have been investigated in *S. cerevisiae* (Deutscher *et al.,* 2006; Papp *et al.,* 2004). It has been found that a gene's function is buffered by duplication in *S. cerevisiae* genomic DNA or by an alternative biochemical pathway. Although only 13% of genes were suggested to be essential by single knockout experiments, simultaneous deletion of

pairs of nonessential genes (>70% of the total metabolic genes) were found to inhibit growth. Invariability of metabolic flux under mutagenic genotypes seems to be an important feature in many biological systems, and thus successful metabolic strategies highly depend on an understanding of robust cellular nature (Heinemann and Sauer 2009; Kol *et al.,* 2010; Tang *et al.,* 2009).

Metabolic engineering of industrial chassis is based on the premise that the yield of a desired product can be increased by identifying and overexpressing the enzymes that catalyze the rate-limiting steps in a given metabolic pathway. However, a method based on overexpressing rate-limiting enzymes will only work if these rate-limiting enzymes exist and remain rate-limiting when their activities are increased. Previous studies have shown that the commonly-believed "rate-limiting" enzymes may not exist in some industrial microbes and an increase in productivity has to be achieved by coordinated expression of entire pathways (Niederberger, *et al.,* 1992). Furthermore, rate-limiting steps in a metabolic network often shift after initial targets have been engineered. For example, phenotypic data in *S. cerevisiae* mutants revealed that some FBA-predicted gene targets for ethanol production are invalid if the cell's respiratory genes have been knocked-out (Dikicioglu *et al.,* 2008). Another example of this phenomenon is highlighted by the metabolic consequences of the deletion of the methionine and cysteine biosynthesis repressor protein (McbR) in Corynebacterium glutamicum, which yielded no overproduction of methionine but drastic accumulation of homolanthionine (Krömer *et al.,* 2006). The above evidence indicates that rate-limiting steps often shift after initial targets have been engineered. Additionally, simultaneous importation and expression of a few heterologous genes to improve the rate-limiting pathway may fail if the nonnative pathway is incompatible with the host. These

efforts often lead to metabolic imbalance and accumulation of toxic metabolites (Atsumi *et al.,* 2008; Atsumi *et al.,* 2009).

Based on the recent publications, we have constructed a linear regression model which shows that the yield of biosynthetic products decreases exponentially as a function of the steps away from central metabolism in *S. cerevisiae* (Figure 3). It is easier to achieve high carbon fluxes to the central metabolites, possibly because enzyme efficiency in central metabolism is usually high (Colletti *et al.,* 2010). However, the yields of secondary metabolites are smaller because each additional enzymatic step may not be perfectly effcient (model regression shows an average of ~67% efficiency in each enzymatic step in secondary metabolisms). This loss of yield is unavoidable due to the metabolism channeling the intermediates away from the desired product. Potential solutions to this problem include (1) designing host-compatible enzymes with high product specificity (Yoshikuni *et al.,* 2006), (2) feeding intermediates to the cell to reduce the number of enzymatic steps to final product (Eshkol *et al.,* 2009), and (3) creating synthetic protein scaffolds, which significantly improve intermediate conversion efficiency and overall biosynthetic yield (Dueber *et al.,* 2009). In conclusion, fluxomics studies enable the quantification of intracellular metabolism. However, this tool is not fully developed, and it remains difficult to deduce cell-wide pathway bottlenecks and to provide effective strategies for biotechnology applications. Numerous technical difficulties in developing flux analysis methods and complicated metabolic regulatory mechanisms have severely limited the scope of fluxomics in industrial biotechnology. It is necessary for the future development of flux analysis to combine other advanced "omics" analysis and molecular biology techniques to resolve challenges in the fluxomics fields.

References

Alper, H., Jin, Y. S., Moxley, J. F., and Stephanopoulos, G. (2005) Identifying gene targets for the metabolic engineering of lycopene biosynthesis in *Escherichia coli*. *Metabol. Eng*. 7, 3:155–164.

Alper, H., Moxley, J., Nevoigt, E., Fink, G. R., and Stephanopoulos, G. (2006) Engineering yeast transcription machinery for improved ethanol tolerance and production. *Science*. 314, 5805:1565–1568.

Alper, H and Stephanopoulos, G. (2009) Engineering for biofuels: exploiting innate microbial capacity or importing biosynthetic potential? *Nat. Rev. Microbiol*., 7, 10: 715–723.

Antoniewicz, M. R., Kelleher, J. K., and Stephanopoulos, G. (2007) Elementary metabolite units (EMU): a novel framework for modeling isotopic distributions. *Metabol. Eng*. 9, 1: 68–86.

Antoniewicz, M. R., Kraynie, D. F., Laffend, L. A., González-Lergier, J. Kelleher, J. K., and Stephanopoulos, G. (2007) Metabolic flux analysis in a nonstationary system: fed-batch fermentation of a high yielding strain of *E. coli* producing 1,3-propanediol. *Met. Eng*. 9, 3: 277– 292.

Asadollahi, M. A., Maury, J., Patil, K. R., Schalk, M., Clark, A., and Nielsen, J. (2009) Enhancing sesquiterpene production in *Saccharomyces cerevisiae* through *in silico* driven metabolic engineering. *Metab. Eng*. 11, 6:328– 334.

Asadollahi, M. A., Maury, J., Schalk, M., Clark, A., and Nielsen, J. (2010) Enhancement of farnesyl diphosphate pool as direct precursor of sesquiterpenes through metabolic engineering of the mevalonate pathway in *Saccharomyces cerevisiae*. *Biotechnol and Bioeng*. 106, 1:86–96.

Atsumi, S. and Liao, J. C. (2008) "Directed evolution of *Methanococcus jannaschii* citramalate synthase for biosynthesis of 1- propanol and 1-butanol by *Escherichia coli*. *Appl. and Env. Microbiol*. 74, 24:7802–7808.

Atsumi, S., Hanai, T., and Liao, J. C. (2008) Non-fermentative pathways for synthesis of branched-chain higher alcohols as biofuels. *Nature*. 451,7174:86–89.

Atsumi, S. Higashide, W., and Liao, J. C., (2009) Direct photosynthetic recycling of carbon dioxide to isobutyraldehyde. *Nat. Biotechnol*. 27,12:1177–1180.

Becker, S. A. Feist, A. M. Mo, M. L. Hannum, G., Palsson, B. Ø., and Herrgard, M. J. (2007) Quantitative prediction of cellular metabolism with constraint-based models: the COBRA toolbox. *Nat. Prot*. 2, 3:727–738.

Bennett, B. D., Yuan, J., Kimball, E. H., and Rabinowitz, J. D. (2008) Absolute quantitation of intracellular metabolite concentrations by an isotope ratio-based approach. *Nat. Prot*. 3, 8:1299–1311.

Blank, L. M., Kuepfer, L., and Sauer, U. (2005) Large-scale ^{13}C-flux analysis reveals mechanistic principles of metabolic network robustness to null mutations in yeast. *Genome Bio*. 6, 6: R49.

Blank, L. M., Lehmbeck, F., and Sauer, U. (2005) Metabolic-flux and network analysis in fourteen hemiascomycetous yeasts. *FEMS Yeast Res.* 5, 6-7:545–558.

Blazeck, J. and Alper, H. (2010) Systems metabolic engineering: genome-scale models and beyond. *Biotechnol*. J. 5, 7:647–659.

Boghigian, B. A., Seth, G., Kiss, R., and Pfeifer, B. A., (2010) Metabolic flux analysis and pharmaceutical production. *Metabol. Eng*. 12, 2:81–95.

Boyle, N. R. and Morgan, J. A. (2009) Flux balance analysis of primary metabolism in *Chlamydomonas reinhardtii. BMC Sys. Biol*. 3, 4.

Bro, C., Regenberg, B., Förster, J., and Nielsen, J. (2006) *In silico* aided metabolic engineering of *Saccharomyces cerevisiae* for improved bioethanol production. *Met. Eng.* 8, 2:102–111.

Burgard, A. P. Pharkya, P. and Maranas, C. D. (2003) Opt- Knock: a bilevel programming framework for identifying gene knockout strategies for microbial strain optimization. *Biotechnol and Bioeng*. 84, 6:647–657.

Carlson, R. and Srienc, F. (2006) Effects of recombinant precursor pathway variations on poly[(r)-3-hydroxybutyrate] synthesis in *Saccharomyces cerevisiae*. *J. Biotechnol*. 124,3: 561–573.

Colletti, P., Goyal, Y., Varman, A., Feng, X., Wu, B., and Tang, Y. J. (2011) Evaluating factors that influence microbial synthesis yields by regression with numerical and categorical variables. *Biotechnol. and Bioeng*. 108,4:893-901.

Colón-López, M. S., Sherman, D. M., and Sherman, L. A. (1997) Transcriptional and translational regulation of nitrogenase in light- dark- and continuous-light-grown cultures of the unicellular cyanobacterium *Cyanothece* sp. strain ATCC 51142. *J. Bact*. 179, 13:4319– 4327.

Dauner, M. (2010) From fluxes and isotope labeling patterns towards *in silico* cells. *Curr. Op. in Biotechnol*. 21,1:55–62.

De Graaf, A. A., Striegel, K., Wittig, R., M. et al. (1999) Metabolic state of *Zymomonas mobilis* in glucose-, fructose-, and xylose-fed continuous cultures as analysed by ^{13}C- and ^{31}P-NMR spectroscopy. *Arch. Microbiol*., 171, 6:371–385.

Deutscher, D., Meilijson, I., Kupiec, M., and Ruppin, E. (2006) Multiple knockout analysis of genetic robustness in the yeast metabolic network. *Nature Genetics*. 38, 9:993– 998.

Dikicioglu, D., Pir, P., Onsan, Z. I., Ulgen, K. O., Kirdar, B., and Oliver, S. G. (2008) Integration of metabolic modeling and phenotypic data in evaluation and improvement of ethanol production using respiration-deficient mutants of *Saccharomyces cerevisiae*. *Appl. and Env. Microbiol*. 74, 18:5809–5816.

Dong, Q. L., Zhao, X. M., Ma, H. W., Xing, X. Y., and Sun, N. X. (2006) Metabolic flux analysis of the two astaxanthin-producing microorganisms *Haematococcus pluvialis* and *Phaffia rhodozyma* in the pure and mixed cultures. *Biotechnol. J*. 1, 11:1283–1292.

Dueber, J. E., Wu, G. C., Malmirchegini G. R., et al., (2009) Synthetic protein scaffolds provide modular control over metabolic flux. *Nat. Biotechnol.* 27, 8:753–759.

Eshkol, N. Sendovski, M., Bahalul, M., Katz-Ezov, T., Kashi, Y., and Fishman, A. (2009) Production of 2-phenylethanol from L-phenylalanine by a stress tolerant *Saccharomyces cerevisiae* strain. *J. Appl. Microbiol*. 106, 2:534–542.

Feist, A. M., Zielinski, D. C., Orth, J. D., Schellenberger, J., Herrgard, M. J., and Palsson, B. Ø. (2010) Model-driven evaluation of the production potential for growth-coupled products of *Escherichia coli. Metabol. Eng.* 12, 3: 173–186.

Feng, X., Mouttaki, H., Lin L. U., et al., (2009) "Characterization of the central metabolic pathways in *Thermoanaerobacter* sp. strain X514 via isotopomer-assisted metabolite analysis. *Appl. and Env. Microbiol*. 75, 15:5001– 5008.

Fischer E., and Sauer, U. (2005) Large-scale *in vivo* flux analysis shows rigidity and suboptimal performance of *Bacillus subtilis* metabolism. *Nat. Genet*. 37, 6:636– 640.

Fong, S. S., Burgard, A. P., Herring, C. D., et al. (2005) *In silico* design and adaptive evolution of *Escherichia coli* for production of lactic acid. *Biotechnol. and Bioeng*., 91, 5:643–648.

Fong, S. S., Nanchen, A. Palsson, B. Ø. and Sauer, U., (2006) Latent pathway activation and increased pathway capacity enable *Escherichia coli* adaptation to loss of key metabolic enzymes. *J. Biol. Chem.* 281. 12:8024– 8033, 2006.

Frick, O. and Wittmann, C. (2005) Characterization of the metabolic shift between oxidative and fermentative growth in *Saccharomyces cerevisiae* by comparative ^{13}C flux analysis. *Microbial Cell Factories*. 4, 30.

Gianchandani, E. P., Chavali, A. K., and Papin, J. A. (2010) The application of flux balance analysis in systems biology. *Wiley Interdisc. Rev: Sys. Bio. and Med*. 2, 3:372–382.

Grotkjær, T., Christakopoulos, P., Nielsen, J., and Olsson, L. (2005) Comparative metabolic network analysis of two xylose fermenting recombinant *Saccharomyces cerevisiae* strains. *Metabol. Eng*., 7, 5-6:437–444.

Heinemann, M., and Sauer, U. (2010) Systems biology of microbial metabolism. *Curr*. *Op. in Microbiol.*, 13, 3:337–343.

Hjersted, J. L., Henson, M. A, and Mahadevan, R. (2007) Genome-scale analysis of *Saccharomyces cerevisiae* metabolism and ethanol production in fed-batch culture. *Biotechnol. and Bioeng*. 97, 5:1190–1204

Hoefnagel, M. H. N., Starrenburg, M. J. C., Martens D. E., et al., (2002) Metabolic engineering of lactic acid bacteria, the combined approach: kinetic modelling, metabolic control and experimental analysis. *Microbiology*. 148, 4:1003–1013.

Howell, D. M., Xu, H., and White, R. H. (1999) (r)-citramalate synthase in methanogenic archaea. *J. Bact*. 181, 1:331–333.

Hua, Q., Joyce, A. R., Palsson, B. Ø. and Fong, S. S. (2007) Metabolic characterization of *Escherichia coli* strains adapted to growth on lactate. *Appl. and Env. Microbiol.* 73, 14:4639–4647, 2007.

Ishii, N., Nakahigashi, K., Baba, T., *et al*. (2007) Multiple high-throughput analyses monitor the response of *E. coli* to perturbations. *Science*. 316, 5824:593–597.

Iwatani, S., Van Dien, S., Shimbo, K., et al. (2007) Determination of metabolic flux changes during fed-batch cultivation from measurements of intracellular amino acids by LC-MS/MS. *J. Biotechnol.* 128, 1:93–111.

Iwatani, S., Yamada, Y., and Usuda, Y. (2008) Metabolic flux analysis in biotechnology processes. *Biotechnol. Lett*. 30, 5:791–799.

Jiang, H., Wood, K. V., and Morgan, J. A., (2005) Metabolic engineering of the phenylpropanoid pathway in *Saccharomyces cerevisiae*. *Appl. and Env. Microbiol.*71, 6:2962–2969.

Jin, Y. L., Jang, Y. S., Lee, J., Papoutsakis, E. T., and Lee, S. Y. (2009) Metabolic engineering of *Clostridium acetobutylicum* M5 for highly selective butanol production. *Biotechnol. J*. 4, 10:1432–1440.

Jung, T. S., Yeo, H. C., Reddy, S. G., Cho, W. S., and Lee, D. Y. (2009) WEbcoli: an interactive and asynchronous web application for *in silico* design and analysis of genome-scale E. *coli* model. *Bioinformatics*. 25, 21:2850–2852.

Kaeberlein, T., Lewis, K., and Epstein, S. S. (2002) Isolating ”uncultivable” microorganisms in pure culture in a simulated natural environment. *Science*. 296,5570: 1127– 1129.

Kleijn, R. J., Buescher, J. M., Le Chat, L., Jules, M., Aymerich, S., and Sauer, U. (2010) Metabolic fluxes during strong carbon catabolite repression by malate in *Bacillus subtilis*. *JBC*. 285, 3:1587– 1596.

Kleijn, R. J., Geertman, J. M. A., Nfor, B. K., et al., (2007) Metabolic flux analysis of a glycerol-overproducing *Saccharomyces cerevisiae* strain based on GC-MS, LC-MS and NMR-derived C-labeling data," *FEMS Yeast Research*. 7, 2:216– 231.

Kleijn, R. J., Van Winden, W. A., Ras, C., Van Gulik, W. M., Schipper, D., and J. J. Heijnen, J. J. (2006) ^{13}C-labeled gluconate tracing as a direct and accurate method for determining the pentose phosphate pathway split ratio in *Penicillium chrysogenum*. *Appl. and Env. Microbiol.* 72, 7:4743–4754.

Kol, S., Elena Merlo, M., Scheltema, R. A., et al., (2010). Metabolomic characterization of the salt stress response in *streptomyces coelicolor*. *Appl. and Env. Microbiol*., 76, 8:2574–2581.

Krömer, J. O., Heinzle, E., Schröder, H., and Wittmann, C. (2006) Accumulation of homolanthionine and activation of a novel pathway for isoleucine biosynthesis in *Corynebacterium glutamicum* McbR deletion strains. *J. Bact.* 188, 2:609–618.

Kumar, V. S., and Maranas, C. D. (2009) GrowMatch: an automated method for reconciling *in silico/in vivo* growth predictions. *PLoS Comp Bio*. 5, 3. Article ID e1000308.

Kwok, R. (2010) Five hard truths for synthetic biology. *Nature*. 463,7279:288–290.

Lee, S. J., Lee, D. Y., Kim, T. Y., Kim, B. H., Lee, J., and Lee, S. Y. (2005) Metabolic engineering of *Escherichia coli* for enhanced production of succinic acid, based on genome comparison and *in silico* gene knockout simulation. *Appl. and Env. Microbiol*. 71, 12:7880– 7887.

Lee, S. Y., Hong, S. H., and Moon, S. Y. (2002) *In silico* metabolic pathway analysis and design: succinic acid production by metabolically engineered *Escherichia coli* as an example. *Genome Informat*. 13:214–223.

Lemuth, K. Hardiman, T. Winter, S. et al. (2008) Global transcription and metabolic flux analysis of *Escherichia coli* in glucose-limited fed-batch cultivations. *Appl. and Env. Microbiol*. 74, 22:7002–7015.

Liao, J. C., Hou, S. Y., and Chao, Y. P. (1996) Pathway analysis, engineering, and physiological considerations for redirecting central metabolism. *Biotechnol. and Bioeng*. 52, 1:129–140.

Mahadevan, R. Edwards, J. S., and Doyle, F. J., (2002) Dynamic flux balance analysis of diauxic growth in *Escherichia coli*. *Biophys. J.* 83, 3:1331–1340.

Malaisse, W. J., Zhang, Y., Jijakli, H., Courtois, P., and Sener, A. (2004) Enzyme-to-enzyme channelling in the early steps of glycolysis in rat pancreatic islets. *Int. J. of Biochem. Cell Biol.* 36, 8:1510–1520.

Meadows, A. L., Karnik, R., Lam, H., Forestell, S., and Snedecor, B. (2010) Application of dynamic flux balance analysis to an industrial *Escherichia coli* fermentation. *Metabol. Eng.* 12, 2:150–160.

McKinlay J. B. and Vieille, C. (2008) ^{13}C-metabolic flux analysis of *Actinobacillus succinogenes* fermentative metabolism at different $NaHCO_3$ and H_2 concentrations. *Metabol. Eng.* 10, 1:55–68.

McKinlay, J. B., Shachar-Hill, Y., Zeikus, J. G., and Vieille, C. (2007) Determining *Actinobacillus succinogenes* metabolic pathways and fluxes by NMR and GC-MS analyses of ^{13}C-labeled metabolic product isotopomers. *Metabol. Eng*. 9, 2:177–192.

Moxley, J. F., Jewett, M., C., Antoniewicz, M. R., et al. (2009) Linking high-resolution metabolic flux phenotypes and transcriptional regulation in yeast modulated by the global regulator Gcn4p. *Proc. Nat. Acad. Sci. USA*.106,16:6477–6482.

Mukhopadhyay, A. Redding, A, M., Rutherford, B. J., and Keasling, J. D. (2008) Importance of systems biology in engineering microbes for biofuel production. *Curr. Op. in Biotechnol.* 19, 3:228–234.

Namjoshi, A. A., Hu, W. S, and Ramkrishna, D. (2003) Unveiling steady-state multiplicity in hybridoma cultures: the cybernetic approach. *Biotechnol. Bioeng*. 81, 1:80–91.

Nanchen, A. Schicker, A., Revelles, O., and Sauer, U. (2008) Cyclic AMP-dependent catabolite repression is the dominant control mechanism of metabolic fluxes under glucose limitation in *Escherichia coli*. *J. Bact*. 190, 7:2323–2330.

Navarro, E., Montagud, A., Fernández de Córdoba, P, and Urchueguía, J. F. (2009) Metabolic flux analysis of the hydrogen production potential in *Synechocystis* sp. PCC 6803. *Int. J. Hyd. Ener.* 34, 21:8828– 8838.

Niederberger, P., Prasad, R., Miozzari, G., and Kacser, H. (1992) A strategy for increasing an *in vivo* flux by genetic manipulations: the tryptophan system of yeast. *Biochem. J.* 287, 2:473–479.

Nöh, K., Grönke, K., Luo, B., Takors, R., Oldiges, M., and Wiechert, W. (2007) Metabolic flux analysis at ultra short time scale: isotopically non-stationary ^{13}C labeling experiments. *J. Biotechnol.* 129, 2:249–267.

Nöh, K., Wahl, A., and Wiechert, W. (2006) Computational tools for isotopically instationary ^{13}C labeling experiments under metabolic steady state conditions. *Metabol. Eng.* 8, 6:554–577.

Oddone, G. M., Mills, D. A., and Block, D. E. (2009) A dynamic, genome-scale flux model of *Lactococcus lactis* to increase specific recombinant protein expression. *Metabol Eng.* 11, 6:367–381.

Oh, Y. K., Palsson, B. Ø. Park, S. M., Schilling, C. H., and Mahadevan, R. (2007) Genome-scale reconstruction of metabolic network in *Bacillus subtilis* based on high-throughput phenotyping and gene essentiality data. *JBC*. 282, 39:28791–28799.

Otero, J. M., Olssona, L., and Nielsen, J. (2007) Metabolic engineering of *Saccharomyces cerevisiae* microbial cell factories for succinic acid production. *J. Biotechnol*. 131, 2:205.

Overkamp, K. M., Bakker, B. M., Kötter, B., Luttik, M. A. H., Van Dijken, J. P., and Pronk, J. T. (2002) Metabolic engineering of glycerol production in *Saccharomyces cerevisiae*. *Appl. Env. Microbiol.* 68, 6:2814–2821.

Papp, B., Pál, C., and Hurst, L. D. (2004) Metabolic network analysis of the causes and evolution of enzyme dispensability in yeast. *Nature*. 429, 6992:661–664.

Park, J. H. and Lee, S. Y. (2008) Towards systems metabolic engineering of microorganisms for amino acid production. *Curr. Opin. in Biotechnol.* 19, 5:454–460.

Quek, L. E. Wittmann, C., Nielsen, L. K. and Krömer, J. O. (2009) OpenFLUX: efficient modelling software for ^{13}C-based metabolic flux analysis. *Microb. Cell Factories*. 8, 25.

Risso, C., Van Dien, S. J., Orloff, A., Lovley, D. R., and Coppi, M. V. (2008) Elucidation of an alternate isoleucine biosynthesis pathway in *Geobacter sulfurreducens. J. Bact*., 190, 7:2266–2274.

Ro, D. K. Paradise, E. M., Quellet, M. et al., (2006) Production of the antimalarial drug precursor artemisinic acid in engineered yeast. *Nature*. 440,7086:940–943.

Rühl, M., Zamboni, N., and Sauer, U. (2010) Dynamic flux responses in riboflavin overproducing *Bacillus subtilis* to increasing glucose limitation in fed-batch culture. *Biotechnol and Bioeng*. 105, 4:795–804.

Sauer, M., Branduardi, P., Valli, M., and Porro, D. (2004) Production of L-ascorbic acid by metabolically engineered *Saccharomyces cerevisiae* and *Zygosaccharomyces bailii*. *Appl. Env. Microbiol*. 70, 10:6086–6091.

Sauer, U., Hatzimanikatis, V., Bailey, J. E., Hochuli, M., Szyperski, T., and Wüthrich, K. (1997) Metabolic fluxes in riboflavin-producing *Bacillus subtilis*. *Nat Biotechnol*. 15, 5:448–452.

Sauer, U., Hatzimanikatis, V., Hohmann,H. P., Manneberg, M., Van Loon, A. P. G. M., and Bailey, J. E. (1996) Physiology and metabolic fluxes of wild-type and riboflavin-producing *Bacillus subtilis*. *Appl. Env. Microbiol*. 62, 10:3687–3696.

Sauer, U., Lasko, D. R., Fiaux, J. (1999) Metabolic flux ratio analysis of genetic and environmental modulations of *Escherichia coli* central carbon metabolism. *J. Bact.* 181, 21:6679–6688.

Schaub, J., Mauch, K., and Reuss, M. (2008) Metabolic flux analysis in *Escherichia coli* by integrating isotopic dynamic and isotopic stationary ^{13}C labeling data. *Biotechnol. Bioeng*. 99, 5:1170–1185.

Schilling, C. H., Edwards, J. S., Letscher, D., and Palsson, B. Ø. (2000) Combining pathway analysis with flux balance analysis for the comprehensive study of metabolic systems. *Biotechnol. Bioeng.* 71, 4: 286–306.

Schuetz, R., Kuepfer, L., and Sauer, U. (2007) Systematic evaluation of objective functions for predicting intracellular fluxes in *Escherichia coli*. *Mol. Sys. Bio*. 3:119.

Shastri A. A. and Morgan, J. A., (2005) Flux balance analysis of photoautotrophic metabolism. *Biotechnol. Prog*. 21, 6:1617–1626.

Szczebara, F. M., Chandelier, C. Villeret, C., et al. (2003) Total biosynthesis of hydrocortisone from a simple carbon source in yeast. *Nat. Biotechnol*. 21, 2:143-149.

Shastri A. A., and Morgan, J. A. (2007) A transient isotopic labeling methodology for ^{13}C metabolic flux analysis of photoautotrophic microorganisms. *Phytochem*. 68,16-18: 2302–2312.

Shiba, Y., Paradise, E. M., Kirby, J., Ro, D. K., and Keasling, J. D. (2007) Engineering of the pyruvate dehydrogenase bypass in *Saccharomyces cerevisiae* for high-level production of isoprenoids. *Metabol Eng.* 9, 2:160-168.

Shimizu, K. (2004) Metabolic flux analysis based on ^{13}C-labeling experiments and integration of the information with gene and protein expression patterns. *Adv. Biochem. Eng./Biotechnol*. 91, 1–49.

Shirai, T., Fujimura, K., Furusawa, C., Nagahisa, K., Shioya, S., and Shimizu, H. (2007) Study on roles of anaplerotic pathways in glutamate overproduction of *Corynebacterium glutamicum* by metabolic flux analysis. *Microbial Cell Factories*. 6, 19.

Sonderegger, M., Jeppsson, M., Hahn-Hägerdal, B., and Sauer, U. (2004) Molecular basis for anaerobic growth of *Saccharomyces cerevisiae* on xylose, investigated by global gene expression and metabolic flux analysis. *Appl. Env. Microbiol*. 70, 4: 2307–2317.

Song, H. S., Morgan, J. A, and Ramkrishna, D. (2009) Systematic development of hybrid cybernetic models: application to recombinant yeast co-consuming glucose and xylose. *Biotechnol. Bioeng*. 103, 5:984-1002.

Stelling, J., Sauer, U., Szallasi, Z., Doyle, F. J., and Doyle, J. (2004) Robustness of cellular functions. *Cell*. 118, 6:675–685.

Stephanopoulos, G. N., Aristidou, A. A., and Nielsen, J. (1998) *Metabolic Engineering Principles and Methodologies*. Academic Press, San Diego, Calif, USA, 1998.

Stolyar, S., Van Dien, S., Hillesland, K. L., et al.(2007) Metabolic modeling of a mutualistic microbial community. *Mol. Sys. Biol.* 3, 92.

Suthers, P. F., Burgard, A. P., Dasika, M. S., et al. (2007) "Metabolic flux elucidation for large-scale models using ^{13}C labeled isotopes," *Metabol. Eng*. 9, 5-6:387–405.

Suthers, P. F., Chang, Y. J., and Maranas, C. D. (2010) Improved computational performance of MFA using elementary metabolite units and flux coupling. *Metabol. Eng.* 12, 2:123–128.

Suthers, P. F., Dasika, M. S., Kumar, V. F., Denisov, G., Glass, J. I., and Maranas, C. D. (2009) Genome-scale metabolic reconstruction of *Mycoplasma genitalium*, iPS189. *PLoS Comp. Bio.* 5, 2. Article ID e1000285.

Suthers, P. F., Zomorrodi, A. and Maranas,C. D. (2009) Genome-scale gene/reaction essentiality and synthetic lethality analysis. *Mol. Sys. Biol*. 5, 301.

Taffs, R. Aston, J. E., Brileya, K., et al.(2009) *In Silico* approaches to study mass and energy flows in microbial consortia: a syntrophic case study. *BMC Sys. Biol.,* 3, 114.

Tang, Y. J., Chakraborty, R., Martín, H. G., Chu, J., Hazen, T. C., and Keasling, J. D. (2007) Flux analysis of central metabolic pathways in *Geobacter metallireducens* during reduction of soluble Fe(III)-nitrilotriacetic acid. *Appl. Env. Microbiol*. 73, 12:3859–3864.

Tang, Y. J., Sapra, R., and Joyner, D. et al. (2009) Analysis of metabolic pathways and fluxes in a newly discovered thermophilic and ethanol-tolerant *geobacillus* strain. *Biotechnol. Bioeng*. 102, 5:1377–1386.

Tang, Y. J., Martin, H. G., Deutschbauer, A., et al., (2009) Invariability of central metabolic flux distribution in *Shewanella oneidensis* MR-1 under environmental or genetic perturbations. *Biotechnol. Prog*. 25, 5:1254–1259.

Tang, Y. J., Martin, H. G., Myers, S., Rodriguez, S., Baidoo, E. E. K., and Keasling, J. D. (2009) Advances in analysis of microbial Metabolic fluxes via ^{13}C isotopic labeling. *Mass Spec. Rev*. 28, 2: 362–375.

Tang, Y. J., Meadows, A. L., and Keasling, J. D. (2007) A kinetic model describing *Shewanella oneidensis* MR-1 growth, substrate consumption, and product secretion. *Biotechnol. and Bioeng.* 96, 1:125–133.

Tännler, S., Decasper, S., and Sauer, U. (2008) Maintenance metabolism and carbon fluxes in *Bacillus* species. *Microbial Cell Factories*. 7,19.

Tännler, S., Fischer, E., Le Coq D., et al. (2008) CcpN controls central carbon fluxes in *Bacillus subtilis*," *J. Bact.* 190, 18:6178–6187.

Toepel, J., Welsh, E., Summerfield, T. C., Pakrasi, H. B., and Sherman, L. A. (2008) Differential transcriptional analysis of the cyanobacterium *Cyanothece* sp. strain ATCC 51142 during light-dark and continuous-light growth. *J. Bact.* 190, 11:3904–3913.

Toivari, M. H., Ruohonen, L., Miasnikov, A. N., Richard, P., and Penttilä, M. (2007) Metabolic engineering of *Saccharomyces cerevisiae* for conversion of D-glucose to xylitol and other five-carbon sugars and sugar alcohols. *Appl. Env. Microbiol*. 73, 17: 5471–5476.

Tokuhiro, K., Muramatsu, M., Ohto, C., et al., (2009) Overproduction of geranylgeraniol by metabolically engineered *Saccharomyces cerevisiae*. *Appl. Env. Microbiol*. 75, 17:5536–5543.

Trinh, C. T., Wlaschin, A., and Srienc, F. (2009) Elementary mode analysis: a useful metabolic pathway analysis tool for characterizing cellular metabolism. *Appl. Microbiol. Biotechnol*. 81,5:813–826.

Tsantili, I. C., Karim, M. N., and Klapa, M. I. (2007) Quantifying the metabolic capabilities of engineered *Zymomonas mobilis* using linear programming analysis. *Microbial Cell Factories.* 6, 8.

Van Maris, A. J. A. Geertman, J. M. A., Vermeulen, A. et al. (2004) Directed evolution of pyruvate decarboxylase-negative *Saccharomyces cerevisiae*, yielding a C2-independent, glucose-tolerant, and pyruvate-hyperproducing yeast. *Appl. Env. Microbiol*. 70, 1:159–166.

Vannelli, T., Wei Qi, W., Sweigard, J., Gatenby, A. A., and Sariaslani, F. S. (2007) Production of p-hydroxycinnamic acid from glucose in *Saccharomyces cerevisiae* and *Escherichia coli* by expression of heterologous genes from plants and fungi. *Met. Eng*. 9, 2:142–151.

Van Winden, W. A., Van Dam, J. C. Ras, C. et al.(2005) "Metabolic- flux analysis of *Saccharomyces cerevisiae* CEN.PK113-7D based on mass isotopomer measurements of ^{13}C-labeled primary metabolites," *FEMS Yeast Res*. 5, 6-7:559–568.

Varma, A. and Palsson, B. Ø. (1994) Metabolic flux balancing: basic concepts, scientific and practical use. *Bio/Technol*. 12, 10:994–998.

Varma, A and Palsson, B. Ø. (1994) Stoichiometric flux balance models quantitatively predict growth and metabolic by product secretion in wild-type *Escherichia coli* W3110. *Appl. Env. Microbiol*. 60, 10:3724–3731.

Verwaal, R., Wang, J. Meijnen, J. P., et al. (2007) High-level production of beta-carotene in *Saccharomyces cerevisiae* by successive transformation with carotenogenic genes from *Xanthophyllomyces dendrorhous*. *Appl. and Env. Microbiol*. 73, 13:4342–4350.

Wahl, S. A., Nöh, K., and Wiechert, W. ^{13}C labeling experiments at metabolic nonstationary conditions: an exploratory study. *BMC Bioinformatics.* 9, 152.

Wang, Q., Chen, X., Yang, Y., and Zhao, X. (2006) Genome-scale *in silico* aided metabolic analysis and flux comparisons of *Escherichia coli* to improve succinate production. *Appl. Microbiol. Biotechnol*. 73, 4:887–894.

Wildermuth, M. C., (2000) Metabolic control analysis: biological applications and insights. *Genome Bio.* 1, 6.

Wu, B. Zhang, B. Feng X., et al., (2010) Alternative isoleucine synthesis pathway in cyanobacterial species. *Microbiol*. 156, 2:596–602.

Yang, C., Hua, Q., and Shimizu, K. (2002) Metabolic flux analysis in *Synechocystis* using isotope distribution from ^{13}C-labeled glucose. *Metabol. Eng*. 4, 3:202–216.

Yegane-Sarkandy, S., Farnoud, A. M., Shojaosadati S. A, et al. (2009) Overproduction of human interleukin-2 in recombinant *Escherichia coli* BL21 high-cell-density culture by the determination and optimization of essential amino acids using a simple stoichiometric model. *Biotechnol. Appl. Biochem*. 54, 1:31–39.

Yoshikuni, Y., Ferrin,T. E., and Keasling, J. D. (2006) Designed divergent evolution of enzyme function. *Nature*. 440, 7087:1078–1082.

Young, J. D., Walther, J. L., Antoniewicz, M. R., Yoo, H., and Stephanopoulos, G. (2008) "An elementary metabolite unit (EMU) based method of isotopically nonstationary flux analysis," *Biotechnol. Bioeng.* 99, 3:686–699.

Yuan, J., Bennett, B. D., and Rabinowitz, J. D. (2008) Kinetic flux profiling for quantitation of cellular metabolic fluxes. *Nat. Prot*. 3, 8: 1328–1340.

Zamboni, N., Fendt, S. M., Rühl, M., and Sauer, U. (2009) C-based metabolic flux analysis. *Nat. Prot.* 4, 6:878–892.

Zamboni, N. Fischer, E. Muffler, A. Wyss, M., Hohmann, H. P., Sauer, U. (2005) Transient expression and flux changes during a shift from high to low riboflavin production in continuous cultures of *Bacillus subtilis*. *Biotechnol. Bioeng*. 89, 2:219–232.

Zamboni, N. and Sauer, U. (2009) Novel biological insights through metabolomics and ^{13}C-flux analysis. *Curr. Opin. Microbiol.* 12, 5:553–558.

Table 1. Recent application of fluxomics in nonmodel microbes to bioproduct synthesis

Species	Product	Substrate	Model Description	Results from Study	Reference
Corynebacterium glutamicum	Lysine	Glucose (sucrose, fructose)	^{13}C-MFA	MFA models (combining transcriptome, metabolome analysis) have been developed to study fluxes inder different cultivation modes (minibioreactor, batch, fed-batch) using various carbon sources.	Iwatani *et al.,* 2008
Corynebacterium glutamicum	Methionine	Glucose	^{13}C-MFA only focuses on flux distribution in the methionine pathway	The *C. glutamicum* mutant (mcbR) showed no overproduction of methionine, but accumulation of homolanthionine.	Krömer *et al.,* 2006
Corynebacterium glutamicum	Glutamate	Glucose	^{13}C-MFA (focus on anaplerotic pathways)	Flux from phosphoenolpyruvate to oxaloacetate catalyzed by phosphoenolpyruvate carboxylase (PEPc) was active in the growth phase, whereas pyruvate carboxylase was inactive.	Shirai *et al.,* 2007
Actinobacillus succinogenes	Succinate, formate, and acetate	Glucose $NaHCO_3$	^{13}C-MFA (via NMR and GC-MS) and enzyme assay	The model indicated (1) NADPH was produced primarily by transhydrogenase and/or by NADP-dependent malic enzyme (2) oxaloacetate and malate were converted to pyruvate (3) the effects of $NaHCO_3$ and H_2 on metabolic fluxes were quantified.	McKinlay *et al.,* 2007; McKinlay and Vielle, 2008
Geobacillus thermoglucosidasius	Ethanol	Glucose	FBA and ^{13}C-MFA	The model characterized the ethanol production under three oxygen conditions. The FBA analysis pointed out several gene targets for improving ethanol production.	Tang *et al*., 2009
Clostridium acetobutylicum	Butanol	Glucose	Genome-Scale-FBA	The engineered strain ws able to produce 154 mM butanol with 9.9 mM acetone at pH 5.5, resulting in a butanol selectivity (a molar ratio of butanol to total solvents) of 0.84.	Jin *et al*., 2009
Pennicillium chrysogenum	Penicillin	Gluconate/ Glucose	^{13}C-MFA (focus on pentose phosphate pathway and glycolysis)	The model determined the pentose-phosphate pathway split ratio and estimated NADPH metabolism.	Kleijn *et al*., 2006
Synechocystis sp. PCC 6803	Hydrogen	CO_2	FBA	The results included H_2 photoproduction, strategies to avoid oxygen inhibition, and analysis of hetero-, auto-, and mixotrophic metabolisms.	Navarro *et a*l., 2009; Shastri and Morgan 2005
Synechocystis sp. PCC 6803	Light Energy and Biomass	Glucose/CO_2	^{13}C-MFA and dynamic ^{13}C-MFA	The model analyzed heterotrophic, autotrophic and mixotrophic metabolisms.	Shastri and Morgan, 2007; Yang *et al*., 2002
Chlamydomonas reinhardtii	Light Energy and Biomass	CO_2	FBA model including three metabolically active compartments	The model indicated that heterotrophic growth had a low biomass yield on carbon, while mixotrophical and autotrophical growth had higher carbon utilization efficiency.	Boyle and Morgan, 2009
Zymomonas mobilis	Ethanol	Glucose/xylose	FBA with various biological objectives	Model analyzed the metabolic boundaries of *Z. mobilis*. The study indicated that ethanol and biomass production depend on anaerobic respiration stoichiometry and activity.	Tsantili *et al.*, 2007
Zymomonas mobilis	Ethanol	Glucose/fructose /xylose	^{13}C-MFA via ^{1}H-NMR ^{31}P-NMR spectroscopy	The model characterized the intracellular metabolic state during growth on glucose, fructose, and xylose in defined continuous cultures.	De Graaf *et al*., 1999
Coculture (*Desulfovibrio vulgaris* and *Methanococcus maripaludis*)	CH_4	Lactate	FBA analysis of microbial consortia	The model predicted the ratio of *D. vulgaris* to *M. maripludis* cells during growth. It was possible to eliminate formate as an interspecies electron shuttle, but H_2 transfer was essential for syntrophic growth.	Stolyar *et al*., 2007
Community (oxygenic phototrophs, filamentous anoxygenicphototrophs, and sulfate-reducing bacteria)	Biomass and nitrogen fixation	CO_2	FBA and elementary mode analysis	The model predicted and described relative abundances of species, by-products, and the metabolic interactions.	Taffs *et al.*, 2009
Phaffia rhodozyma and *Haemotococcus pluvialis*	Astaxanthin	Glucose (with Peptone and Yeast Extract)	FBA analysis of mix culture	The two major astaxanthin-producing microorganisms exhibited elevated yields (2.8-fold) under mixed culture conditions compared to pure culture.	Dong *et al*., 2006

Figure 1. An interative approach of fluxomic analysis and rational metabolic engineering.

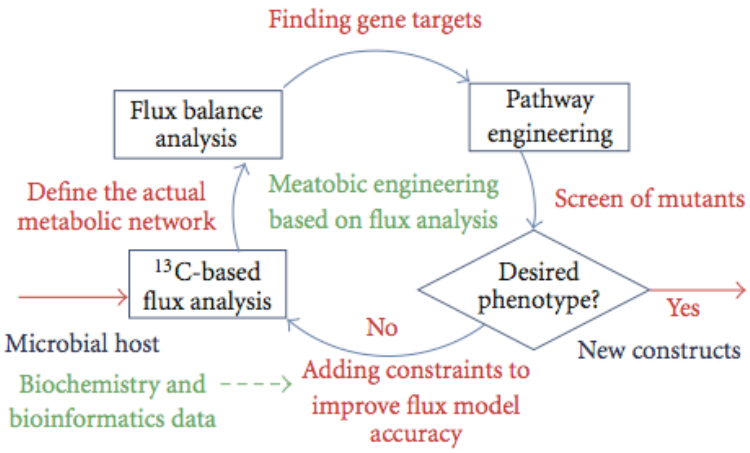
Finding gene targets
Flux balance analysis
Pathway engineering
Define the actual metabolic network
Meatobic engineering based on flux analysis
Screen of mutants
^{13}C-based flux analysis
Desired phenotype?
Yes
No
Microbial host
New constructs
Biochemistry and bioinformatics data
Adding constraints to improve flux model accuracy

Figure 2. ^{13}C-assisted cellular metabolism analysis.

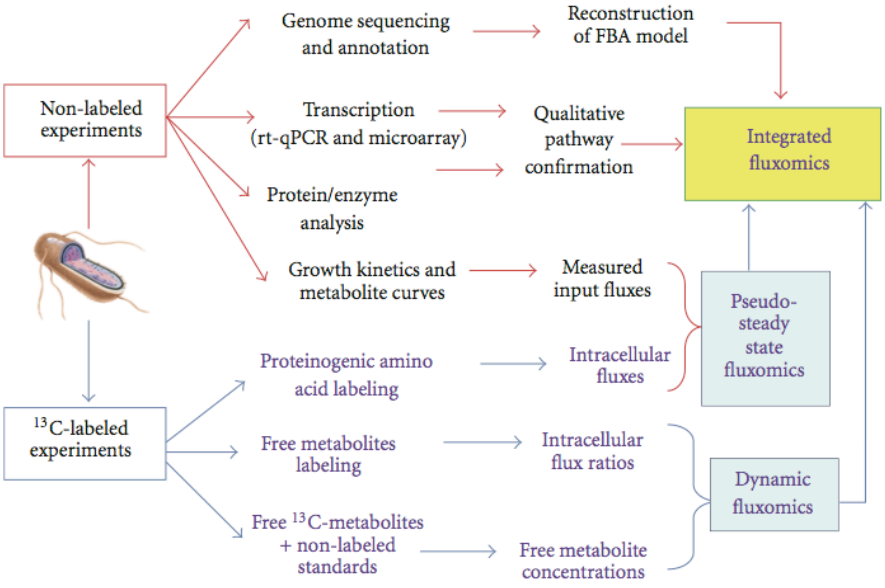

FIGURE 2: ^{13}C-assisted cellular metabolism analysis.

Figure 3. Product yields as a function of enzymatic steps from central metabolism. The solid line is the regression of published product yields by *S. cerevisiae* as a function of reaction steps from intermediate steps in the central metabolism (including glycolysis, TCA cycle and pentose-phosphate pathways). The yield declines exponentially as the number of reaction steps increases. The dotted lines are boundary curves with yield efficiencies of 30% and 70% respectively. All yield data from initial carbon sources are estimated from recent papers using our best judgement. The synthesized products and reaction steps are: Poly (R-3-hydroxybutyrate) (Carlson and Srienc, 2006) (steps=3); Glycerol (Overkamp *et al.,* 2002) (steps=2); Artemisinic Acid (Ro *et al.,* 2006)(steps=10); Amorphadiene (Shiba *et al.,* 2007) (steps=9); Pyruvate (Van Maris *et al.,* 2004) (steps=0); Geranylgeraniol (Tokuhiro *et al.,* 2009) (steps=10); Hydrocortisone (Szczebara *et al.,* 2003) (steps=19); Squalene (Asadollahi *et al.,* 2010) (steps=9); β-carotene (Verwaal *et al.,* 2007) (steps=12); Lycopene (Verwaal *et al.,* 2007) (steps=11); Phytoene (Verwaal *et al.,* 2007) (steps=10); p=hydroxycinnamic acid (Vannelli *et al.,* 2007) (steps=12); Naringenin (Jiang *et al.,* 2005) (steps=14); Pinocembrin (Jiang *et al.,* 2005) (steps=14); Xylitol and Ribitol (Toivari *et al.,* 2007) (steps=3); Ethanol (Alper *et al.,* 2006) (steps=2); L-ascorbic acid (Sauer *et al.,* 2004) steps=8).

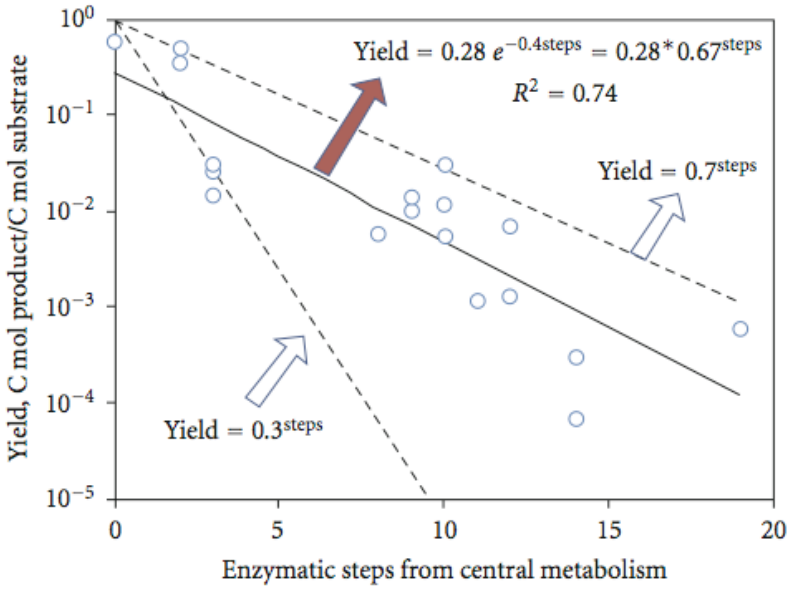
Yield = 0.28 $e^{-0.4steps}$ = 0.28*0.67^{steps}
R^2 = 0.74
Yield = 0.7^{steps}
Yield = 0.3^{steps}
Yield, C mol product/C mol substrate
Enzymatic steps from central metabolism
10^0
10^{-1}
10^{-2}
10^{-3}
10^{-4}
10^{-5}
0
5
10
15
20

Appendix Chapter 3

Mixotrophic and photoheterotrophic metabolism in *Cyanothece* sp. ATCC 51142 under continuous light

Summary

The unicellular diazotrophic cyanobacterium, *Cyanothece* sp. ATCC 51142 (*Cyanothece* 51142) is able to grow aerobically under nitrogen-fixing conditions with alternating light-dark cycles or continuous illumination. This study investigated the effects of carbon and nitrogen sources on *Cyanothece* 51142 metabolism via ^{13}C-assisted metabolite analysis and biochemical measurements. Under continuous light (50 μmol photons/m^2/s) and nitrogen-fixing conditions, we found that glycerol addition promoted aerobic biomass growth (by twofold) and nitrogenase-dependent hydrogen production [up to 25 μmol H_2 (mg chlorophyll)$^{-1}$ h^{-1}], but strongly reduced phototrophic CO_2 utilization. Under nitrogen-sufficient conditions, *Cyanothece* 51142 was able to metabolize glycerol photoheterotrophically, and the activity of light dependent reactions (e.g. oxygen evolution) was not significantly reduced. In contrast, *Synechocystis* sp. PCC 6803 showed apparent mixotrophic metabolism under similar growth conditions. Isotopomer analysis also detected that *Cyanothece* 51142 was able to fix CO_2 via anaplerotic pathways, and to take up glucose and pyruvate for mixotrophic biomass synthesis.

Introduction

Rising concerns about global warming due to the greenhouse effect have renewed research focused on biological capture of CO_2. Cyanobacteria have versatile metabolic capabilities, which allow them to grow under autotrophic, heterotrophic, and mixotrophic conditions (Bottomley & Baalen, 1978; Eiler, 2006; Yang *et al.*, 2002). More importantly, some cyanobacteria can capture solar energy to fix nitrogen and generate H_2, thereby serving as a source of biofertilizer and biofuel, while simultaneously consuming atmospheric CO_2 (Bernat *et al.*, 2009; Dutta *et al.*, 2005; Fay, 1992; Madamwar *et al.*, 2000; Tamagnini *et al.*, 2007; Tuli *et al.*, 1996). *Cyanothece,* sp. ATCC 51142 (*Cyanothece* 51142), a unicellular diazotrophic cyanobacterium, is able to grow aerobically under nitrogen-fixing conditions and has been recognized as contributing to the marine nitrogen cycle (Zehr et al., 2001). The recent sequencing of the *Cyanothece* 51142 genome and its transcriptional analysis have uncovered the diurnally oscillatory metabolism of the bacterium in alternating light-dark cycles (photosynthesis during the day and nitrogen fixation at night) (Stöckel *et al.*, 2008; Toepel *et al.*, 2008; Welsh *et al.*, 2008). In general, cyanobacteria use spatial or temporal separation of oxygen-sensitive nitrogen-fixation and oxygen-evolving photosynthesis as a strategy for diazotrophic growth (Benemann & Weare, 1974; Fay, 1992). Interestingly, *Cyanothece* 51142 demonstrates simultaneous N_2 fixation and O_2 evolution under continuous-light conditions, though it appears to be unicellular (Colon-Lopez *et al.*, 1997; Huang & Chow., 1986). For example, a recent study on transcriptional and translational regulation of continuously-illuminated *Cyanothece* has revealed strong synthesis capability for nitrogenase and circadian expression of 10% of its genes (Toepel *et al.*, 2008). Furthermore, *Cyanothece* strains usually utilize exogenous carbon substrates for mixotrophic growth under light conditions and for heterotrophic growth under dark

conditions (Reddy *et al.,* 1993). Carbon substrates are key factors controlling the efficiency of cyanobacterial aerobic growth and hydrogen production (Berman-Frank *et al.*, 2003; Reddy *et al.*, 1993; Tamagnini *et al.*, 2007). Genome analysis studies have revealed that *Cyanothece* 51142 has a unique gene cluster on its linear chromosome that contains key genes involved in glucose and pyruvate metabolism (Welsh *et al.*, 2008). However, the ability of this strain to metabolize glucose or pyruvate remains unknown.

To quantitatively examine the effect of carbon and nitrogen sources on *Cyanothece* central metabolism, this study investigated the effects of three carbon sources (glucose, glycerol, and pyruvate as representatives of sugar, lipid derivatives, and organic acids from central metabolic pathways, respectively) on *Cyanothece* 51142 growth and metabolism. Two nitrogen sources other than N_2, ammonia and nitrate, were also examined. Precise readouts on metabolic state and activity were based on ^{13}C-assisted metabolite analysis integrated with biochemical assays and the gene expression patterns obtained by reverse transcription PCR (RT-PCR) (Fong *et al.*, 2006; Pingitore *et al.*, 2007; Tang *et al.*, 2007c; Tang *et al.*, 2009; Wu *et al.*, 2010). Our work demonstrates that ^{13}C-assisted metabolite analysis can be used as a high throughput tool to study cyanobacterial metabolisms. Superior to the traditional ^{14}C method (Bottomley & Baalen, 1978), the non-radioactive ^{13}C method can provide rich information about which carbons within a metabolite are labeled, and thus enable an in-depth understanding of carbon utilization and metabolic regulation in *Cyanothece* 51142.

Materials and Methods

Bacterial strains and growth conditions.

Cyanothece 51142 was first grown in 150 mL Erlenmeyer flasks fed with ASP2 medium (Reddy *et al.*, 1993) without nitrate. Ambient CO_2 provided the sole carbon source. For experiments examining the effect of nitrogen sources, 18 mM $NaNO_3$ or 17 mM NH_4Cl was added into the medium. Cultures were grown aerobically under continuous light (50 μmol photons$\cdot m^{-1} \cdot s^{-1}$) on a shaker at 150 r. p. m. and 30°C. Cells at late-mid exponential phase were sub-cultured into different culture media with various nitrogen and carbon sources. Isotopically-labeled carbon substrates (Cambridge Isotope Laboratories, Andover, MA) were used for mixotrophic growth, including 54 mM glycerol (2-^{13}C, >98%), 26 mM glucose (U-^{13}C, >98%) and 11 mM sodium pyruvate (3-^{13}C, >98%). For tracer experiments, a 3% inoculum from unlabeled stock culture was used to inoculate a 50 mL medium containing labeled carbon sources. At the mid-exponential phase of growth, a 3% inoculum from the first isotopic labeled culture was used to inoculate 50 mL sub-cultures with the same medium to remove the effect of unlabeled carbon introduced from the initial inoculum. Cell growth was monitored by a UV-Vis spectrometer (GENESYS, Thermo Scientific, USA) at 730 nm. To perform a comparative study, a glucose tolerant *Synechocystis* strain PCC 6803 (a model cyanobacterium for studying fundamental processes of photosynthetic metabolism) was also cultured in BG11 medium (pH=7.6) under the same growth conditions (continuous light and 30 ^{o}C, Stanier *et al.*, 1971). The BG11 medium was supplemented with 6 mM glucose (U-^{13}C, >98%) to support mixotrophic growth. *Synechocystis* PCC 6803 was also sub-cultured in the same labeled medium twice before sampling for ^{13}C-labeled metabolite analysis.

Metabolite and photosynthetic activity analysis.

To analyse metabolites in *Cyanothece* 51142, biomass was harvested at the mid-exponential phase of growth (~90 h) by centrifugation at 7,000 rpm for 15 min at 10˚C. The concentrations of pyruvate, glucose and glycerol were analyzed with enzymatic assay kits (R-Biopharm). To measure hydrogen produced by *Cyanothece* 51142, 20 ml of culture solution was taken from the culture flask after three days and transferred into a 35.2 ml glass vial sealed with a rubber septum and kept under continuous light (50 μmol photons m^{-2} s^{-1}). A modified protocol was used to quantify hydrogen (Rey *et al.*, 2007). Briefly, hydrogen that accumulated in the headspace of the sealed culture vials (for 5 h) was withdrawn with a Hamilton gas-tight syringe and quantified on an Agilent 6890N Gas Chromatograph with a molseive 5A 60/80 column [inner dimensions 6'×1/8" (1830x3.17 mm)] and Thermal Conductivity Detector. Injection, oven, and detector temperatures were 100°C, 50°C, and 100°C, respectively. Argon was the carrier gas (flow rate of 65 ml min^{-1}). All measurements included three biological replicates.

Photosynthesis activities were determined based on measurements of chlorophyll fluorescence and oxygen evolution. Chlorophyll fluorescence profiles of photosystem II (PSII) of *Cyanothece* 51142 under different nutrient conditions were detected by a FL100 fluorometer (Photon Systems Instruments, Brno, Czech Republic) as described previously (Roose & Pakrasi, 2004). All samples taken for measurement were diluted to OD_{730} ~0.2 using cell-free ASP2 medium. The samples were first adapted for 3 min in total darkness. During the measurement (performed at room temperature), the fluorometer emitted saturating light pulses to determine the fluorescence yield of the samples. The photosynthesis activity was derived by the maximum quantum yield (F_v/F_m) according to the formula $F_v/F_m = (F_m - F_0)/F_m$, where F_0 is initial fluorescence and F_m is maximum fluorescence at the beginning of measurement (Krause & Weis, 1991).

Oxygen evolution rates of *Cyanothece* 51142 grown under different nutrient conditions were measured with a Hansatech oxygen electrode. Assays were performed at 30 °C on whole cells in ASP2 media with a saturating light intensity of 8,250 μmol photons m^{-2} s^{-1} for 2 min at a 2.5 ml reaction volume. For each reaction, the chlorophyll concentration of each sample was diluted and ~6 μg mL^{-1}. The oxygen evolution rates [μmol O_2 (mg chlorophyll)$^{-1}$ h^{-1}] were then measured and normalized based on chlorophyll concentration.

RNA extraction and RT-PCR

The bacteria grown under different cultural conditions were harvested at mid-exponential phase according to the corresponding growth curves. The total RNA was extracted by using a PureLinkRNA Mini kit (Invitrogen), following the manufacturer's instruction. cDNA was synthesized from ~2 μg RNA by using a High-Capacity cDNA Reverse Transcription Kit (Invitrogen). The primers for RT-PCR were designed using Primer Premier 5 software (PREMIER Biosoft) and analyzed by OligoAnalyzer 3.0 software (Integrated DNA Technologies). The forward primer 5'-AGCGGTGGAGTATGTGGT-3' and reverse primer 5'-GGCTGGGTTTGATGAGATT-3' were employed to amplify a 16S rRNA gene as a control. The forward primer 5'-CCGACTACACTCCGAAAG-3' and reverse primer 5'-ACGTAACGCCCGTAATGC-3' were used to amplify the Rubisco (*rbcL*) gene and the forward primer 5'-TAATCACGAAACGGGAG-3' and reverse primer 5'-CACCACATCAGCGTATTG-3' to amplify the *prk* gene. The PCRs were conducted with the following cycle conditions: 2 min of activation of the polymerase at 94 °C, followed by 30 cycles consisting of 1 min at 94 °C, 30 s at 53 °C and 2 min at 72 °C; finally, a 10 min extension was performed at 72 °C. The final PCR product was observed directly on 2% agarose gels after electrophoresis.

Isotopic analysis.

The preparation and isotopic analysis of proteogenic amino acids were performed as previously described (Tang *et al.*, 2007a,b). In brief, exponentially growing biomass from ~20 ml culture was collected by centrifugation (8,000×*g*, 10 min, 4˚C) and hydrolyzed in 6 M HCl at 100°C for 24 h. The amino acid mix was dried and derivatized in tetrahydrofuran (THF) and N-(tert-butyl dimethylsilyl)-N-methyl-trifluoroacetamide (Sigma-Aldrich) at 70°C for 1 h. A gas chromatograph (Hewlett-Packard model 7890A, Agilent Technologies) equipped with a DB5-MS column (J&W Scientific) and a mass spectrometer (5975C, Agilent Technologies) were used for analyzing amino acid labeling profiles. The ion $[M\text{-}57]^+$ from unfragmented amino acid was detected and mass fractions of key amino acids were calculated (Wahl *et al.*, 2004). The substrate utilization ratios R (reflecting the degree of mixotrophic metabolism) for an amino acid X was calculated from the labeling patterns of proteogenic amino acids by the following equation:

$$\text{Amino acid X: } \frac{0.98 \times n \times V_{sub} + 0.01 \times V_{CO2}}{m \times V_{sub} + V_{CO2}} = \frac{(\sum_{i=1}^{C} i \times M_i)}{C} \Longrightarrow \quad R = \frac{V_{sub}}{V_{CO2}} \qquad (1)$$

where the ratio R indicates the utilization of labeled carbon substrate over unlabeled CO_2 for producing an amino acid X (and its precursors). M_i is the GC-MS isotopomer fraction for amino acid X (i.e., M_0 is the unlabeled fraction, M_1 is the singly labeled fraction, M_2 is the doubly labeled fraction, M_3 is the triply labeled fraction, etc), C is the total number of carbon atoms in the amino acid molecule, V_{sub} is the carbon flux from ^{13}C labeled substrate, V_{CO2} is the carbon flux from CO_2, *0.98* is the purity of the labeled carbon substrate; *0.01* is the natural abundance of ^{13}C, m is the total number of carbons in the substrate molecule, and n is the total number of labeled carbons in the substrate molecule. R indicates the amount of labeled carbon that percolated through the central metabolic networks (Figure 1).

Results

Cell growth with different carbon and nitrogen sources.

Figure 2 and Supplementary Figure S-1 show the effect of carbon and nitrogen substrates on the growth of *Cyanothece* 51142 under continuous light. Biomass growth was significantly enhanced by the addition of glycerol to ASP2 medium. For example, glycerol addition doubled the specific growth rate from 0.28 to 0.63 day^{-1} under N_2-fixing conditions. These results are consistent with an earlier report on two *Cyanothece* strains (Reddy *et al.*, 1993). On the other hand, *Cyanothece* growth was not apparently enhanced by either glucose or pyruvate (Supplementary Figure S-1), and a high concentration of pyruvate (64 mM) inhibited *Cyanothece* growth. Compared with nitrogen fixing cultures, the presence of nitrate salts in the growth media increased *Cyanothece* autotrophic growth rates from 0.28 day^{-1} (N_2-fixation condition) to 0.37 day^{-1} (nitrate-sufficient condition). Similarly, the presence of glycerol enhanced growth rate by approximately two-fold (from 0.60 to 1.02 day^{-1}). As expected, high concentrations of ammonium salts (17 mM) fully inhibited growth (data not shown) because of their well-known deleterious effect on the photosystems of cyanobacteria (Drath *et al.*, 2008; Dai *et al.*, 2008).

Isotopic analysis of amino acids.

^{13}C enrichment patterns in key metabolites were used to estimate the relative utilization of labeled carbon substrates (i.e., glucose, pyruvate, and glycerol) and CO_2 for metabolite synthesis under mixotrophic growth. Figure 1 shows the central metabolic pathways in *Cyanothece* 51142 (http://www.genome.jp/kegg/). The labeling of five amino acids was analyzed: histidine (precursors: ribose-5-phosphate and 5,10-methyl-THF), synthesized from the Calvin cycle and pentose phosphate pathway; serine (precursor: 3-phosphoglycerate, a product

from the Calvin cycle); alanine (precursor: pyruvate, originated from carbon substrate or CO_2 fixation); and aspartate and glutamate (precursors: oxaloacetate and 2-oxoglutarate, respectively, synthesized from the citric acid cycle). Under nitrate-sufficient conditions, glycerol could be used as the sole carbon source for synthesis of alanine, serine, and histidine (as indicated by R values approaching infinity). This indicates that the cell was undergoing completely heterotrophic metabolism. R values of some of the key amino acids in glucose and pyruvate cultures were positive and thus these two carbon sources were actually utilized for biomass synthesis (Table 1). However, their measured R values were between 0 and 0.3, which indicated that CO_2 was the main carbon source for metabolite synthesis. This result was consistent with the fact that glucose and pyruvate did not apparently improve the biomass growth. Compared with nitrogen-sufficient conditions, nitrogen fixing conditions further limited glucose and glycerol utilization, as shown by the decreased labeling fractions of three key amino acids (i.e., alanine, serine, and histidine) (Table 1).

Nitrogenase-dependent hydrogen production, photosynthesis and Calvin Cycle activity.

Hydrogen production was under continuous light with different carbon substrates (N_2 as the sole nitrogen source) was measured in the exponential (day 4) and stationary (day 9) growth phases (Supplementary Figure S-2). In the exponential growth phase under nitrogen fixing conditions, hydrogen production rates were as follows: glycerol, 25±6 μmol H_2 (mg chlorophyll)$^{-1}$ h^{-1}; glucose, 13±9 μmol H_2 (mg chlorophyll)$^{-1}$ h^{-1}; pyruvate, 4±2 μmol H_2 (mg chlorophyll)$^{-1}$ h^{-1} ; and under photoautotrophic conditions; 5±1 μmol H_2 (mg chlorophyll)$^{-1}$ h^{-1}. Under all nitrate or ammonium chloride conditions, hydrogen production was not detected, regardless of the carbon substrate.

The measurement of photosynthetic parameters (Fig. 3) suggested that, compared with photoautotrophic conditions, addition of an exogenous carbon source (glycerol, glucose, or pyruvate) did not strongly suppress the maximal quantum yield of PSII (F_v/F_m) or the oxygen evolution rate. Nitrate-sufficient conditions enhanced the oxygen evolution rates by two- to threefold compared with nitrogen-fixing conditions, while the changes of quantum yields of PSII were much less significant (10-30%). Gene expression in the carbon fixation pathway was also determined (Fig. 4). RT-PCR results indicated that two key enzymes in Calvin Cycle ([Rubisco, (*rbcL*) and phosphoribulokinase (*prk*)] were functional under conditions of growth with glyverol or glucose. The above measurements confirmed that the light-dependent reactions were active under all culture conditions, even though carbon substrates reduced the relative contribution of CO_2 fixation to biomass synthesis.

Discussion

Carbon substrate utilization and regulation.

In continuous light, *Cyanothece* 51142 can efficiently utilize glycerol for aerobic growth. Based on the measurement of carbon substrates in the culture medium during the exponential growth phase, the uptake rates for glycerol were 0.22±0.05 g (g dry biomass)$^{-1}$ day^{-1} under nitrogen fixing and 0.35±0.06 g (g dry biomass)$^{-1}$ day^{-1} under nitrate-sufficient conditions. Glycerol promoted *Cyanothece* 51142 growth because it provided carbon and energy sources. Under nitrate-sufficient conditions, the high values of R for the serine, alanine and histidine labeling data indicated that 3-phosphoglycerate, pyruvate and ribose-5-phosphate nodes in the central metabolic pathways (Figure 1) originating completely from glycerol, while the contribution of CO_2 photofixation to these metabolite nodes was negligible. As a comparison, the glucose-tolerant strain of *Synechocystis* sp. 6803 was cultured with fully labeled glucose under continuous light and nitrogen-sufficient conditions (Supplementary Figure S3). The measured R values (Table 1) for serine (0.87), alanine (0.92) and histidine (1.73) indicated that *Synechocystis* 6803 had a typical mixotrophic growth. In general, cyanobacterial heterotrophic growth has been reported only under three conditions: complete darkness, dim light and pulses of light (Anderson & McIntosh, 1991; Van Baalen *et al.*, 1971). When the light is sufficient for photoautotrophy, *Cyanothece* photoheterotrophic growth is only achieved by addition of PSII inhibitors (Reddy *et al.*, 1993). This study shows that rapidly growing *Cyanothece* 51142 cells can shift their metabolic strategies from mixotrophic or autotrophic growth to photoheterotrophic growth, possibly because maximal utilization of an energy-rich carbon substrate (glycerol) can reduce energy costs related to CO_2 fixation (fixation of one CO_2 consumes two ATP and one NADPH) and building block synthesis, so that maximal biomass growth can be achieved.

On the other hand, glucose was not apparently consumed by *Cyanothece* 51142 (the consumed concentrations were below 1 mM in all experiments). In the [U-^{13}C] glucose experiments (Table 1), all five amino acids contained labeled carbons, which indicated that the labeled glucose had percolated through all the entire central metabolic pathways, thereby confirming the ability of *Cyanothece* 51142 to metabolize glucose. The R values of all key amino acids were below 0.05 for both nitrogen-fixation and nitrate-sufficient conditions, suggesting that a large fraction of the carbon in the biomass had originated from CO_2 fixation. In contrast, glucose is the most favorable carbon source for *Synechocystis* species (Yang *et al.*, 2002), and the R values (Table 1) from key amino acids were around ~0.4-1.7. While both *Synechocystis* 6803 and *Cyanothece* 51142 have completely annotated central pathways for glucose metabolism, *Synechocystis* 6803 contains a glucose transporter (gene code Sll0771) that shares a sequence relationship with mammalian glucose transporters (Bottomley & Baalen, 1978; Flores & Schmetterer, 1986; Schmetterer, 1990). So far, the presence of a glucose transporter in *Cyanothece* 51142 has not been rigorously verified. From the genome database (DOE Joint Genome Institute, www.jgi.doe.gov/), a gene (cce_3842) has been identified as a glucose transport protein that shared weak (25%) amino acid identity with the Sll0771 protein of *Synechocystis* PCC 6803. Based on the glucose-dependent growth data, we conclude that the enzymes involved in glucose transport or utilization in *Cyanothece* 51142 may not be as efficient as those of *Synechocystis* PCC 6803.

Analysis of labeled pyruvate-grown *Cyanothece* cells showed that serine (precursor 3-phosphoglycerate) and histidine (precursor ribose-5-phosphate) were completely unlabeled (R=0). Such a labeling profile suggests that CO_2 was used as the sole carbon source for synthesis of metabolites in glycolysis and the pentose phosphate pathway (i.e., there was no

gluconeogenesis activity). Pyruvate was used only to synthesize alanine (R=0.3~0.6) and metabolites in the tricarboxylic acid cycle: (pyruvate→oxaloacetate→Asp) (pyruvate→acetylCoA→citrate→2-oxoglutarate→Glutamate), as reflected by the labeled carbon present in glutamate and aspartic acid. Interestingly, the R values for alanine (0.60) and glutamate (1.25) were higher under nitrogen-fixing conditions than under nitrate-sufficient conditions, indicating that relatively more labeled pyruvate was used for glutamate synthesis under these conditions. The nitrogen fixation was via nitrogenase: $N_2 + 6\ H^+ + 6\ e^- \rightarrow 2\ NH_3$, and the nitrogenase-generated ammonium was assimilated into amino acids through the glutamine synthetase/glutamate synthase pathway (Postgate, 1998). Utilization of supplemented pyruvate for glutamate synthesis could facilitate the nitrogen fixation process.

The enzyme RuBisCO is known to be the rate-limiting factor in the Calvin Cycle for capturing CO_2 to synthesize three-carbon sugars (glycerate 3-phosphate) (Atsumi *et al.*, 2009). We examined RuBisCO (*rbcL*) and phosphoribulokinase (*prk*) gene expression to reveal the metabolic regulation in the Calvin cycle at transcription level. Under photoautotrophic, mixotrophic, and heterotrophic growth conditions, expression of the two genes was clearly observed. Although Calvin cycle genes were expressed, *Cyanothece* 51142 still grew heterotrophically in the presence of glycerol and nitrate, based on the isotopomer data (no apparent incorporation of CO_2 from the Calvin cycle). These inconsistencies indicate that ^{13}C-assisted metabolite analysis provides a direct readout of actual metabolic status, while gene expression results alone cannot be relied upon, as there are many points of possible post-transcriptional regulation.

Furthermore, *Cyanothece* 51142 can fix CO_2 via anaplerotic pathways (i.e., C4 carbon fixation) (Slack & Hatch, 1967). In the presence of glycerol and under nitrate-sufficient

conditions (Table 1), R ratios for aspartate synthesis was 1.53, much smaller than the R ratios (R=∞) for Ala, Ser, and His. This indicates that, even though phototrophic CO_2 fixation was significantly inhibited, CO_2 was utilized for the synthesis of C4 metabolites in the tricarboxylic acid cycle via anaplerotic pathways: (1) PEP+CO_2→oxaloacetate (catalyzed by phosphoenolpyruvate carboxylase or phosphoenolpyruvate carboxykinase) or (2) pyruvate+CO_2→malate (catalyzed by malic oxidoreductase). Such anaplerotic pathways synthesized key TCA cycle metabolites such as oxaloacetate and succinate (precursors for chlorophyll).

Meanwhile, CO_2 was generated by two reactions (i.e., pyruvate→acetylCoA+CO_2; isocitrate→2-oxoglutarate+CO_2), which are essential steps for glutamate synthesis. These catabolic processes cause the loss of unlabeled carbon when the 2nd position labeled glycerol is used as the main carbon source. Therefore, the coefficients V_{CO2} (CO_2 utilization flux) and R (carbon utilization ratio) were both negative for glutamate synthesis (Equation 1) in glycerol supplemented cultures (under both nitrogen fixation and nitrate-sufficient conditions) (Table 1).

Photosynthesis activity.

Photosynthesis activity was estimated by the F_v/F_m parameter (maximum quantum efficiency of photosystem II) (Pirintsos *et al.*, 2009). When glycerol or glucose was utilized, the maximum quantum yield F_v/F_m (i.e, efficiency of PSII) in *Cyanothece* 51142 was not significantly affected (changes were within ~30%, Figure 3a). Although chlorophyll fluorescence estimation is not an accurate method for determination of absolute PSII activity (Schreiber *et al.*, 1995; Ting & Owens, 1992), we have used it in our study as a tool only to confirm active photon capture in the light-harvesting antenna complexes of PSII under both heterotrophic and mixotrophic conditions.

Oxygen evolution was measured as one molecule of the pigment chlorophyll absorbs one photon and uses its energy to generate NADPH, ATP, and O_2 in the light-dependent reactions (Kaftan *et al.*, 1999). The oxygen evolution rates in *Cyanothece* 51142 rose by 2-3 fold under all nitrate-sufficient conditions compared to corresponding nitrogen fixation conditions (Fig. 3b). The significantly higher rates of oxygen evolution indicated that the photosynthetic process of water splitting was more active and provided more energy (ATP and NADPH) to support biomass growth.

Finally, precise determination of the photosynthesic activity of *Cyanothece* 51442 is difficult, as its metabolic behavior fluctuates under continuous light due to its circadian rhythm (Colon-Lopez *et al.*, 1997; Toepel *et al.*, 2008). The photoreaction activity data in Fig. 3 represent only qualitative (not quantitative) evidence to support the presence of active light-dependent reactions under all culture conditions.

Nitrogen utilization and nitrogenase-dependent hydrogen production.

Under anaerobic conditions (using argon gas to flush the culture), hydrogen production rates of *Cyanothece* 51142 were as high as 100 μmol (mg chlorophyll)$^{-1}$ hr^{-1} (Data not shown). Under aerobic conditions, the hydrogen production enzyme (hydrogenase) is completely inactivated by oxygen (Tamagnini *et al.*, 2007). *Cyanothece* 51142 uses nitrogenase for both nitrogen fixation and hydrogen production. Nitrate, ammonium and some amino acids inhibit nitrogenase activity and thus fully prohibit aerobic hydrogen production by cyanobacteria (Rawson, 1985). Furthermore, NH_4^+ is a direct nitrogen source (nitrate is reduced to NH_4^+) that can be incorporated into biomass via glutamine/glutamate synthase (Muro-Pastor *et al.*, 2005). *Cyanothece* 51142, however, only grows at low concentrations of NH_4^+ (below 1 mM) because of an inhibition effect (Galmozzi *et al.*, 2007; Rawson, 1985). Nitrogen fixation is an energy

demanding process: $N_2+8H^++\mathbf{8e^-}+\mathbf{16ATP}\rightarrow 2NH_3+H_2+16ADP+16P_i$. The addition of glycerol reduces CO_2 fixation via the Calvin Cycle, so more energy (ATP and NADH) can be directed to nitrogen fixation, thus promoting hydrogen production by 4-5 fold (Dutta *et al.*, 2005; Madamwar *et al.*, 2000). Glucose and pyruvate cannot significantly promote hydrogen production because their utilization is very low and their effect on the energy economy limited. Hydrogen production rates dropped for all mixotrophic cultures of *Cyanothece* 51142 after 9 days, suggesting that inhibitory metabolites that reduced nitrogenase activity accumulated during cultivation (Atsumi *et al.*, 2009; Nyström, 2004). Finally, the coexistence of oxygen-evolving photosynthesis and oxygen-sensitive nitrogen fixation (indicated by hydrogen evolution) is an attractive characteristic in some cyanobacteria (Benemann & Weare, 1974; Huang & Chow., 1986). Unlike filamentous cyanobacterial species, in which nitrogen fixation and oxygenic photosynthesis are spatially segregated (Berman-Frank *et al.*, 2001), *Cyanothece* 51142 is able to maintain activities for N_2 fixation, respiration, and photosynthesis within the same cell under continuous light. This strain not only has a strong ability to scavenge intracellular oxygen and synthesize nitrogenase (Colon-Lopez *et al.*, 1997; Fay, 1992), but also develops a highly circadian mechanism for nitrogen fixation (Elvitigala *et al.*, 2009).

This study improves our understanding of *Cyanothece* 51142 physiology with different carbon and nitrogen sources as well as its potential application for hydrogen production. In general, exogenous carbon substrates may improve cellular growth but have strong negative effects on CO_2 fixation. Continuously illuminated *Cyanothece* 51142 shows simultaneous oxygen evolution and nitrogenase-dependent hydrogen production, while hydrogen production can be significantly enhanced by the addition of glycerol. A comparison of metabolic status under autotrophic, mixotrophic and heterotrophic growth conditions indicated that *Cyanothece*

51142 has an inherent metabolic strategy for maximal biomass production at low energy cost. Finally, this study has further confirmed that ^{13}C-assisted metabolite analysis is a high-throughput method which can provide new and precise information to understand a biological system.

References

Anderson, S. L. & McIntosh, L. (1991). Light-activated heterotrophic growth of the cyanobacterium *Synechocystis* sp. strain PCC 6803: a blue-light-requiring process. *Journal of Bacteriology* 173, 2761-2767.

Atsumi, S., Higashide, W. & Liao, J. C. (2009). Direct photosynthetic recycling of carbon dioxide to isobutyraldehyde. *Nature Biotechnology* 27, 1177-U1142.

Benemann, J. R. & Weare, N. M. (1974). Hydrogen Evolution by Nitrogen-Fixing *Anabaena cylindrica* Cultures. *Science* 184, 174-175.

Berman-Frank, I., Lundgren, P., Chen, Y.-B., Küpper, H., Kolber, Z., Bergman, B. & Falkowski, P. (2001). Segregation of Nitrogen Fixation and Oxygenic Photosynthesis in the Marine Cyanobacterium *Trichodesmium*. *Science* 294, 1534-1537.

Berman-Frank, I., Lundgren, P. & Falkowski, P. (2003). Nitrogen fixation and photosynthetic oxygen evolution in cyanobacteria. *Research in Microbiology* 154, 157-164.

Bernat, G., Waschewski, N. & Rogner, M. (2009). Towards efficient hydrogen production: the impact of antenna size and external factors on electron transport dynamics in *Synechocystis* PCC 6803. *Photosynth Res* 99, 205-216.

Bottomley, P. J. & Baalen, C. V. (1978). Characteristics of Heterotrophic Growth in the Blue-Green Alga *Nostoc* sp. Strain Mac. *Journal of General Microbiology* 107, 309-318.

Colon-Lopez, M. S., Sherman, D. M. & Sherman, L. A. (1997). Transcriptional and translational regulation of nitrogenase in light-dark- and continuous-light grown cultures of the unicellular cyanobacterium *Cyanothece* sp. strain ATCC 51142. *Journal of Bacteriology* 179, 4319-4327.

Dai, G., Deblois, C. P., Liu, S., Juneau, P. & Qiu, B. (2008). Differential sensitivity of five cyanobacterial strains to ammonium toxicity and its inhibitory mechanism on the photosynthesis of rice-field cyanobacterium Ge-Xian-Mi (Nostoc). *Aquatic toxicology* 89, 113-121.

Drath, M., Kloft, N., Batschauer, A., Marin, K., Novak, J. & Forchhammer, K. (2008). Ammonia triggers photodamage of photosystem II in the cyanobacterium *Synechocystis* sp strain PCC 6803. *Plant Physiology* 147, 206-215.

Dutta, D., De, D., Chaudhuri, S. & Bhattacharya, S. K. (2005). Hydrogen production by Cyanobacteria. *Microb Cell Fact* 4.

Eiler, A. (2006). Evidence for the Ubiquity of Mixotrophic Bacteria in the Upper Ocean: Implications and Consequences. *Applied and Environmental Microbiology* 72, 7431-7437.

Elvitigala, T., Stöckel, J., Ghosh, B. K. & Pakrasi, H. B. (2009). Effect of continuous light on diurnal rhythms in *Cyanothece* sp. ATCC 51142. *BMC Genomics* 10, 226.

Fay, P. (1992). Oxygen relations of nitrogen fixation in cyanobacteria. *Microbiological Reviews* 56, 340-373.

Flores, E. & Schmetterer, G. (1986). Interaction of fructose with the glucose permease of the cyanobacterium *Synechocystis* sp. strain PCC 6803. *Journal of Bacteriology* 66, 693-696.

Fong, S. S., Nanchen, A., Palsson, B. O. & Sauer, U. (2006). Latent pathway activation and increased pathway capacity enable *Escherichia coli* adaptation to loss of key metabolic enzymes. *Journal of Biological Chemistry* 281, 8024-8033.

Galmozzi, C. V., Fernandez-Avila, M. J., Reyes, J. C., Florencio, F. J. & Muro-Pastor, M. I. (2007). The ammonium-inactivated cyanobacterial glutamine synthetase I is reactivated in vivo by a mechanism involving proteolytic removal of its inactivating factors. *Mol Microbiol* 65, 166-179.

Huang, T. C. & Chow., T. J. (1986). New type of N_2-fixing unicellular cyanobacterium (blue-green alga). *FEMS Microbiology Letter* 36, 109-110.

Kaftan, D., Meszaros, T., Whitmarsh, J. & Nedbal, L. (1999). Characterization of Photosystem II Activity and Heterogeneity during the Cell Cycle of the Green Alga *Scenedesmus quadricauda*. *Plant Physiology* 120, 433-441.

Krause, G. H. & Weis, E. (1991). Chlorophyll fluorescence and photosynthesis: the basics. *Ann Rev Plant Physiol Plant Mol Biol* 42, 313-349.

Madamwar, D., Garg, N. & Shah, V. (2000). Cyanobacterial hydrogen production. *World J Microbiol Biotechnol* 16, 757-767.

Muro-Pastor, M. I., Reyes, J. C. & Florencio, F. J. (2005). Ammonium assimilation in cyanobacteria. *Photosynthesis Research* 83, 135-150.

Nyström, T. (2004). Stationary phase physiology. *Annual Review of Microbiology* 58, 161-181.

Pingitore, F., Tang, Y. J., Kruppa, G. H. & Keasling, J. D. (2007). Analysis of amino acid isotopomers using FT-ICR MS. *Analytical Chemistry* 79, 2483-2490.

Pirintsos, S. A., Munzi, S., Loppi, S. & Kotzabasis, K. (2009). Do polyamines alter the sensitivity of lichens to nitrogen stress? *Ecotoxicology and Environmental Safety* 72, 1331-1336.

Postgate, J. (1998).Nitrogen Fixation, 3rd Edition: Cambridge University Press, Cambridge UK.

Rawson, D. M. (1985). The effects of exogenous amino acids on growth and nitrogenase activity in the cyanobacterium *Anabaena cylindrica* PCC 7122. *Journal of General Microbiology* 134, 2549-2544.

Reddy, K. J., Haskell, J. B., Sherman, D. M. & Sherman, L. A. (1993). Unicellular, aerobic nitrogen-fixing cyanobacteria of the genus *Cyanothece*. *J Bacteriol* 175, 1284-1292.

Rey, F. E., Heiniger, E. K. & Harwood, C. S. (2007). Redirection of Metabolism for Biological Hydrogen Production. *Applied and Environmental Microbiology* 73, 1665-1671.

Roose, J. L. & Pakrasi, H. B. (2004). Evidence that D1 processing is required for manganese binding and extrinsic protein assembly into photosystem II. *J Biol Chem* 279, 45417-45422.

Schmetterer, G. R. (1990). Sequence conservation among the glucose transporter from the cyanobacterium *Synechocystis* sp. PCC 6803 and mammalian glucose transporters. *Plant Molecular Biology* 14, 697-706.

Schreiber, U., Endo, T., Mi, H. & Asada, K. (1995). Quenching Analysis of Chlorophyll Fluorescence by the Saturation Pulse Method: Particular Aspects Relating to the Study of Eukaryotic Algae and Cyanobacteria. *Plant and Cell Physiology* 36, 873-882.

Slack, C. R. & Hatch, M. D. (1967). Comparative studies on the activity of carboxylases and other enzymes in relation to the new pathway of photosynthetic carbon dioxide fixation in tropical grasses. *Biochem J* 103, 660-665.

Stanier, R. Y., Kunisawa, R., Mandel, M. & Cohen-Bazire, G. (1971). Purification and properties of unicellular blue-green algae (order Chroococcales). *Bacteriol Rev* 35, 171-205.

Stöckel, J., Welsh, E. A., Liberton, M., Kunnvakkam, R., Aurora, R. & Pakrasi, H. B. (2008). Global transcriptomic analysis of *Cyanothece* 51142 reveals robust diurnal oscillation of central metabolic processes. *Proc Natl Acad Sci* 105, 6456-6461.

Tamagnini, P., Leitao, E., Oliveira, P., Ferreira, D., Pinto, F., Harris, D. J., Heidorn, T. & Lindblad, P. (2007). Cyanobacterial hydrogenases: diversity, regulation and applications. *Fems Microbiology Reviews* 31, 692-720.

Tang, Y. J., Hwang, J. S., Wemmer, D. & Keasling, J. D. (2007a). The *Shewanella oneidensis* MR-1 fluxome under various oxygen conditions. *Applied and Environmental Microbiology* 73, 718-729.

Tang, Y. J., Meadows, A. L., Kirby, J. & Keasling, J. D. (2007b). Anaerobic central metabolic pathways in *Shewanella oneidensis* MR-1 reinterpreted in the light of isotopic metabolite labeling. *Journal of Bacteriology* 189, 894-901.

Tang, Y. J., Pingitore, F., Mukhopadhyay, A., Phan, R., Hazen, T. C. & Keasling, J. D. (2007c). Pathway confirmation and flux analysis of central metabolic pathways in *Desulfovibrio vulgaris* Hildenborough using GC-MS and FT-ICR mass spectrometry. *Journal of Bacteriology* 189, 940-949.

Tang, Y. J., Martin, H. G., Myers, S., Rodriguez, S., Baidoo, E. E. K. & Keasling, J. D. (2009). Advances in metabolic network and flux analysis of microorganisms via 13C isotopic labeling. *Mass Spectrometry Reviews* 28, 362-375.

Ting, C. S. & Owens, T. G. (1992,). Limitations of the pulse-modulated technique for measuring the fluorescence characteristics of algae. *Plant Physiol* 100, 367-373.

Toepel, J., Welsh, E., Summerfield, T. C., Pakrasi, H. B. & Sherman, L. A. (2008). Differential transcriptional analysis of the cyanobacterium *Cyanothece* sp strain ATCC 51142 during light-dark and continuous-light growth. *J Bacteriol* 190, 3904-3913.

Tuli, R., Naithani, S. & Misra, H. S. (1996). Cyanobacterial photosynthesis and the problem of oxygen in nitrogen-fixation: A molecular genetic view. *Journal of Scientific & Industrial Research* 55, 638-657.

Van Baalen, C., Hoare, D. S. & Brandt, E. (1971). Heterotrophic growth of blue-green algae in dim light. *Journal of Bacteriology* 105, 685-689.

Wahl, S. A., Dauner, M. & Wiechert, W. (2004). New tools for mass isotopomer data evaluation in ^{13}C flux analysis: mass isotope correction, data consistency checking, and precursor relationships. *Biotechnology and Bioengineering* 85, 259-268.

Welsh, E. A., Liberton, M., Stöckel, J. & other authors (2008). The genome of *Cyanothece* 51142, a unicellular diazotrophic cyanobacterium important in the marine nitrogen cycle. *Proc Natl Acad Sci USA* 105, 15094-15099.

Wu, B., Zhang, B., Feng, X., Rubens, J. R., Huang, R., Hicks, L. M., Pakrasi, H. B. & Tang, Y. J. (2010). An Alternate Isoleucine Biosynthesis Pathway involves Citramalate Synthase in Cyanothece sp. ATCC 51142. *Microbiology* 156, 596-602.

Yang, C., Hua, Q. & Shimizu, K. (2002). Metabolic flux analysis in *Synechocystis* using isotope distribution from ^{13}C-labeled glucose. *Metab Eng* 4, 202-216.

Table 1. Isotopic analysis of the labeling profiles of amino acids in *Cyanothece* 51142 and *Synechocystis* 6803 under different growth conditions (the standard error for GC-MS measurement is below 0.02, technical replicates, n=2)

Amino Acids	$[M-57]^+$	N_2						$NaNO_3$						*Synechocystis* 6803 (nitrate-medium)	
		Glucose	R^1	Pyruvate	*R*	Glycerol	*R*	Glucose	*R*	Pyruvate	*R*	Glycerol	*R*	Glucose	*R*
Ala	M0	0.67		0.41		0.19		0.61		0.51		0.07		0.04	
	M1	0.19	***0.032***	0.55	***0.597***	0.71	***4.2***	0.19	***0.042***	0.48	***0.327***	0.85	+∞	0.05	***0.92***
	M2	0.11		0.03		0.10		0.17		0.01		0.07		0.28	
Ser	M0	0.65		0.98		0.20		0.58		0.97		0.08		0.04	
	M1	0.22	***0.033***	0.02	***0***	0.72	***3.7***	0.22	***0.046***	0.03	***0***	0.81	+∞	0.06	***0.87***
	M2	0.10		0		0.09		0.16		0		0.10		0.28	
Asp	M0	0.58		0.54		0.10		0.59		0.94		0.07		0.04	
	M1	0.24	***0.030***	0.43	***0.195***	0.64	***2.2***	0.20	***0.032***	0.06	***0.005***	0.78	***1.53***	0.05	***0.44***
	M2	0.11		0.04		0.25		0.17		0		0.15		0.19	
	M3	0.06		0		0.01		0.03		0		0		0.47	
Glu^2	M0	0.43		0.15		0.02		0.38		0.47		0.01		0.02	
	M1	0.26	***0.041***	0.44	***1.25***	0.14	***- 1.78***	0.22	***0.051***	0.49	***0.170***	0.15	***- 2.11***	0.02	***0.76***
	M2	0.21		0.37		0.62		0.27		0.04		0.74		0.04	
	M3	0.07		0.04		0.21		0.09		0		0.10		0.07	
	M4	0.02		0		0.01		0.03		0		0		0.53	
His	M0	0.44		0.91		0.05		0.33		0.92		0.01		0.01	
	M1	0.28		0.08		0.28		0.24		0.08		0.21		0.01	
	M2	0.17	***0.032***	0	***0***	0.50	***2.83***	0.22	***0.049***	0	***0***	0.55	+∞	0.02	***1.73***
	M3	0.07		0		0.16		0.12		0		0.20		0.03	
	M4	0.03		0		0		0.07		0		0.03		0.06	
	M5	0		0		0		0.01		0		0		0.22	

Note: 1. Bold values were the carbon substrate (glycerol, pyruvate, or glucose) utilization ratios (substrate/CO_2 fixation) for amino acid synthesis calculated according to Equation (1).
2. The glutamate synthesis pathway involved the loss of two carbons from pyruvate to ketoglutarate. Such a microbial process changed the labeling enrichment, and the negative value indicated the net loss of unlabeled CO_2.

Figure 1. Central metabolic pathways of *Cyanothece* 51142 with glucose, glycerol, and pyruvate as carbon substrates. The dashed line shows the metabolic pathway with glycerol as carbon substrate; the bold line indicates glucose; the solid line shows the common pathway for all carbon conditions. Abbreviations: ACCOA, acetyl-coenzyme A; Ala, alanine; E4P, erythrose-4-phosphate; F6P, fructose-6-phosphate; G6P, glucose-6-phosphate; GAP, glyceraldehyde 3-phosphate; 3PG, 3-phosphoglycerate; GLY, glycerol; GLU, glucose; His, histidine; ICIT, citrate/isocitrate; MAL, malate; OAA, oxaloacetate; OXO, 2-oxoglutarate; PEP, phosphoenolpyruvate; PYR, pyruvate; R5P, ribose-5-phosphate (or ribulose-5-phosphate); R15P, ribulose-1,5-bisphosphate; S7P, sedoheptulose-7-phosphate; Ser, serine; Xu5P: xylulose-5-phosphate.

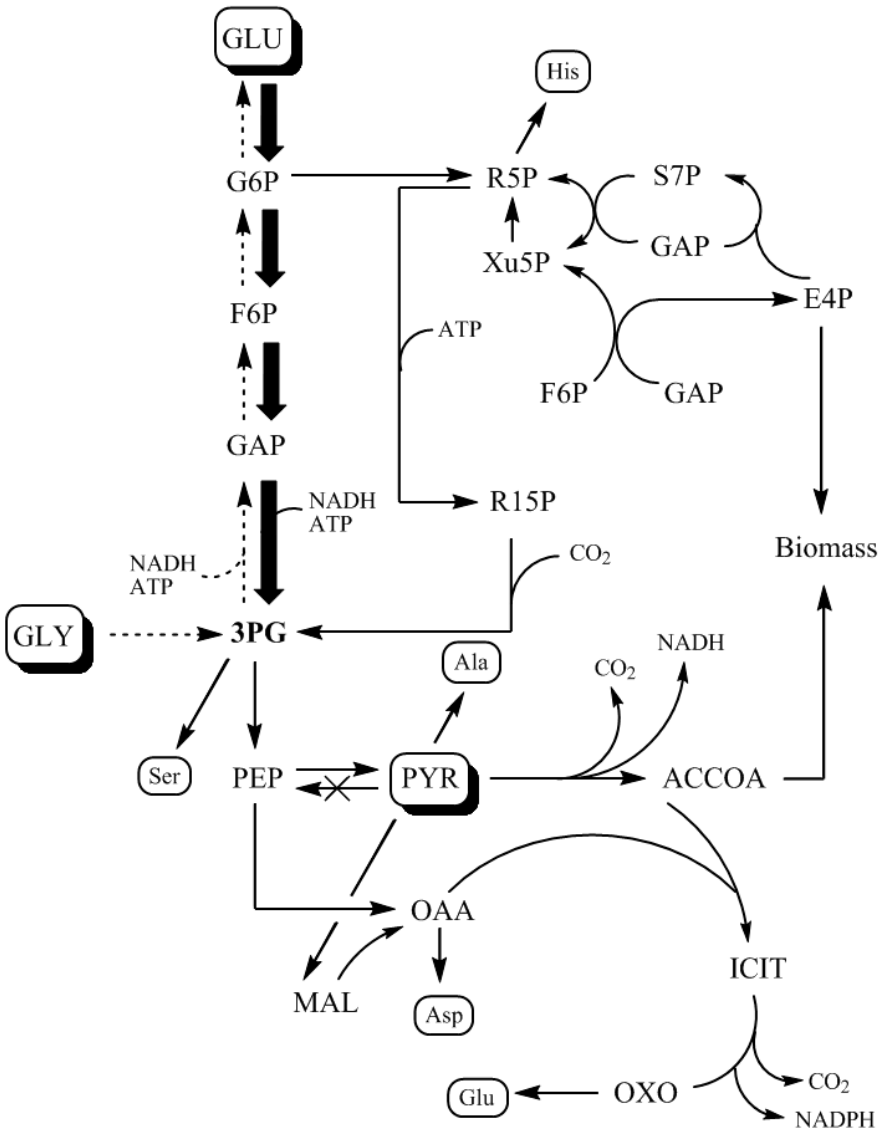
GLU
His
G6P
R5P
S7P
GAP
Xu5P
E4P
F6P
ATP
F6P
GAP
GAP
NADH
ATP
R15P
Biomass
NADH
ATP
CO2
GLY
3PG
Ala
CO2
NADH
Ser
PEP
PYR
ACCOA
OAA
ICIT
MAL
Asp
Glu
OXO
CO2
NADPH

Figure 2. *Cyanothece* 51142 growth curves under different nitrogen and carbon sources (biological replicates, n=3). Diamond: Gly+Nitrate; Square: Gly+N_2; Triangle: CO_2+ Nitrate; Circle: CO_2+N_2. The glycerol-growing samples were taken at day four when the remained glycerol in the culture medium was sufficient for biomass growth (>30mM).

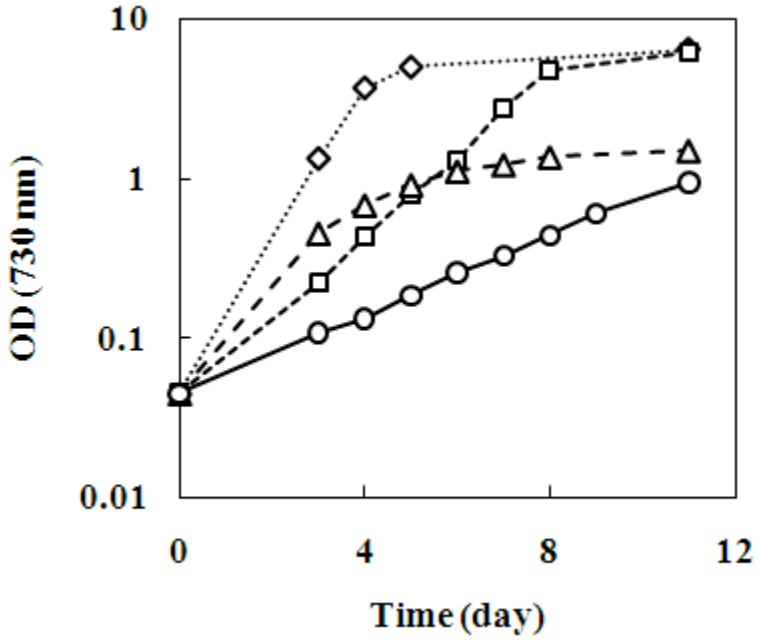
10
1
0.1
0.01
OD (730 nm)
0
4
8
12
Time (day)

Figure 3. Maximum quantum yields (Figure 2a) of PSII and oxygen evolution rates (Figure 2b) in *Cyanothece* 51142 under different growth conditions (biological replicates, n=3). All samples were taken at the exponential growth phase based on the growth curve. Black column, N_2 as nitrogen source; white column, $NaNO_3$ as nitrogen source.

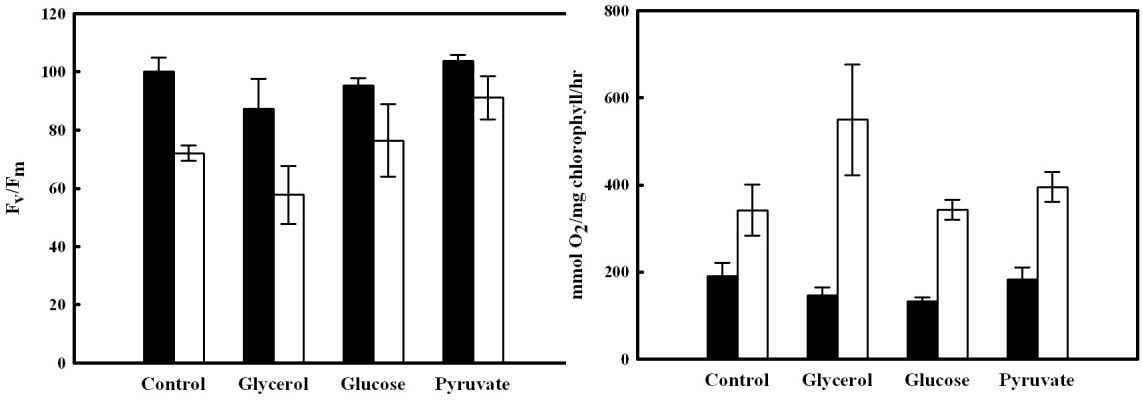
120
100
80
60
40
20
0
F_v/F_m
Control
Glycerol
Glucose
Pyruvate
800
600
400
200
0
nmol O_2/mg chlorophyll/hr
Control
Glycerol
Glucose
Pyruvate

Figure 4. Reverse transcription PCR (RT-PCR) study for ribulose-1,5-bisphosphate carboxylase oxygenase (*rbcL*) and phosphoribulokinase (*prk*) under different mixotrophic growth conditions. (a) CO_2+N_2; (b) CO_2+$NaNO_3$; (c) glycerol+$NaNO_3$; (d) glucose+$NaNO_3$. The 16S rRNA gene was used as the internal reference; the no template control (NTC) was added under each mixotrophic growth conditions.

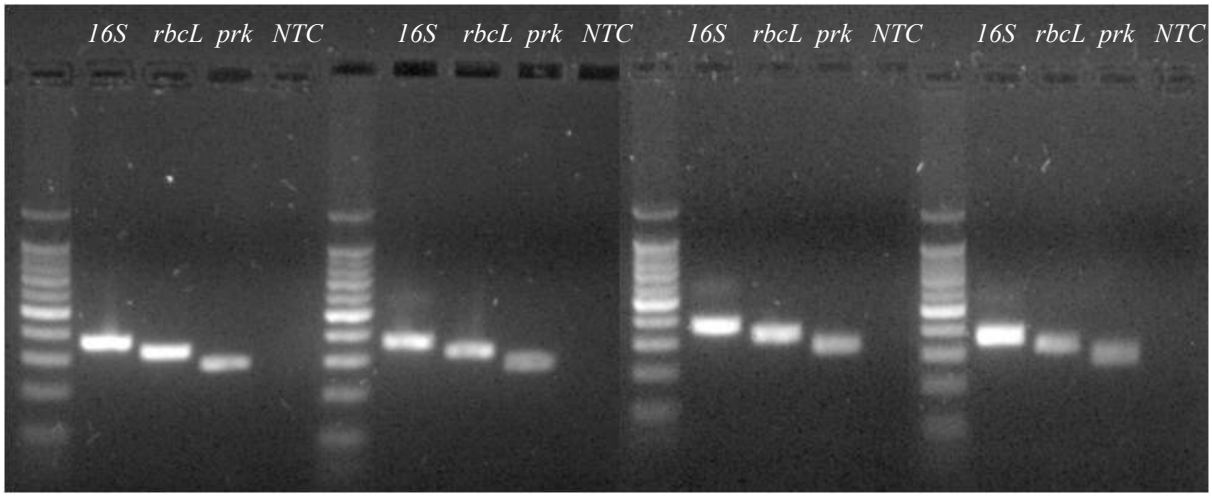
16S rbcL prk NTC
16S rbcL prk NTC
16S rbcL prk NTC
16S rbcL prk NTC

(a) **(b)** **(c)** **(d)**

Appendix Chapter 4

The Genome of Heliobacterium modesticaldum, a Phototrophic Representative of the Firmicutes Containing the Simplest Photosynthetic Apparatus

Summary

Despite the fact that heliobacteria are the only phototrophic representatives of the bacterial phylum *Firmicutes*, genomic analyses of these organisms have yet to be reported. Here we describe the complete sequence and analysis of the genome of *Heliobacterium modesticaldum*, a thermophilic species belonging to this unique group of phototrophs. The genome is a single 3.1-Mb circular chromosome containing 3,138 open reading frames. As suspected from physiological studies of heliobacteria that have failed to show photoautotrophic growth, genes encoding enzymes for known autotrophic pathways in other phototrophic organisms, including ribulose bisphosphate carboxylase (Calvin cycle), citrate lyase (reverse citric acid cycle), and malyl coenzyme A lyase (3-hydroxypropionate pathway), are not present in the *H. modesticaldum* genome. Thus, heliobacteria appear to be the only known anaerobic anoxygenic phototrophs that are not capable of autotrophy. Although for some cellular activities, such as nitrogen fixation, there is a full complement of genes in *H. modesticaldum*, other processes, including carbon metabolism and endosporulation, are more genetically streamlined than they are in most other low-G+C gram-positive bacteria. Moreover, several genes encoding photosynthetic functions in phototrophic purple bacteria are not present in the heliobacteria. In contrast to the nutritional flexibility of many anoxygenic phototrophs, the complete genome sequence of *H. modesticaldum* reveals an organism with a notable degree of metabolic specialization and genomic reduction.

Introduction

Heliobacteria are photosynthetic bacteria that uniquely employ bacteriochlorophyll (Bchl) *g* as the major antenna pigment and primary electron donor within a type I reaction center (RC) (Amesz, 1995, Trost and Blankenship, 1989). Bchl *g* is related to chlorophyll (Chl) *a* but has an ethylidine functional group at the C-8^1 position and is esterified with farnesol rather than phytol (Madigan, 2006). An oxidized form of Chl *a*, 8^1-hydroxy-Chl *a*, is the primary electron acceptor from the RC special pair (Amesz, 1995; van de Meene *et al.,* 1991). Unlike other anoxygenic phototrophic bacteria, heliobacteria have no Bchl-containing internal membranes or structures, such as lamellae (purple bacteria) or chlorosomes (green bacteria). In the heliobacteria, photosynthetic pigments are confined to RCs in the cytoplasmic membrane (Fuller *et al.,* 1985, Miller *et al.,* 1986). Carotenoids are also unusual in heliobacteria in that they consist of C_{30} pigments rather than the C_{40} derivatives present in other phototrophs (Takaichi, 1999). The dominant carotenoid in nonalkaliphilic heliobacteria is 4,4'-diaponeurosporene (Takaichi *et al.,* 1997). In addition to their unique photosynthetic properties, heliobacteria can be distinguished from all other anaerobic anoxygenic phototrophs in at least three major ways. In terms of carbon metabolism, heliobacteria are obligately heterotrophic. Growth occurs either photoheterotrophically (anoxic, with light) on a limited range of organic substrates or by fermentation of pyruvate in the dark (Kimble *et al.,* 1994; Madigan *et al.,* 1995). By contrast, autotrophic growth, the hallmark of photosynthetic organisms, has not been observed with cultures of any heliobacterium species (Madigan *et al.,* 1995). Heliobacteria are phylogenetically unique, as they are the only phototrophic organisms that group within the bacterial phylum *Firmicutes* using 16S rRNA gene sequence analyses (Bryantseva, *et al.,* 1999; Madigan, 2001). Finally, heliobacteria are unique among all phototrophs in that they produce endospores

(Kimble-Long *et al.,* 2001), a key property of nonphototrophic *Firmicutes*, such as *Bacillus* and *Clostridium*.

A complete genome sequence analysis of *Heliobacterium modesticaldum*, the first heliobacterial genome to be sequenced, reveals an organism with a full complement of nitrogen fixation genes but only a limited capacity for carbon metabolism and no apparent mechanism for autotrophic growth. Many genes linked to endosporulation in *Bacillus subtilis* were not found in *H. modesticaldum*, which may have relevance for the ambiguous sporulation patterns observed in heliobacterial cultures (Kimble-Long *et al.,* 2001). These results describe *H. modesticaldum* strain Ice1, the type strain of this species isolated from Icelandic hot spring volcanic soils (Kimble *et al.,* 1995).

Materials and Methods

Genome sequencing.

H. modesticaldum strain Ice1^T genomic DNA was fragmented randomly by kinetic shearing, and two shotgun libraries were constructed: a small insert library in plasmid pOTWI3 (using 3- to 4-kb size fractions) and a large insert fosmid library in pEpiFOS-5 (with insert sizes ranging from 28 to 47 kb), which was used as a scaffold. The relative amounts of sequence coverage obtained from the small and large insert libraries were approximately 11x and 2x, respectively. The whole genome sequence was established from 51,795 end sequences derived from these libraries using dye terminator chemistry with Applied Biosystems 3730xl automated sequencers. The sequence was assembled with the program ARACHNE (Batzoglou *et al.,* 2002) and finished as described previously (Swingley *et al.,* 2007).

Annotation.

Initial automated annotation of the genome was performed with the TIGR/JCVI annotation engine (www.tigr.org/AnnotationEngine), and it was processed by The Institute for Genome Research's prokaryotic annotation pipeline using gene finding with Glimmer, SignalP predictions, and BLAST extendrepraze (BER), HMM, and TMHMM searches. Automatic annotations were created using AutoAnnotate. Manatee (manatee.sourceforge.net) was used to manually review and confirm the annotation of all genes. Pseudogenes contained one or more mutations that could ablate expression; each inactivating mutation was subsequently checked against the original sequencing data. A circular genome map was created using the program CGView (Stothard and Wishart, 2005).

Phylogenetic analyses.

Sequence identity analyses were performed using the Basic Local Alignment Search Tool (BLAST) (Altschul *et al.,* 1990). Gene sequences were aligned and phylogenetic trees were constructed using MEGA, version 3.1 (Kumar *et al.,* 2004). Bootstrap values were determined using 500 replicates. Sequences used in phylogenetic analyses were obtained from NCBI genome databases (http://www.ncbi.nlm .nih.gov/).

Nucleotide sequence accession number.

The complete and annotated sequence of the genome of *H. modesticaldum* strain Ice1^{T} has been deposited in the DDBJ/EMBL/GenBank database under accession number CP000930.

Results and Discussion

Genome properties.

H. modesticaldum strain Ice1^T has a single 3,075,407-bp circular chromosome containing 3,138 open reading frames (ORFs), eight pseudogenes, and no plasmids (Table 1). The genomic G+C content of *H. modesticaldum*, 56.0%, is at the upper end of the range for heliobacteria (Madigan, 2006) (Table 1 and Fig. 1). The total protein-encoding content of the chromosome is 87%, and the average gene length is 882 nucleotides. Eight rRNA operons are randomly dispersed throughout the chromosome. Each operon contains one copy each of 5S, 16S, and 23S rRNA genes, giving a total of 24 rRNA genes. This number is high but consistent with the numbers for other endospore-forming *Firmicutes* (Klappenbach *et al.,* 2000). A summary of the number and percentage of genes in each primary category is shown in Table 2.

An unusual feature of the *H. modesticaldum* genome is the prevalence of gene strand bias, where large numbers of genes cluster predominately on one strand or the other throughout the chromosome (Fig. 1). One strand of the chromosome contains approximately two-thirds of the protein coding sequences (CDSs) (Fig. 1, outer ring), while the other strand contains the other one-third. This degree of strand asymmetry of coding sequences is unusual in bacteria and, to our knowledge, is equaled only by the close phylogenetic but not phototrophic relative *Desulfitobacterium hafniense* Y51 among completely sequenced prokaryotes having a circular chromosome (Nonaka *et al.,* 2006).

CDSs encoding conserved hypothetical proteins make up approximately 11% of the total CDSs, and an additional 1.7% of the ORFs contain domain regions having sequence identity to known motifs. The genome contains 70 ORFs that show significant sequence identity to genes that encode transposases. Although this number is high compared to the numbers for many other

completely sequenced *Firmicutes*, it is comparable to the 71 (2 confirmed and 69 putative) transposase genes found in *D. hafniense* Y51 (Nonaka, *et al.,* 2006) and the 60 transposase genes of *Desulfotomaculum reducens* MI-1 (U.S. DOE Joint Genome Institute, NCBI genome database); these two strains are nonphototrophic gram-positive bacteria that are close phylogenetic relatives of *Heliobacterium* spp. (Stackenbrandt *et al.,* 1997).

Most of the 20 common aminoacyl-tRNAs can be synthesized directly in *H. modesticaldum*; the only exception is asparaginyl-tRNA, which cannot be synthesized due to the apparent absence of a gene encoding asparaginyl-tRNA synthetase. An alternative pathway that could allow asparaginyl-tRNA synthesis involves aspartyl/glutamyl-tRNA amidotransferase, a heterotrimeric enzyme that can catalyze the conversion of aspartyl-tRNA to asparaginyl-tRNA in *Pseudomonas aeruginosa* (Akochy *et al.,* 2004). Although this function is more commonly observed in *Archaea* (Curnow *et al.,* 1998), genes predicted to encode all three subunits of aspartyl-tRNA amidotransferase (gatABC) are present in *H. modesticaldum*. These genes may have functions similar to those of *P. aeruginosa* genes for synthesis of a full complement of aminoacyl-tRNAs. In addition, the *H. modesticaldum* genome contains the *selABCD* genes, which allow the synthesis and incorporation of selenocysteine into proteins.

Carbon metabolism.

Genomic analyses of *H. modesticaldum* supported the restricted capacity for organic carbon photoassimilation previously observed in physiological studies (Kimble *et al.,* 1995). Although photoheterotrophic growth using fatty acids, such as butyrate and propionate, has been observed for some species of heliobacteria (Asao *et al.,* 2006; Beer-Romero and Gest, 1987; Bryantseva *et al.,* 2000; Ormerod *et al.,* 1996), *H. modesticaldum* is limited to photoassimilation

of pyruvate, lactate, or acetate (Kimble *et al.,* 1995). Growth of *Heliobacterium gestii*, but not growth of *H. modesticaldum*, is supported by ethanol plus CO_2 (Ornerod *et al.,* 1996). Although three genes predicted to encode alcohol dehydrogenase are present in *H. modesticaldum*, a lack of peripheral enzymes, such as NADdependent aldehyde dehydrogenase, may preclude the catabolism of alcohols. Glucose and fructose utilization has also been reported in *H. gestii* (Madigan, 2006). However, despite the presence of genes predicted to encode a four-subunit monosaccharide-transporting ATPase (*rbsABCD*) in the genome, sugars did not support growth of *H. modesticaldum* (Kimble *et al.,* 1995). Genes corresponding to complete glycolytic and nonoxidative pentose phosphate pathways were identified (data not shown), so it remains unclear why monosaccharides are unsuitable growth substrates for *H. modesticaldum*.

Pyruvate supports both photoheterotrophic and fermentative (dark anoxic) growth of heliobacteria (Madigan, 2006). Consistent with biochemical studies carried out by Pickett *et al*. (Pickett, *et al.,* 1994), no gene encoding pyruvate dehydrogenase was found in the *H. modesticaldum* genome. However, the oxidation of pyruvate to acetyl coenzyme A (acetyl-CoA) can alternatively be catalyzed by a predicted pyruvate:ferredoxin oxidoreductase (HM1_0807). This enzyme showed 65 to 70% amino acid sequence identity to the pyruvate:ferredoxin oxidoreductase of closely related, nonphototrophic *Firmicutes* and 83% sequence identity to the pyruvate:ferredoxin oxidoreductase of *Heliobacillus mobilis*. During photoheterotrophic growth, the oxidation of lactate to pyruvate (and the concomitant reduction of NAD^+ to NADH) is catalyzed by a putative lactate dehydrogenase (HM1_2756) (Fig. 2). Acetate is presumably photometabolized through an acetyl adenylate intermediate to acetyl-CoA via an AMP-forming acetyl-CoA synthetase (HM1_0951) (Fig. 2). A gene predicted to encode acetate kinase (HM1_2157), which phosphorylates acetate to acetyl-P, was also found in the genome.

The mechanism of pyruvate fermentation in *H. modesticaldum* is complicated by the lack of a gene encoding phosphotransacetylase, which converts acetyl-CoA to acetyl-phosphate. Either a highly unusual phosphotransacetylase is present, or there is an alternative mechanism of pyruvate fermentation in *H. modesticaldum*. One possibility for this is reverse activity of enzymes involved in the photoassimilation of acetate (reactions 1 and 12 in Fig. 2). In this scenario, CO_2 and reduced ferredoxin are products of the oxidation of pyruvate to acetyl-CoA. The production of ATP would occur with the conversion of acetyl-adenylate (from acetyl-CoA) to acetate via acetyl-CoA synthetase (Fig. 2), an enzyme known to have reversible activity (Webster, 1967).

Genes encoding a putative [FeFe] hydrogenase that could oxidize ferredoxin with the production of H_2 were identified in *H. modesticaldum* and are shown schematically in Fig. 3A. These genes, *nuoEF* (HM1_1028) and *nuoG* (hydA; HM1_ 1029), showed levels of sequence identity of 79 and 81%, respectively, to genes of *Heliobacillus mobilis*. The arrangement of *nuoE* and *nuoF* varies among *Firmicutes* containing an [FeFe] hydrogenase. In both *H. modesticaldum* and *Heliobacillus mobilis*, these genes are fused to produce a single transcript, but in some other *Firmicutes*, such as *Pelotomaculum thermopropionicum* SI, the genes are separate (Ludwig *et al.,* 2006) (Fig. 3A). The fusion of *nuoE* and *nuoF* does not occur exclusively in heliobacteria, however, since these genes are also fused in *Symbiobacterium thermophilum*, an uncultivated commensal bacterium phylogenetically related to *Firmicutes* (Ludwig *et al.,* 2006).

No mechanism for autotrophic growth has been identified in any heliobacterial species, in contrast to all other anaerobic anoxygenic phototrophs (Heinnickel *et al.,* 2007). Consistent with these physiological observations, genes encoding essential enzymes of all known autotrophic pathways were not found in the *H. modesticaldum* genome, including genes encoding ribulose

1,5-bisphosphate carboxylase and phosphoribulokinase (Calvin cycle), citrate lyase (reverse citric acid cycle), carbon monoxide dehydrogenase (reductive acetyl-CoA pathway), and malyl-CoA lyase (3-hydroxypropionate pathway). Moreover, there is no evidence for a gene encoding 4-hydroxybutyryl-CoA dehydratase, a key enzyme of the recently described 3-hydroxypropionate/ 4-hydroxybutyrate pathway of carbon fixation (Berg *et al.,* 2007; Thauer 2007). The absence of citrate lyase may be the key factor distinguishing the carbon metabolism of heliobacteria from that of green sulfur bacteria, autotrophic phototrophs that fix CO_2 via the reverse citric acid cycle. In addition, no gene encoding citrate synthase was found in the genome. Thus, *H. modesticaldum* appears to have an incomplete citric acid cycle, which is typical of organisms using this cycle for biosynthesis.

A putative anapleurotic carbon fixation pathway for heliobacteria, in which CO_2 assimilation occurs through phosphoenolpyruvate (PEP) carboxylase activity, was proposed by Pickett et al. (Pickett *et al.,* 1994) and recently examined again by Heinnickel and Golbeck (Heinnickel *et al.,* 2007). A similar mechanism was proposed as a means of mixotrophic growth in the aerobic phototrophic proteobacterium *Roseobacter denitrificans* (Swingley *et al.,* 2007). The enzymes needed to carry out these transformations have been identified in the *H. modesticaldum* genome, and thus a small amount of nonautotrophic CO_2 assimilation likely takes place. A summary of the proposed pathways of carbon metabolism in H. modesticaldum is shown in Fig. 2.

Nitrogen fixation.

H. modesticaldum is an active dinitrogen fixer, and this species and the green sulfur bacterium *Chlorobaculum tepidum* are the only cultured anoxygenic phototrophs that are capable

of N_2 fixation at temperatures above 50°C (Kimble *et al.,* 1995; Madigan, 1995). The organization of the *nif* regulon in *H. modesticaldum* is identical to that in *Heliobacterium chlorum* (Enkh-Amgalan *et al.,* 2006). The *nif* regulon consists of 11 genes: *nif$_I$1, nif$_I$2, nifH, nifD, nifK, nifE, nifN, nifX, fdxB, nifB*, and *nifV*. In a phylogenetic analysis using a concatenated alignment of the nitrogenase structural genes *nifHDK*, *H. modesticaldum* grouped within a clade containing both a closely related species belonging to the *Firmicutes* (*D. hafniense*) and a distantly related deltaproteobacterium (*Geobacter sulfurreducens*) (Fig. 4). The high level of similarity of heliobacterial *nifHDK* genes to the genes of *Geobacter* was also noted in phylogenetic analyses using *nif* genes from *H. chlorum* (Enkh-Amgalan *et al.,* 2006) and suggests that either these genes had a common ancestor or there was a lateral transfer event.

Although some heliobacteria contain an alternative iron (Fe)-only group III type nitrogenase (Kimble and Madigan, 1992; Loveless and Bishop 1999), *H. modesticaldum* contains a molybdenum-dependent, group I nitrogenase (Raymond *et al.,* 2004). The products of *nif$_I$1* and *nif$_I$2*, which encode proteins belonging to the P_{II} signal transduction family, are located between the *nifH* and *nifD* products in group II and III nitrogenases, but they are not present in most group I nitrogenases (Enkh-Amgalan, *et al.,* 2006a, Raymond *et al.,* 2004). The presence of *nif$_I$1* and *nif$_I$2* upstream of *nifH* in *H. modesticaldum*, as well as in other species of *Heliobacterium* and in *D. hafniense* Y51, suggests that the nitrogenase of these organisms may be an evolutionary intermediate between group I and group II/III nitrogenases (Enkh-Amgalan, *et al.,* 2006ab).

The *H. modesticaldum* genome contains an ORF (HM1_ 0869) with 90 and 74% sequence identity to the recently described *orf1* in *H. gestii* and *H. chlorum*, respectively (Enkh-Amgalan, *et al.,* 2006a). The *orf1* product shares some amino acid sequence identity (~27%)

with the *hutP* product, a positive regulator of the histidine utilization (*hut*) operon in *B. subtilis*. Similar to the regulatory mechanism for histidine utilization by *HutP*, *orf1*, situated upstream of the *nif* regulon, may be involved in ammonia switch-off regulation of *nif* gene expression in heliobacteria (Enkh-Amgalan, *et al.,* 2006a; Madigan, 1995). The activation of the *orf1* product in the absence of sufficient levels of fixed nitrogen may allow transcription to continue through a terminator-like structure in the intergenic region of *orf1* and *nifI1*, resulting in expression of the *nif* structural genes (Enkh-Amgalan, *et al.,* 2006a). In *H. modesticaldum* the terminator-like structure shows 94 and 83% sequence identity to the terminator regions of *H. gestii* and *H. chlorum*, respectively. This regulatory mechanism is distinct from that of most diazotrophs, which employ the *nifA* gene product, which is not present in heliobacteria (Chen, 2004; Enkh-Amgalan, *et al.,* 2006a), as a transcriptional activator (Merrick, 2004).

An operon containing genes involved in the assembly of an uptake [NiFe] hydrogenase was also found in the genome of *H. modesticaldum*. In contrast to the [FeFe] hydrogenase involved in hydrogen production during pyruvate fermentation, the uptake [NiFe] hydrogenase is likely associated with nitrogenase, catalyzing the oxidation of hydrogen produced in the following nitrogen-fixing reaction: $8H^+ + 8e^- + N_2 \rightarrow 2NH_3 + H_2$ (Rey *et al.,* 2006). A total of 10 genes are present in the uptake [NiFe] hydrogenase operon (Fig. 3B). Six genes (*hypABCDEF*) encode assembly/maturation proteins, and *hypA* (HM1_1482) encodes the Ni insertion protein. Three genes encode hydrogenase structural proteins; *hupS*, *hupL*, and *hupC* encode the small, large, and b-type cytochrome subunits, respectively. One gene, *hupD* (HM1_1481), encodes an accessory formation protein. Genes encoding an uptake [NiFe] hydrogenase, including three copies each of *hupC*, *hupL*, and *hupS*, are also present in *D. hafniense* Y51. In contrast to the

single gene cluster present in *H. modesticaldum*, however, these genes occur in separate operons found in different regions of the *D. hafniense* chromosome (Fig. 3B).

Endospore formation.

Endosporulation appears to be universal among heliobacteria (Kimble-long *et al.,* 2001), and the ability of endospores to survive pasteurization (heating to 80°C for 15 min) can be exploited for selective enrichment of these organisms (Madigan, 2006; Stevenson *et al.,* 1997). *H. modesticaldum* contains genes encoding all five sigma factors deemed essential for sporulation in B. subtilis (σH, σE, σF, σG, and σK). However, in a genome-wide comparison of the two organisms, several sporulation-specific genes were not found in *H. modesticaldum*.

An ortholog of the *spo0M* gene, which is involved in the regulation of endospore formation in *B. subtilis* (Han *et al.,* 1998), was not identified in *H. modesticaldum*. Although this gene is not essential for viability of *B. subtilis*, inactivation of it significantly hinders initiation of endosporulation (Han *et al.,* 1998). The absence of this gene in *H. modesticaldum* is curious since it is present in many species of *Bacillus*, as well as in sporulating organisms more closely related to heliobacteria, such as *D. reducens* and *P. thermopropionicum*. Likewise, no homolog of the *spoIIB* gene, which is involved in septum formation during stage II of sporulation in *B. subtilis*, could be found in the *H. modesticaldum* genome. Although genetic studies in which the *B. subtilis spoIIB* gene was altered resulted in only minor impairment of sporulation (Margolis *et al.,* 1993), the apparent absence of both *spoIIB* and *spo0M* in heliobacteria could adversely affect the ability of these organisms to sporulate. Consistent with this hypothesis is the fact that sporulation of pure cultures of heliobacteria is rarely observed (Kimble-Long and Madigan, 2001).

None of the 20 known *cot* genes in *B. subtilis*, whose products form the inner and outer spore coat and ostensibly function in a protective capacity (Naclerio *et al.,* 1996), showed significant sequence identity to genes in the *H. modesticaldum* genome. Although it is not known whether the lack of cot genes is universal among heliobacteria, heliobacterial endospores do not appear to be compromised in terms of heat resistance, as evidenced by the presence of viable cells in pasteurized cultures (Stevenson *et al.,* 1997).

Pigment biosynthesis and photosynthetic proteins.

Bchl *g* is one of two Chl derivatives (along with Bchl *b*) that contain an ethylidene substituent on ring B. The biosynthetic pathway of Bchl *g* (or Bchl *b*) has not been established yet. The genome data for *H. modesticaldum* revealed no gene predicted to encode a divinyl reductase; however, this cannot be correlated to Bchl *b*-containing organisms since, to date, the genomes of none of these organisms have been sequenced. Homologues of neither *bciA* nor slr1923, genes recently shown to encode C-8 divinyl reductases in *C. tepidum* (Chow and Bryant, 2007) and *Synechocystis* sp. strain PCC 6803 (Ito *et al.,* 2008), respectively, were identified in the *H. modesticaldum* genome. Thus, it is possible that heliobacteria contain a third, unknown type of divinyl reductase, as has been proposed for species of *Roseiflexus*, a filamentous anoxygenic phototroph that also lacks *bciA* and slr1923 (Ito *et al.,* 2008). However, a proposed alternative pathway of Bchl *g* synthesis that circumvents the absence of divinyl reductase and incorporates the somewhat unexpected presence of the chlorophyllide reductase enzyme complex (BchX, BchY, and BchZ) is shown in Fig. 5. We propose that in this pathway, the C-7–C-8 double bond is reduced by chlorophyllide reductase, and the ethylidene group is then formed by isomerization of the C-8^1 vinyl substituent. Although the gene that encodes the

enzyme responsible for this isomerase activity has not been identified, this mechanism seems plausible, as it would require the reduction of only one double bond on ring B and is completely consistent with the gene presence/absence patterns described above.

Farnesol, the esterifying alcohol of Bchl *g*, is synthesized in a complete nonmevalonate pathway, in which pyruvate and glyceraldehyde 3-phosphate are condensed to yield isopentenyl-pyrophosphate and dimethylallyl-pyrophosphate through a cascade of enzymatic reactions (Dubey *et al.,* 2003). Farnesyl-pyrophosphate is produced from these precursors through a geranyl-pyrophosphate intermediate (Dubey *et al.,* 2003).

The gene encoding Bchl synthetase (*bchG*) in *H. modesticaldum* (HM1_0692) has a high level of sequence identity (74.7%) to *bchG* from *Heliobacillus mobilis* (see Fig. S1 in the supplemental material). As it is in *Heliobacillus mobilis* (Xiong *et al.,* 1998), *bchG* is situated between *bchJ* (HM1_0693), a gene recently shown to not encode divinyl reductase in green sulfur bacteria (Chew and Bryant, 2007), and *pshA* (HM1_0690) in *H. modesticaldum* (Fig. 3C). PshA is the type I RC core polypeptide homologous to PscA and PsaA of other phototrophs with type I RCs (see Fig. S2 in the supplemental material). These genes are members of a large photosynthesis gene cluster (PGC) that also contains genes encoding all four cytochrome *bc* complex subunits (PetA, PetB, PetC, and PetD), the 18-kDa cytochrome c553 (PetJ), a carotenoid biosynthesis protein (CrtN), and several proteins involved in vitamin biosynthesis (Xiong *et al.,* 1998) (Fig. 3C). The *bchXYZ* genes are located on the opposite strand in an adjacent operon (Fig. 3C). The phylogenetic relationship of concatenated amino acid sequences from protochlorophyllide reductase (*bchLNB*) and chlorophyllide reductase (*bchXYZ*) genes from *H. modesticaldum* and other organisms is shown in Fig. 4. The distinctly separate lineages of the

H. modesticaldum bchXYZ and *bchLNB* genes and the genes of other anoxygenic phototrophs are evident.

The grouping of photosynthetic genes into superoperonal clusters is a trait found only in heliobacteria and purple bacteria. However, as these organisms are phylogenetically distinct phototrophs, it is significant that the PGC of purple bacteria shows little gene synteny with that of heliobacteria. A comparison of the PGCs of *Rhodobacter capsulatus* and *H. modesticaldum* shows that most of the photosynthesis genes in *R. capsulatus* are not present in *H. modesticaldum* (Fig. 3C). It is also notable that while nearly all of the genes in the PGC of *R. capsulatus* encode proteins with photosynthetic functions, the products of more than one-half of the genes in the PGC of *H. modesticaldum* appear to be involved in nonphotosynthetic processes (Fig. 3C).

The relative simplicity of heliobacterial photosynthesis is suggested first by the absence of three Bchl biosynthesis genes in *H. modesticaldum* that are present in *R. capsulatus* (*bchCPF*). Conversely, *R. capsulatus* contains all 13 *bch* genes present in *H. modesticaldum* (Fig. 3C). Perhaps even more indicative of the simplicity of the heliobacterial photosynthetic apparatus is the lack of a heteromeric RC, such as that encoded by the *pufLM* genes in purple bacteria, and the absence of additional light-harvesting complexes, which are encoded by the *pufAB* and *pucAB* genes in purple bacteria. It is therefore difficult to envision a close evolutionary connection between the PGCs of heliobacteria and purple bacteria due to extensive gene rearrangements and divergent transcription. Instead, the high degree of genetic disparity suggests that these superoperon clusters developed convergently rather than having a common origin. The possible functional significance of this is not apparent.

Electron transfer pathways.

Genes predicted to encode all 14 subunits of NADH:quinone oxidoreductase (*nuoA* to *nuoN*) were identified in the *H. modesticaldum* genome. Presumably, electrons from NADH are transferred to menaquinone through this complex and donated to the cytochrome *bc* complex, which reduces the Rieske [2Fe-2S] subunit (PetC) and cytochrome b_L (Heinnickel and Golbeck, 2007) (Fig. 6). Electrons from the cytochrome *bc* complex are transferred to the RC primary electron donor, P798, via cytochrome c_{553} (Oh-Oka *et al.,* 2002). A complete ATP synthase, having all eight subunits encoded in a single conserved operon, catalyzes ATP synthesis. Phylogenetic and physiological similarities between photosystem I and the heliobacterial RC, as well as kinetic studies conducted with *Heliobacillus mobilis* (Kramer *et al.,* 1997), suggest that proton motive force generation through cyclic electron flow occurs in *H. modesticaldum*, but this has not been confirmed.

Electron transfer within the RC of heliobacteria is not well understood. It is known that rapid transfer occurs from the excited state of the primary electron donor, P798, to the primary acceptor, 8^1-OH-Chl *a* (*A0*), but the existence of a secondary quinone acceptor (*A1*) has not been confirmed (Oh-Oka, 2007). PshA exists as a homodimer containing two cysteine residues per subunit that are believed to bind to an FX-like [4Fe-4S] cluster (Kleinherebrink *et al.,* 1994; Miyamoto *et al.,* 2006; Oh-Oka, 2007). In addition to *pshA*, a *pshB* gene (HM1_1462), which encodes an RC-associated [4Fe-4S]-binding ferredoxin, was confirmed to be present in the *H. modesticaldum* genome. A recent study showed that PshB binds the terminal Fe/S dicluster electron acceptors, FA and FB (Heinnickel *et al.,* 2007). Electrons are likely transferred from the Fe/S clusters to a cytoplasmic ferredoxin, which can supply reducing equivalents for cellular processes, such as carbon assimilation and nitrogen fixation (Fig. 6).

No clear homolog of a gene encoding ferredoxin:$NADP^+$ reductase (FNR) is present in the genome. A well-conserved thioredoxin reductase encoded by a gene in the *H. modesticaldum* genome (HM1_0984) showed 30 and 28% sequence identity to the FNR of *Bacillus thuringiensis* and *C. tepidum*, respectively. The gene encoding FNR in *C. tepidum* was originally annotated as a putative thioredoxin reductase gene, but the product has since been shown to have FNR activity (Seo and Sakurai, 2002). However, the low levels of sequence identity of these enzymes to HM1_0984, as well as the equivalog-level support of the ORF as a thioredoxin reductase gene, suggest that the enzyme is not FNR. Therefore, the mechanism of $NADP^+$ reduction in *H. modesticaldum* remains unknown.

Our analysis of the *Heliobacterium* genome provides the first glimpse of the genetic capacity of the unique anoxygenic phototrophs belonging to this genus. Further genomic analyses, especially analyses of species of heliobacteria that inhabit agricultural soils (such as *Heliophilum fasciatum*) or alkaline soils (such as *Heliorestis species*), should further unravel the unusual patterns of carbon metabolism, photosynthetic energy conversion, and sporulation found here.

References

Akochy, P.-M., Bernard, D., Roy, P. H. and Lapointe, J. (2004) Direct glutaminyl- tRNA biosynthesis and indirect asparaginyl-tRNA biosynthesis in *Pseudomonas aeruginosa* PAO1. *J. Bacteriol*. 186:767–776

Altschul, S. F., Gish, W. Miller, W., Myers, E. W., and Lipman, D. J. (1990) Basic local alignment search tool. *J. Mol. Biol*. 215:403–410.

Amesz, J. (1995) The antenna-reaction center complex of heliobacteria, p. 687–697. *In* R. E. Blankenship, M. T. Madigan, and Bauer, C. E. (*ed*.), Anoxygenic photosynthetic bacteria. Kluwer Academic Publishers, Dordrecht, The Netherlands.

Asao, M., Jung, D. O., Achenbach, L. A., and Madigan, M. T. (2006) *Heliorestis convoluta* sp. nov., a coiled, alkaliphilic heliobacterium from the Wadi El Natroun, Egypt. *Extremophiles.* 10:403–410

Batzoglou, S., Jaffe, D. B., Stanley, K., Butler, J., Gnerre, S., Mauceli, E., Berger, B., Mesirov, J. P., and Lander, E. S. (2002) ARACHNE: a whole-genome shotgun assembler. *Genome Res.* 12:177–189

Beer-Romero, P., and Gest, H. (1987) *Heliobacillus mobilis*, a peritrichously flagellated anoxyphototroph containing bacteriochlorophyll g. *FEMS Microbiol*. *Lett*. 41:109–114

Berg, I. A., Kockelkorn, D., Buckel, W., and Fuchs, G. (2007) A 3-hydroxypropionate/ 4-hydroxybutyrate autotrophic carbon dioxide assimilation pathway in Archaea. *Science.* 318:1782–1786

Bryantseva, I. A., Gorlenko, V. M., Kompantseva, E. I., Achenbach, L. A., and Madigan, M. T. (1999) *Heliorestis daurensis*, gen. nov. sp. nov., an alkaliphilic rod-to-coiled-shaped phototrophic heliobacterium from a Siberian soda lake. *Arch. Microbiol*. 172:167–174

Bryantseva, I. A., Gorlenko, V. M., Kompantseva, E., I., Tourova, T. P., Kuznetsov, B. B., and Osipov, G. A. (2000) Alkaliphilic heliobacterium *Heliorestis baculata* sp. nov. and emended description of the genus *Heliorestis*. *Arch. Microbiol*. 174:283–291.

Chen, J. S. 2004. Nitrogen fixation in the clostridia, p. 53–64. In Klipp, W., Masepohl, B., Gallon, J. R., and Newton, W. E. (*ed*.), Genetics and regulation of nitrogen fixation in free-living bacteria. Kluwer Academic Publishers, Dordrecht, The Netherlands

Chew, A. G. M., and Bryant, D. A. (2007) Characterization of a plant-like protochlorophyllide a divinyl reductase in green sulfur bacteria. *J. Biol. Chem*. 282:2967–2975

Curnow, A. W., Tumbula, D. L., Pelaschier, J. T., Min, B., and D. Söll. (1998) Glutamyl-tRNAGln amidotransferase in Deinococcus radiodurans may be confined to asparagine biosynthesis. *Proc. Natl. Acad. Sci. USA* 95:12838– 12843

Dubey, V. S., Bhalla, R., and Luthra, R. (2003) An overview of the nonmevalonate pathway for terpenoid biosynthesis in plants. *J. Biosci*. 28:637– 646

Enkh-Amgalan, J., Kawasaki, H., Oh-oka, H., and Seki, T. (2006) Cloning and characterization of a novel gene involved in nitrogen fixation in *Heliobacterium chlorum*: a possible regulatory gene. *Arch. Microbiol*. 186:327–337

Enkh-Amgalan, J., Kawasaki, H., and Seki, T. (2006) Molecular evolution of the nif gene cluster carrying *nifI*$_1$ and *nifI*$_2$ genes in the Gram-positive phototrophic bacterium *Heliobacterium chlorum*. *Int. J. Syst. Evol. Microbiol*. 56:65–74

Fuller, R. C., Sprague, S. G., Gest, H., and Blankenship, R. E. (1985) A unique photosynthetic reaction center from *Heliobacterium chlorum. FEBS Lett.* 182:345–349

Han, W.-D., Kawamoto, S., Hosoya, Y., Fujita, M., Sadaie, Y., Suzuki, K., Ohashi, Y., Kawamura, F., and Ochi, K. (1998) A novel sporulation-control gene (*spo0M*) of *Bacillus subtilis* with a s^H-regulated promoter. *Gene.* 217:31–40

Heinnickel, M., and Golbeck, J. H. (2007) Heliobacterial photosynthesis. *Photosynth. Res*. 92:35–53.

Heinnickel, M., Shen, G., and Golbeck, J. H. (2007) Identification and characterization of *PshB*, the dicluster ferredoxin that harbors the terminal electron acceptors FA and FB in *Heliobacterium modesticaldum. Biochemistry.* 46:2530–2536

Ito, H., Yokono, M., Tanaka, R., and Tanaka, A. (2008) Identification of a novel vinyl reductase gene essential for the biosynthesis of monovinyl chlorophyll in *Synechocystis* sp. PCC 6803. *J. Biol. Chem*. 283:9002–9011

Kimble, L. K., and Madigan, M. T. (1992) Evidence for an alternative nitrogenase in *Heliobacterium gestii. FEMS Microbiol. Lett.* 100:255–260

Kimble, L. K., Stevenson, A. K., and Madigan, M. T. (1994) Chemotrophic growth of heliobacteria in darkness. *FEMS Microbiol. Lett*. 115:51–55

Kimble, L. K., Mandelco, L., Woese, C. R., and Madigan, M. T. (1995) *Heliobacterium modesticaldum*, sp. nov., a thermophilic heliobacterium of hot springs and volcanic soils. *Arch. Microbiol*. 163:259–267

Kimble-Long, L. K., and Madigan, M. T. (2001) Molecular evidence that the capacity for endosporulation is universal among phototrophic heliobacteria. *FEMS Microbiol. Lett*. 199:191–195

Klappenbach, J. A., Dunbar, J. M., and Schmidt, T. M. (2000) rRNA operon copy number reflects ecological strategies of bacteria. *Appl. Environ. Microbiol*. 66:1328–1333

Kleinherenbrink, F. A. M., Chiou, H. C., LoBrutto, R., and Blankenship, R. E. (1994) Spectroscopic evidence for the presence of an iron-sulfur center similar to FX of photosystem I in *Heliobacillus mobilis. Photosynth. Res.* 41:115–123

Kramer, D. M., Schoepp, B., Liebl, U., and Nitschke, W. (1997) Cyclic electron transfer in *Heliobacillus mobilis* involving a menaquinol-oxidizing cytochrome *bc* complex and an RCI-type reaction center. *Biochemistry.* 36:4203– 4211

Kumar, S., Tamura, K., and Nei, M. (2004) MEGA3: integrated software for molecular evolutionary genetics analysis and sequence alignment. *Brief Bioinform*. 5:150–163

Loveless, T. M., and Bishop, P. E. (1999) Identification of genes unique to Mo-independent nitrogenase systems in diverse diazotrophs. *Can. J. Microbiol*. 45:312–317.

Ludwig, M., Schulz-Friedrich, R., and Appel, J. (2006) Occurrence of hydrogenases in cyanobacteria and anoxygenic photosynthetic bacteria: implications for the phylogenetic origin of cyanobacterial and algal hydrogenases. *J. Mol. Evol*. 63:758–768

Madigan, M. T. (1995) Microbiology of nitrogen fixation by anoxygenic photosynthetic bacteria, p. 915–928. In Blankenship, R. E., Madigan, M. T., and Bauer, C. E. (*ed*.), Anoxygenic photosynthetic bacteria. Kluwer Academic Publishers, Dordrecht, The Netherlands

Madigan, M. T. (2001) Heliobacteriaceae, p. 625–630. In D. R. Boone, R. W. Castenholz, and G. M. Garrity (*ed*.), Bergey's manual of systematic bacteriology, 2nd ed., vol. 1. Springer-Verlag, New York, NY

Madigan, M. T. (2006) The family Heliobacteriaceae, p. 951–964. In Dworkin, M., Falkow, S., Rosenberg, E., Schleifer, K.-H., and Stackebrandt, E. (*ed*.), The prokaryotes, 4th ed. Springer, New York, NY

Madigan, M. T., and Ormerod, J. G. (1995) Taxonomy, physiology, and ecology of heliobacteria, p. 17–30. In R. E. Blankenship, M. T. Madigan, and C. E. Bauer (*ed*.), Anoxygenic photosynthetic bacteria. Kluwer Academic Publishers, Dordrecht, The Netherlands

Margolis, P. S., Driks, A., and Losick, R. (1993) Sporulation gene *spoIIB* from *Bacillus subtilis. J. Bacteriol*. 175:528–540

Merrick, M. J. (2004) Regulation of nitrogen fixation in free-living diazotrophs. p. 197–223. In Klipp, W., Masepohl, B., Gallon, J. R., and Newton, W. E. (*ed*.), Genetics and regulation of nitrogen fixation in free-living bacteria. Kluwer Academic Publishers, Dordrecht, The Netherlands

Miller, K. R., Jacob, J. S., Smith, U., Kolaczkowski, S., and Bowman, M. K. (1986) *Heliobacterium chlorum*: cell organization and structure. *Arch. Microbiol*. 146:111–114

Miyamoto, R., Iwaki, M., Mino, H., Harada, J., Itoh, S., and Oh-oka, H. (2006) ESR signal of the iron-sulfur center FX and its function in the homodimeric reaction center of *Heliobacterium modesticaldum. Biochemistry.* 45:6306– 6316

Naclerio, G., Baccigalupi, L., Zilhao, R., De Felice, M., and Ricca, E. (1996) *Bacillus subtilis* spore coat assembly requires *cotH* gene expression. *J. Bacteriol*. 178:4375–4380

Nonaka, H., Keresztes, G., Shinoda, Y., Ikenaga, Y., Abe, M., Naito, K., Inatomi, K. Furukawa, K., Inui, M., and Yukawa, H. (2006) Complete genome sequence of the dehalorespiring bacterium *Desulfitobacterium hafniense* Y51 and comparison with *Dehalococcoides ethenogenes* 195. *J. Bacteriol*. 188: 2262–2274

Oh-oka, H. (2007) Type 1 reaction center of photosynthetic heliobacteria. *Photochem. Photobiol*. 83:177–186

Oh-oka, H., Iwaki, M., and Itoh, S. (2002) Electron donation from membrane bound cytochrome c to the photosynthetic reaction center in whole cells and isolated membranes of *Heliobacterium gestii. Photosynth. Res.* 71:137–147

Ormerod, J. G., Kimble, L. K., Nesbakken, T., Torgersen, Y. A., Woese, C. R., and Madigan, M. T. (1996) *Heliophilum fasciatum* gen. nov. sp. nov. and *Heliobacterium gestii* sp. nov.: endospore-forming heliobacteria from rice field soils. *Arch. Microbiol*. 165:226–234

Pickett, M. W., Williamson, M. P., and Kelly, D. J. (1994) An enzyme and ^{13}C-NMR study of carbon metabolism in *heliobacteria. Photosynth. Res*. 41:75–88

Raymond, J., Siefert, J. L., Staples, C. R., and Blankenship, R. E. (2004) The natural history of nitrogen fixation. *Mol. Biol. Evol*. 21:541–554

Rey, F. E., Oda, Y., and Harwood, C. S. (2006) Regulation of uptake hydrogenase and effects of hydrogen utilization on gene expression in *Rhodopseudomonas palustris. J. Bacteriol.* 188:6143–6152

Seo, D., and Sakurai, H. (2002) Purification and characterization of ferredoxin- NAD(P)$^+$ reductase from the green sulfur bacterium *Chlorobium tepidum*. *Biochim. Biophys. Acta* 1597:123–132

Stackebrandt, E., Sproer, C., Rainey, F. A., Burghardt, J., Pauker, O., and Hippe, H. (1997) Phylogenetic analysis of the genus *Desulfotomaculum*: evidence for the misclassification of *Desulfotomaculum guttoideum* and description of *Desulfotomaculum orientis* as *Desulfosporosinus orientis* gen. nov., comb. nov. *Intl. J. Syst. Bacteriol*. 47:1134–1139

Stevenson, A. K., Kimble, L. K., Woese, C. R., and Madigan, M. T. (1997) Characterization of new phototrophic heliobacteria and their habitats. *Photosynth. Res*. 53:1–12

Stothard, P., and Wishart, D. S. (2005) Circular genome visualization and exploration using CGView. *Bioinformatics.* 21:537–539

Swingley, W. D., Sadekar, S., Mastrian, S. D., Matthies, H. J., Hao, J., Ramos, H., Acharya, C. R., Conrad, A. L., Taylor, H. L., Dejesa, L. C., Shah, M. K., O'Huallachain, M. E., Lince, M. T., Blankenship, R. E., Beatty, J. T., and Touchman, J. W. (2007) The complete genome sequence of *Roseobacter denitrificans* reveals a mixotrophic rather than photosynthetic metabolism. *J. Bacteriol*. 189:683–690

Takaichi, S., Inoue, K., Akaike, M. Kobayashi, M., Oh-oka, H., and Madigan, M. T. (1997) The major carotenoid in all known species of heliobacteria is the C_{30} carotenoid 4,4'-diaponeurosporene, not neurosporene. *Arch. Microbiol*. 168:277–281

Takaichi, S. (1999) Carotenoids and carotenogenesis in anoxygenic photosynthetic bacteria, p. 39–69. In H. A. Frank, R. J. Cogdell, A. Young, and G. Britton (*ed*.), The photochemistry of carotenoids: applications in biology. Kluwer Academic Publishers, Dordrecht, The Netherlands

Thauer, R. K. (2007) A fifth pathway of carbon fixation. *Science* 318:1732– 1733

Trost, J. T., and Blankenship, R. E. (1989) Isolation of a photoactive photosynthetic reaction center-core antenna complex from *Heliobacillus mobilis*. *Biochemistry.* 28:9898–9904

van de Meent, E. J., Kobayashi, M., Erkelens, C., van Veelen, P. A., Amesz, J., and Watanabe, T. (1991) Identification of 81-hydroxychlorophyll a as a functional reaction center pigment in heliobacteria. *Biochim. Biophys. Acta.* 1058:356–362

Webster, L. T. (1967) Studies of the acetyl coenzyme A synthetase reaction. *J. Biol. Chem.* 242:1232–1240

Xiong, J., Inoue, K., and Bauer, C. E. (1998) Tracking molecular evolution of photosynthesis by characterization of a major photosynthesis gene cluster from *Heliobacillus mobilis. Proc. Natl. Acad. Sci. USA* 95:14851–14856.

Table 1. Features of the *H. modesticaldum* strain Ice[1]T (=ATCC 51547[T]) genome.

Characteristic	Value
Chromosome size (bp)	3,075,407
G+C content (%)	56.0
% Genome coding	87
Total no. of ORFs	3,138
Avg ORF length (bp)	882
% ATG initiation codons	62.1
% GTG initiation codons	19.1
% TTG initiation codons	18.8
No. of rRNAs (no. of genes/no. of operons)	24/8
No. of tRNAs	104
No. of structural RNAs	1
No. of tmRNA	1
% Conserved hypothetical proteins	11.1
% Hypothetical proteins	23.8
No. of transposases	70
No. of pseudogenes	8

Table 2. Characterization of selected gene categories of the *H. modesticaldum* strain Ice[1]T (=ATCC 51547T) genome.

Category	No. of genes	% of genome content
Energy and central intermediary metabolism	389	13.0
Amino acid biosynthesis	113	3.8
Transport	157	5.2
Cofactor and prosthetic group biosynthesis	152	5.1
DNA metabolism	135	4.5
Transcription	44	1.5
Protein synthesis, modification, and degradation	247	8.2
Regulatory functions and signal transduction	177	5.9
Cellular processes (cell division, motility, sporulation, etc.)	273	9.1
Fatty acid and phospholipid metabolism	45	1.5
Phage/insertion elements	123	4.1
Surface features	145	4.8

Figure 1. Circular genome map of the 3.1-Mb *H. modesticaldum* chromosome. The rings indicate (from outside to inside) all the genes and insertion elements, color coded by functional category (rings 1 and 2), the deviation from the average G+C content (ring 3), and the GC skew (ring 4). The approximate location of the origin of replication is at the beginning of the *dnaA* gene. The colors indicate the following: turquoise, small-molecule biosynthesis; yellow, central or intermediary metabolism; orange, energy metabolism; red, signal transduction; light blue, DNA metabolism; blue, transcription; purple, protein synthesis/fate; dark green, surface-associated features; gray, miscellaneous features; pink, phage and insertion elements; light green, unknown function; dark gray, conserved hypothetical proteins; black, hypothetical proteins; brown, pseudogenes.

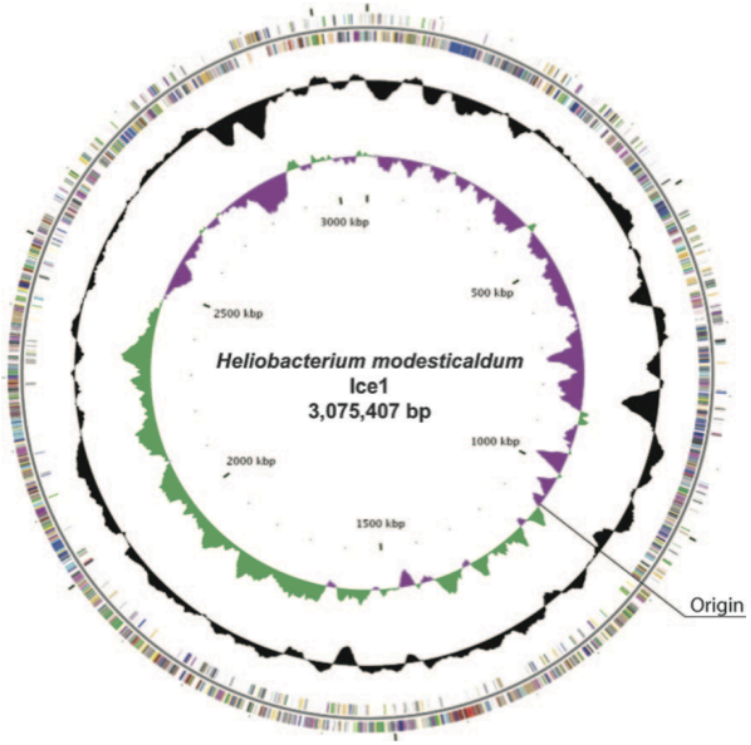
3000 kbp
500 kbp
2500 kbp
Heliobacterium modesticaldum
Ice1
3,075,407 bp
1000 kbp
2000 kbp
1500 kbp
Origin

Figure 2. Putative pathway of carbon metabolism in *H. modesticaldum* (adapted from Pickett *et al.,* 1994). A partial reverse citric acid cycle with CO_2 incorporation via PEP carboxykinase is shown. The enzymes involved in the reduction of acetate to pyruvate putatively function in an oxidative direction during chemotrophic (dark) growth on pyruvate. The oxidation of pyruvate to acetyl-CoA is likely accompanied by hydrogen evolution via an [FeFe] hydrogenase. The numbers indicate the following enzymes: 1, pyruvate:ferredoxin oxidoreductase; 2, pyruvate-phosphate dikinase; 3, PEP carboxykinase; 4, oxaloacetate decarboxylase; 5, malate dehydrogenase; 6, fumarase; 7, fumarate reductase; 8, succinyl-CoA synthetase; 9, 2-oxoglutarate:ferredoxin oxidoreductase; 10, NADP-dependent isocitrate dehydrogenase; 11, aconitate hydratase; 12, AMP-forming acetyl-CoA synthetase; 13, lactate dehydrogenase.

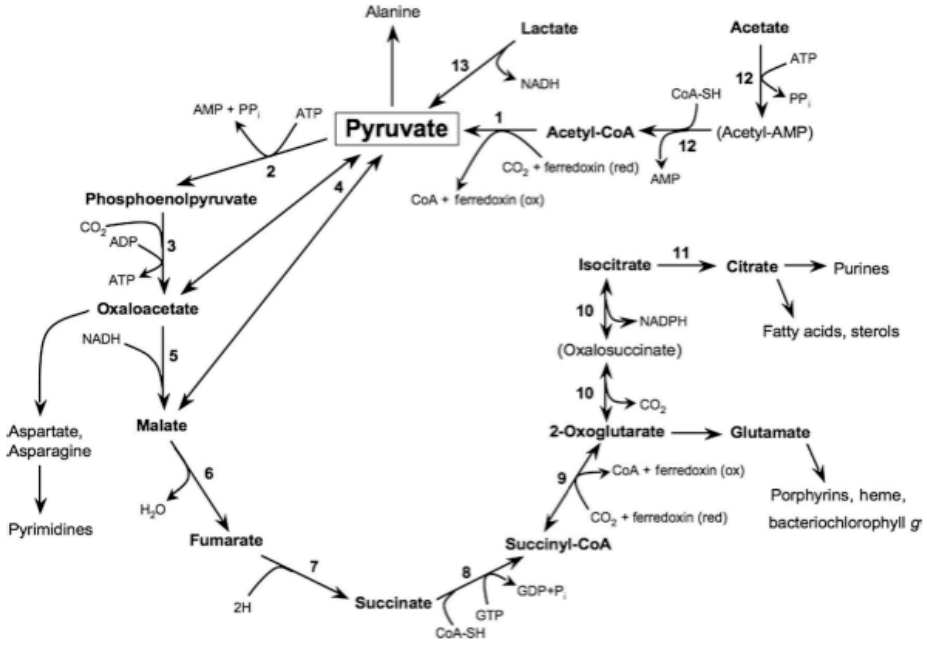
Alanine
Lactate
Acetate
13
NADH
12
ATP
PPi
CoA-SH
AMP + PPi
ATP
Pyruvate
1
Acetyl-CoA
(Acetyl-AMP)
12
2
CO2 + ferredoxin (red)
AMP
CoA + ferredoxin (ox)
Phosphoenolpyruvate
4
CO2
ADP
3
ATP
Oxaloacetate
Isocitrate
11
Citrate
Purines
10
NADPH
Fatty acids, sterols
(Oxalosuccinate)
NADH
5
10
CO2
Aspartate,
Asparagine
Malate
2-Oxoglutarate
Glutamate
9
CoA + ferredoxin (ox)
6
H2O
CO2 + ferredoxin (red)
Porphyrins, heme,
bacteriochlorophyll g
Pyrimidines
Fumarate
Succinyl-CoA
7
8
2H
Succinate
GDP+Pi
GTP
CoA-SH

Figure 3. Schematic representation of hydrogenase and photosynthesis gene clusters in *H. modesticaldum*. Arrows represent individual genes and indicate the direction of transcription. (A) Putative [FeFe] hydrogenase genes in *H. modesticaldum* and the close phylogenetic relative *P. thermopropionicum* SI. As in *Heliobacillus mobilis*, *nuoE* and *nuoF* are fused in *H. modesticaldum*, suggesting that this feature may be universal in heliobacteria. Colors indicate the following: gold, NADH dehydrogenase subunits; orange, [FeFe] hydrogenase structural genes. (B) Uptake [NiFe] hydrogenase genes in related *Firmicutes*. The genes are located in a single operon in *H. modesticaldum*, whereas they are dispersed in different regions of the *D. hafniense* Y51 chromosome. Colors indicate the following: blue, [NiFe] hydrogenase structural genes; purple, hydrogenase expression/formation; red, hydrogenase assembly/maturation. (C) Photosynthesis gene clusters from *H. modesticaldum* and the purple bacterium *R. capsulatus*. Shared genes are outlined with bold lines. Lines indicate gene synteny, as follows: black lines, single gene rearrangements; red lines, inverted genes; blue lines, inverted genes with a gene insertion. Dashed boxes indicate *R. capsulatus* photosynthesis genes absent from *H. modesticaldum*. The colors of the arrows indicate the following: green, Bchl biosynthesis (*bch*); orange, carotenoid biosynthesis (*crt*); pink, proteobacterial reaction centers (*puf*) and light harvesting complexes (*puh*); olive, heliobacterial reaction center (*psh*); teal, regulatory proteins; light green, electron transport (*pet*); red, cofactor biosynthesis; purple, cell division and sporulation; light blue, nitrogen fixation; gray, transcription; light gray, other nonphotosynthetic genes; white, uncharacterized genes.

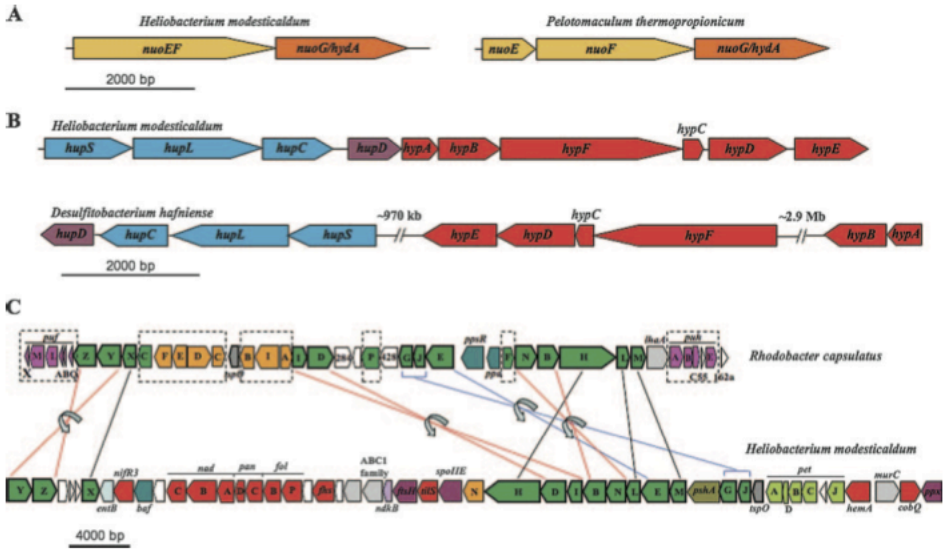
A
Heliobacterium modesticaldum
nuoEF
nuoG/hydA
Pelotomaculum thermopropionicum
nuoE
nuoF
nuoG/hydA
2000 bp
B
Heliobacterium modesticaldum
hupS
hupL
hupC
hupD
hypA
hypB
hypF
hypC
hypD
hypE
Desulfitobacterium hafniense
hupD
hupC
hupL
hupS
~970 kb
hypE
hypD
hypC
hypF
~2.9 Mb
hypB
hypA
2000 bp
C
Rhodobacter capsulatus
Heliobacterium modesticaldum
4000 bp

Figure 4. Phylogenetic tree showing the relationship of concatenated *bchXYZ*, *bchLNB*, and *nifHDK* genes from *H. modesticaldum* to those of other organisms containing these genes. Although not present in *H. modesticaldum*, alternative nitrogenase genes, *anfHDK* and *vnfHDK*, are also included to balance the tree. Organisms containing more than one set of genes used in the comparison appear multiple times in the tree. The following organisms were included in the analysis: *Anabaena siamensis* strain TISTR8012, *Azospirillum brasilense*, *Azotobacter vinelandii*, *Bradyrhizobium* sp. strain BTAi1, *Bradyrhizobium* sp. strain ORS278, *Chlorobaculum tepidum*, *Chloroflexus aurantiacus*, *Clostridium acetobutylicum*, *Clostridium pasteurianum*, *Clostridium kluyveri*, *Desulfitobacterium hafniense* strain Y51, *Geobacter sulfurreducens*, *Heliobacterium modesticaldum*, *Jannaschia* sp. strain CCS1, *Klebsiella pneumoniae*, *Methanothermobacter thermoautotrophicus*, *Methanococcus maripaludis*, *Methanosarcina acetivorans* strain C2A, *Nostoc* sp. strain PCC7120, *Prosthecochloris aestuarii*, *Rhodobacter capsulatus*, *Rhodopseudomonas palustris*, *Roseiflexus castenholzii*, *Roseobacter denitrificans*, *Synechococcus elongatus* strain PCC6301, and *Synechocystis* sp. strain PCC6803.

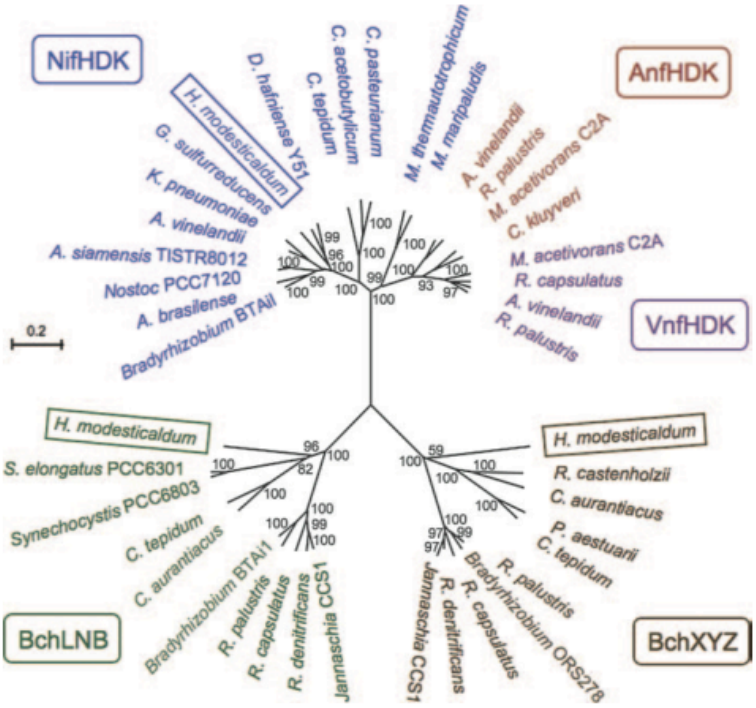
NifHDK
AnfHDK
VnfHDK
BchLNB
BchXYZ
H. modesticaldum
D. hafniense Y51
C. tepidum
C. acetobutylicum
C. pasteurianum
M. thermautotrophicum
M. maripaludis
G. sulfurreducens
K. pneumoniae
A. vinelandii
A. siamensis TISTR8012
Nostoc PCC7120
A. brasilense
Bradyrhizobium BTAii
A. vinelandii
R. palustris
M. acetivorans C2A
C. kluyveri
M. acetivorans C2A
R. capsulatus
A. vinelandii
R. palustris
0.2
H. modesticaldum
S. elongatus PCC6301
Synechocystis PCC6803
C. tepidum
C. aurantiacus
Bradyrhizobium BTAii
R. palustris
R. capsulatus
R. denitrificans
Jannaschia CCS1
H. modesticaldum
R. castenholzii
C. aurantiacus
P. aestuarii
C. tepidum
R. palustris
Bradyrhizobium ORS278
R. capsulatus
R. denitrificans
Jannaschia CCS1

Figure 5. Proposed pathway of later steps in Bchl *g* biosynthesis in *H. modesticaldum*. Divinyl protochlorophyllide *a* is reduced to 8-vinyl chlorophyllide *a* by the activity of the *bchLNB* gene products. This is followed by the reduction of the C-7—C-8 double bond via the *bchXYZ* gene products, which yields C-8 vinyl bacteriochlorophyllide *a*. Bacteriochlorophyllide *g* is produced by the isomerization of the 8^1-vinyl group to an ethylidene group. Bchl synthetase (BchG) then catalyzes the addition of a farnesyl group, which yields the completed Bchl *g*.

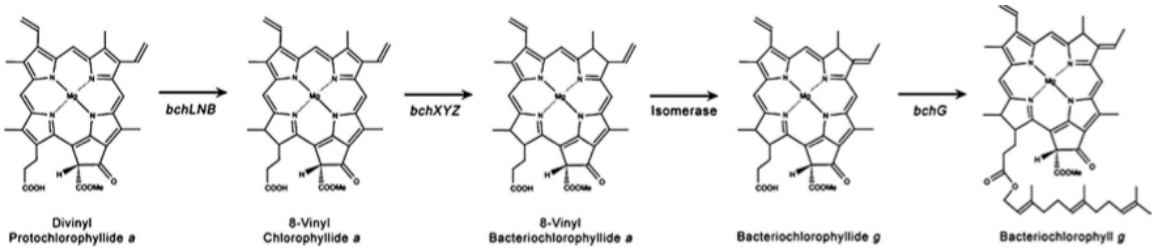
bchLNB
bchXYZ
Isomerase
bchG
Divinyl
Protochlorophyllide a
8-Vinyl
Chlorophyllide a
8-Vinyl
Bacteriochlorophyllide a
Bacteriochlorophyllide g
Bacteriochlorophyll g

Figure 6. Diagram showing a putative pathway of electron transfer based on genetic components present in *H. modesticaldum*. Cyclic electron transfer has not been confirmed in heliobacteria. In addition, the reduction of NAD^+ by cytoplasmic ferredoxin has not been confirmed, as a gene encoding FNR was not identified in the genome. Despite this, genes encoding all 14 subunits of NADH:quinone oxidoreductase (*nuoA* to *nuoN*) were putatively identified.

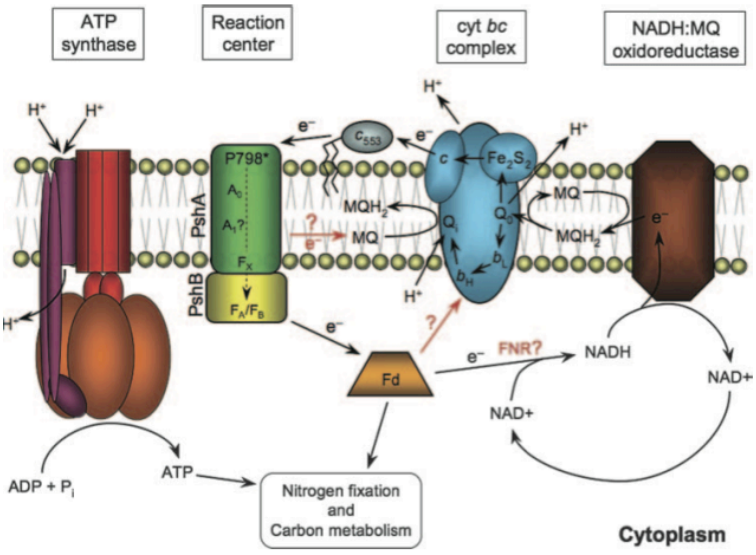
ATP synthase
Reaction center
cyt bc complex
NADH:MQ oxidoreductase
H+
H+
e−
c_{553}
P798*
A_0
A_1?
F_X
PshA
PshB
F_A/F_B
MQ
MQH_2
?
c
Fe_2S_2
Q_i
Q_o
b_L
b_H
e−
Fd
FNR?
NADH
NAD+
ADP + P_i
ATP
Nitrogen fixation and Carbon metabolism
Cytoplasm

Appendix Chapter 5

Niche adaptation and genome expansion in the chlorophyll *d*-producing cyanobacterium *Acaryochloris marina*

Summary

Acaryochloris marina is a unique cyanobacterium that is able to produce chlorophyll d as its primary photosynthetic pigment and thus efficiently use far-red light for photosynthesis. *Acaryochloris* species have been isolated from marine environments in association with other oxygenic phototrophs, which may have driven the niche-filling introduction of chlorophyll *d*. To investigate these unique adaptations, we have sequenced the complete genome of *A. marina*. The DNA content of *A. marina* is composed of 8.3 million base pairs, which is among the largest bacterial genomes sequenced thus far. This large array of genomic data is distributed into nine single-copy plasmids that code for >25% of the putative ORFs. Heavy duplication of genes related to DNA repair and recombination (primarily *recA*) and transposable elements could account for genetic mobility and genome expansion. We discuss points of interest for the biosynthesis of the unusual pigments chlorophyll *d* and α-carotene and genes responsible for previously studied phycobilin aggregates. Our analysis also reveals that *A. marina* carries a unique complement of genes for these phycobiliproteins in relation to those coding for antenna proteins related to those in *Prochlorococcus* species. The global replacement of major photosynthetic pigments appears to have incurred only minimal specializations in reaction center proteins to accommodate these alternate pigments. These features clearly show that the genus *Acaryochloris* is a fitting candidate for understanding genome expansion, gene acquisition, ecological adaptation, and photosystem modification in the cyanobacteria.

•

- **Introduction**

  - The cyanobacteria are oxygenic photosynthetic prokaryotes that span a tremendous variety of light-available environments, ranging from hot springs to ice cores, tropical forests to polar tundra, and desert crusts to the open ocean. They play important roles for carbon and nitrogen cycles in each of these environments where they modify their morphology, metabolism, and light-harvesting systems for survival in their respective niches. To date, genomes of 55 cyanobacterial strains in 21 genera have been completed or are under construction (National Center for Biotechnology Information). These cyanobacterial genomes are diverse in size, ranging from 1.66 to 9.1 Mbp. The differences may arise from the expansion or reduction of genome size as the result of adaptation to the light or nutrient conditions in their particular niches. For example, the 1.66-Mbp genome of *Prochlorococcus marinus* strain CCMP1986 (MED4) seems to contain a minimal set of genes for survival in the stable oligotrophic open ocean (Difresne *et al.,* 2003). In contrast, the 7.21-Mbp genome of *Nostoc* sp. PCC7120 (also known as *Anabaena*) is characteristic of the genetic adapt ability of filamentous cyanobacteria that thrive under both free-living and symbiotic conditions where they fix nitrogen; form a number of distinct cell morphologies; and grow photoautotrophically, photoheterotrophically, and chemoheterotrophically (Kaneko *et al.,* 2001).

The cyanobacterium *Acaryochloris marina* was found to be the only oxygenic photoautotroph that uses the pigment chlorophyll (Chl) *d* as the predominant photosynthetic pigment, with only trace amounts of Chl *a* (Miyashita *et al.,* 1996; Miyashita *et al.,* 1997; Miyashita *et al.,* 2003). Although *A. marina* produces phycobiliproteins (PBPs), they do not form phycobilisomes (PBS), a typical structure for cyanobacterial peripheral antenna, but instead accumulate rod-shaped PBP complexes (Marquardt *et al.,* 1997). Previous work has shown that chlorophylls in both reaction centers, photosystem (PS)I and PSII, have been replaced by Chl *d*, which absorbs light with a wavelength up to 30 nm red-shifted from Chl *a* (Tomo *et al,* 2007; Hu *et al.,* 1998). Although it was anticipated that the Chl *d*-PSII *in A. marina* would harvest insufficient energy to cleave water molecules during oxygen evolution, Shevela *et al* (Shevela *et al.,* 2006) showed that the redox potential of the *A. marina* PSII-special pair was within 0.1 eV of that in other cyanobacteria and would thus not present an energetic barrier to water oxidation.

Acaryochloris ecotypes have been found in marine environments in close association with other oxygenic phototrophs such as *Prochloron* (associate with colonial ascidians) (Miyashita *et al.,* 2003; Miyashita *et al.,* 1996; Kuhl *et al.,* 2005), eukaryotic macroalgae (Ohkubo *et al.,* 2006;Mirakami *et al.,* 2004), and in a microbial mat in the Salton Sea, a saline and highly eutrophic California lake (Miller *et al.,* 2005). In each environment, the photosynthetically available radiation is likely completely used by organisms that absorb light using Chl *a* and/or Chl *b*. By using Chl *d*, *A. marina* thrives in these environments with low visible light intensity but high near-infrared intensity where no other photosynthetic organisms absorb strongly. Recent metagenomic analyses indicate that *Acaryochloris* is also distributed as a member of epilithic and/or endolithic communities in Antarctic rocks and in limestone from a Mayan archeological site in Mexico (de los Rios *et al.,* 2007; McNamara *et al.,* 2006; Smith *et al.,* 2006). These results clearly show the global population of *Acaryochloris* species has a range of lifestyles from free-living to symbiotic and marine to terrestrial.

We report here the complete genome sequence of *A. marina* str. MBIC11017, the first *A. marina* strain isolated from the *Prochloron*-dominated colonial ascidian *Lissoclinum patella* off the tropical coast of the Palau islands (Miyashita *et al.,* 1996, Miyashita *et al,* 2003). This represents a previously uncharacterized genome sequence for a Chl *d*-containing organism.

Materials and Methods

DNA Preparation.

A. marina was grown as described (Swingley *et al.,* 2005) on 1.5% agar plates. Genomic DNA was isolated by using the U.S. Department of Energy Joint Genome Initiative "DNA Isolation Bacterial CTAB Protocol" (http://my.jgi.doe.gov/general/index.html).

Genome Sequencing.

The *A. marina* genome was sequenced by using a pyrosequencing approach on a Roche-454 GS20 instrument at 454 Life Sciences. Approximately 24-fold sequence coverage was achieved from 1,860,686 short sequence reads. A total of 775 contigs were assembled from these reads representing 7,570,764 nonredundant bases. This assembly was supplemented with reads generated by a traditional Sanger sequencing strategy (Swingley *et al.,* 2007). Briefly, genomic DNA was fragmented by kinetic shearing, and three shotgun libraries were generated: small and medium insert libraries in pOTWI3 (using size fractions of 2–3 and 6 – 8 kb, respectively) and a large insert fosmid library in pEpiFOS-5 (insert sizes ranging from 28 to 47 kb), which was used as a scaffold. The relative amount of sequence coverage obtained from the small, medium, and large insert libraries was 4.4X, 0.6X, and 0.6X, respectively. A total of 56,419 end sequences derived from these libraries were generated by using dye-terminator chemistry on Applied Biosystems 3730xl automated sequencers. The combined 454 and Sanger sequence datasets were assembled with the program Arachne and finished as described (Swingley *et al.,* 2007).

Phylogenetic Analysis.

Homology matching was performed by using the Basic Local Alignment Search Tool (BLAST) (Altschul *et al*., 1990), and neighbor-joining (NJ) trees were constructed by using MEGA 4.0 (Tamura *et al.,* 2007). Bootstrapped NJ trees (1,000x) were constructed by using a JTT substitution model. To generate protein families, Markov clustering (Enright *et al., 2002*) was performed iteratively on a matrix generated from BLAST e values with an inflation parameter of 2.8.

Annotation.

Initial automated annotation of the genome was performed with the TIGR/JCVI Annotation Engine (www.tigr.org/AnnotationEngine), where it was processed by TIGR's prokaryotic annotation pipeline using gene finding with Glimmer, SignalP predictions, Blast-extend-repraze (BER), HMM, and TMHMM searches. Automatic annotations were created by AutoAnnotate. Manatee(manatee.sourceforge.net) was used to manually review and confirm the annotation of all genes. Pseudogenes contained one or more mutations that would ablate expression; each mutation was confirmed by using the original sequencing data. The circular genome map was created by using the program CGView (Stothard and Wishart, 2005).

Results and Discussion

Genome Properties.

The genome of *A. marina* was sequenced to completion by a combined pyrosequencing/Sanger approach (see *Materials and Methods*). It consists of a single circular chromosome and nine distinct plasmids (Table 1 and Fig. 1). The genome has an average G+C content of 47.0% and a coding capacity of 84.1%. The largest category of ORFs (35%) are those that code for hypothetical proteins with little homology to any proteins or motifs. An additional 17% of ORFs code for hypothetical proteins with some conservation among other species. Although this large number of proteins without an assigned function is higher than most sequenced organisms, it is similar to that found in *Nostoc* sp. PCC7120 (Kaneko *et al.,* 2001).

Although sequence comparisons indicate that none of the plasmids in *A. marina* arise from very recent duplication events, several of the plasmids do share significant regions of homologous sequence. The largest homology is that between pREB7 and pREB8, with 29% of pREB7 (or 38% of pREB8) nucleotides sharing 75% identity. The matching regions range from <100 to >8,500 bp with an average of 1,800 bp. Several plasmids also share a few very large homologous regions (>10 kbp) but do not share a significant global sequence identity. The internal homology between all *A. marina* plasmids exceeds that seen between its plasmids and those from other bacteria, suggesting that no recent lateral transfer events are responsible for any of the plasmids.

Although all tRNA, rRNA, and ribosomal proteins are encoded by the main chromosome, several of the plasmids code for key metabolic proteins [supporting information (SI) Table 2]. Notable among these are: uridine kinase and aliphatic amidase (pREB2), all phycocyanin (PC)-related genes (pREB3), *hoxEF-HUWY*/*hypABCDEF* genes for a full complement of bidirectional

hydrogenase subunits (pREB4), cobalamin-independent *metE* methionine synthase and *nrdAB* ribonucleotide-diphosphate reductase (pREB6) that clearly arose from lateral transfer, and a full second set of genes for an alternate ATP synthase (discussed below). A summary of not able plasmid-encoded proteins can be found in SI Table 2.

The *A. marina* genome contains a large number of genes for the adaptive regulation of biological activities. Over 170 genes were identified as members of the two-component regulatory system, consisting of sensory kinases and response regulators. Although this number is higher than that in most cyanobacteria, it is still lower than the *Nostocales* (Kaneko *et al.,* 2001). *A. marina* also contains a number of genes encoding members of the LuxR, LysR, AraC, and TetR transcription factor families. The large number of these regulatory mechanisms indicates that the genome expansion in *A. marina* is not superfluous but could play a very important role in its adaptation to specialized environmental niches.

Genome Expansion.

The *A. marina* genome is considerably larger than that in most other single-celled cyanobacteria [see *Synechocystis* sp. PCC6803 (Kaneko *et al.,* 1996)], especially that in other sequenced marine strains [see *Prochlorococcus* (Dufresne *et al.,* 2003; Rocap *et al.,* 2003) and marine *Synechococcus* strains (Palenik *et al.,* 2003; Palenik *et al.,* 2006)]. The high percent age of ORFs with no homologous matches (compared with other sequenced cyanobacteria) suggests that a large part of *A. marina* codes for either novel proteins or pseudogenes. Large genomes in other bacteria do not tend to accumulate so many hypothetical ORFs (Konstantinidis and Tiedje, 2004). A large number of putative transposases (~350) could account for much of this genetic mobility. Transposase coding regions were in near proximity (1 kb) to predicted transposable

regions for <20% of the genes, significantly lower than the~70% found in *Nostoc* sp. PCC7120 (Kaneko *et al.,* 2001). This is partly because of the vast disparity in transposable elements in the two similarly-sized genomes, with nearly 1,300 detected in *Nostoc* and only 500 in *A. marina*. Surprisingly, a large number of transposases and integrases in *A. marina* cluster together in regions with no detect able mobile sequences. Further investigation into the mechanisms of genetic mobility in *A. marina* and other cyanobacteria may clarify this apparent disparity.

Despite the smaller number of transposable elements in *A. marina*, the genome contains a significant level of duplication. A pair-wise comparison of the *A. marina* chromosome nucleotide sequence (vs. itself) shows 18.7% of the sequence (not including the original, duplicated sequence) has a homology of greater than $E=1x10^{-10}$ to another location on the chromosome. This is significantly higher than the 11.2% and 5.8% duplication in *Synechocystis* PCC6803 and *Nostoc* sp. PCC7120, respectively. *A. marina* actually has far fewer duplicated regions than *Nostoc*, but its contiguous matching regions are much longer, averaging 743 vs. 134 bp. Markov clustering of protein families reveals a similar trend, where 11.6% of the protein families in *A. marina* contain duplicated copies, accounting for 46.7% of all proteins, considerably higher than *Synechocystis* and *Nostoc* at 8.4% (28.1%) and 9.8% (36.1%), respectively.

Another possible influence on the expansion is the presence of duplicate copies of *recA*, an import ant multifunctional DNA repair and recombination enzyme found in nearly every organism (reviewed in Smith, 2004). There are an astounding seven distinct copies of this gene (*recA*) found in the *A. marina* genome, far greater than the previously published record of two for *Myxococcus xanthus* (Norioka *et al.,* 1995). Four of the *recA* genes are located on four separate plasmids (pREB1, -2, -4, and -5), and the other three are on the main chromosome. Multiple copies of *umuD* (4x) and *umuC* (3x), two sets of which are plasmid-encoded, and two

putative proteins with a lambda-phage cI motif are also likely correlated with the extra *recA* (Smith, 2004; Pham *et al.,* 2001). The presence of multiples copies of *recA* and related enzymes could account for gene duplication and/or integration of foreign genes that would lead to genome expansion.

Based on the comparative analysis of many genomes, Konstantinidis et al . (Konstantinidis *et al.,* 2004) hypothesized that species with large genomes may dominate noncompetitive environments where resources are scarce but diverse in nature. This hypothesis appropriately fits the nature of *Acaryochloris* species. By using far-red light that is not absorbed by other aerobic photoautotrophs, *Acaryochloris* species fill a noncompetitive niche where they are apparently free to specialize their metabolic library.

ATP Synthase.

One interesting case of the idiosyncratic plasmid gene library in *A. marina* is the inclusion of a second full set of ATP synthase genes on plasmid pREB4 (AM1 D0157-67). These genes are arranged into a unique operon and the individual proteins do not clearly fit into any of the described families (SI Fig. 5) (Cross and Muller, 2004). This unusual operon is conserved with full synteny in a remarkable array of organisms, including cyanobacteria, archaea, planctomycetes, chlorobi, and proteobacteria (SI Fig. 5). This alternate AT P synthase was briefly noted in the genome publication for *Syntrophus aciditrophicus* (McInerney *et al.,* 2007), where it was predicted to be involved in Na^+-transport. However, it is clear that this class of ATP synthase does not share any greater degree of similarity to Na^+-transport systems in *Ilyobacter tartaricus* and others (Meier *et al.,* 2005) than to other ATP synthases. The primary

sequences of these proteins are so divergent from other ATP synthases that a thorough biochemical study is needed to confidently propose a functional role.

Chlorophyll Biosynthesis.

The most significant feature of *A. marina* is its ability to produce Chl *d* as a major photosynthetic pigment, which accounts for up to 99% of all cellular chlorophyll (Gloag *et al.,* 2007; Swingley *et al.,* 2005). Molecular and biochemical work has yet to identify any candidate ‘‘Chl d synthase’’ genes. *A. marina* contains close homologs to all known chlorophyll *a* biosynthesis genes. The two proteins responsible for the biosynthesis of Chl *a* from protoporphyrin IX, magnesium-protoporphyrin IX monomethyl ester oxidative cyclase (AcsF) and chlorophyll synthase (ChlG) (Beale, 1999), are highly homologous to those in other cyanobacteria, including a common conserved duplication of *acsF*. This indicates that Chl *d* is likely synthesized from chlorophyllide *a* or Chl *a*.

Both Chl *b* and Chl *d* contain a formyl side-chain, although at different positions (C-7 and C-3) in the chlorophyll macrocycle. This suggests that a putative Chl *d* synthase could be a member of the super family encompassing a wide range of aromatic ring-degradation proteins including the plant and *Prochlorococcus* enzymes responsible for the synthesis of Chl *b* from chlorophyllide *a*, chlorophyllide *a* oxygenase (CAO) (Fig. 2) (Tanaka *et al.,* 1998). Five putative proteins containing a CAO-type Rieske-FeS motif are encoded by *A. marina*. Most of the candidate genes in *A. marina* fall into orthologous clusters with other hypothetical cyanobacterial proteins (Fig. 2). Only one protein, AM1 5665, does not have any significant homologs and diverges early with consistently long branch lengths.

Anaerobic bacteria use a method of oxygenation using enzymes that proceed via radical chemistry and use *S*-adenosylmethionine (SAM) to transfer oxygen from water rather than O2 as in aerobic species (Layer *et al.,* 2004). Such enzymes could provide another means for Chl *d* biosynthesis. *A. marina* codes for 12 proteins with putative radical SAM motifs, far more than expected from an oxygen-producing cyanobacterium. Of these 12, two (AM1 5023 and AM1 5798) share very little homology with other sequenced cyanobacteria.

- The Chl *d* biosynthesis pathway may not be as simple as expected. Unlike the formyl side chain of Chl *b* at C-7 in the chlorin macrocycle, which is derived from a methyl group, the formyl group of Chl *d* at C-3 is derived from a vinyl group. This loss of a carbon is chemically difficult and could require multiple enzymes for a two-step oxidative cleavage of the double bond. Although it is possible that the means of Chl *d* synthesis could be completely unrelated to anything familiar in chlorophyll chemistry, it is far more likely that an enzyme has been recruited from related pathways. Major sources of interest are the large pool of proteins orthologous to ‘‘Chl degradation’’ and aromatic ring breakage, which likely provided the origin for CAO, and other poorly understood enzymes, such as the phylogenetically aberrant divinyl chlorophyllide reductase (Nagata *et al.,* 2005), which shows an unusual phylogenetic topology in A. marina (AM1 2394), where it branches near the alphaproteobacteria (SI Fig. 6). This enzyme is of special interest, because *A. marina* appears to contain a (phylogenetically) normal copy of the newly discovered cyanobacterial-type divinyl reductase (Ayumi Tanaka, personal communication).

Carotenoid Biosynthesis.

Most cyanobacteria and higher plants contain β-carotene as a primary carotenoid found in both PSI and PSII (Fig. 3). In the case of A. marina, α-carotene was detected instead of β-carotene, and zeaxanthin, an oxidative product of β-carotene, was identified as a major carotenoid (Miyashita *et al.,* 1997; Miller *et al.,* 2005). A similar carotenoid composition has been reported only in *Prochlorococcus* species that contain atypical, divinyl-Chls, and α-carotene , β-carotene, and other carotenoids (Stickforth *et al.,* 2003). Surprisingly, only α-

carotene was detected in the purified PSI and PSII complexes from *A. marina* (Tomo *et al.,* 2007; Hu *et al.,* 1998).

The absence of β-carotene challenges the established understanding of carotenoid biosynthesis and the role of reaction center carotenoids. Higher plants also synthesize both α- and β-carotene; however, α-carotene is used primarily as a precursor of lutein, and only β-carotene is found in reaction centers. Future biochemical work may indicate whether a preferential interaction between Chl *d* and α-carotene (rather than β-carotene) could account for its exclusivity in the reaction center.

The chromosome of *A. marina* codes for 11 proteins predicted to be associated with the biosynthesis of α-carotene and zeaxanthin (SI Table 3). These genes are distributed throughout the chromosome, with no clear operons and no related genes found in plasmid DNA. There are two copies each of *crtH*, *cruA*, and *crtQ*; however, phylogenetic analyses indicate that these genes are more closely related to those in filamentous cyanobacteria than the other α-carotene-containing *Prochlorococcus* species. *A. marina* is the only cyanobacterium found to contain both *cruA* and *cruP*, responsible for γ- and β-carotene synthesis, in addition to lycopene cyclase (*crtL*) (Maresca *et al.,* 2007; Cunningham *et al.,* 1994). One class of cyclase, CrtL-e for ε-cyclase, was identified as the enzyme responsible for α-carotene synthesis in *Prochlorococcus* (Stickforth *et al.,* 2003). However, the *A. marina* CrtL groups closer to another CrtL found in marine *Synechococcus* and *Prochlorococcus* (Stickforth *et al.,* 2003; Maresca *et al.,* 2007) that acts as both a β- and ε-cyclase. In *A. marina*, this enzyme may catalyze the formation of both α- and β-carotene synthesis (Fig. 3). There is no clear differentiation that would explain the near-complete conversion of β-carotene to zeaxanthin by β-carotene hydroxylase (CrtR), the enzyme responsible for zeaxanthin biosynthesis. We suggest a putative carotene biosynthesis pathway

(Fig. 3) that accommodates the distinct complement of the carotenoid bio-synthesis enzymes and their end products in *A. marina*.

Light-Harvesting Systems.

Two major accessory light-harvesting and protection systems exist in cyanobacteria, PBPs (reviewed in Adir, 2005), and accessory chlorophyll-binding proteins (CBPs) (Chen *et al.,* 2008; Chen and Bibby, 2005; Bibby *et al.,* 2003). Like other ‘‘alternative Chl’’ cyanobacteria, *A. marina* does not construct the supramolecular PBP assemblies, the PBSs. However, the presence of both PBP aggregates and CBPs has been reported in *A. marina* (Marquardt *et al.,* 1997; Chen *et al.,* 2001).

Genes for PBP biosynthesis and assembly in the *A. marina* genome are summarized in SI Table 4. There are multiple copies of genes encoding PC core and linker proteins (*cpcA-cpcG*) but no genes for phycoerythrin. Unexpectedly, we found that the only PBP-related genes found on the main chromosome were three copies of *apcA* and one copy of *apcB*. All other PBP-related genes were found on plasmid pREB3 in a number of large gene clusters. No *apcE* gene, which encodes a core-membrane linker peptide, was identified. Phylogenetic analysis suggests that the three copies of *cpcG* genes in *A. marina* belong to the *CpcG2* group (data not shown), consistent with the fact that *A. marina* possesses a minor component of allophycocyanin (APC) cores (Marquardt *et al.,* 1997).

The detected rod-shaped PBP structures, composed of four ring-shaped subunits, are a likely result of linked PC and/or APC subunits without the core-membrane linker required to construct typical PBS assemblies. The presence of a gene coding for a single rod-core linker (CpcG), which connects a central core to the radiating rods in a PBS, could form the assemblage

of PC and APC subunits. It is unlikely that the presence of only α and β subunits of APC is sufficient to form a core structure similar to that in other cyanobacteria. The biochemical identification of all proteins present in PBP assemblies will serve to clarify the role of these peptides in the unique *A. marina* light-harvesting antenna.

Although most cyanobacteria contain IsiA, a CBP that is produced during iron-deficiency stress, most *Prochlorococcus* species have a number of other CBPs (Pcb) for additional light harvesting. Although the cloning and characterization of two CBP-like genes was previously reported in *A. marina* (Chen *et al.,* 2005), the genome revealed an additional eight CBP genes (for a total of 10) and one *isiA* that will require further biochemical study.

In all cyanobacterial systems studied thus far, the expression of PBP and CBP systems is mutually exclusive. *Prochlorococcus*, which lack or have only very primitive PBPs, constitutively express their CBP systems (Bibby *et al.,* 2003). Conversely, the expression of the CBPIII (*IsiA*) is activated only under iron-stress conditions during which PBP expression is strictly repressed (Michel and Pistorius, 2004). The exclusive expression of these systems has evolved into a chasm separating the relative gene content in these species (Fig. 4). Low-light *Prochlorococcus* strains encode a large number of CBPs (Garczarek *et al.,* 2000) and have lost nearly all genes responsible for PBPs. The evolutionarily and environmentally related marine *Synechococcus* strains encode a large number of PBP-related proteins with very few CBP genes. Only *A. marina* bucks this trend with its large number of both types of genes that show evidence of concurrent expression (Fig. 4) (Marquardt *et al.,* 1997; Chen *et al.,* 2005). This indicates that *A. marina* may be adapted to varying availability of green/orange vs. far-red light. The genetic rift between these two cyanobacterial lifestyles is an intriguing issue that warrants additional investigation.

Photosynthetic Proteins.

A. marina contains a full complement of genes to code for functional cyanobacterial photosystems (SI Table 5). Only genes coding for the small PSI subunits *PsaI* and *PsaX* were not detected. Crystallographic analysis suggests that these small single-transmembrane proteins are associated with the stabilization of PSI trimers (Jordan *et al.,* 2001), although a stable trimer was isolated without them in *Gloeobacter violaceus* (Inoue *et al.,* 2004). Like several other cyanobacteria, *A. marina* contains three copies of *psbA* (the D1 core subunit of PSII) and three copies of *psbD* (the D2 core subunit of PSII). Two of the *psbA* sequences (AM1_2166 and AM1_2889) share 97% nucleotide and 100% amino acid identity, whereas the third (AM1_0448) shares only 61% amino acid identity and is more closely related to a divergent *PsbA* in *Anabaena variabilis* (YP_324615) and *Crocosphaera watsonii* (ZP_00515211). Two of the *psbD* sequences (AM1_1083 and AM1_4084) share 99% nucleotide and 100% amino acid identity, whereas the third (AM1_6045) shares 93% amino acid identity; these likely arose from internal duplications within *A. marina*. The primary sequence of both D1 and D2 is highly conserved with other cyanobacteria and Chl *d* likely binds naturally into Chl *a*-binding sites (Itoh *et al.,* 2007; Chen *et al.,* 2005).

Several other genes coding for photosystem-associated proteins have been duplicated in *A. marina*. Two of four unique copies of psbU (AM1_G0114 and AM1_D0138) are plasmid encoded, with a protein identity ranging from 36% to 82%. Both *psaK* and *psbE* share a conserved duplication found in many other cyanobacteria, with 32% and 68% identity, respectively. Last, all genes responsible for coding cytochrome b_6f are present in single copies, with the exception of *petH* (x3) and *petJ* (x2).

Conclusions

Although several marine *Synechococcus* and *Prochlorococcus* species have been sequenced (Dufresne *et al.,* 2003; Rocap *et al.,* 2003), there is a paucity of genome information for marine cyanobacteria belonging to the traditional ‘‘cyanophyte’’ clade. Our completion of the genome sequence of *A. marina*, a marine organism with a novel epiphytic/mutualistic lifestyle and a unique light-acclimation method (in Chl *d*), provides this genetic infrastructure to understand the relationship between marine cyanobacterial species. The number of surprising features, ranging from genome size and gene duplication to *recA* copy number and light-harvesting protein complement, accentuates the need for complete sequence coverage. Because the incorporation of Chl *d* in *A. marina* has eliminated a major source of competitive stress, its expansive genome serves as a model for understanding the relationship between metabolic capacity and niche adaptation.

References

Adir, N. (2005) Elucidation of the molecular structures of components of the phycobilisome: reconstructing a giant. *Photosynth. Res*. 85:15–32.

Altschul, S. F., Gish, W., Miller, W., Myers, E. W., and Lipman, D. J. (1990) Basic local alignment search tool. *J. Mol. Biol*. 215:403– 410.

Beale, S. I. (1999) *Photosynth. Res*. 60:43–73.

Bibby, T. S., Nield, J., Chen, M., Larkum, A. W. D., and Barber, J. (2003) Structure of a photosystem II supercomplex isolated from *Prochloron didemni* retaining its chlorophyll *a/b* light-harvesting system. *Proc. Nat. Acad. Sci. USA*. 100:9050 –9054.

Chen, M., and Bibby, T. S. (2005) Photosynthetic apparatus of antenna-reaction centres supercomplexes in oxyphotobacteria: insight through significance of Pcb/IsiA proteins. *Photosynth. Res*. 86:165–173.

Chen, M., Bibby, T. S., Nield, J., Larkum, A. W. D., and Barber, J. (2005) Structure of a large photosystem II supercomplex from *Acaryochloris marina*. *FEBS Lett.* 579:1306 –1310.

Chen, M., Eggink, L. L., Hoober, J. K., and Larkum, A. W. D. (2005) Influence of structure on binding of chlorophylls to peptide ligands. *J. Am. Chem. Soc*. 127:2052–2053.

Chen, M., Hiller, R. G., Howe, C. J., and Larkum, A. W. D (2005) Unique origin and lateral transfer of prokaryotic chlorophyll-*b* and chlorophyll-*d* light-harvesting systems. *Mol. Biol. Evol*. 22:21–28.

Chen, M., Quinnell, R. G., and Larkum, A. W. (2002) The major light-harvesting pigment protein of *Acaryochloris marina*. *FEBS Lett*. 514:149 –152.

Chen, M., Zhang, Y., and Blankenship, R. E. (2008) Nomenclature for membrane-bound light-harvesting complexes of cyanobacteria. *Photosynth. Res*. 95:147–154.

Cross, R. L., and Muller, V. (2004) The evolution of A-, F-, and V-type ATP synthases and ATPases: reversals in function and changes in the H+/ATP coupling ratio. *FEBS Lett.* 576:1– 4.

Cunningham, F. X., Sun, Z. R., Chamovitz, D., Hirschberg, J., and Gantt, E. (1994) Molecular structure and enzymatic function of lycopene cyclase from the cyanobacterium *Synechococcus* sp strain PCC7942. *Plant Cell* 6:1107–1121.

de los Rios, A., Grube, M., Sancho, L. G., and Ascaso, C. (2007) Ultrastructural and genetic characteristics of endolithic cyanobacterial biofilms colonizing Antarctic granite rocks. *FEMS Microbiol. Ecol.* 59:386 –395.

Dufresne, A., Salanoubat, M., Partensky, F., Artiguenave, F., Axmann, I. M., Barbe, V., Duprat, S., Galperin, M. Y., Koonin, E. V., Le Gall, F., Makarova, K.S., Ostrowski, M., Oztas, S., Robert, C., Rogozin, I. B., Scanlan, D.J., Tandeau de Marsac, N., Weissenbach, J., Wincker, P., Wolf, Y. I., and Hess, W. R. (2003) Genome sequence of the cyanobacterium *Prochlorococcus marinus* SS120, a nearly minimal oxyphototrophic genome. *Proc. Natl. Acad. Sci. USA*. 100:10020-10025.

Enright, A. J., Van Dongen, S., and Ouzounis, C. A. (2002) An efficient algorithm for large-scale detection of protein families. *Nucleic Acids Res*. 30:1575–1584.

Garczarek, L., Hess, W. R., Holtzendorff, J., van der Staay, G.W.M., and Partensky, F. (2000) Multiplication of antenna genes as a major adaptation to low light in a marine prokaryote. *Proc. Nat. Acad. Sci. USA*. 97:4098 – 4101.

Gloag, R. S., Ritchie, R. J., Chen, M., Larkum, A. W. D., and Quinnell, R. G. (2007) Chromatic photoacclimation, photosynthetic electron transport and oxygen evolution in the chlorophyll *d*-containing oxyphotobacterium *Acaryochloris marina*. *Biochim. Biophys. Acta.* 1767:127–135.

Hu, Q., Miyashita, H., Iwasaki, II., Kurano, N., Miyachi, S., Iwaki, M., and Itoh, S. (1998) A photosystem I reaction center driven by chlorophyll d in oxygenic photosynthesis. *Proc. Natl. Acad. Sci. USA*. 95:13319-13323.

Inoue, H., Tsuchiya, T., Satoh, S., Miyashita, H., Kaneko, T., Tabata, S., Tanaka, A., and Mimuro, M. (2004) Unique constitution of photosystem I with a novel subunit in the cyanobacterium *Gloeobacter violaceus* PCC 7421. *FEBS Lett*. 578:275–279.

Itoh, S., Mino, H., Itoh, K., Shigenaga, T., Uzumaki, T., and Iwaki, M. (2007) Function of chlorophyll *d* in reaction centers of photosystems I and II of the oxygenic photosynthesis of *Acaryochloris marina*. *Biochemistry.* 46:12473–12481.

Jordan, P., Fromme, P., Witt, H. T., Klukas, O., Saenger, W., and Krauss, N. (2001) Three-dimensional structure of cyanobacterial photosystem I at 2.5 A resolution. *Nature.* 411:909–917.

Kaneko, T., Nakamura, Y., Wolk, C. P., Kuritz, T., Sasamoto, S., Watanabe, A., Iriguchi, M., Ishikawa, A., Kawashima, K., Kimura, T., Kishida, Y., Kohara, M., Matsumoto, M., Matsuno, A., Muraki, A., Nakazaki, N., Shimpo, S., Sugimoto, M., Takazawa, M., Yamada, M., Yasuda, M., and Tabata, S. (2001) Complete genomic sequence of the filamentous nitrogen-fixing cyanobacterium *Anabaena* sp. strain PCC 7120. *DNA Res.* 8:205–213.

Kaneko, T., Sato, S., Kotani, H., Tanaka, A., Asamizu, E., Nakamura, Y., Miyajima, N., Hirosawa, M., Sugiura, M., Sasamoto, S., Kimura, T., Hosouchi, T., Matsuno, A., Muraki, A., Nakazaki, N., Naruo, K., Okumura, S., Shimpo, S., Takeuchi, C., Wada, T., Watanabe, A., Yamada, M., Yasuda, M., and Tabata, S. (1996) Sequence analysis of the

genome of the unicellular cyanobacterium *Synechocystis* sp. strain PCC6803. II. Sequence determination of the entire genome and assignment of potential protein-coding regions. *DNA Res.* 3:109 –136.

Konstantinidis, K. T. and Tiedje, J. M. (2004) Trends between gene content and genome size in prokaryotic species with larger genomes. *Proc. Nat. Acad. Sci. USA*. 101:3160 –3165.

Kuhl, M., Chen, M., Ralph, P. J., Schreiber, U., and Larkum, A. W. D. (2005) Ecology: a niche for cyanobacteria containing chlorophyll d. *Nature*. 433:820.

Layer, G., Heinz, D. W., Jahn, D., and Schubert, W. D. (2004) Structure and function of radical SAM enzymes. *Curr. Opin. Chem. Biol*. 8:468 – 476.

Maresca, J. A., Graham, J. E., Wu, M., Eisen, J. A., and Bryant, D. A. (2007) Identification of a fourth family of lycopene cyclases in photosynthetic bacteria. *Proc. Nat. Acad. Sci. USA*. 104:11784 –11789.

Marquardt, J., Senger, H., Miyashita, H., Miyachi, S., and Morschel, E. (1997) Isolation and characterization of biliprotein aggregates from *Acaryochloris marina*, a Prochloron-like prokaryote containing mainly chlorophyll d. *FEBS Lett*. 410:428-432.

McInerney, M. J., Rohlin, L., Mouttaki, H., Kim, U., Krupp, R. S., Rios-Hernandez, L., Sieber, J., Struchtemeyer, C. G., Bhattacharyya, A., Campbell, J. W., and Gunsalus, A.W. (2007) The genome of *Syntrophus aciditrophicus*: life at the thermodynamic limit of microbial growth. *Proc. Nat. Acad. Sci. USA*. 104:7600 –7605.

McNamara, C., Perry, T., Bearce, K., Hernandez-Duque, G., and Mitchell, R. (2006) Epilithic and endolithic bacterial communities in limestone from a Maya archaeological site. *Microb. Ecol*. 51:51– 64.

Meier, T., Polzer, P., Diederichs, K., Welte, W., and Dimroth, P. (2005) Structure of the rotor ring of F-Type Na+-ATPase from *Ilyobacter tartaricus*. *Science.* 308:659 – 662.

Michel K. P. and Pistorius, E. K. (2004) Adaptation of the photosynthetic electron transport chain in cyanobacteria to iron deficiency: The function of IdiA and IsiA. *Physiol. Plant*. 120:36 –50.

Miller, S. R., Augustine, S., Le Olson, T. L., Blankenship, R. E., Selker, J., and Wood, A. M. (2005) Discovery of a free-living chlorophyll d-producing cyanobacterium with a hybrid proteobacterial/cyanobacterial small-subunit rRNA gene. *Proc. Natl. Acad. Sci. USA.* 102:850-855.

Miyashita, H., Adachi, K., Kurano, N., Ikemoto, H., Chihara, M., and Miyachi, S. (1997) *Plant Cell Physiol*. 38:274 –281.

Miyashita, H., Ikemoto, H., Kurano, N., Adachi, K., Chihara, M., and Miyachi, S. (1996) *Nature* 383:402.

Miyashita, H., Ikemoto, H., Kurano, N., Miyachi, S., and Chihara, M. (2003) *J. Phycol*. 39:1247–1253.

Murakami, A., Miyashita, H., Iseki, M., Adachi, K., and Mimuro, M. (2004) Chlorophyll *d* in an epiphytic cyanobacterium of red algae. *Science*. 303:1633.

Nagata, N., Tanaka, R., Satoh, S., and Tanaka, A. (2005) Identification of a vinyl reductase gene for chlorophyll synthesis in *Arabidopsis thaliana* and implications for the evolution of *Prochlorococcus* species. Plant Cell. 17:233–240.

Norioka, N., Hsu, M. Y., Inouye, S., and Inouye, M. (1995) Two *recA* genes in *Myxococcus xanthus*. *J. Bact*. 177:4179 – 4182.

Ohkubo, S., Miyashita, H., Murakami, A., Takeyama, H., Tsuchiya, T., and Mimuro, M. (2006) Molecular detection of epiphytic *Acaryochloris* spp. on marine macroalgae. *Appl. Environ. Microbiol.* 72:7912-7915.

Palenik, B., Brahamsha, B., Larimer, F. W., Land, M., Hauser, L., Chain, P., Lamerdin, J., Regala, W., Allen, E. E., McCarren, J., Paulsen, I., Dufresne, A., Partensky, F., Webb, E. A., and Waterbury, J. (2003) The genome of a motile marine *Synechococcus*. *Nature* 424:1037–1042.

Palenik, B., Ren, Q., Dupont, C. L., Myers, G. S., Heidelberg, J. F., Badger, J. H., Madupu, R., Nelson, W. C., Brinkac, L. M., Dodson, R. J., Durkin, A. S., Daugherty, S. C., Sullivan, S. A., Khouri, H., Mohamoud, Y., Halpin, R., and Paulsen, I.T. (2006) Genome sequence of *Synechococcus* CC9311: Insights into adaptation to a coastal environment. *Proc. Nat. Acad. Sci. USA*. 103:13555–13559.

Pham, P., Rangarajan, S., Woodgate, R., and Goodman, M. F. (2001) Roles of DNA polymerases V and II in SOS-induced error-prone and error-free repair in *Escherichia coli*. *Proc. Nat. Acad. Sci. USA*. 98:8350 – 8354.

Rocap, G., Larimer, F. W., Lamerdin, J., Malfatti, S., Chain, P., Ahlgren, N. A., Arellano, A., Coleman, M., Hauser, L., Hess, W. R., Johnson, Z. I., Land, M., Lindell, D., Post, A. F., Regala, W., Shah, M., Shaw, S.L., Steglich, C., Sullivan, M. B., Ting, C. S., Tolonen, A., Webb, E. A., Zinser, E. R., and Chisholm, S. W. (2003) Genome divergence in two *Prochlorococcus* ecotypes reflects oceanic niche differentiation. *Nature* 424:1042–1047.

Shevela, D., Noring, B., Eckert, H. J., Messinger, J., and Renger, G. (2006) *Phys. Chem.Chem. Phys*. 8:3460–3466.

Smith, K. C. (2004) Recombinational DNA repair: the ignored repair systems. *BioEssays* 26:1322–1326.

Smith, M. C., Bowman, J. P., Scott, F. J., and Line, M. A. (2000) *Antarct. Sci*. 12:177–184.

Stickforth, P., Steiger, S., Hess, W. R., and Sandmann, G. (2003) A novel type of lycopene epsilon-cyclase in the marine cyanobacterium *Prochlorococcus marinus* MED4. Arch. Microbiol. 179:409 – 415.

Stothard, P., and Wishart, D. S. (2005) Circular genome visualization and exploration using CGView. *Bioinformatics* 21:537–539.

Swingley, W. D., Hohmann-Marriott, M. F., Le Olson, T., and Blankenship, R. E. (2005) Effect of iron on growth and ultrastructure of *Acaryochloris marina*. *Appl. Environ. Microbiol*. 71:8606 – 8610.

Swingley, W. D., Sadekar, S., Mastrian, S. D., Matthies, H. J., Hao, J., Ramos, H., Acharya, C. R., Conrad, A. L., Taylor, H. L., Dejesa, L. C., et al. (2007)The complete genome sequence of *Roseobacter denitrificans* reveals a mixotrophic rather than photosynthetic metabolism. *J. Bact.* 189:683– 690.

Tamura, K., Dudley, J., Nei, M., and Kumar S (2007) MEGA4: Molecular Evolutionary Genetics Analysis (MEGA) software version 4.0. *Mol. Biol. Evol*. 24:1596 –1599.

Tanaka, A., Ito, H., Tanaka, R., Tanaka, N. K., Yoshida, K., and Okada K. (1998) Chlorophyll *a* oxygenase (CAO) is involved in chlorophyll *b* formation from chlorophyll *a*. *Proc. Nat. Acad. Sci. USA*. 95:12719 –12723.

Tomo, T., Okubo, T., Akimoto, S., Yokono, M., Miyashita, H., Tsuchiya, T., Noguchi, T., and Mimuro, M. (2007) Identification of the special pair of photosystem II in a chlorophyll d-dominated cyanobacterium. *Proc. Natl. Acad. Sci. USA.* 104:7283-7288.

Table 1. General features of the *A. marina* genome.

	Genome	pREB1	pREB2	pREB3	pREB4	pREB5	pREB6	pREB7	pREB8	pREB9	Total
Genome size	6,503,723	374,161	356,087	273,121	226,680	177,162	172,728	155,110	120,693	2,133	8,361,598
G + C content	47%	47%	45%	45%	46%	45%	47%	46%	45%	43%	47%
Open reading frames	6,342	392	417	384	279	224	192	174	120	4	8,528
Pseudogenes	14	5	4	2	1	0	0	0	0	0	26
Coding density	85%	85%	84%	76%	85%	82%	83%	83%	78%	67%	84%
Average gene length	867	814	713	541	693	647	744	737	785	286	824
Ribosomal RNAs	6	0	0	0	0	0	0	0	0	0	6
Transfer RNAs	69	0	0	0	0	0	0	0	0	0	69
Percent CDS without similarities	28%	44%	50%	52%	50%	66%	50%	61%	67%	100%	35%
Percent conserved hypothetical	18%	15%	13%	15%	14%	12%	18%	17%	7%	0%	17%
Insertion elements	285	30	28	19	9	27	16	21	51	1	487
Copy number (approximate)	1	1	1	1	1	1	1	1	1	1	

Figure 1. Circular representation of *the A. marina* chromosome and plasmids. The different rings represent (from outer to inner) all genes and insertion elements, color-coded by functional category (rings 1 and 2), deviation from average GC content (ring 3), and GC skew (ring 4). All plasmids are represented at X10 scale for visualization except pREB9 at 500. Color codes are as follows: turquoise, small-molecule biosynthesis; yellow, central or intermediary metabolism; orange, energy metabolism; red, signal transduction; light blue, DNA metabolism; blue, transcription; purple, protein synthesis/fate; dark green, surface-associated features; gray, miscellaneous features; pink, phage and insertion elements; light green, unknown function; dark gray, conserved hypothetical proteins; black, hypothetical proteins; and brown, pseudogenes.

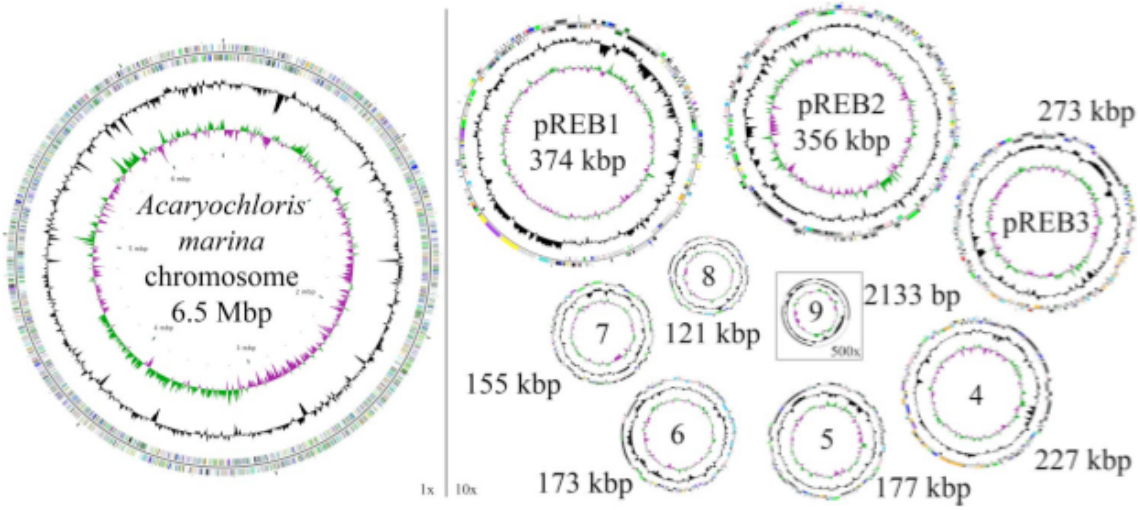
Acaryochloris marina
chromosome
6.5 Mbp
1x
10x
pREB1
374 kbp
pREB2
356 kbp
273 kbp
pREB3
8
121 kbp
9
2133 bp
500x
7
155 kbp
4
227 kbp
6
173 kbp
5
177 kbp

Figure 2. Phylogenetic relationship of CAO superfamily proteins constructed using maximum-likelihood. *Acaryochloris* sequences are listed by their locus tag. Note that the phylogenetic space between *Prochlorococcus* and plant CAO enzymes includes a number of undescribed proteins implicated in degradation of aromatic ring molecules including chlorophyll.

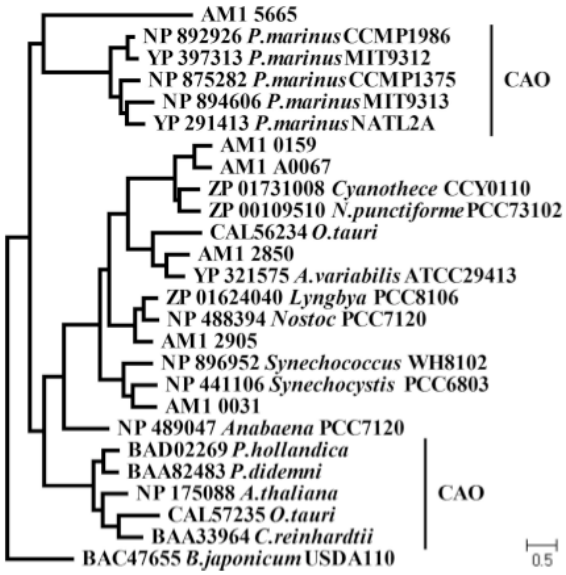
AM1 5665
NP 892926 P.marinus CCMP1986
YP 397313 P.marinus MIT9312
NP 875282 P.marinus CCMP1375
NP 894606 P.marinus MIT9313
YP 291413 P.marinus NATL2A
CAO
AM1 0159
AM1 A0067
ZP 01731008 Cyanothece CCY0110
ZP 00109510 N.punctiforme PCC73102
CAL56234 O.tauri
AM1 2850
YP 321575 A.variabilis ATCC29413
ZP 01624040 Lyngbya PCC8106
NP 488394 Nostoc PCC7120
AM1 2905
NP 896952 Synechococcus WH8102
NP 441106 Synechocystis PCC6803
AM1 0031
NP 489047 Anabaena PCC7120
BAD02269 P.hollandica
BAA82483 P.didemni
NP 175088 A.thaliana
CAL57235 O.tauri
BAA33964 C.reinhardtii
CAO
BAC47655 B.japonicum USDA110
0.5

Figure 3. A schematic of the putative carotenoid biosynthesis pathway in *Acaryochloris*. The reaction catalyzed by CrtR passes through the intermediate β-cryptoxanthin.

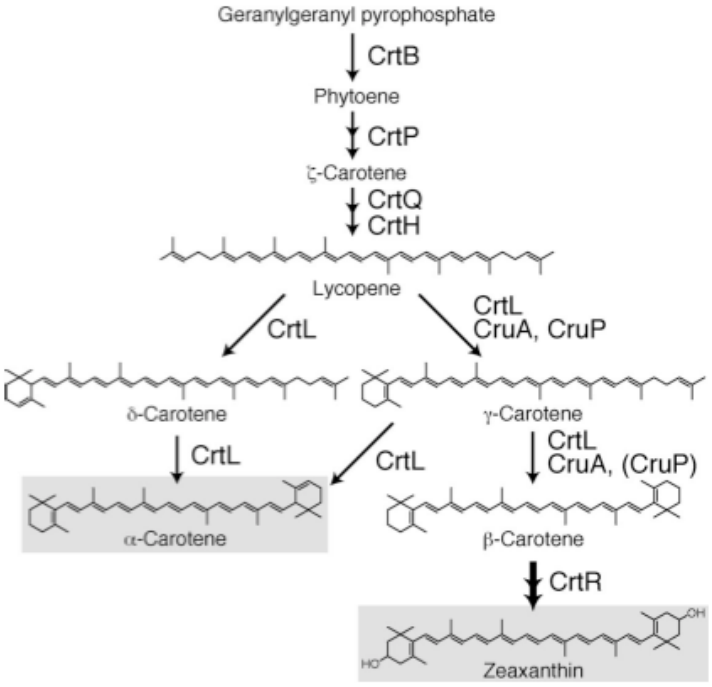
Geranylgeranyl pyrophosphate
CrtB
Phytoene
CrtP
ζ-Carotene
CrtQ
CrtH
Lycopene
CrtL
CrtL
CruA, CruP
δ-Carotene
γ-Carotene
CrtL
CrtL
CrtL
CruA, (CruP)
α-Carotene
β-Carotene
CrtR
HO
OH
Zeaxanthin

Figure 4. The relationship between the usage of PBPs and accessory CBPs in cyanobacteria. Green diamonds represent *Prochlorococcus* species, blue triangles represent marine *Synechococcus* species, a red square represents *Acaryochloris*, and black circles represent all other cyanobacteria. Points including two or more species are bordered in black.

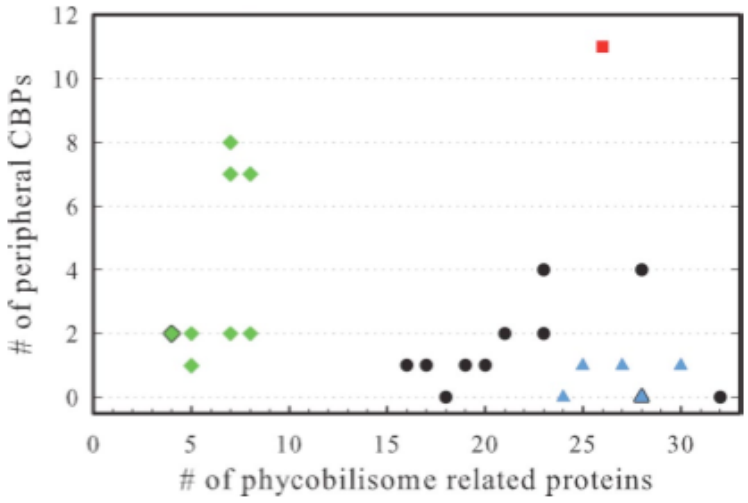
# of peripheral CBPs
# of phycobilisome related proteins
0
2
4
6
8
10
12
0
5
10
15
20
25
30